1-1-1992

Use of solid-state NMR to probe the order, dynamics and conformations of poly(p-phenylene vinylene) and poly(2,5-dimethoxy-p-phenylene vinylene)/

Jeffrey Harper Simpson
University of Massachusetts Amherst

USE OF SOLID-STATE NMR TO PROBE THE ORDER, DYNAMICS AND CONFORMATIONS OF POLY(*p*-PHENYLENE VINYLENE) AND POLY(2,5-DIMETHOXY-*p*-PHENYLENE VINYLENE)

A Dissertation Presented

by

JEFFREY HARPER SIMPSON

Submitted to the Graduate School of the

University of Massachusetts in partial fulfillment

of the requirements for the degree of

DOCTOR OF PHILOSOPHY

September, 1992

Department of Polymer Science and Engineering

USE OF SOLID-STATE NMR TO PROBE THE ORDER, DYNAMICS AND CONFORMATIONS OF POLY(*p*-PHENYLENE VINYLENE) AND POLY(2,5-DIMETHOXY-*p*-PHENYLENE VINYLENE)

A Dissertation Presented

by

JEFFREY HARPER SIMPSON

Approved as to style and content by:

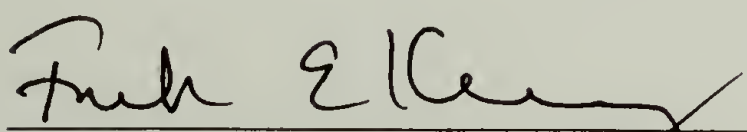

Frank E. Karasz, Chair of Committee

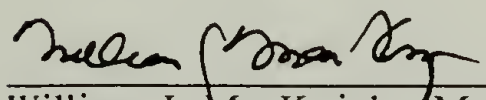

William J. MacKnight, Member

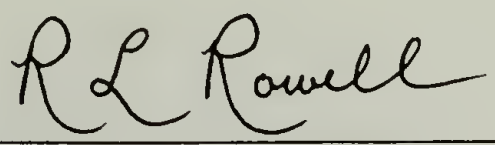

Robert. L. Rowell, Member

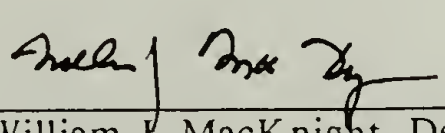

William J. MacKnight, Department Head
Department of Polymer Science and Engineering

To Scott A. Nitzsche

ACKNOWLEDGEMENTS

I wish to thank Professor Frank E. Karasz for making my stay here at the University a successful one, for giving me the right balance of guidance and freedom in the pursuit of my studies, and for showing me how to get things done. I also wish to thank the other members of my committee, Professor William J. MacKnight and Professor Robert L. Rowell. Both of these gentlemen have been patient and wise in their dealings with me.

Dr. David M. Rice also deserves a tremendous amount of thanks. Dave showed me some of the ropes and for this I will always be in his debt. In addition, I must mention Dr. Michael A. Masse who started on the PPV project and who let me share his office for a year. Next, I have to thank Dr. L. Charles Dickinson for his presence, patience and thoughtfulness. Dr. Michael J. Winokur is heartily lauded for useful discussions and physical perspective. Mr. Frank C. Rossitto, Mr. Ananda Sarker and Professor Paul M. Lahti are thanked for their assistance and helpful discussions.

For help in the quick-and-dirty manufacture of a number of projects, I am truly indebted to Mr. Thomas Scott and Mr. Todd Sunderland. Their willingness to help me do something when they should have been doing their own work does not go unnoticed. In the same vein, the administrative and secretarial staff of the Karasz group deserve an immense amount of praise for the expedition of various tasks that has enabled me to be the first in my class to obtain my degree.

And speaking of my class, I wish to acknowledge the powerful impact that the late Mr. Scott A. Nitzsche had on me during the time I knew him. His work-hard/play-hard attitude taught me more than I dare say.

Finally, I must thank all of the other friends and loved ones who have supported me. I thank my fiance Andrea M. Morawski for putting up with the emotional rollercoaster that is the essence of the graduate student experience. I save special thanks

for Mr. John Savage, Mr. Frank C. Rossitto and Mr. Michael DeRosa, the collaborative musical effort we have shared has been a source of strength and inspiration.

ABSTRACT

USE OF SOLID-STATE NMR TO PROBE THE ORDER, DYNAMICS AND CONFORMATIONS OF POLY(*p*-PHENYLENE VINYLENE) AND POLY(2,5-DIMETHOXY-*p*-PHENYLENE VINYLENE)

SEPTEMBER 1992

JEFFREY HARPER SIMPSON, B.A. BOWDOIN COLLEGE

Ph.D., UNIVERSITY OF MASSACHUSETTS

Directed by: Professor Frank E. Karasz

Solid-state ^{13}C cross-polarization magic-angle-spinning (CPMAS) nuclear magnetic resonance (NMR) spectra have been obtained for films of poly (*p*-phenylene vinylene) (PPV) and PPV-d_4, poly (*p*-2,3,5,6-tetradeutero-phenylene vinylene). All four phenylene and vinylene resonance have been assigned. The ^{13}C CPMAS NMR spectra show the presence of phenylene ring 180° rotation jumps.

Solid-state ^{2}H quadrupole-echo nuclear magnetic resonance spectra of PPV-d_4 films show that all the phenylene rings of PPV undergo 180° rotational jumps about the 1,4 ring axis with a median activation energy, E_a = 15 kcal/mol and a distribution of activation energies of less than ±2 kcal/mol.

The effects of concentrated sulfurice acid doping of PPV-d_4 have been examined with ^{2}H quadrupole echo NMR spectroscopy. The activation energy for ring flips is observed to increase upon doping, as does the width of the jump rate distribution.

Stretched PPV films have been prepared in which the vinylene protons have been substituted with deuterium (PPV-d_2). ^{2}H spectra of aligned samples at high temperature

show molecular motion. The observed chain motion is consistent with a 180° rotational jump of the PPV chain about the crystallographic **c** axis. Inversion recovery quadrupole echo spectra also support a chain jump model and indicate the jump rate distribution is similar to that of the phenylene rings.

^{2}H quadrupole echo NMR spectra of oriented PPV-d_4 aligned in the NMR magnetic field have been simulated and thereby have yielded the chain orientation distribution in these films. ^{2}H spectra obtained at -58 °C are well simulated by an orientation distribution consisting of two Gaussian components. In addition, the average tilt of the phenylene ring relative to the chain axis has been found to be 7.7°, not the 9.2° predicted for a *trans*-stilbene-like structure.

PPV has been doped with sodium metal. The chemistry of this process has been examined with elemental analysis. ESR spectroscopy has followed the evolution of unpaired spins as the doping reaction proceeds. The ^{2}H NMR line shape of sodium-doped PPV-d_4 is relatively insensitive to changes in temperature and consists of two distinct components. The origin of these components is considered.

Two-dimensional ^{13}C-^{1}H HETCOR CP-MAS NMR spectra of *p*-dimethoxybenzene (DMB) and poly(2,5-dimethoxy-*p*-phenylene vinylene) (PDMPV) with variable ^{1}H dipolar mixing times have been analyzed to determine the rates of ^{1}H magnetization transfer between chemically distinct protons. Internuclear distances have been obtained from these rates and the conformation of the PDMPV repeat unit has been calculated and discussed.

TABLE OF CONTENTS

LIST OF TABLES

LIST OF FIGURES

CHAPTER 1

INTRODUCTION

1.1 Motivation for Studies

Fully-conjugated polymers have been studied for a number of years, dating back to the 1970s when high-molecular weight polyacetylene (PA) was first prepared[1]. The doping of PA with AsF_5[2] to obtain a relatively highly conductive material has stirred much interest in the field and led to the dubbing of these materials conducting polymers. Since 1977, a large number of other conducting polymers have been synthesized and characterized (see Table 1.1) and a number of texts have appeared on the subject.[3,4]

Fully-conjugated polymers continue to be widely studied. Extended π-conjugation in organic systems gives rise to many interesting physical properties and phenomena, including some with potentially important practical device applications in areas such as electronics[5,6] and optics[7,8]. Many different sub-disciplines from the physical sciences have been brought together in the study of these materials. Figure 1.1 shows how the field of conducting polymers fits into the scientific spectrum.

From the onset of work in this field, researchers have realized that besides having a unique structure on the molecular level, fully-conjugated polymers must retain their macroscopic structural integrity. Early fully-conjugated organic materials synthesized by direct methods[9-11] yielded products that were oligomeric in nature and also insoluble, presenting the researchers with powder samples unsuitable for many measurements and applications. The insolubility of these systems is in general due to the stiffness of the polymer backbone caused by the full conjugation. Figure 1.2 shows a picture of how the p-orbitals of the conducting polymer chain force it to adopt a planar conformation to maximize orbital overlap. The powdery nature of direct synthesis products is caused by product insolubility which causes precipitation at low degrees of

polymerization. The resulting low-molecular weight material has extremely poor mechanical properties. For example, some of the early characterizations of these materials involved compressing the powdery materials into pellets. The attainment of high-molecular-weight materials via different synthetic pathways soluble in either their fully-conjugated form[12-16] or in a precursor polymer form[17,18] has resulted in materials that can be processed into oriented films and fibers.

While solubility and processibility are important technological hurdles, these materials are primarily intended for solid-state applications. Therefore, any true understanding of these materials must include the study of them in the solid state. This dissertation contains work focused on the understanding of the solid-state of poly(*p*-phenylene vinylene) (PPV) and a ring-functionalized analog, poly(2,5-dimethoxy-*p*-phenylene vinylene) (PDMPV) with nuclear magnetic resonance (NMR) spectroscopy.

The unique physical properties of fully-conjugated polymers arise from their electronic structure. That is, the π-electrons which are delocalized along the polymer backbone are responsible for the interesting attributes of these systems. And yet in order to properly understand how the electron clouds of these systems are perturbed by various external forces, it is necessary to understand how the electron clouds are constrained by the molecules on which they reside. For example, drawn PPV doped with any of a number of oxidizing agents will show a marked conductivity anisotropy.[19,20] This anisotropy is caused by the fact that the electron-pair holes (bipolarons[21]) are able to migrate much more readily along the polymer chains than perpendicular. This anisotropy serves to simply illustrate how the molecular framework of the PPV chain has a profound effect on the electronic properties of the system.

1.2 Objectives

The work contained in this dissertation seeks to determine the structure of the PPV chains, with the hope that the data and conclusions presented here will assist in the

understanding of how the electronic properties of the system are affected by various molecular influences for all conducting polymers. In order to development the picture of the molecular framework of PPV, this dissertation presents data on bonding, degree of crystalline perfection, chain orientation, defect structure, chain motion, repeat unit conformation, and changes induced in structure and molecular dynamics caused by doping. Table 1.2 lists the aspects of PPV that have been studied in the completion of this work.

1.3 Organization

This dissertation is organized as follows.

Chapter two presents a brief and relevant history of one, conducting polymers and two, the NMR techniques that have been used to compile the data included in this work.

Chapter three describes the experimental procedures and techniques used for the preparation of samples and collection of data.

Chapter four focuses on solid-state carbon-13 nuclear magnetic resonance (NMR) data of PPV and how this data provides information on the bonding and crystallinity of the PPV system.

Chapter five describes how solid-state deuterium NMR reveals that the phenylene rings of ring-deuterated PPV (PPV-d_4) undergo substantial molecular motion on the NMR time scale.

Chapter six examines the effect of various dopants on this motion and discusses these effects in the context of changes in the electronic and physical structure of the PPV system.

Chapter seven relates how deuterium NMR of vinylene-labeled PPV (PPV-d_2) gives information on chain motions that are present in PPV. This is addition to the more local ring motion covered in chapter five.

Chapter eight shows how deuterium NMR reveals the complete chain orientation distribution in drawn, deuterated samples. Both ring- and vinylene-labeled PPV have been studied to confirm the presence of defects in the PPV backbone.

Chapter nine examines the chemistry of sodium doping of PPV. This chapter utilizes data from a several techniques that together present a coherent picture of the change induced in the PPV structure as a result of doping.

Chapter ten presents a two-dimensional proton-carbon NMR study of poly(2,5-dimethoxy-*p*-phenylene vinylene) that reveals the conformation of the repeat unit.

Chapter eleven summarizes the material presented in chapters four through ten and also suggest potentially fruitful future studies on PPV and related systems.

Table 1.1

Major Groups of Conducting Polymer

Name	Structure
Polyacetylene	
Poly-*p*-phenylene	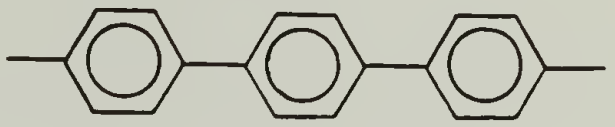
Poly(*p*-phenylene vinylene)	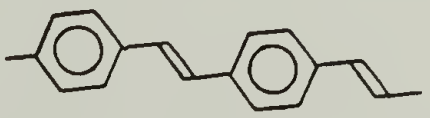
Polythiophene	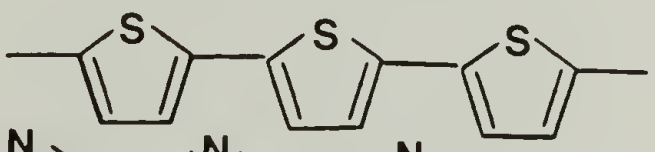
Polypyrrole	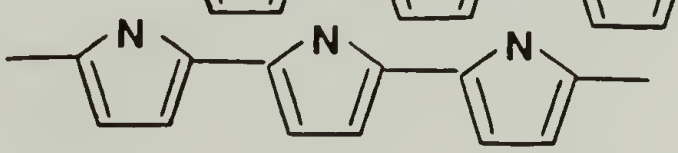
Polyaniline	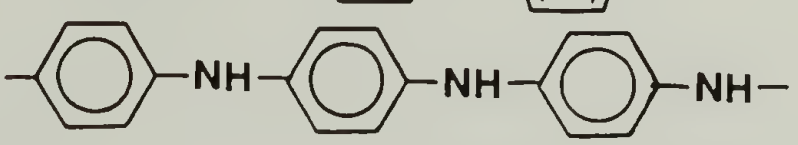

Table 1.2

Aspects of PPV to Study

Bonding
Chemical defects
Repeat unit conformation
Crystallinity
Chain ordering
Defect structure
Dynamic disorder
Molecular motions
Effects of heat treatment
Effects of drawing
Effects of doping

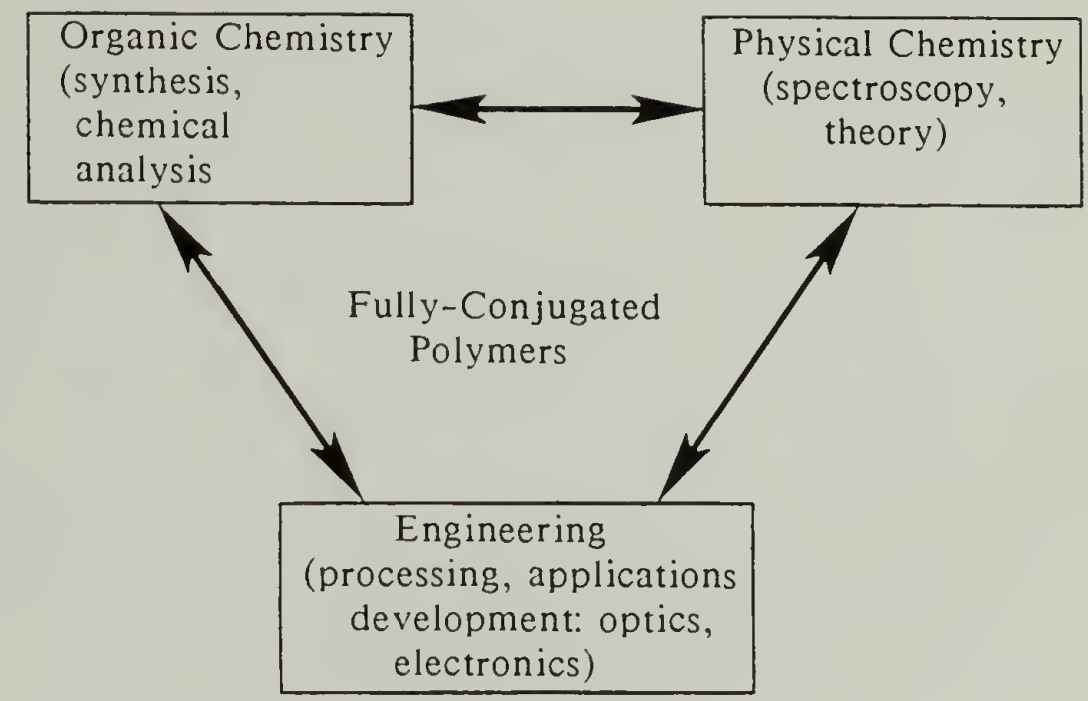

Figure 1.1 A schematic diagram showing where conducting polymer research fits into the scientific spectrum or continuum.

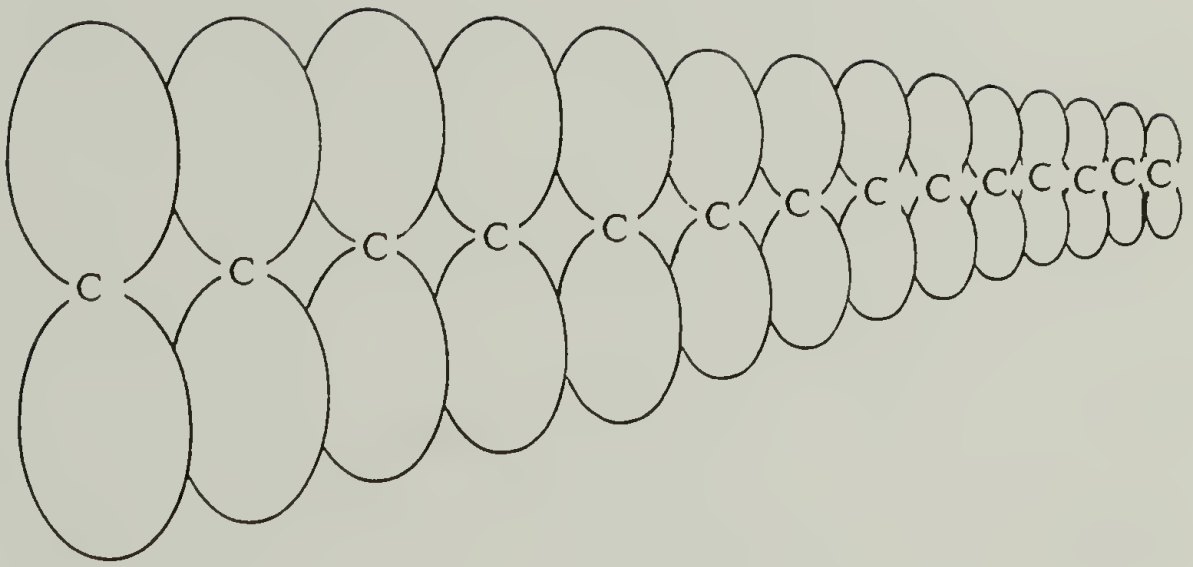

Figure 1.2 Depiction of a stiff polymer chain with overlapping p-orbitals.

CHAPTER 2

HISTORY AND OVERVIEW

This chapter will give the reader background information in two main sections, the first on fully-conjugated polymers and the second on solid-state NMR. Information on fully-conjugated polymers will be presented with the goal of giving the reader a good understanding the relevant work that has taken place up to now in the field. The first main section will be further divided into the three subsections: the first on the variety of fully-conjugated polymers in existence, the second on the various synthetic and processing options that exist for PPV, and the third on the spectroscopic characterization results for PPV. The second main section will discuss the kinds of information that are accessible with solid-state NMR that are relevant to the study of PPV and other related polymeric systems.

2.1 Past Studies of Fully Conjugated Polymers

There are different requirements for conjugated polymers depending on the application for which they are to be used. For instance, electrical conduction applications require a far different electronic structure than do non-linear optical (NLO) second-harmonic generation (SHG) applications. In the former case a polymer with a high degree of crystalline perfection, excellent molecular orientation, a fibrillar morphology and a small bandgap might give good electrical properties[22] and in the latter case a polymer that contains electron donating and electron withdrawing groups linked by conjugation and oriented in a non-centrosymmetric manner could potentially be a useful SHG NLO material.[7]

For conducting polymers, there is a tradeoff between the magnitude of a specific property of interest and the processability of the material. This is due to the fact that

the properties of interest are dependent on the concentration of π-electrons and the planarity of the molecular backbone. Both of these factors tend to impart substantial chain stiffness into the polymer chains rendering them insoluble. A lack of solubility in turn prevents them from being easily processed (or processed at all). Dilution of the concentration of π-electron density gives more flexible and hence more soluble chains but this enhancement comes at the price of reduced property magnitudes.

2.1.1 Types of Fully-Conjugated Polymers

There is a wide array of conjugated materials that have been reported in the literature. The simplest material that can be envisioned is also the most widely studied.[3] Polyacetylene (PA) consists of a hydrocarbon backbone with alternating single and double carbon-carbon bonds. It has a number of interesting physical properties in both its doped and undoped forms. One important aspect of PA is that it becomes electrically conducting when oxidized with an appropriate chemical agent such as AsF_5.[23,24] Early claims that organic conductors would soon replace inorganic (i.e. metallic) conductors for electrical applications have proved to be premature.[25,26] Even highly oriented, doped PA still fails to achieve electrical conductivities comparable to copper.[27] Another important problems associated with PA is that it is not air stable, even it its undoped form.[1,3,18] In spite of these difficulties, many research efforts into the field of fully-conjugated or conducting polymers continue unabated.

Other fully-conjugated polymers that have been reported and continue to appear in the literature include poly(p-phenylene) (PPP),[28-30] poly(p-phenylene vinylene) (PPV),[9,10] polyaniline (PAn),[31,32] polythiophene (PTh)[33,34] and polypyrrole (PPy).[35,36] Variation of polymer backbone structure while retaining full conjugation gives materials with substantially different properties. Further variations can be accomplished by the addition of different substituents as side groups along the chain, either in a regular

fashion[9-11,37-43] or as a copolymer.[41,44-46] Figure 2.1 shows how a conducting polymer may evolve synthetically.

Variation of the polymer structure is found to give the materials designer a wide array of physical properties. The inclusion of aromatic rings in the backbone enhances product stability and also tunes the bandgap.[37,47,48] Incorporation of heteroatoms into the polymer repeat unit as pendant groups further alters the physical properties of these systems such as the solubility.[11,26,38,48-50] Other approaches toward controlling morphology and polymer miscibility have involved blending a conducting polymer with other polymeric systems.[51-53]

2.1.2 Synthetic and Processing Methods for PPV

Early attempts at making fully-conjugated, high molecular-weight polymers failed. This was due to the synthetic methods employed. As soon as the degree of polymerization reached ten or so, the polymer chain would no longer be soluble and would precipitate out of solution, away from unreacted monomer.[9-11,54]

The synthesis of polyacetylene via a transition metal catalyst produced the first high molecular-weight, fully-conjugated polymer.[1] The polymer produced via this route comes in a sheet-like form that is difficult to process.

An important innovation in the area of synthesis was the advent of the precursor polymer route.[17,18,55] The idea is simply to polymerize some material that can be subsequently treated in some manner to yield a fully-conjugated product.
The attractiveness of this synthetic scheme is that the precursor polymer is soluble and can be fabricated into various desirable geometries (e.g. fibers and films). A number of fully-conjugated polymers can be produced with this technique, including PPV.

The concept for the polymerization of a sulfur-containing precursor polymer dates back to 1968.[17] This method has produced PPV precursor polymer with a molecular weight on the order of 10^6.[56] The precursor polymer is soluble in a number

of common solvents such as water and methanol.[50,57-59] Solutions with concentrations on the order of 10-15% polymer by weight can be routinely prepared. These solutions can be cast into films simply by pouring them out on an appropriate surface such as polymethylmethacrylate) (PMMA).[22] The main advantage of this synthetic pathway, however, is realized when this material is heated and placed under tension. The sample heating liberates volatiles from the precursor polymer structure that plasticize the chains, making the material extremely plastic for a short amount of time.[20,60,61] Figure 2.2 shows depicts how the liberation of volatiles can plasticize the polymer chains. Moderate stresses can yield very high strains (maximum draw ratios on the order of 10 are typical but have been reported as high as 20[19,20]). The orientation of the chains within these films is excellent as measured with x-ray diffraction and ir dichroism.[20,47,60,62,63]

Orientation methods vary from the simple hand-stretching operation[19] to the more elaborate machine-stretching procedure.[59] The construction of a machine that can take undrawn PPV film from one roll and wind it on another in a oriented state takes the production of drawn PPV from a batch process to a continuous one. After proper annealing of a drawn film, the mechanical properties of the film will be excellent parallel to the draw direction.[64] The tensile modulus will be very high and will be highly anisotropic due to the orientation of the chains parallel to the draw direction. Cleaving of a film along the draw direction requires breaking a much higher number of covalent bonds than does cleavage perperdicular to the draw direction.

After orientation has taken place, the PPV precursor films are only partly converted into PPV. That is, the chains will be random copolymers of the precursor polymer and PPV. Figure 2.3 shows the random copolymer of PPV, poly(*p*-xylylidene tetrahydrothiophenium chloride) and poly-7-chloro-p-xylylene. Extensive sample heating is required to achieve full elimination of the precursor polymer volatiles.[61,65] This is accomplished by heating the films in an oxygen free vessel at 300 °C for at least

four hours. The heating/elimination can be done in either an inert atmosphere such as argon or in a high vacuum environment. Heating the films at too low a temperature gives incomplete elimination and heating at too high a temperature induces sample degradation.

In certain cases, sample degradation associated with the annealing step is desirable. In recent years there has been much interest in carbon fibers obtained via pyrolysis methods. Pyrolysis of PPV to form graphite films has been undertaken by several research groups in Japan.[66-68] The procedure simply involves heating a sample of PPV to a very high temperature (> 2000 °C) under vacuum and removing all of the liberated volatiles. What is left the untrained eye might see as charcoal but is actually relatively pure in molecular terms. Unfortunately, the relatively high cost of PPV makes it a poor choice for the production of graphite.

Chemical treatment or doping is also used to alter the physical properties of PPV films. There are a number of applicable dopants for the PPV system. Table 2.1 lists these dopants. The list expands when copolymers of PPV and some closely related system such as PDMPV are considered. For pure PPV, the list of dopants included AsF_5,[57] SbF_5,[61,63] H_2SO_4,[63] ClO_4^- anion,[42] and the alkalis.[69-71] For copolymers of PPV such as PDMPV, weaker oxidizing or reducing agents may be used such as iodine.[44] Doping can be accomplished either by either bulk methods (e.g. by immersing the film in H_2SO_4 directly or exposing the film to the appropriate chemical vapor)[57] or by electrochemical means.[51,72] While electrochemical means offer greater control of the doping reaction, they are necessarily done in solution which gives rise to the complication of solvent coinsertion.[22,69] Solvent coinsertion is potentially a problem because one, it introduces an additional level of complexity to the system by adding another component and two, the solvent molecules cannot be expected to indefinitely reside in the doped-PPV matrix.

Other chemical species are observed to accelerate doping reactions. For example, AsF_3 (present as an impurity in commercially-available AsF_5) is observed to act as a co-dopant.[22] That is, AsF_3 does not actually participate in the doping reaction but nevertheless is somehow able to speed along the doping reaction, perhaps by facilitating the diffusion of AsF_5 into the PPV matrix.

Overdoping is observed to occur in some cases, either due to too long a doping time or to too powerful a reagent. HNO_3, for example, is too strong an oxidizer and degrades a film of PPV entirely. A PPV film immersed in nitric acid for an hour becomes so completely oxidized that it loses its structural integrity and eventually disappears.[73]

Variation of the doping times has been found to strongly affect the final physical properties of the PPV films. Masse *et al.* have studied how arsenic penetrates into the PPV bulk.[74] Some doping reactions are observed to occur homogeneously and others are very heterogeneous in nature. Most doping reactions involve a crystal-crystal phase transition wherein the PPV unit cell undergoes a first-order phase transition to a unit cell that includes dopant counterions.[22,75]

2.1.3 Characterization Methods for PPV

Because PPV is insoluble in its fully converted form, solid-state instrumental techniques have had to be employed in the study of these materials. While there are other conducting polymers which are soluble even in their conducting forms,[12-14] but this is not the case for PPV. A number of spectroscopic techniques have been used to study PPV in its fully converted form. These techniques have yielded a wealth of information on PPV, and this is the foundation on which the studies described in this thesis are based. For other conducting polymers such as PA, there is the additional complication of air instability.[3] To some extent, PPV suffers from this drawback as well. PPV is not air stable in its doped forms. Perhaps the most stable of all of the

doped forms of PPV is H_2SO_4-doped PPV. Air stability often complicates sampling handling procedures and some analytical techniques are complicated or compromised as a result. Nevertheless, a great abundance of data has been collected on PPV and related systems.

Elemental analysis has been used to study the elimination/annealing steps of the PPV preparation procedure.[22,61,65] This has allowed the assessment of how much oxygen is incorporated into the samples and also whether or not the elimination step(s) has(have) gone to completion. If a film of PPV precursor polymer is heated for too short a time or at too low a temperature, the volatile components (HCl and tetrahydrothiophene, THT) will be incompletely removed from the sample. Elemental analysis has determined that the sulfur content drops off more quickly than does the chlorine content,[76] suggesting that the chloride ions displace the THT moieties prior to the formation of the vinylene double bond.

Thermogravimetric analysis (TGA) data is also consistent with this scheme.[77] As a film of PPV precursor is heated, it shows three distinct weight loss regimes. One occurs at just above 100 °C and is associated with the loss of water, the second occurs in the 170-240 °C range and corresponds to the loss of THT, the third occurs in the 250-300 °C temperature range and is assigned to the loss of HCl. It should be noted that the second and third weight loss regimes overlap to a large extent, making an exact determination of their origin difficult. Nevertheless, the approximate percentages of weight loss are in agreement with the ratio of the THT and HCl molecular weights to that of the PPV precursor repeat unit (less the water weight). Finally, at around 450-500 °C the PPV sample begins to irreversibly degrade into graphite and related structures. Figure 2.4 diagrams the evolution of the PPV precursor polymer as it is heated.

Density measurements have been used to determine the crystallinity of PPV samples. This is done by comparison with the theoretical density determined from the

x-ray crystallographic structure. Density measurements on oriented and unoriented PPV films have shown that PPV possesses a similar percentage of crystalline regions in both drawn and undrawn samples.[22,63] This indicates that on the molecular level, the chains are able to still pack quite efficiently even though at the macroscopic level they are randomly oriented.

Mechanical testing methods have been used to determine the tensile strength and modulus of PPV films and fibers.[61,64] PPV was originally of great interest to the United States Air Force because of its potential as a high modulus fiber. Indeed, PPV does possess very good mechanical properties in its pristine form, but doping is observed to significantly degrade these properties.[64]

Dynamic mechanical testing (DMT) and calorimetric methods have been used to look for the glass transition and other cooperative transitions in PPV.[22,61,65] Interestingly, PPV is observed to undergo none of these phenomena below its degradation temperature, indicating that PPV is frozen in the solid state. Only redox reactions are able to pry the PPV chains apart, illustrating the stability of the PPV structure.

Infrared spectroscopy has been used very successfully to examine PPV.[22,59-62,78,79] Ir spectra have shown that the elimination reaction that produces PPV from the PPV precursor polymer gives *trans* vinylene linkages exclusively. Ir spectra have further been used to assess the order present in PPV. Ir dichroism measurements[59,60,79] have been used to follow the orientation induced in PPV films as a function of the draw ratio.

X-ray and electron diffraction techniques have also been used to both quantify the orientation induced in PPV films as a result of sample drawing,[80-82] to elucidate the unit cell of pristine[81] and doped PPV[63] and to follow the conversion of the precursor polymer into PPV.[83,84] From this work, PPV is known to adopt a *trans, transoid* configuration wherein all of the *trans*-vinylene groups in a given chain are aligned

parallel. This is arrangement is shown in Figure 2.5. Furthermore, the chains, when viewed end on, pack in a herringbone arrangement, as shown in Figure 2.6.

X-ray diffraction[22,63] and electron diffraction[81,82] have also shown that PPV packs into the unit cell with a certain amount of disorder, referred to as paracrystallinity.[85-88] This disorder corresponds to a lack of axial registry of the chains (see Figure 2.7). This means that there is a very shallow potential well in which the chains reside along the polymer backbone. In addition, diffraction methods have shown that the direction of the vinylene group is unspecified. That is, the vinylene groups can vary their tilt from one layer of chains to the next.

Besides electron diffraction methods, electron microscopy has been used to examine PPV.[75] This technique has revealed the morphology of PPV. It has been used to show that a PPV chain spans a number of small (10 nm), equiaxed crystallites. Orientation of PPV films is observed to not change the size of the crystallites appreciably but to instead merely align them more or less parallel with the draw direction.

To examine the penetration of dopant into bulk PPV, Rutherford backscattering spectroscopy has been employed Masse *et al.*[74] found that AsF_5 doping of PPV occurs primarily as a skin doping. Significant penetration of dopant counterions beyond the first 100 nm of the films examined was not observed. This indicates that the highly dense PPV matrix in not hospitable to large molecules or ions and once agains affirms the intractability of this and related materials.

2.1.4 Understanding of the Electronic Structure of PPV

Not only are the mechanical properties anisotropic, but so are the electrical properties of drawn, doped PPV films.[19,20] The alignment of conjugated units along a common axis serves to give a very large electrical conductivity anisotropy. The ratio of the parallel to perpendicular conductivities is high but not infinite. This is because of

two things, one the chain orientation is not perfect but spans a finite width of angles within a few degrees of the draw director and two, the charge carriers are able to hop between the chains (because a typical film of several cm does not have chains which span the entire length of the chain). In fact, the typical length of a region in which a chain is planar and otherwise unperturbed (by a rotational defect, for example) is on the order of 10 nm.[75] This means that the charge carriers must be hopping between chains or past the high energy sites where the extended conjugation is disrupted.

It is interesting to note that polyisoprene, a non-conjugated polymer, has been doped with iodine to obtain modest conductivities (in the semiconductor range).[12,89] Initially, it was thought that this proved that conjugation is not required for electrical conduction. However, a later report[90] has shown that the iodine doping process not only oxidizes the material but also induces an isomerization reaction that produces regions of full conjugation and regions of saturation along the chains. Electrical conduction is able to occur as it would in a block copolymer of polyacetylene and polymethylene (ignoring the pendant methyl groups of the chain). That is, the charge can move along the conjugated regions and then, when it reaches a saturated region for a given chain, it can hop over to the conjugated region of nearby chain.

The nature of the charge carriers in these materials has been widely studied.[21,91-96] In order for oxidation (or reduction) to occur on the molecular level, single electrons must be removed from (or donated to) the polymer chains. The removal of one electron generates and unpaired spin that is trapped on one specific portion of a chain. This unpaired spin is termed a polaron.[91,94] In general, the electron will be confined by the chain ends and by kinked regions in the polymer chain which impede the *p*-orbital overlap or by saturated regions where oxygen has added to a vinylene group or the chemical species of the precursor polymer have failed to be eliminated. Covalent addition of dopant molecules also must be considered in the assessment of the molecular structure on which electrical conduction takes place.

Removal of a second electron from the same region of a chain presents two options. One is that the two holes repel each other because of their like charge, another is that the two spins combine to form a spinless entity called a bipolaron.[21,91] There is substantial evidence from ESR[42,97] and other techniques[21,98-100] that bipolaron migration is the dominant charge conducting mechanism in many conducting polymers, including PPV.

On the other hand, groups studying PPV for applications in light emitting devices (LEDs)[5,101] have reported that oppositely charged polarons are the charge carriers for this experimental configuration. LEDs are made by injecting opposites charges on opposing sides of a thin layer of PPV that has been spun coated onto an optically clear, electrically conducting substrate (e.g. indium-tin-oxide glass). By applying a modest potential, a thin film (on the order of 100 nm) of PPV will have the opposite charges migrate through the bulk of the film a combine. This combination of charges gives a spinless excited state that can decay non-radiatively to liberate heat or radiatively to liberate a photon. Currently, some of the problems with these LEDs are that the non-radiative decay pathways are dominant leading to one, a low device efficiency and two, excessive local device heating which leads to sample degradation and ultimately to device failure.

2.2 Solid State NMR Studies of Other Polymers

There are two sub-disciplines of solid state NMR spectroscopy which have been employed in this work. One involves using the carbon-13 cross-polarization, magic-angle-spinning (CPMAS) pulse sequence[102,103] and the other involves broadline quadrupole echo deuterium NMR.[104-108] Carbon NMR work gives the scientist a variety of chemical and structural information, including data on motion and chemical exchange. Deuterium NMR reveals information about order and molecular dynamics. Although

carbon NMR is also able to furnish information of this nature, deuterium NMR is better able to quantify order and molecular motion than carbon is NMR.

2.2.1 CPMAS ^{13}C NMR

Most solid-state carbon NMR gives the scientist information analogous to that obtained with solution-state techniques. That is, the majority of the solid-state data collected consists of one-dimensional spectra showing chemical shift information. Samples are typically ground into powders and loaded into a magic-angle-spinning (MAS) rotors where they are spun at a sufficient speed (typically 5 kHz) to average out the anisotropy of the chemical shift tensor. The resulting spectrum so is simply what would be observed for a liquid sample.

However, notable differences are present for the solid-state experiment and these are described in much greater depth elsewhere.[109-112] For one, the carbon nuclei are invariably in close proximity to the near 100% abundant proton spins in the sample, giving a large dipolar coupling which wipes out the carbon magnetization. This impediment is overcome by using high-power proton decoupling to saturate the proton resonances while the carbon free induction decay is acquired.

Other differences include the resonance widths in solids. The virtually continuous ensemble of minutely varying chemical environments give line widths which are substantially broader than what is seen for solution-state spectra.[113-115] While detracting from the spectral resolution, the broader line widths associated with the solid state can be used to determine the variation of the chemical environment for various chemically distinct carbons. The variation of line widths for amorphous versus crystalline materials is well-documented.[113-121]

Molecular motions of various portions of polymer chains have also been extensively studied and reported.[122-129] This particular area of carbon NMR is still one of the most active areas in the polymer journals. Aside from the averaging of chemical

shifts, molecular motion is also observed to affect the relaxation rates of protons and carbons in the solid state.[127] The spin-lattice relaxation rate passes through a minimum as the spectral density passes through a maximum at the spectrometer frequency.[109,112] This and other relaxation rates enable to scientist to better quantify the nature of the molecular motions taking place.

A particularly elegant method for the elucidation of molecular dynamics using carbon NMR detection methods is two-dimensional NMR.[130-133] Specific information such as jump angles associated with conformational changes in polymer chains have been unequivocally demonstrated.[134,135] Table 2.2 summarizes the information available with solid-state ^{13}C NMR methods.

2.2.2 Broadline ^{2}H Quadrupole-Echo NMR

Deuterium NMR is a technique which is not as commonly used as carbon NMR. One of the principle reasons for this is that deuterium labeling of the material to be studied must be carried out. This requires not just the physical chemist to analyze the material, but it also requires a proficient synthetic chemist to prepare the material without the annoyance of mixed labels. Fortunately, a text has been published to help accomplish this end.[136] For deuterium NMR to serve as a valuble tool for the polymer scientist, the deuterium atoms are ideally to be incorporated into the molecule or polymer at only one or a very few sites.

With this accomplished, the information that can be obtained from a sample of specifically deuterated material is quite large. First and foremost, the deuterium spectra will reveal give information about the atom to which it is bonded. The quadrupolar coupling constant of a deuterium nuclei is found to depend on the bond hybridization of the carbon nuclei to which it is attached.[110]

The observed deuterium line shape is also depends on the orientation of the C-D bonds in space.[111,112] This dependence allows the complete determination of the

distribution of bond orientations within an oriented sample. Spiess and coworkers have used this technique to characterize the orientation of liquid crystalline polymers.[105,108,137,138]

Modern deuterium NMR techniques use pulsed methods, and this necessitates using the quadrupole echo pulse sequence so that the magnetization is refocussed at some small time interval after the last pulse to allow transient ringdown. Typical delays are on the order of five to ten microseconds. In some cases, the deuterium nuclei will undergo relaxation during this short time period and the resulting line shape will be attenuated and distorted.[139-141] These effects are most pronounced when there is molecular motion or exchange occuring at a frequency similar to the spectrometer frequency. For very narrow distributions of correlation times, the height of the spin echo will be attenuated by as much as a factor of ten when passing through this intermediate exchange regime.

The deuterium line shape is also very sensitive to molecular motion. The symmetry of a jump motion can often be determined by the resulting line shape.[104,105]

Relaxation data obtained from deuterated compounds is also able to furnish information on molecular motions.[140,142,143] By adapting the inversion-recovery pulse sequence to the quadrupolar deuterium nucleus, specific components of a complicated line shape can be assigned to regions with different mobilities.

There are also two-dimensional experiments that have been devised for probing exchange processes in deuterated materials.[130,132,144-146] This experiment takes advantage of the fact that the exchange will alter the orientation of a given C-D bond vector with respect to the applied magnetic field and will hence change the energy of the spin levels, giving a transition at a different frequency. For isotropic samples, this technique yields distinctive elipses when exchange is occuring. For oriented samples, distinct cross-peaks are observed similar in appearance to carbon-proton correlations. Furthermore, varying the time delay during which the exchange takes place allows the

complete characterization of the distribution of jump rates (limited only by the relaxation of the coherent magnetization which degrades the signal-to-noise of the experiment). Table 2.3 lists the types of information available using solid-state ^2H NMR methods.

2.3 Conclusion

Using carbon and deuterium NMR, it is possible to learn a great deal more about the structure and ordering of PPV. Examination of carbon line widths will indicate the degree of crystalline perfection within the PPV structure, and relaxation data will reveal any motional heterogeneities which may be present. Two-dimensional NMR results reveal the conformation of the PDMPV repeat unit.

Deuteron NMR will show how ordered the PPV chains are and these results will be compared with diffraction results and ir dichroism measurements. Deuteron NMR will also be shown to give information on molecular motions in the solid PPV lattice which go undetected using calorimetric or dynamic mechanical testing instrumentation. The specific molecular basis of various molecular motions will also be examined using carbon and deuteron NMR.

Table 2.1

Applicable Dopant for PPVs

Dopant	Type
AsF_5	p-type, vapor
$SbCl_5$	p-type, vapor
H_2SO_4	p-type, liquid
ClO_4^-	p-type, electrochemical
Na	n-type, vapor
K	n-type, vapor
Rb	n-type, vapor
Cs	n-type, vapor

Table 2.2

Information Available with ^{13}C NMR Methods

Information	Technique/Interaction
Chemical environment	Chemical shift tensor analysis Isotropic chemical shifts
Molecular distances	Spin-diffusion Dipolar mixing Nuclear Overhauser effect Rotational resonance
Molecular motions	Resonance coalescence Relaxation Two-dimensional techniques
Molecular ordering	Shift tensor analysis Dipolar interactions

Table 2.3

Information Available with ^{2}H NMR Methods

Information	Technique/Interaction
Chemical environment	Quadrupole coupling Line shape assymmetry
Molecular motion	Line shape analysis Quadrupole-echo attenuation Relaxation rates Relaxation anisotropy Two-dimensional methods
Molecular ordering	Line shape analysis Relaxation anisotropy

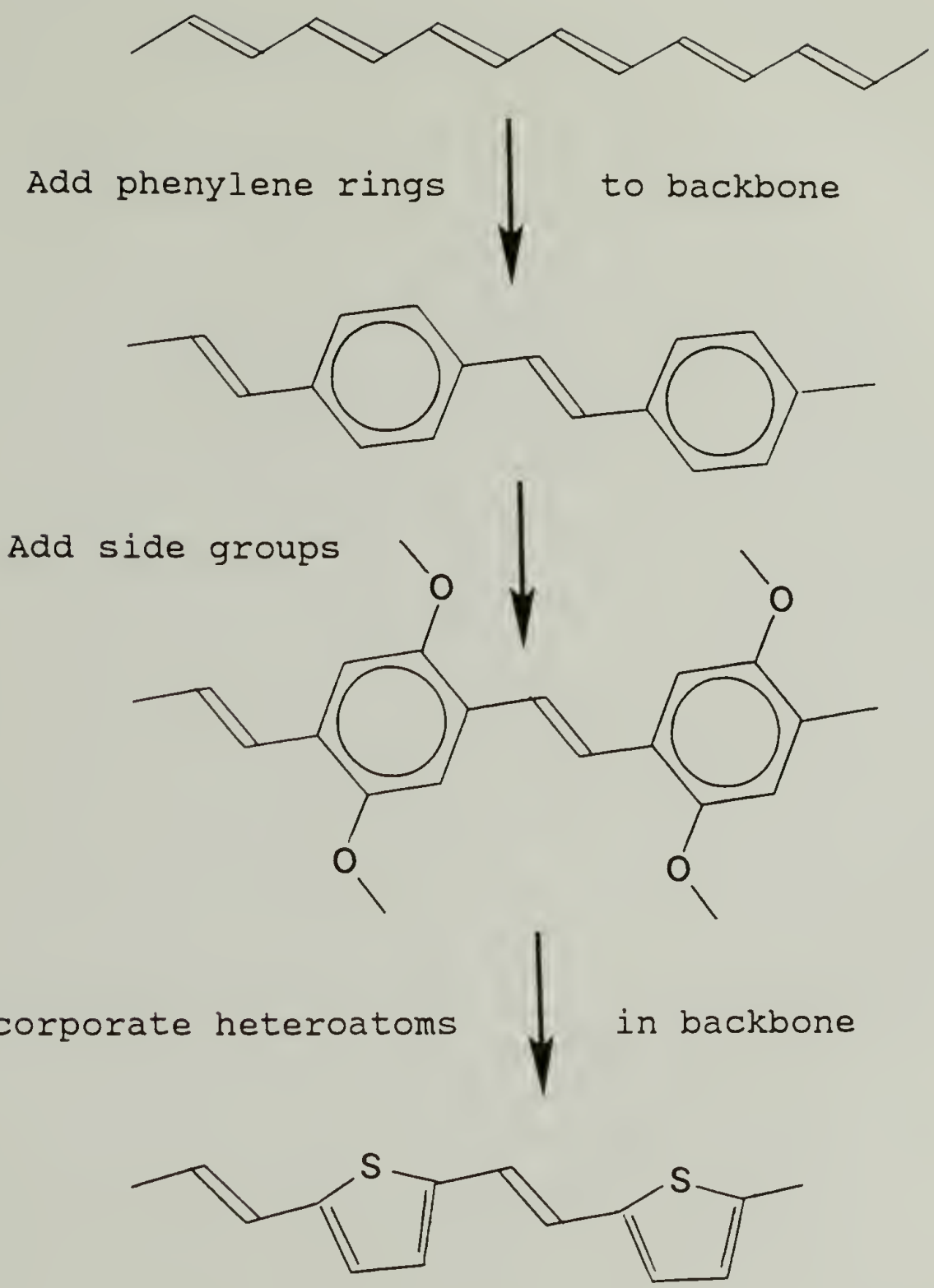

Also, oxidation and reduction, copolymers, blends, and various combinations of these.

Figure 2.1 Evolution of a conducting polymer.

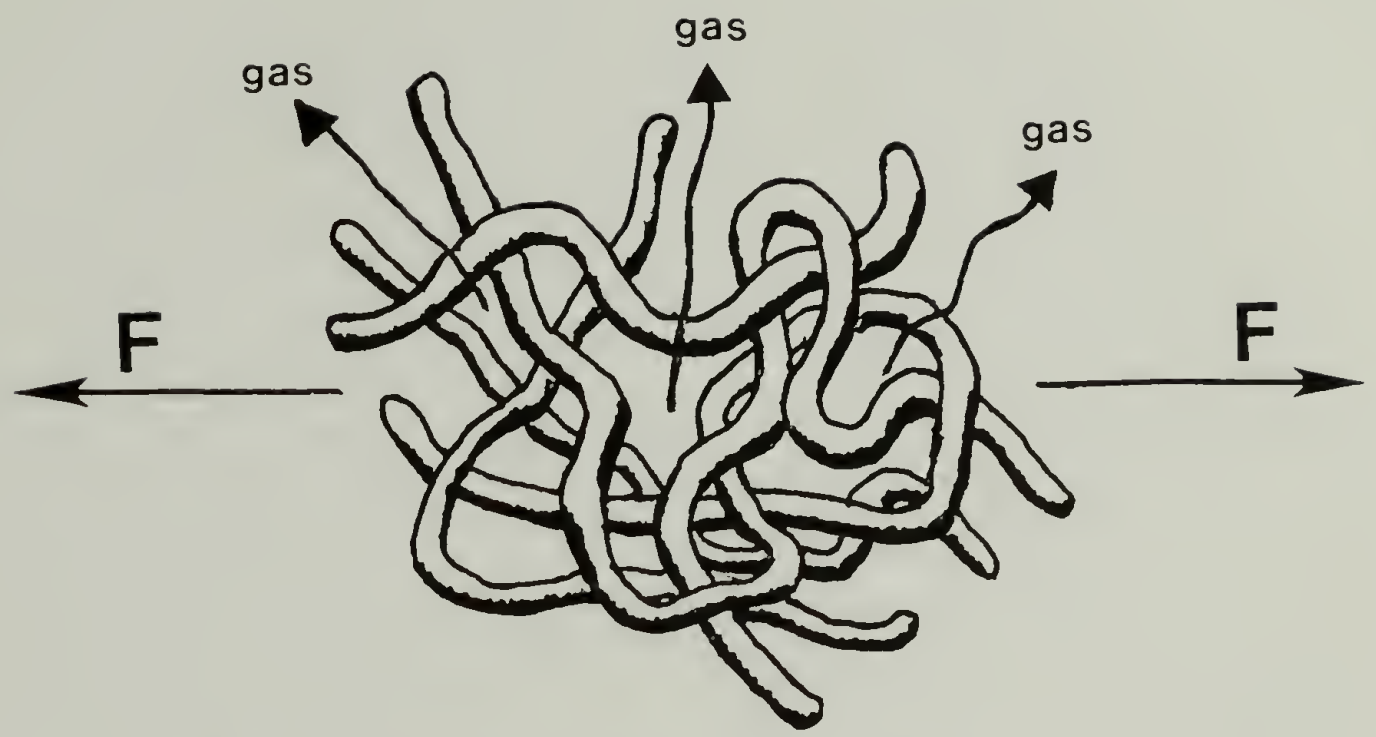

Figure 2.2 Elimination of volatile components from the polymer bulk allows the chains to slip past one another and become highly oriented under tension.

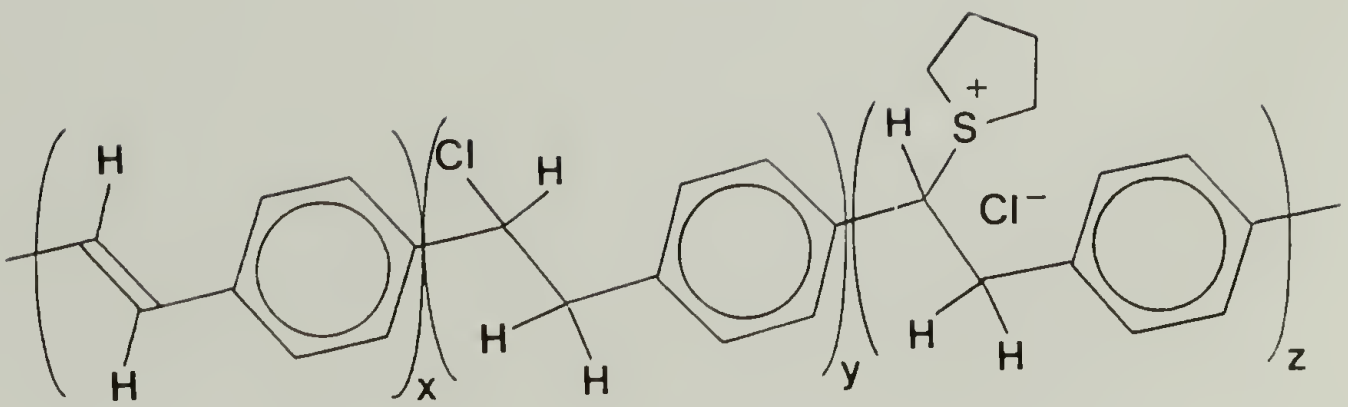

Figure 2.3 Copolymeric structure of partially eliminated PPV precursor polymer.

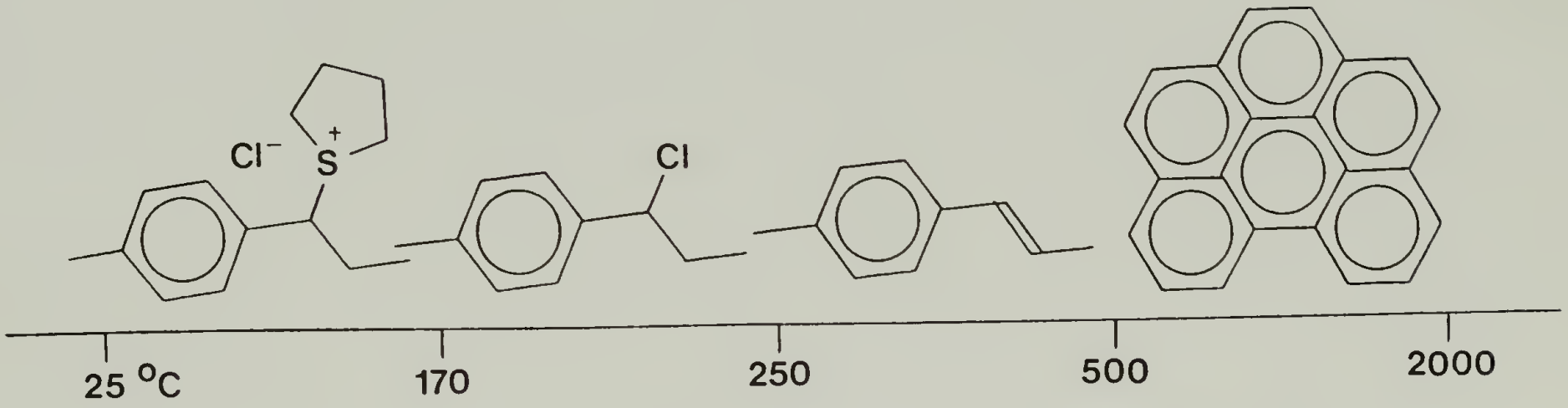

Figure 2.4 Thermal evolution of the PPV precursor polymer into PPV and beyond.

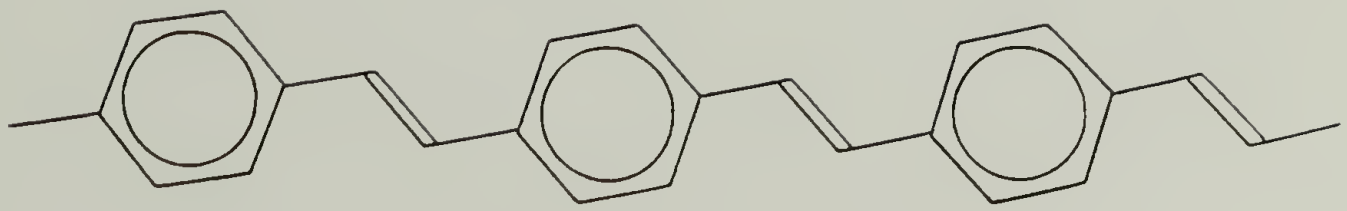

Figure 2.5 *Trans, transoid* structure of PPV repeat units.

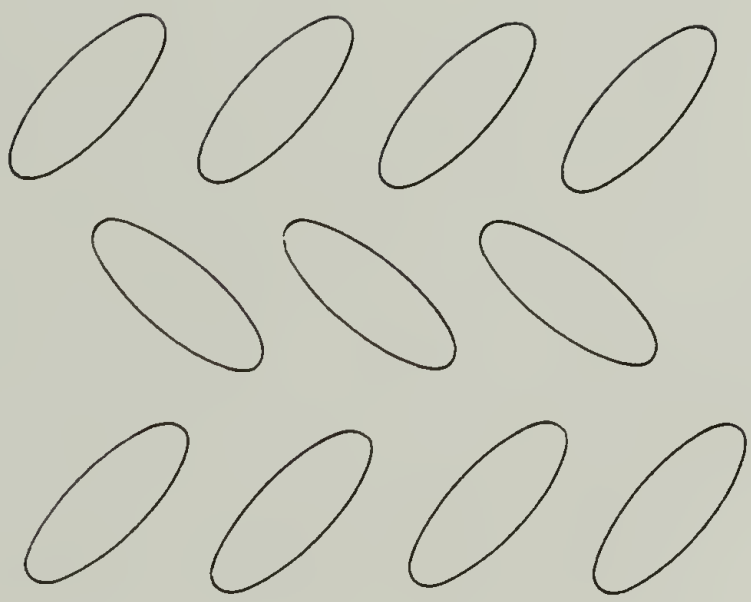

Figure 2.6 Herringbone packing arrangement of undoped PPV chains when viewed end-on.

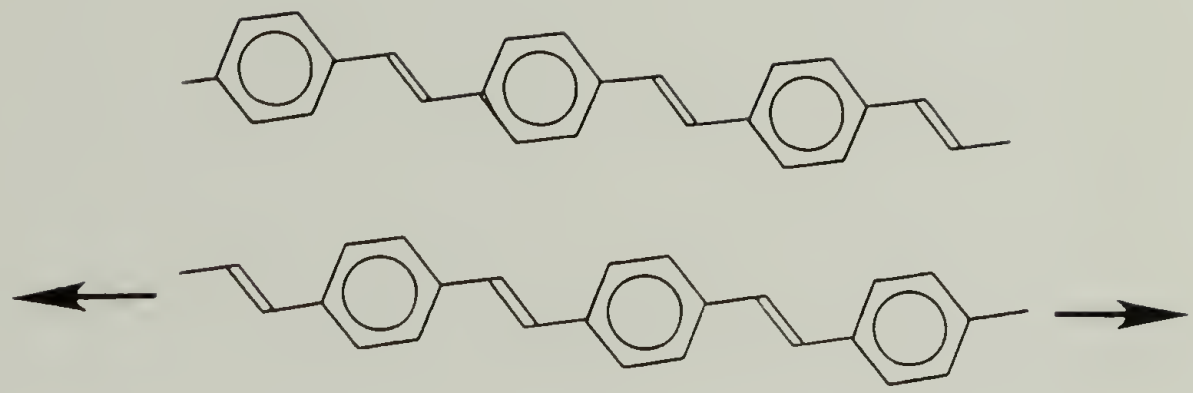

Figure 2.7 Axial (paracrystalline) disorder between adjacent chains in PPV.

CHAPTER 3

EXPERIMENTAL PROCEDURES

This chapter details the various laboratory procedures employed to acquire the data presented in this thesis. The first section focusses on the preparation of the PPV samples and the second deals with the spectroscopic methods employed in the analysis of these materials.

3.1 PPV Precursor Synthesis and Solution Preparation

Poly (*p*-phenylene vinylene) (PPV) films used in all of the work contained in this thesis were prepared via the precursor polymer route.[55,57,58] This pathway involves first polymerizing a monomer to form a precursor polymer (which is processable) and then heating (or annealing or eliminating) the polymer to form the desired polymer. The synthetic scheme used to make the monomer is shown in Figure 3.1 and the synthetic scheme used to make the precursor polymer, poly (*p*-xylylidene tetrahydrothiophenium chloride), from the monomer is shown in Figure 3.2. For preparing PPV deuterated at either the vinylene sites or at the phenylene ring sites, the procedure or starting material needs to be modified.

3.1.1 Preparation of Vinylene-Deuterated PPV (PPV-d_2)

To prepare vinylene labeled material, the undeuterated monomer is prepared exactly as in Figure 3.1 but for the polymerization reaction shown in Figure 3.2, the polymerization step is carried out in D_2O instead of H_2O. The labile benzyl protons of the monomer exchange with D_2O solvent to obtain full deuteration of the precursor polymer.[136,147] Thus the deuterons from the solvent exchange onto the aliphatic positions which eventually become the vinylene positions. Slow back-exchange occurs

during subsequent dialysis and film casting to achieve a net deuteration of the vinylene sites of 60% as determined by the method described in reference 148.

3.1.2 Preparation of Phenylene-Ring-Deuterated PPV (PPV-d_4)

To prepare the ring labeled material, the starting monomer must be deuterated. This means that there is an extra step in the synthesis because α,α'-dichloro-*p*-xylene-d_8 is not available commercially (recall that the vinylene protons exchange with the solvent during the polymerization step). As a result, perdeuterated *p*-xylene (*p*-xylene-d_{10}) must be chlorinated and isolated using the procedure shown in Figure 3.3.

To ensure that only the ring protons remained deuterated, the monomer was allowed to equilibrate 60 minutes in aqueous solution before addition of base (see Figure 3.2) to allow exchange of the methylene deuterons with protons, taking advantage of the well-known lability of the benzyl protons of benzyl sulfonium salts.[136]

The specificity of labeling of the precursor polymer was determined by ^{13}C NMR through observation of the ^{1}H-coupled spectrum in H_20/D_20 solution (90% v/v) using a Varian XL-300 spectrometer in the University of Massachusetts NMR Facility. Ring deuteration was determined to be greater than 95% through observation of the absence of a phenylene ring ^{13}C-^{1}H doublet. Methylene deuteration was determined to be less than 5% through observation of ^{13}C-^{1}H multiplets for the methylene carbons of the monomer and precursor polymer.

3.1.3 Precursor Polymer Purification

After preparing the precursor polymer, the precursor polymer solution was either dialyzed with distilled water or precipitated and washed to remove salt by-products. Dialysis of the precursor polymer solution was done using Spectro-por dialysis tubing with a molecular weight cutoff between 3500 and 10,000. Tubes of the precursor polymer solution were placed in a large beaker and the beaker was filled to the top with distilled water. The distilled water was typically changed three times in 24 hours.

Elemental analysis revealed that no residual sodium was present (< 0.1% by weight), indicating that the dialysis procedure employed was sufficient to remove the sodium chloride present in solution after polymerization.

One important difficulty associated with the above procedure is that the precursor polymer solution obtained via this procedure tends to be too dilute which renders it inappropriate for some subsequent film casting procedures which require concentrated solutions. That is, the resulting solutions take up a great deal of water inside the dialysis tubing due to osmotic pressure. Films cast from these dilute solutions tend to be too thin (< 10 μm). Using a great deal of a dilute solution causes the solvent evaporation step to take a prohibitve length time. As a result the PPV precursor polymer films are already partly eliminated by the time they are drawn and hence difficult to process.

An alternative procedure has been developed to circumvent the above problems. The PPV precursor polymer is precipitated from solution by adding an excess of cold (0 °C) isopropanol. The precipitate is collected with vacuum filtration and vigorously washed in a blender with a 3:1 isopropanol/water (v/v) solution repeatedly (typically five times) to remove the salt. The isopropanol/water solution is sufficient to swell the polymer but not to dissolve it. As a result, the solution is able to intimately mix with the PPV precursor polymer chains and wash out the salt but does not dissolve that chains and create a solution that is too dilute. If a solution of an exactly known concentration is desired, the precursor polymer is lastly washed with cold diethyl ether to remove the water and alcohol and then pumped on overnight at -20 °C. After this, the precursor polymer is a fluffy white solid with a slight yellow tinge (the more yellow, the more elimination has taken place). At this point the precipitate can be weighed out and added to distilled water or methanol to make a solution with an exactly known concentration.

If the exact concentration of the solution is not so important, the ether washing step can be omitted and the gelatinous solid can be made into a solution directly. One

difficulty associated with the dissolution step is that the rate of dissolution can be very slow. What happens is that a chunk of this material will absorb water on the outside and form a very viscous solution at the surface of the solid chunk of the precursor polymer. Simple mechanical stirring of the solution will not overcome this problem. It has been found that making up the solution in a blender is the only practical method known. Mastication of the chunks of precursor polymer greatly increases the surface area of the solid and allows concentrated solutions of the precursor polymer to be prepared in short amounts of time. Figure 3.4 summarizes the procedure for the precursor polymer washing, solution preparation.

3.1.4 Film Casting

Films of the precursor polymer are prepared in a variety of ways. One method entails pouring the solution onto a silanized glass surface (a glass surface that has been treated with dichlorodimethylsilane).[22] This procedure produces films which are not always homogeneous because the polymer does not adhere well to the silanized glass surface and tends to debond, disturbing nearby regions of the film which are not yet completely dry. Furthermore, this procedure is messy because of the dichlorodimethylsilane waste produced.

An alternative method method is to pour the solution out on a polymethylmethacrylate (PMMA or plexiglas) sheet. The adhesion of the precursor polymer to the PMMA surface will be sufficient so that debonding does not occur prematurely.

Film casting can be done in air, in an inert atmosphere such as argon or nitrogen or under vacuum. Casting in air introduces the problem of oxygen being incorporated into the films which may react and give undesirable properties (i.e. short conjugation lengths). Casting under vacuum can cause the films to adopt a porous morphology due to the volatization of solvent in the sample interior. While this procedure may be good

for the production of samples with very large surface areas, it is not appropriate for the production of dense, homogeneous films amenable to study with NMR because the maximum amount of sample must be packed into the space inside the coil.

Casting films under a dry nitrogen atmosphere on a PMMA sheet was determined to be the most reproducible and trouble-free method of film preparation. The author constructed a clear PMMA box for this operation in which the bottom piece of PMMA could be replaced as often as necessary. Scratching of the casting surface would prevent easy debonding of the precursor polymer film. When casting a film, it is important to remove it from the casting box as soon as it is dry and place it in a freezer. Failure to do so will allow the film to eliminate to such an extent that it will be difficult to process (draw) later.

If proper care is taken in following the above procedure, then a good quality film of PPV precursor polymer will be obtained. The film will be a light yellow in color and will have no cloudy or translucent regions. In addition, a micrometer will measure the same sample thickness throughout the entire film except near the edges where the film may be observed to be thicker. Casting a large area film (15 cm x 50 cm) is typical and can be conveniently trimmed to yield a film measuring 10 cm x 40 cm that is suitable for orientation. Typical film thicknesses obtained from solutions in the 1-5% range were 20-30 μm.

3.1.5 Film Orientation

There are two methods used to orient the PPV precursor films. One simply involves grasping two ends of a strip of the film and pulling on them as the film is placed on a heated teflon surface (a temperature of 125 °C was determined to be optimal).[20] It is important to do this step in a hood as the liberated tetrahydrothiophene has a powerful odor. By marking a region of film with ink graduations, the draw ratio

(the ratio the final sample length to the initial length) can be determined for the regions of homogeneous drawing (so the ends are not counted).

The other film drawing method involves mechanically passing the film over a heated roller (typical temperature of 125 °C) as described by Machado *et al.*[59] In this method, the takeup roller is adjusted to rotate at a faster rate than the feed roller (with the PPV precursor film wrapped on it). Precise control of the sample draw ratio is maintained using this technique. The only difficulty encountered using this technique occurred when the film to be drawn had already eliminated to such an extent that it was not able to become fully plasticized and would catastrophically fail under the large applied stress of the drawing apparatus. The hand-drawing procedure avoids this problem because the operator is able to determine (after a bit of practice) how much stress a film can handle. Table 3.1 lists the advantages and disadvantages of the two stretching methods.

3.2 PPV Film Annealing

After drawing, the film will contain polymer chains that are a random copolymer of three distinct repeat units as shown in Figure 2.3. At this point, the films are sandwiched between two pieces of teflon clamped between two pieces of aluminum to retain the shape of the film. The aluminum/teflon/film unit is placed in a vacuum oven or glass vessel and heated to 300 °C for at least four hours. This heating procedure can be done either under vacuum or in an argon atmosphere. The former method was employed in this work.

The specificity of labeling for the ring-deuterated PPV (PPV-d_4) following elimination was determined by solid-state ^{13}C CPMAS NMR through the use of interrupted decoupling methods.[148] These spectra will be shown below. The specificity of labeling was also examined by means of infrared spectroscopy, along with a study of

the chemistry of ^{1}H-^{2}H exchange during polymerization.[147] There is no observable scrambling of the ring label during elimination and annealing.

Elemental analysis determined that the optimal heating time was four hours and and optimal heating temperature was 300 °C. Table 3.2 shows the results obtained for samples annealed at a variety of temperatures for three or four hours. Heating the sample below 300 °C or for less than four hours was observed to yield samples that were incompletely eliminated. Samples still contained significant amounts of sulfur and chlorine when prepared with too low a temperature or too short an elimination time. Heating the samples above 300 °C was observed to degrade the samples and result in higher oxygen contents. Although these heatings were done on a vacuum line under high vacuum conditions, the glass elimination vessels were observed to be prone to leakage at the large o-ring connections necessary for sample introduction into the vessel. Higher temperature eliminations were observed to exacerbate this problem.

The PPV films prepared in this manner were yellow-orange in color and had excellent mechanical stability. Films were cut up and powdered using a Spex Industries Cryomill. The PPV powders prepared using the cryomill were ideal for packing evenly into magic-angle-spinning (MAS) rotors.

3.3 PDMPV Sample Preparation

For the PDMPV study, *p*-Dimethoxybenzene (DMB) was obtained from Aldrich Chemical and used without further purification. PDMPV films were prepared by Dr. G. Ruggeri according to a previously published procedure[149] and were ground into a powder using a cryomill (Spex Industries). Samples were run in 7 mm zirconia MAS rotors with Kel-F caps.

3.4 PPV Doping

Samples were doped with sulfuric acid and sodium metal. Sulfuric acid oxidizes the chains, removing an electron from them (p-doping). Sodium doping donates an

electron to the chains (n-doping). Sulfuric acid doping was accomplished by simply placing a clean PPV film in a solution of concentrated sulfuric acid for four hours as described by Masse.[22] After removal from the H_2SO_4, the film was washed with acetonitrile and placed in an evacuated chamber overnight. The resulting films had a blue, metallic luster.

Sodium doping was accomplished by sealing a sample of PPV film in an evacuated glass ampule with a chunk of sodium metal. The ampule was then placed in a glassware oven at 200-250 °C for two to seven days, depending on the degree of doping desired. This doping reaction was observed to proceed heterogeneously using the above procedure. First, the film would take on a bluish hue and then later it would take on a gold, metallic luster. Portions of the film closer to the sodium metal were observed to dope first, and portions far removed from the sodium were observed to doped slowly or not at all. In the limit of very long doping times, the film would develop an ashy, gray appearance that is assumed to be the result of overdoping (the incorporation of so much dopant into the PPV structure that chain scission is taking place and the morphology is drastically altered). Figure 3.5 shows the experimental configuration used to dope PPV with sodium.

The glass ampules containing the doped PPV were removed from the oven and placed in a glove box with an argon atmosphere for handling.

3.4.1 Dopant Uptake

To measure the amount of dopant incorporated in a sample, the mass uptake of the samples was determined by obtaining the mass of the film in a tared, sealed container before and after doping. After doping, the sample was kept in an inert (argon) atmosphere to prevent reaction with atmospheric oxygen or water vapor.

3.4.2 Conductivity Measurements

Conductivity measurements were carried out using the standard four contact geometry[19] and a Keithley Autoranging Multimeter. The doped films were affixed to the contact using low resistance graphite cement (E.F. Fullam #14820).

3.5 Handling of PPV Samples

3.5.1 Handling of Unoriented, Deuterated Samples for ^{2}H NMR

Unstretched PPV films were mechanically disordered by cutting into pieces or were ground into powders using a SPEX cryomill to remove any small orientation effects associated with film casting. The samples were sealed under vacuum in a 5 mm solids NMR tube (Wilmad 506-pp, cut to 4 cm length). Spectra from these samples are referred to as powder spectra.

3.5.2 Handling of Oriented, Deuterated Samples for ^{2}H NMR

Powder samples of stretched and unstretched PPV-d_4 were obtained by cutting films into pieces with dimensions of approximately 1 mm^2. The pieces were packed in a 5 mm solids NMR tube (Wilmad 506-PP cut to a 3 cm length).

Aligned samples were prepared from both stretched and unstretched PPV-d_4. Films (10 mm wide) were folded with folds perpendicular to the stretch axis and inserted into a 5 mm diameter rod containing a slot along its axis. Films were affixed to Kapton tape (CHR Industries) to preserve their structural integrity during folding. The folded edges were removed to leave an aligned stack of 5 mm x 10 mm films. The uncertainty of alignment was estimated at ±5° or less. The angle, Θ, between the stretching axis and the applied field was varied by rotating the film holder about its long axis in the NMR coil, an axis perpendicular to the NMR magnetic field. Figure 3.6 shows the geometry of the PPV sample holder and its relation to the NMR coil and applied magnetic field $\mathbf{B}_0$.

3.6 ^{13}C NMR Methods

3.6.1 One-Dimensional ^{13}C NMR Methods

^{13}C cross-polarization magic-angle spinning (CPMAS) NMR spectra were obtained at 75 MHz with a Bruker MSL-300 NMR spectrometer and at 50 MHz with an IBM AF-200 NMR spectrometer. The spinning rate was 4500 or 3000 Hz, respectively. The 90° pulse width was 6.0 μs at 50 MHz and 3.5 μs at 75 MHz. Chemical shifts are reported relative to the chemical shift of tetramethylsilane (TMS). The interrupted decoupling spectra[148] contained a 100 μs delay between cross-polarization and proton decoupling to cause irreversible defocusing of the protonated carbon resonances. The FID was acquired with a spectral width of 20 kHz with quadrature detection. 10^4 scans were averaged to obtain good S/N. The FID was 2048 points long and was zero padded to a total size of 4096 points. The recycle time between scans was 3 s. Figure 3.7 shows a schematic diagram of the CPMAS pulse sequence.

Samples were spun as films or powders and were either cut into 1 x 10 mm strips, were wrapped concentrically in the magic-angle rotor, or were ground into a fine powder with a SPEX cryomill.

Simulation of ^{13}C line shapes was carried out with Lorentzian line-fitting software supplied with the MSL-300.[150]

3.6.2 Two-Dimensional ^{13}C NMR Methods

3.6.2.1 Two-Dimensional Data Acquisition

Spectra were obtained using a Bruker MSL-300 NMR Spectrometer (^1H, 300 MHz; ^{13}C, 75 MHz) under conditions of MAS. Spinning rates of 4.00 kHz for DMB and 3.66 kHz for PDMPV were set to avoid sideband overlap. The ^1H 90° pulse was 4.0 μs and the ^{13}C 90° pulse was 4.5 μs. The pulse sequence used to acquire the data is schematically shown in Figure 3.8. During the ^1H evolution period, 0-63 cycles of the multiple pulse ^1H decoupling sequence, BLEW-12,[151] were applied in the ^1H channel to suppress ^1H-^1H dipolar interaction. BB-12 ^{13}C decoupling[152] was applied synchronously

with BLEW-12 to suppress ^{13}C-^{1}H dipolar interaction. During this time only ^{1}H chemical shift evolution remained, with an experimental chemical shift scaling factor of 0.41. During the mixing period the ^{1}H magnetization was aligned along the **z** axis, allowing ^{1}H-^{1}H dipolar interaction to take place. The magnetization was then rotated by 90° to the x-y plane and the multiple-pulse, WIM-24 cross-polarization[153] was applied to transfer ^{1}H magnetization to nearby ^{13}C nuclei without the effects of further ^{1}H-^{1}H interactions. All 64 ^{13}C spectra were obtained with single-frequency ^{1}H decoupling (1024 data points were collected in quadrature with a spectral width of 22.7 kHz). Spin lattice relaxation was negligible during the mixing period and was neglected in the modeling of the dipolar interaction. For DMB, 16 scans per slice were sufficient. For PDMPV, the broader resonances required 1024 scans per slice.

3.6.2.2 Two-Dimensional Data Analysis

2D spectra were processed on the ASPECT 3000 computer of the MSL-300 spectrometer. The data was zero-filled in the ^{1}H dimension to a matrix size of 1024x1024. 64 Fourier transforms were applied in the ^{13}C dimension with exponential multiplication and a Lorentzian line broadening of 50 Hz. The ^{13}C rows were weighted with a 90° phase-shifted sine-bell before the transform in the ^{1}H dimension. Specific columns of the data matrix corresponding to the individual ^{13}C resonances were extracted and deconvoluted into their parent ^{1}H chemical shift components using a Lorentzian-Gaussian line shape simulation program.[154]

Curve-fitting of intensities was carried out with a FORTRAN program using the simplex algorithm[155] to minimize the sum of the squares of the residuals. The uncertainties of the determined rates were determined by evaluating the second derivative of χ^2 as a function of the parameters.[156]

3.7 ^{2}H NMR Methods

There are two types of deuterium NMR experiments that were performed in the completion of this work. One involved using the conventional quadrupole echo pulse sequence to obtain information about molecular motion and orientation and the other entails using an inversion-recovery pulse sequence to reveal the anisotropic nature of relaxations taking place.

3.7.1 Quadrupole-Echo ^{2}H NMR Measurements

^{2}H quadrupole echo NMR spectra[113] were acquired at 46 MHz using a Bruker MSL-300 NMR spectrometer with a 5mm insert in the HP probe. 90° pulses were 2.3 μs in duration and were spaced by 20 μs to allow for transient decay. Acquisition of the free induction decay (FID) was begun approximately 3.2 μs prior to the echo maximum; the accumulated average of all the scans was later left shifted to the echo maximum before Fourier transformation. Figure 3.9 shows the quadrupole-echo pulse sequence. The pulse sequence employed an eight-member phase cycle to minimize instrumental artifacts. A spectral width of 2.5 MHz (an A/D rate of 5 MHz) was used. For a typical acquisition, 1024 scans of 2048 points were averaged together. Prior to Fourier transforming, the FIDs were zero padded to a total size of 4096 points and exponentially multiplied with a Lorentzian line broadening of 4 kHz. The equilibrium recycle delay was determined by progressive saturation methods[140] using the echo height; the equilibrium delay was 60 s at -58 °C, 20 s at 25 °C, and 2 s at 225 °C.

3.7.2 Inversion-Recovery, Quadrupole-Echo ^{2}H NMR Measurements

The ^{2}H spin lattice relaxation was measured with a three-pulse inversion recovery quadrupole echo.[115,140] For this pulse sequence, a 180° pulse was followed by a time delay, DE for inversion recovery. The intensity after the delay was sampled by a two-pulse quadrupole echo sequence. Figure 3.10 shows the inversion-recovery quadrupole-echo pulse sequence. T_1 was measured from the echo height. Partially

relaxed spectra are obtained to characterize the T_1 anisotropy. The T_1 anisotropy is defined as the frequency dependence of T_1 in the powder spectrum of the unoriented sample and is most easily seen at the null point (where the spectrum integral passes through zero intensity).

3.7.3 Simulation of ^2H NMR Line Shapes

Theoretical ^2H lineshapes for various jump models are calculated using a specially written program which makes use of the method of Wittebort *et al.*[157] to calculate the effects of intermediate exchange and the method of planar moments to calculate the effects of film orientation.[137,138]

3.7.3.1 Calculation of Powder ^2H Line Shapes

Powder spectra, in the absence of motion, are described by a quadrupole splitting and the asymmetry parameter. For the phenylene ring, these parameters are related to the three principal axis quadrupole tensor components ν_{zz} (aligned with the C-D bond), ν_{yy} (perpendicular to the ring), and ν_{xx}.

The ring flip motion of the *p*-phenylene group of PPV-d_4 was modeled as a two site exchange. The inclinations of the two sites with respect to the crystallographic **c** axis were taken as 67.7° and 52.3°. The simulated spectra appearing in the figures in chapters 5 and 6 are modeled as a weighted sum of individual spectra of varying flip rates. The width of the distribution of flip rates for the observed spectra is determined by comparing the change in normalized quadrupole echo height with the calculated echo height for various sums of simulated spectra.[139] In all cases the distribution of the logarithm of flip rates is modeled as a Gaussian.[158] Chain motion at elevated temperatures was analyzed according to two possible mechanisms: either a 180° jump or small angle diffusion, as described in chapter 7.

For jump motions, the theoretical line shape calculation includes the effect of anisotropic T_2 relaxation during the quadrupole echo. These echo distortions occur when

the jump rate k is approximately equal to $\Delta\nu_Q$, and the simulations are also corrected for the effect of finite pulsewidths.[104,140,158] Simulations are obtained for a log-Gaussian distribution of jump rates by superposition of spectra for different jump rates.

$$P(\log(k)) = \exp - \{[\log(k) - \log(k_m)] / \Delta\log(k)\}^2 \qquad (3.1)$$

where $P(\log(k))$ is the probability, $\log(k_m)$ is the logarithm of the median jump rate, and $\Delta\log(k)$ is the width of the distribution.[137,140] The changes in the quadrupole splitting and the asymmetry parameter with temperature are described by analytical integration of the quadrupole coupling parameters for fast small-angle rotation of the phenylene ring within a square-well potential about the 1,4 ring axis.

Partially relaxed ^2H lineshapes resulting from the inversion recovery quadrupole echo pulse sequence were calculated with the method of Torchia and Szabo[159] as described by Wittebort *et al.*[157] The anisotropy of the spin lattice relaxation time, T_1, is related to the spectral density functions J_1 and J_2 as follows:

$$1/T_1(\beta,\alpha) = (3/8)\nu_{zz}[J_1(\omega_0,\beta,\alpha) + 4J_2(2\omega_0,\beta,\alpha)] \qquad (3.2)$$

$$J_m(\omega_0,\alpha,\beta) = \sum_{a,a'=-2}^{2} d_{ma}^{(2)}(\beta)\, d_{ma'}^{(2)}(\beta)\, d_{0a}^{(2)}(\beta_0)\, d_{0a'}^{(2)}(\beta_0)\, J_{aa'}(\omega_0) \qquad (3.3)$$

where m = 1, 2 and the values of $d_{aa'}^{(2)}$ are second rank rotation matrix elements. For calculation of T_1, the axial asymmetry of the C-D bond quadrupole coupling is neglected. The anisotropy of T_1 for a particular mechanism is determined by the spectral density functions $J_{aa'}(\omega_0)$. For the two site jump model:

$$J_{aa'}(\omega_0) = (1/4) \sum_{l,j=1}^{2} (-1)^l(-1)^k \cos[a_l\Phi + a_j'\Phi]\, [\tau_c/(1+\omega_0^2\tau_c^2)] \qquad (3.4)$$

where $\beta_0 = 71.7°$, Φ_l, Φ_j = a + 0° or a + 180°. The spectrometer frequency in radians is ω_0, $\tau_c = 1/2k$, the jump correlation time (an experimental parameter), and k is the jump rate. Equations 3.2-3.4 result from equations 3.21 and 3.22 of Wittebort *et al.*[157] for the

case of two site exchange with equal populations. For the diffusion model:[104,141]

$$J_{aa'}(\omega_0) = \sum_{n=1}^{N} aa'\Phi^2 \frac{[\cos(a\Phi)\cos(a'\Phi)(1-(-1)^n)+\sin(a\Phi)\sin(a'\Phi)(1+(-1)^n)]}{[(a\Phi)^2+(n\pi/2)^2]\,[(a\Phi)^2+(n\pi/2)^2]}$$

$$\cdot \cos((a+a')a)\,[\tau_n/(1+\omega_0^2\tau_n^2)] \qquad (3.5)$$

where $\Phi = 38°x(2\pi/360°)$ and N = 20. Equation 3.5 results from the analytical solution of the diffusion equation within a square-well potential with boundaries at $\pm\Phi$ and is the spectral density function which corresponds to the correlation function shown in Equations 3.12a to 3.12c of reference 141. For equation 3.5 each term of the summation depends upon a correlation time $\tau_n = Dn^2\pi^2/4\Phi^2$ where D is the rotational diffusion constant, an experimental parameter. During the powder average over α and β each subspectrum was scaled by the factor $(1-2e^{DE/T_1})$ where DE is the delay for inversion recovery.

3.7.3.2 Calculation of Line Shapes for Oriented PPV

Figure 3.11 describes the coordinate systems used to represent oriented PPV. The ^2H splitting, $\Delta\nu$, is a function of the normalized cartesian coordinates of the magnetic field vector, $\mathbf{B}_0$, in the principal axis system (PAS, Figure 3.11) of the C-D bond:[160]

$$\Delta\nu = \nu_{xx}\mathbf{B}_x^2 + \nu_{yy}\mathbf{B}_y^2 + \nu_{zz}\mathbf{B}_y^2 \qquad (3.6)$$

where ν_{xx}, ν_{yy}, ν_{zz} are the principal axis quadrupole splittings (tensor components) and $\mathbf{B}_x$, $\mathbf{B}_y$ and $\mathbf{B}_z$ are the normalized cartesian coordinates of $\mathbf{B}_0$ in the principal axis system. The principal axes for the rigid lattice C-D bond are **z** along the C-D bond, y perpendicular to the ring plane. The average principal axes for a phenylene ring undergoing fast rotational jumps are **z** along the ring axis, y perpendicular to the ring plane. Equation (3.6), when expressed in spherical coordinates, has the form[138]

$$\Delta\nu = \Delta\nu_Q\,[(3\cos^2\Theta - 1) - \eta\sin^2\Theta\cos 2\Phi] \qquad (3.7)$$

where Θ and Φ are the spherical coordinates for $\mathbf{B}_0$, $\Delta\nu_Q = \nu_{zz}/2$, the quadrupolar splitting, and $\eta = (\nu_{yy}-\nu_{xx})/\nu_{zz}$, the asymmetry parameter. The definitions of the

principal axes are reordered such that $\nu_{xx} < \nu_{yy} < \nu_{zz}$. Values of $\Delta\nu_Q$ and η are included only for reference. Calculations are based upon Equation (3.6), which includes no assumption about the relative magnitudes of ν_{xx} and ν_{yy}.

Values of $\mathbf{B}_x$, $\mathbf{B}_y$ and $\mathbf{B}_z$ in Equation (3.6) were calculated by rotating the normalized value of $\mathbf{B}_0$ in the laboratory (LAB, Figure 3.11) frame of reference (0,0,1) through three rotation matrix transformations, $\underline{\underline{\mathbf{R}}}_1$, $\underline{\underline{\mathbf{R}}}_2$ and $\underline{\underline{\mathbf{R}}}_3$ about axes of the C-D bond PAS coordinates (Figure 3.11). The transformation $\underline{\underline{\mathbf{R}}}_1(\alpha_0,\beta_0,\gamma_0)$ relates the PAS coordinates to a coordinate system fixed in the PPV chain (CHAIN, z axis along the chain axis; y axis perpendicular to the ring plane, $\alpha_0 = 0$, $\beta_0 = 60° \pm \Psi$ and $\gamma_0 = 0°$ or 180°). The value of Ψ, the phenylene ring tilt, is an experimental parameter, determined by simulation.

Best-fit simulations were found through an automatic search of the parameters through calculation of least squares. The uncertainties for each simulation parameter were determined both from statistical analysis and by visual inspection to assess the accuracy of the fit.

The transformation $\underline{\underline{\mathbf{R}}}_2(\alpha,\beta,\gamma)$ relates the CHAIN coordinate system to a coordinate system fixed in the PPV film (FILM, z axis along the stretch axis, y axis in the film plane, $\alpha = 0°$ to 360°, $\beta = 0°$ to 180° and $\gamma = 0°$ to 360°). A powder average over α, β and γ was performed using an appropriate chain orientation distribution as described in the chapter 8. The transformation $\underline{\underline{\mathbf{R}}}_3(\Theta)$ relates the FILM coordinate system to the LAB coordinate system and the angle Θ is an experimental parameter, the angle between the stretching axis of the film and $\mathbf{B}_0$.

A value of the Hermans orientation function[161], $f = \langle 3/2\cos\beta - 1/2 \rangle$, was also calculated from the best-fit orientation distribution by numerical integration. The orientation functions obtained by NMR were compared to those previously obtained from the measurement of the infrared dichroism of similarly stretched, protonated films.[61]

For the simulation of the line shapes obtained from vinylene deuterated material (PPV-d_2, chapter 7), the angles and orientation functions used in the calculation of the oriented PPV-d_2 spectra are similar to those used for simulation of the ^2H spectra of PPV-d_4 (deuterated at the phenylene ring positions). The observed splitting, $\Delta\nu$, is determined by the coordinates of the magnetic field vector, $\mathbf{B}_0$ in the principal axis system (PAS) of the C-D bond and the principal axis tensor components, ν_{xx}, ν_{yy}, ν_{zz}. The C-D bond PAS is related to the chain axis system (or unit cell **c** axis) by a rotational transformation about three Euler angles: $\underline{\underline{R}}_1(\alpha_0,\beta_0,\gamma_0)$. Both C-D bonds of PPV should have the same inclination, β_0, to the chain axis as they are related by an inversion center (see Figure 3.2 and 7.1, $b_0 = 72.3°$ for a *trans*-stilbene-like geometry).[81,82,162] The spectra of chapter 8 indicate that there is a 1.5° tilt or disorder of the chain direction relative to the **c** axis of the unit cell. This tilt is predicted to also affect the vinylene groups and lead to $\beta_0 = 71.7°$, $\alpha_0 = 0°$, $\gamma_0 = 0°$ (or 0° and 180° for chain jumps). The chain axis system is related to the stretching axis of the film through the transformation $\underline{\underline{R}}_2(\alpha,\beta,\gamma)$. For oriented films the film stretching axis was related to the laboratory axis system through $\underline{\underline{R}}_3(\Theta)$, where Θ is the angle between the film stretch-axis and the magnetic field, an experimental parameter.

3.8 Electron Microscopy Methods

Dark-field (DF) transmission electron microscopy (TEM) was used to directly observe the crystallites in PPV films. Microscopy was performed using a JEOL 100 CX instrument operated at 100 keV. Dark-field images were formed using a JEOL 100 CX operated at 100 keV with the combined equatorial reflection $g(_{100/200})$. The diffracted beam was passed to the image plane through a 20 μm objective aperture, limiting the diffracted beam to image a full angular breadth of 4 mrad. Images were collected on Kodak SO-163 electron microscope film and the latent images were developed using

full-strength Kodak D-19 developed for 10 minutes. The average crystallite size was determined from measurement of 40-50 crystallites in each micrograph.

Table 3.1

Pros and Cons of Hand Versus Machine Stretching

Method	Pros	Cons
Hand	Can process small amounts Simple and cheap to do Does not break film	Not always reproducible Sample necking occurs Not a continuous process
Machine	Continuous process Excellent reproducibility	Breaks partially-eliminated films Requires large amount of film

Table 3.2

Elemental Analysis Results for PPV Elimination

Temp	Time	C	H	Cl	S	O	Total
200 °C	3 h.	83.94	5.80	10.32	0.23	<0.1	100.39
250 °C	3 h.	86.38	5.97	7.73	0.32	<0.1	100.40
300 °C	3 h.	85.33	6.12	5.25	0.37	0.3	97.07
350 °C	3 h.	89.68	5.96	4.13	0.37	<0.1	100.14
200 °C	4 h.	88.72	5.82	3.37	0.10	1.0	99.01
250 °C	4 h.	92.48	5.92	0.96	0.10	0.4	99.93
300 °C	4 h.	92.46	5.89	0.84	0.06	0.4	99.61
350 °C	4 h.	92.57	5.93	1.19	0.17	0.2	100.03

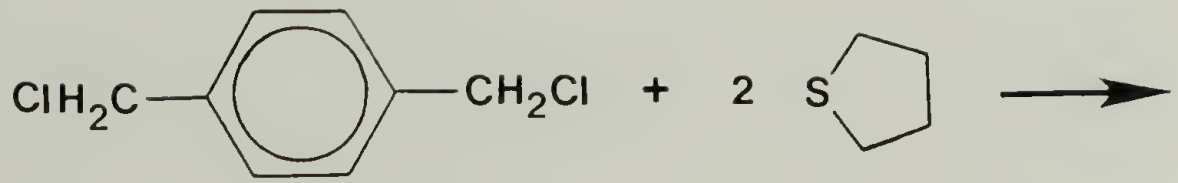

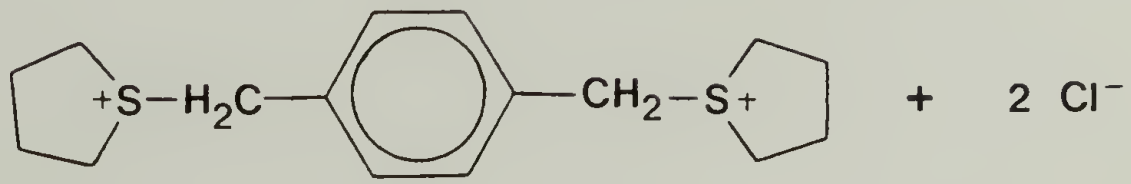

Figure 3.1 Monomer synthesis for PPV.

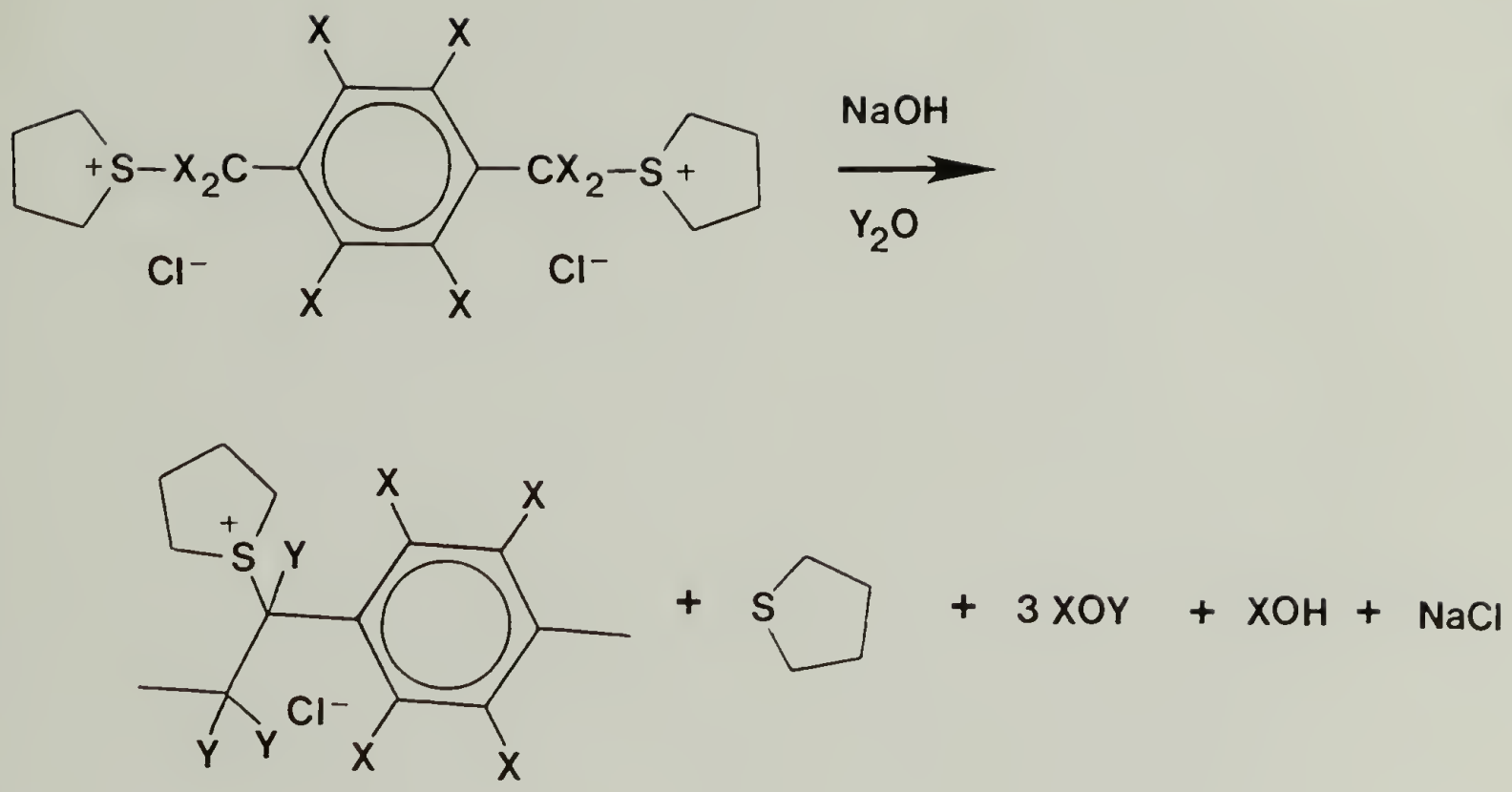

for PPV-d_0 X,Y = H

PPV-d_2 X = H, Y = D

PPV-d_4 X = D, Y = H

Figure 3.2 PPV precursor polymer synthesis.

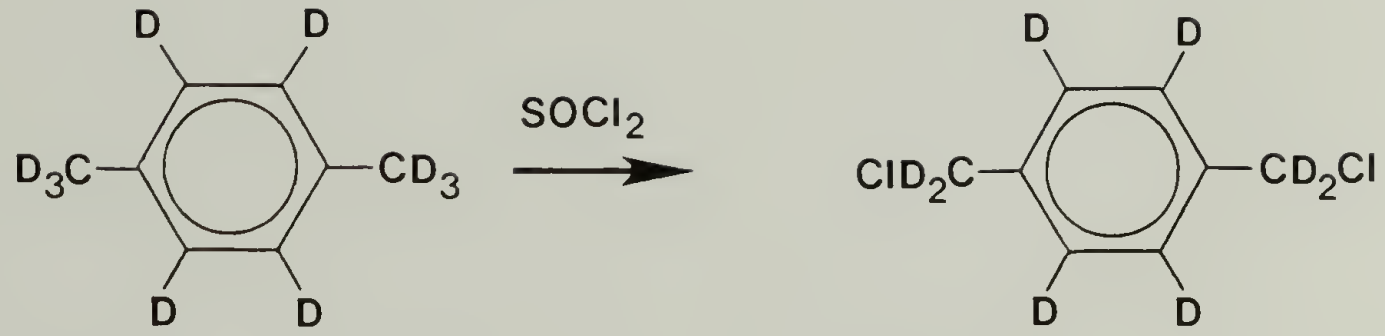

Figure 3.3 Synthesis of α,α'-dichloro-*p*-xylene-d_8 required for synthesis of ring-deuterated PPV (PPV-d_4).

1. Add an excess of cold isopropanol to polymer in aqueous solution to precipitate it. Collect by vacuum filtration.

2. Put precipitate in a blender, add enough isopropanol/water (3:1 v/v mixt.) to cover, blend vigorously.

3. Remove solutions by vacuum filtration.

4. Repeat steps 2 and 3 four more times.

5. Blend precipitate with pure isopropanol.

6. Remove isopropanol with vacuum filtration.

7. Pour diethyl ether through polymer (still in funnel) to remove water.

8. Pull vacuum on precipitate at -20 °C for 12 h.

9. Weigh out dry polymer, place in clean blender.

10. Add distilled water or methanol to blender in proper amount for concentration desired. Blend vigorously.

11. Degas solution and pour out on PMMA sheet with a dry nitrogen purge.

12. When film is dry (about 24 h.), peel off PMMA and refrigerate in freezer until ready to draw.

Figure 3.4 PPV precursor polymer washing and solution preparation procedure.

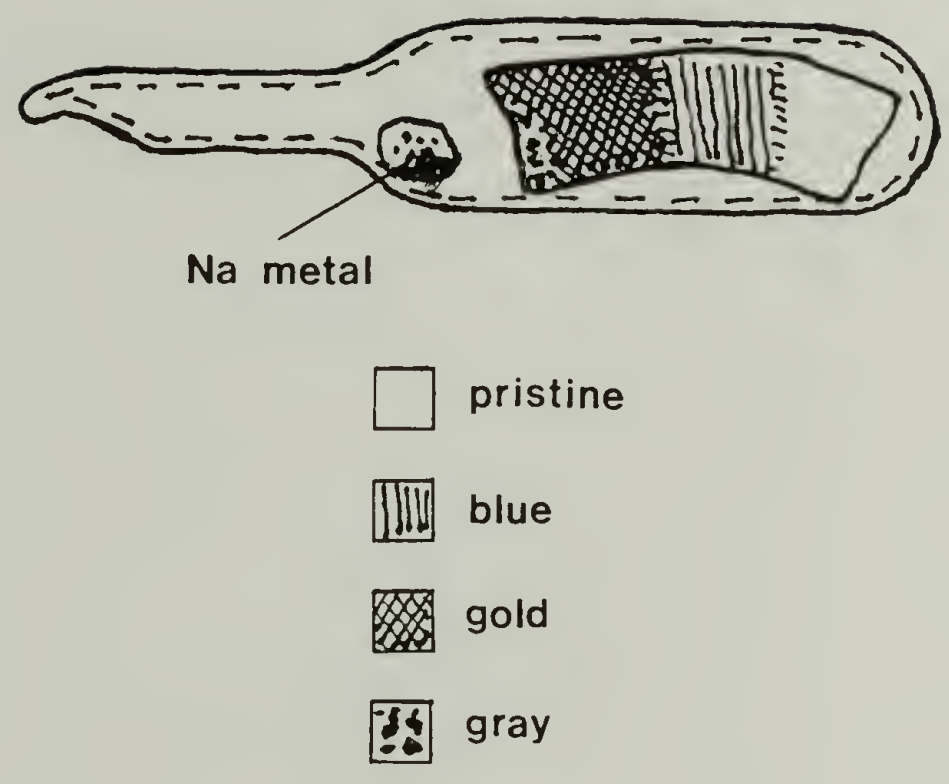

Figure 3.5 Geometry of the sodium-doping vessel.

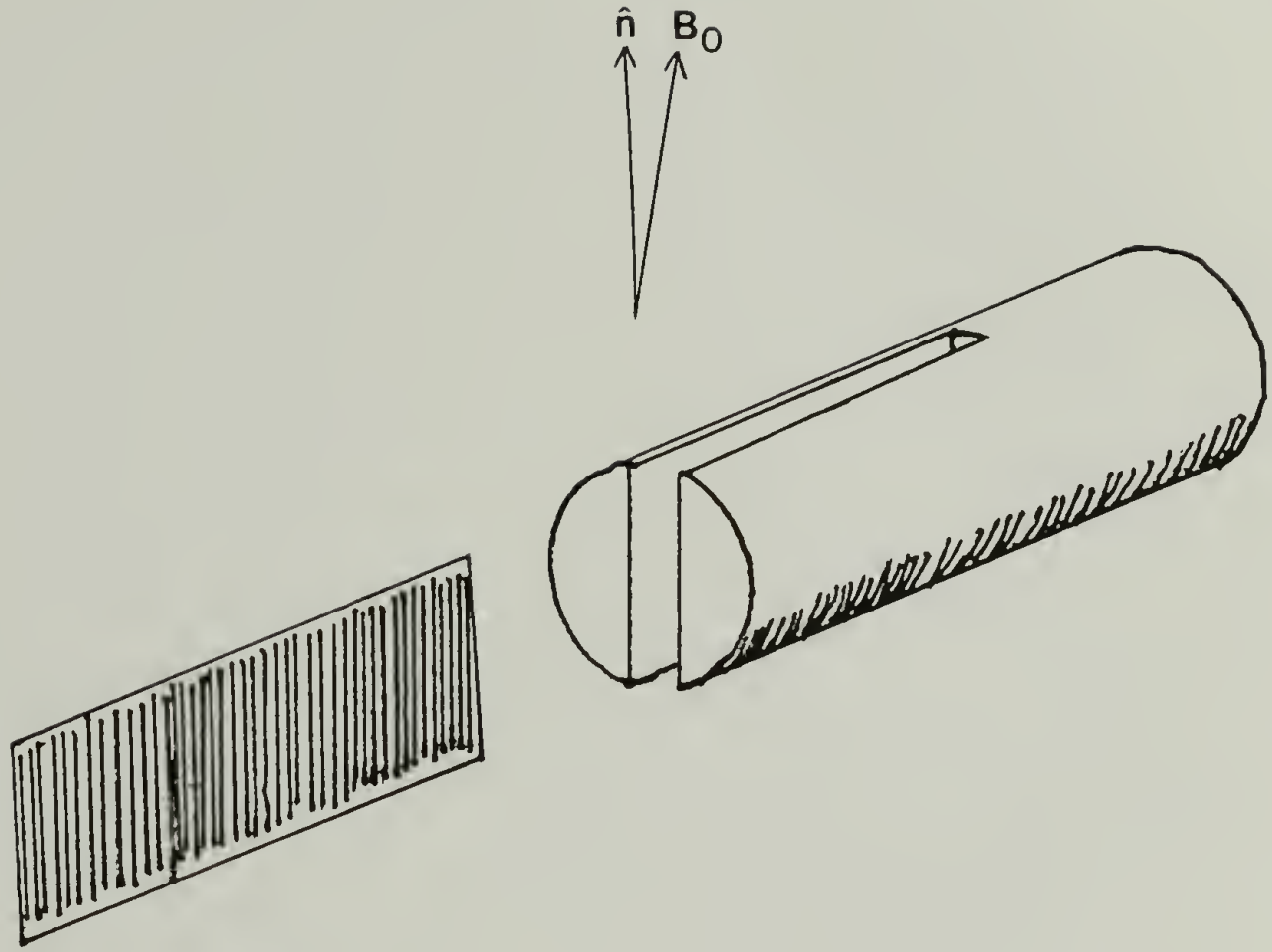

Figure 3.6 Geometry of the oriented-film clip for ^2H NMR.

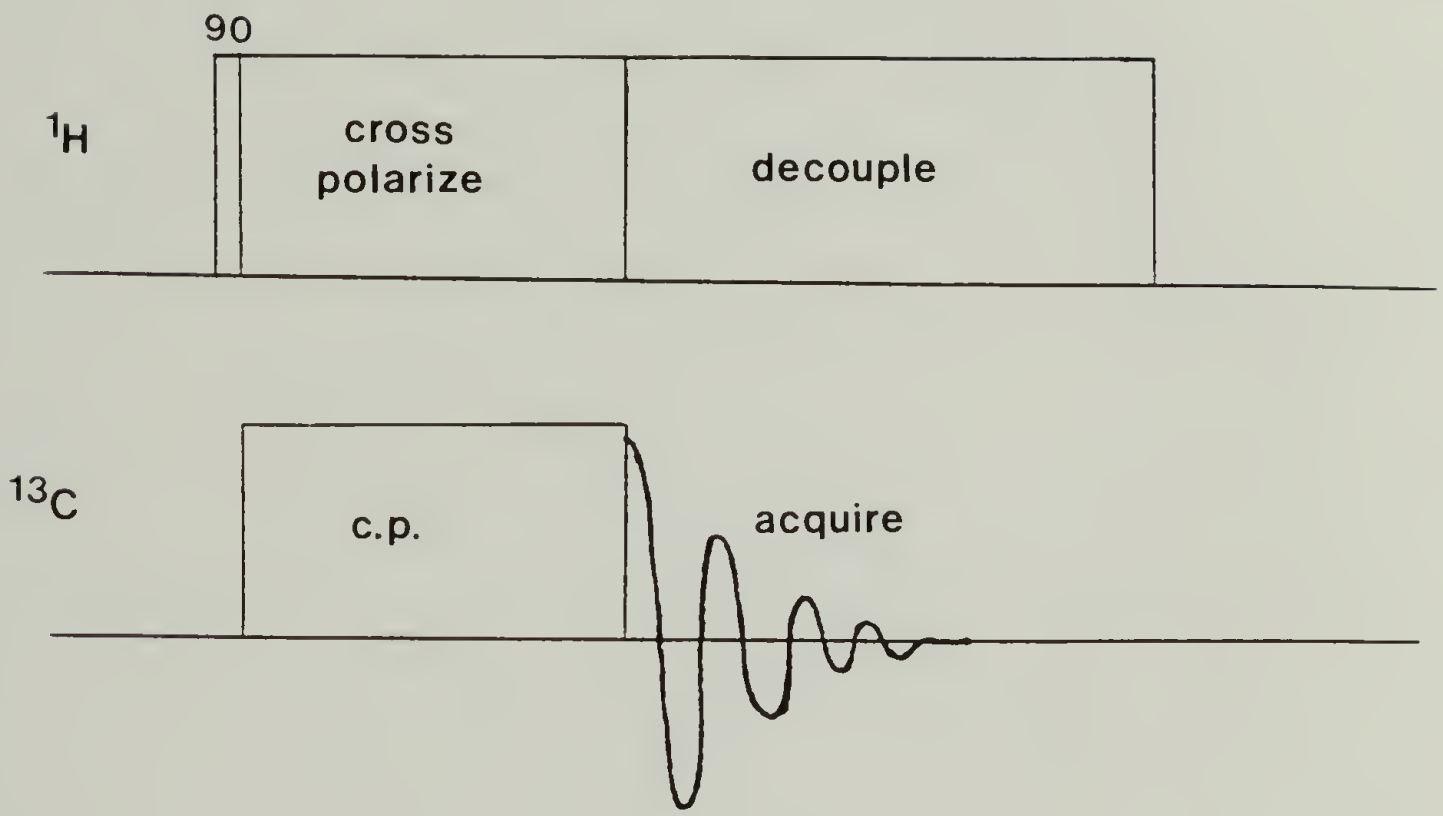

Figure 3.7 Cross-polarization, magic-angle-spinning (CPMAS) ^{13}C NMR pulse sequence.

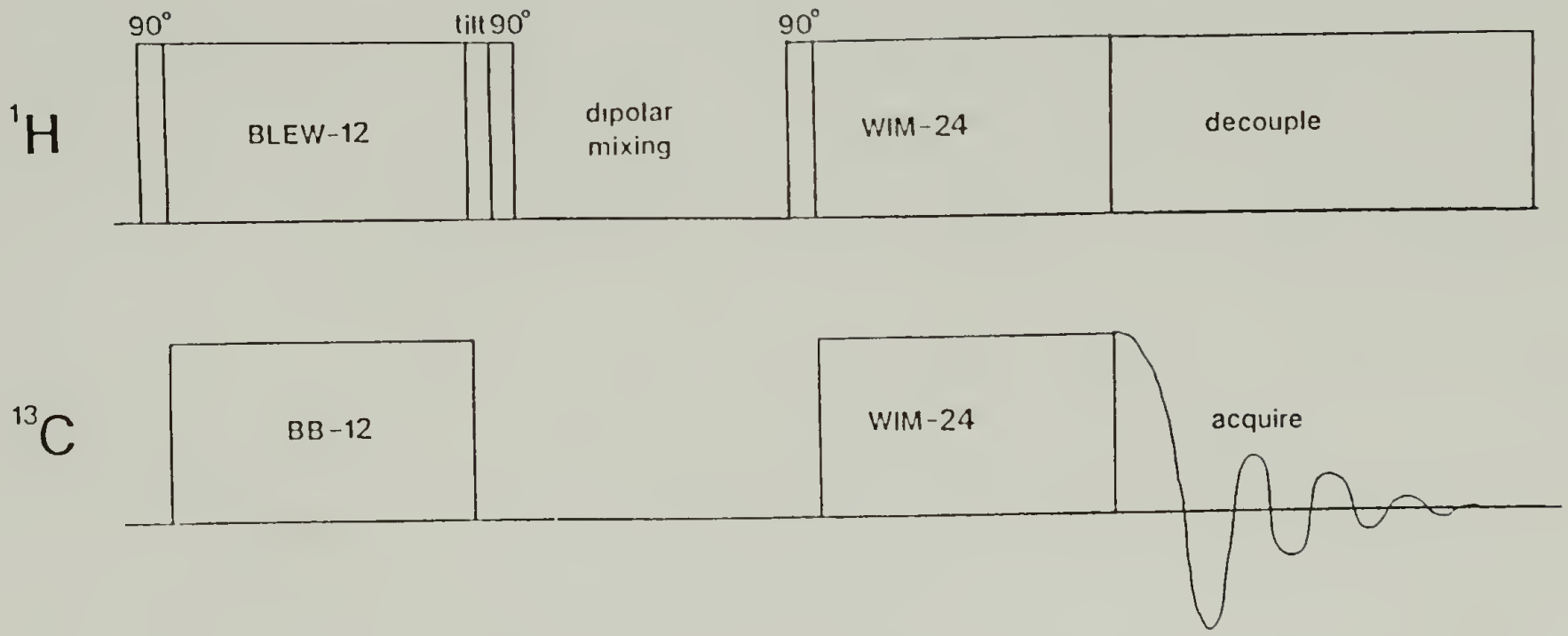

Figure 3.8 Two-dimensional, CPMAS, ^{1}H-^{13}C heteronuclear-correlation pulse sequence

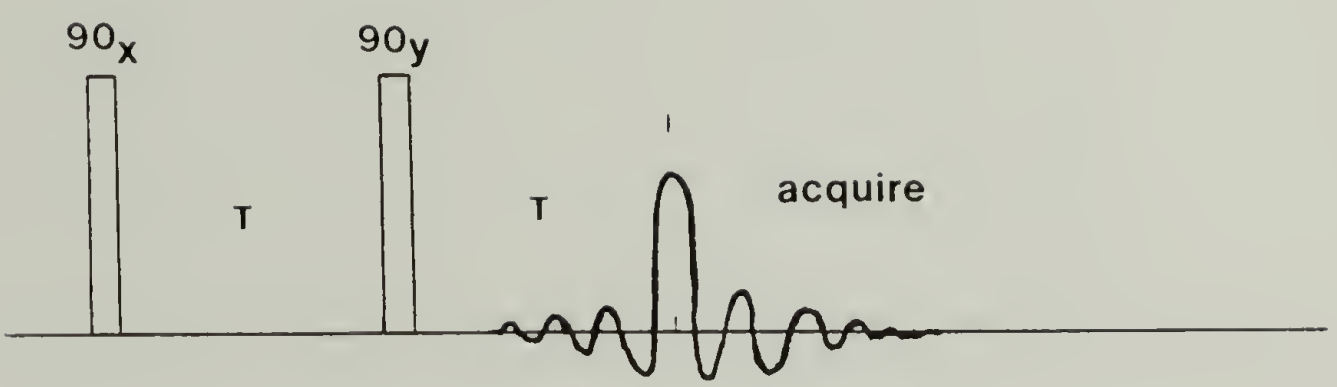

Figure 3.9 ^{2}H quadrupole-echo NMR pulse sequence.

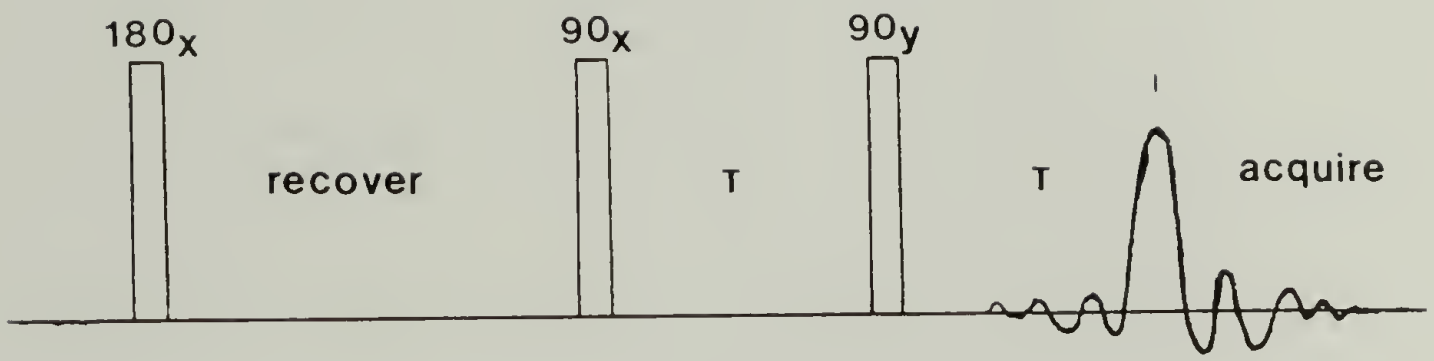

Figure 3.10 ^{2}H inversion-recovery, quadrupole-echo NMR pulse sequence.

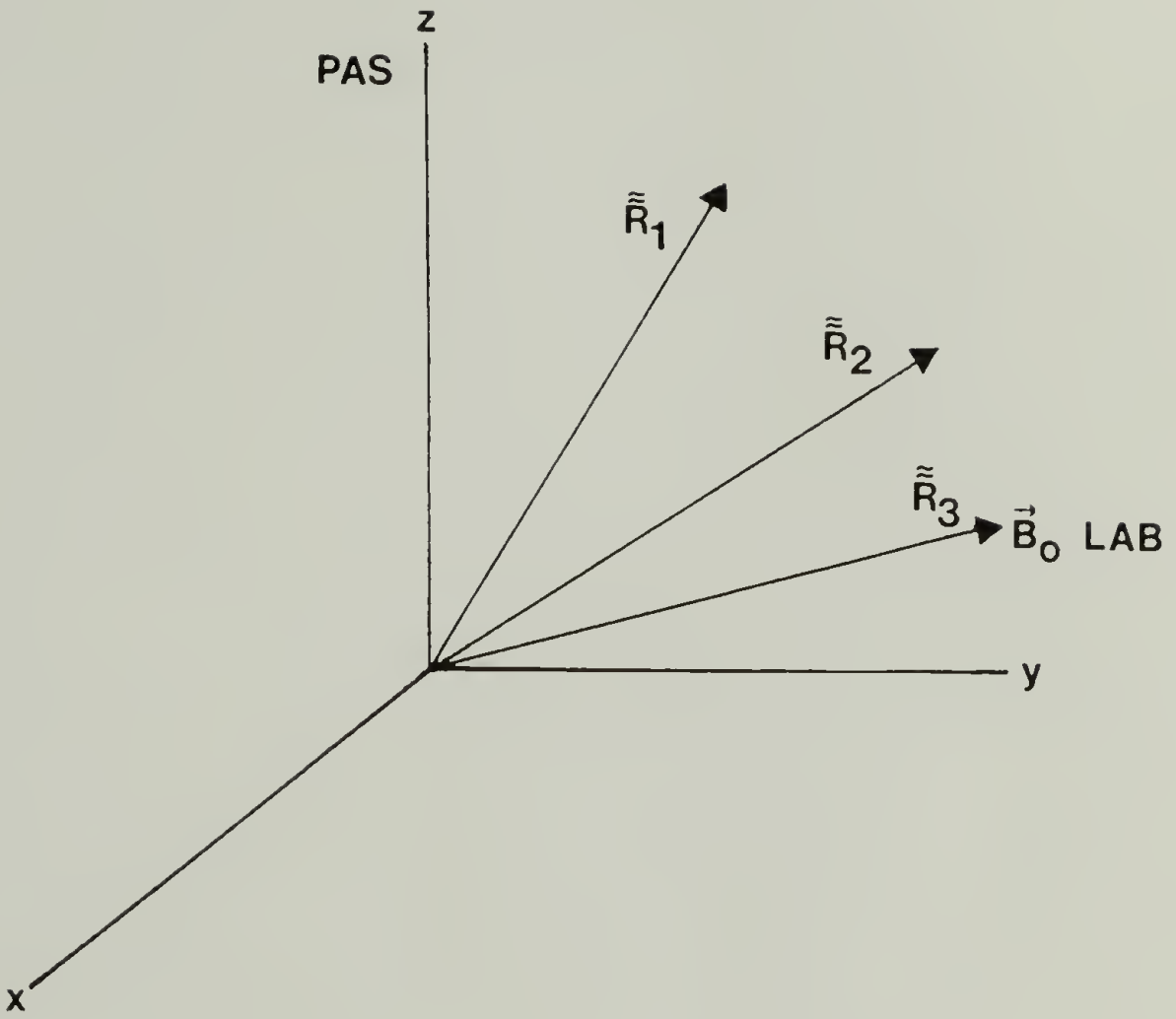

Figure 3.11 Coordinate systems used to simulate the line shapes of oriented PPVs.

CHAPTER 4

^{13}C CPMAS NMR SPECTRA OF PPV AND PPV-d_4

Solid-State ^{13}C cross-polarization magic-angle spinning (CPMAS) spectra can provide detailed information about the crystallinity and morphology of PPV films. The nuclear magnetic resonance (NMR) spectral line shapes of PPV depend upon the conditions employed for film processing, and NMR spectra can be used to monitor the quality of films produced by different processing procedures. In this chapter, a full assignment will be presented for the ^{13}C CPMAS NMR spectrum of PPV. This spectrum has been found to contain information about both the crystallinity of PPV and its molecular dynamics.

The ^{13}C NMR data presented here are consistent with the conclusion that properly annealed PPV films have nearly full crystallinity.[64,81,82] The spectral resolution of these PPV films is high, and greater than previously reported for other PPV films.[163] The resolution for stretched films has also been shown to be independent of draw ratio. There is no evidence from the ^{13}C CPMAS spectrum of a particular amorphous component in properly annealed PPV films. However, it will be shown that the resolution of the ^{13}C spectrum does depend upon annealing temperature, and it will be suggested that the resolution of the ^{13}C CPMAS spectrum is related to rotational disorder about the phenylene-vinylene single bonds.

4.1 ^{13}C CPMAS Spectra of Annealed PPV Films at 25 °C

Figure 4.1 shows ^{13}C CPMAS spectra of two annealed PPV films. The bottom trace is the spectrum of an unstretched PPV film (draw ratio $l/l_0 = 1$) and the top trace is the spectrum of a stretched film ($l/l_0 > 6$). It can be seen that the two spectra are similar, and that stretching does not alter the chemical shifts or resolution of the ^{13}C

CPMAS spectrum. Each spectrum contains four resonance lines in the sp^2-hybridized region (136, 131, 128, and 124 ppm). The remaining resonances are CPMAS sidebands due to the chemical shift anisotropy (B_0 = 4.7T) and the 3.0 kHz spinning rate for this sample. No resonances are observable in the aliphatic region of the spectrum indication that the films are fully eliminated. NMR results support the results of elemental analysis which show that substitution of chlorine or oxygen (which would cause aliphatic resonances) is on the order of 1%.

The all-*trans* PPV chain (Figure 4.2) contains four magnetically inequivalent carbon sites, and the ^{13}C spectra of Figure 4.1 can be completely assigned. Data supporting this assignment will be presented below. The farthest downfield resonance, at 136 ppm, has been assigned to the two nonprotonated carbons at the 1 and 4 positions of the phenylene ring. Nonprotonation was shown with an interrupted decoupling spectrum.[148] This resonance position and assignment is in aggreement with that of previously presented spectra of PPV prepared by a different method.[163] The remaining resonances result from the protonated phenylene and vinylene carbons. The phenylene ring carbons have two distinct chemical shifts, a downfield shift at 131 ppm and an upfield shift at 124 ppm. Position 3 and 6 of the phenylene ring are in the c position relative to the vinylene group, and these carbons have a *cis*-like configuration. It is probable that these carbons have the upfield shift at 124 ppm, similar to the upfield shift of *cis*-polyacetylene.[164] The protonated aromatic carbons in the 2 and 5 positions can therefore be assigned to the resonance at 131 ppm. The fact that the two shifts are distinguishable indicates that a substantial fraction of the phenylene rings of PPV do not undergo 180° rotational jumps about the 1-4 ring axis at 25 °C. The remaining resonance at 128 ppm is due to the two vinylene carbons. It will be shown that this resonance line also contains a contribution from a fraction of phenylene ring carbons which undergo 180° rotational jumps. Evidence for the assignments, and for ring flips will be presented below.

The resolution of the spectra in Figure 4.1 is greater than that for previously published spectra of PPV.[163] The line width for each of the resonance in Figure 4.1 is about 2 ppm. Previous spectra of PPV showed a greater line width, and the protonated resonance between 124 and 131 ppm were not resolved. The difference between the resolution of the present spectra and the earlier spectra can be attributed to the method of film preparation. The earlier PPV samples were not prepared through the precursor route, and the authors concluded that this PPV was amorphous. Likewise, the first unstretched PPV films prepared by the precursor route were also thought to be amorphous, and early ^{13}C spectra from this laboratory also possessed line widths similar to those reported in reference 163.[73]

The higher resolution of the spectra of Figure 4.1 is consistent with a crystalline PPV structure, and the similarity of the spectra in Figure 4.1a and b indicates that the local structure of the chains is not altered by stretching. Usually the ^{13}C CPMAS line widths in crystalline domains are narrower than those of amorphous domains and the broad widths can be attributed to the extent of uncertainty in chain conformation and packing. For example, the line widths of the crystalline component of polyethylene are 1-2 ppm, while the line widths of most amorphous polymers are 5 ppm or more.[121] The line widths of Figure 4.1 are closer to those of a crystalline polymer than an amorphous polymer, and the lack of a dependence upon draw ratio suggests that the local conformational order is similar in stretched and unstretched PPV. Wide-angle x-ray diffraction data now also indicate that unstretched PPV, prepared through the precursor route, has a high degree of crystallinity.[22,47,75] The ^{13}C CPMAS NMR spectra of Figure 4.1 support this conclusion and indicate that PPV films are substantially crystalline.

The intensities of the sidebands of Figure 4.1a and b are also similar. The pattern of sideband intensities of a ^{13}C CPMAS spectrum contains information about the ^{13}C chemical shift tensor components. The sideband intensities of Figure 4.1 (and those of an experiment with a lower magic-angle spinning frequency) have been analyzed by

the graphical method of Herzfeld and Berger[165] to yield shift tensor components (σ_{ii}, where i = x,y,z), and these values are shown in Table 4.1. The tensor components associated with lines a, b, and d are similar to the rigid-lattice tensor components obtained for other phenyl and phenylene rings and values obtained with crystalline xylene are shown in Table 4.1 for comparison.[109] The observation of rigid lattice chemical shift tensor components for PPV confirms that, at room temperature, most segments of both stretched and unstretched PPV do not undergo substantial molecular motion.

The tensor components associated with line c are anomalous and do not agree with those obtained for vinylene groups of polyacetylene (Table 4.1). The anomalous sideband intensities have been attributed to the resonance of the protonated phenylene ring carbons of rings undergoing fast 180° rotational jumps.

4.2 ^{13}C CPMAS Spectra of Ring-Deuterated PPV (PPV-d_4) Films

Figure 4.3a and d show the aromatic region of the ^{13}C CPMAS spectra of unstretched (l/l_0 = 1) films of PPV-d_4. Figure 4.3a shows the spectrum at 25 °C and Figure 4.3d shows the spectrum at -25 °C. In these films, the phenylene ring carbons are completely deuterated and the vinylene carbons are completely protonated. The spectrum of PPV-d_4 obtained at 25 °C is similar in appearance to the spectrum of protonated PPV with the exception that line widths are slightly larger. Larger line widths do not necessarily indicate greater disorder in deuterated PPV, but could possibly be the result of ^{13}C-^{2}H dipole interactions incompletely averaged by spinning. One should also note that in Figure 4.3a the intensity of the vinylene carbons relative to that of the ring carbons is greater than that in Figure 4.1. The difference in intensity can be attributed to the fact that the deuterated phenylene ring carbons of Figure 4.3a cross-polarize to a lesser extent than the protonated carbons of Figure 4.1.

Figure 4.3b and e show carbon spectra of the same deuterated film, obtained by means of interrupted decoupling methods.[148] Only unprotonated (deuterated and quaternary) carbons contribute to these spectra. In Figure 4.3d the resonance at 128 ppm is absent, and this spectrum proves the assignment of the vinylene carbons. A peak is present at 128 ppm in the spectrum (Figure 4.3b) obtained at 25 °C. This resonance can be attributed to a population of deuterated phenylene ring carbons which undergo 180° rotational jumps, and the chemical shift of this resonance is approximately the average of the two rigid-ring chemical shifts. The apparent intensity of this resonance has been determined by line shape simulation to be approximately 40% of the deuterated ring carbon intensity. For a fast sample spinning rate, an average chemical shift would be obtained if the jump rate were greater than the frequency difference between the two isotropic chemical shifts (3.0×10^3 s^{-1}). One can conclude that at ambient temperature approximately 40% of the phenylene rings in ths sample of PPV undergo 180° rotational jumps with a rate greater than 3.0×10^3 s^{-1}. It should be noted that quantification of the percentage of flipping rings by this method is complicated by the additional broadening and relaxation of the fast jump line, which could result from the ^{13}C shift tensor reorientation when the jump rate is close to the spinning rate (3.0×10^4 s^{-1}).[166] An analysis of this effect is not presented here, but it should be noted that the actual percentage of flipping rings at 25 °C could be higher owing to these effects.

The ring-flip resonance is also present in the spectra of protonated PPV. The intensity of line c (Figure 4.1) is greater than that of lines b and d. If resonance c resulted only from the vinylene carbons, one would expect the three peaks (b, c, and d) to have equal intensity. The intensities of all three (protonated carbon) resonances have the same pattern of cross polarization buildup and decay, and so the extra intensity of line c must be attributed to the additional carbon resonance. At low temperature (-58 °C, where the jump motion is slow), peaks b, c, and d have equal intensities. It should be noted that the intensities of line c in Figure 4.1a and b are similar, but not identical,

and probably the ring-flip rate distributions of these two spectra are slightly different. Measurement of the intensity of line c for several samples has shown that the difference is the result of experimental scatter and not necessarily the effect of stretching.

The value of $T_{1\rho}^{H}$, the proton rotating-frame spin-lattice relaxation time, has also been measured at 25 °C for both stretched and unstretched PPV. The value of $T_{1\rho}^{H}$ = 4.8±0.4 ms has been found to be the same for all resonances and independent of draw ratio. This value is slightly greater than that reported by Grobelny *et al.*, "about 4 ms."[167] Decay curve can be fitted by a single exponential, and it has not been possible to separate crystalline and amorphous domains through their relaxation behavior. The most probable explanation for the short $T_{1\rho}^{H}$ of PPV is the presence of the 180° jump motion, similar to that observed, for example, in amorphous polyethylene terephthalate,[115,168] two polyethersulfones,[115,169] and polystyrene.[170] If this explanation is correct, then segments which undergo flips must be distributed homogeneously throught the film.[170] Such behavior is consistent with both the small crystallte size of PPV or the possibility that ring flips occur within crystalline regions of PPV.

Previously, ring-flip motion has been attributed only to the glassy amorphous and boundary domains of semicrystalline polymers.[115] If this assumption were true for PPV, then these ^{13}C NMR data would suggest that a sizable amorphous fraction was present in PPV films, a result in conflict with diffraction data.[22,63,81,82] With the above assumption, the observed increase in the ring-flip population with temperature, would suggest that a crystalline to amophous transition occurs at elevated temperature. However, PPV does not undergo a melting transition at any temperature below its decomposition temperature. One must conclude that the ring-flip motion is present in the crystalline domains of PPV. Ring flips have been observe in some small molecular crystals.[171] It is suggested that a similar motion is present in PPV.

The relationship between the ring-flip rate and conformational disorder of PPV is of considerable interest. PPV films have been shown to be paracrystalline[81] and to

possess some disorder. This disorder could allow a mechanism of chain motion which could propagate the ring-flip motion from boundary domains in to crystallites. In contrast, the ring-flip motion might be an isolated event coupled only to the high frequency motions of the crystalline lattice. Preliminary data suggest that wide amplitude PPV chain motion is the study of the ring-flip mechansim for amorphous polymers.

For Figure 4.3b and e, the integral of the deuterated carbons is twice that of the quaternary carbons (136 ppm). The cross polarization properties of quaternary and deuterated carbons should be similar; therefore, a 2 : 1 integral ratio is consistent width 100% ring deuteration. The lack of a vinylene signal in Figure 4.3e also indicates that these carbons are not deuterated. Scrambling or loss of the deuterium label does not occur during the annealing step of these films. A lack of scrambling has also been verified by infrared spectroscopy of these deuterated films.[147]

Figure 4.3c and f shows the difference spectra between the normal and interrupted decoupling spectra. In each case, the spectra show only the resonance line of the vinylene carbons. The line width of the vinylene carbons resonance is broader than that of the other resonances of PPV and closer to that of an amorphous polymer. Usually a large ^{13}C CPMAS line width is due to conformation heterogeneity, and it is suggested that the greater vinylene line width for PPV is due to a distribution of bond rotation angles about the phenylene-vinylene single bonds or perhaps to molecular motion associated with the ring-flip process.

4.3 Dependence of the ^{13}C CPMAS Spectrum on Annealing Temperature

Figure 4.4 shows ^{13}C CPMAS spectra of three unstretched PPV films which have been annealed at different temperatures between 200 °C and 300 °C. It can be seen from the figure that the resolution of the protonated carbon resnances is dependent upon annealing temperature, with the best resolution obtained for an annealing temperature of

300 °C. It has been shown above that the resolution of the ^{13}C CPMAS spectrum is related to the quality of PPV crystallinity. The spectra in Figure 4.4 suggest that the quality is affected by the annealing temperature.

A previous investigation of PPV by means of transmission electron microscopy (TEM) has shown PPV to be composed of relatively small equiaxed crystallites (crystallites with the same lateral and axial dimensions).[75] In the present study, TEM has been used to determine the effect of annealing temperature upon crystallite size and to determine whether ^{13}C CPMAS resolution is related to crystallite size. Crystallite sizes of 6-7 nm are obtained by annealing at 200-250 °C. For the higher annealing temperatures (300 °C and 350 °C) an increase in size is observed to 11 nm. Annealing above 350 °C results in diminished crystallite sizes, possibly due to the onset of thermal degradation.

The improved resolution of the ^{13}C CPMAS spectrum for annealing temperatures of 300 °C could result from the increase in crystallite size. Becasue the PPV crystallite size is small, a substantial number of PPV segments should be found in the regions between crystallites. In the boundary regions. The near doubling of crystallite dimensions at 300 °C could substatially reduce the fraction of disordered segments and improve NMR resolution.

Grobelny *et al.*[167] have reported a similar improvement in resolution for a 30/70 wt % PPV/polyethylene oxide (PEO) blend which had been annealed at a lower temperature (250 °C). The effect was not explained. The present results suggest that the higher resolution in PPV/PEO blends also resulted from formation of a more perfect crystalline structure. At 250 °C, PEO is in the melt state where greater freedom of motion could allow crystallization in a more perfect structure. TEM data are not available, but it is suggested that this improvement is also related to crystallite size.

Table 4.1

Chemical Shifts and Shift Tensor Components

peak	PPV				*p*-Xylene[109]		
	σ_{ISO}	σ_{11}	σ_{22}	σ_{33}	σ_{11}	σ_{22}	σ_{33}
a	136 ppm	84	34	-106	99	28	-127
b	131	92	13	-105	99	9	-108
c	128	86	-2	-84	97	28	-105*
d	125	92	13	-105	99	9	-108

*Polyacetylene[109]

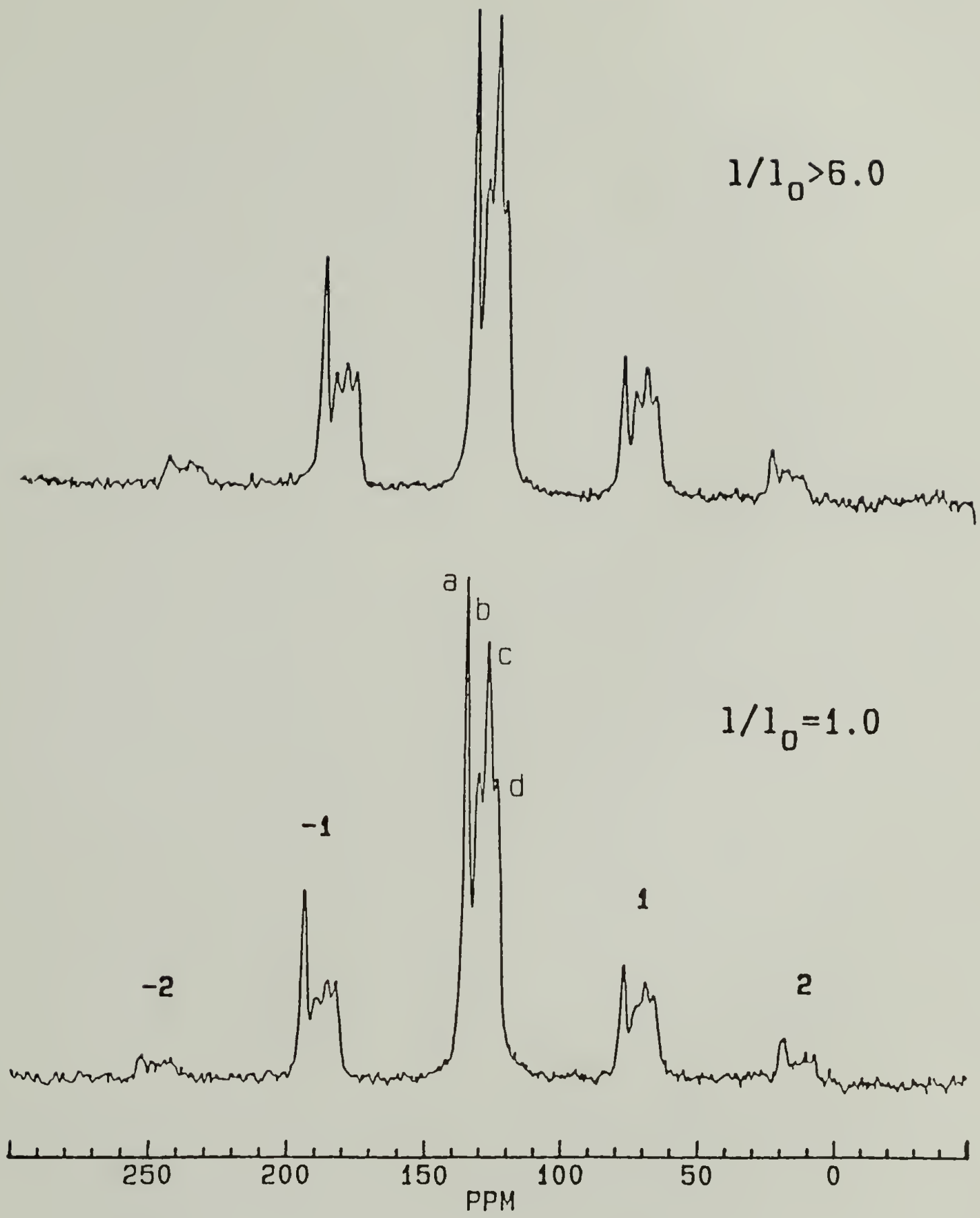

Figure 4.1 ^{13}C CPMAS NMR spectra of annealed PPV films obtained at 50 MHz, unstretched (l/l_0 = 1) and stretched (l/l_0 > 6). The assignment is a) 136 ppm; C1 and C4; b) 131 ppm; C2 and C5; c) 127 ppm; C7 and C8 plus (C2, C3, C5, C6) of rings which undergo 180^{O} jumps; d) 124 ppm; C3 and C6.

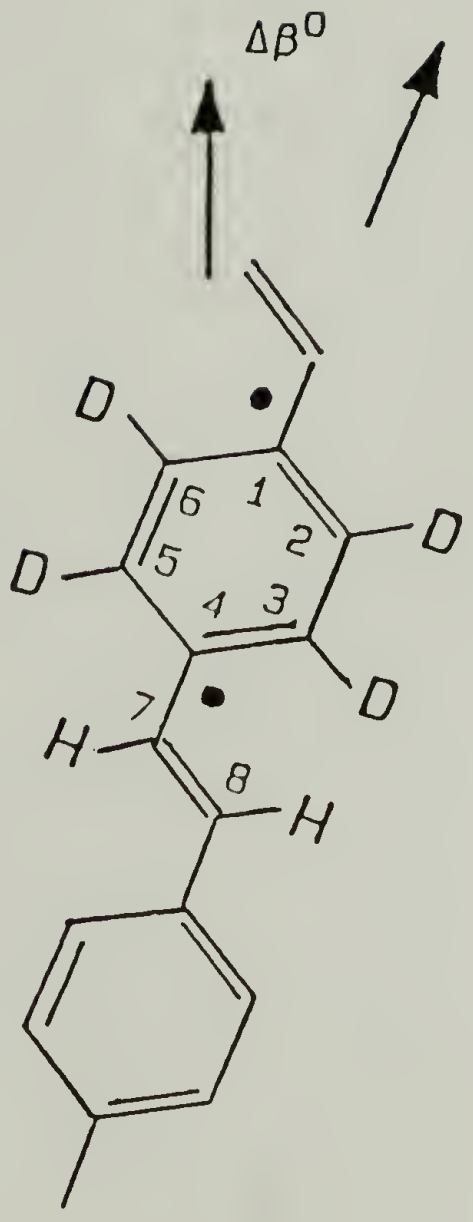

Figure 4.2 The structure of PPV-d_4.

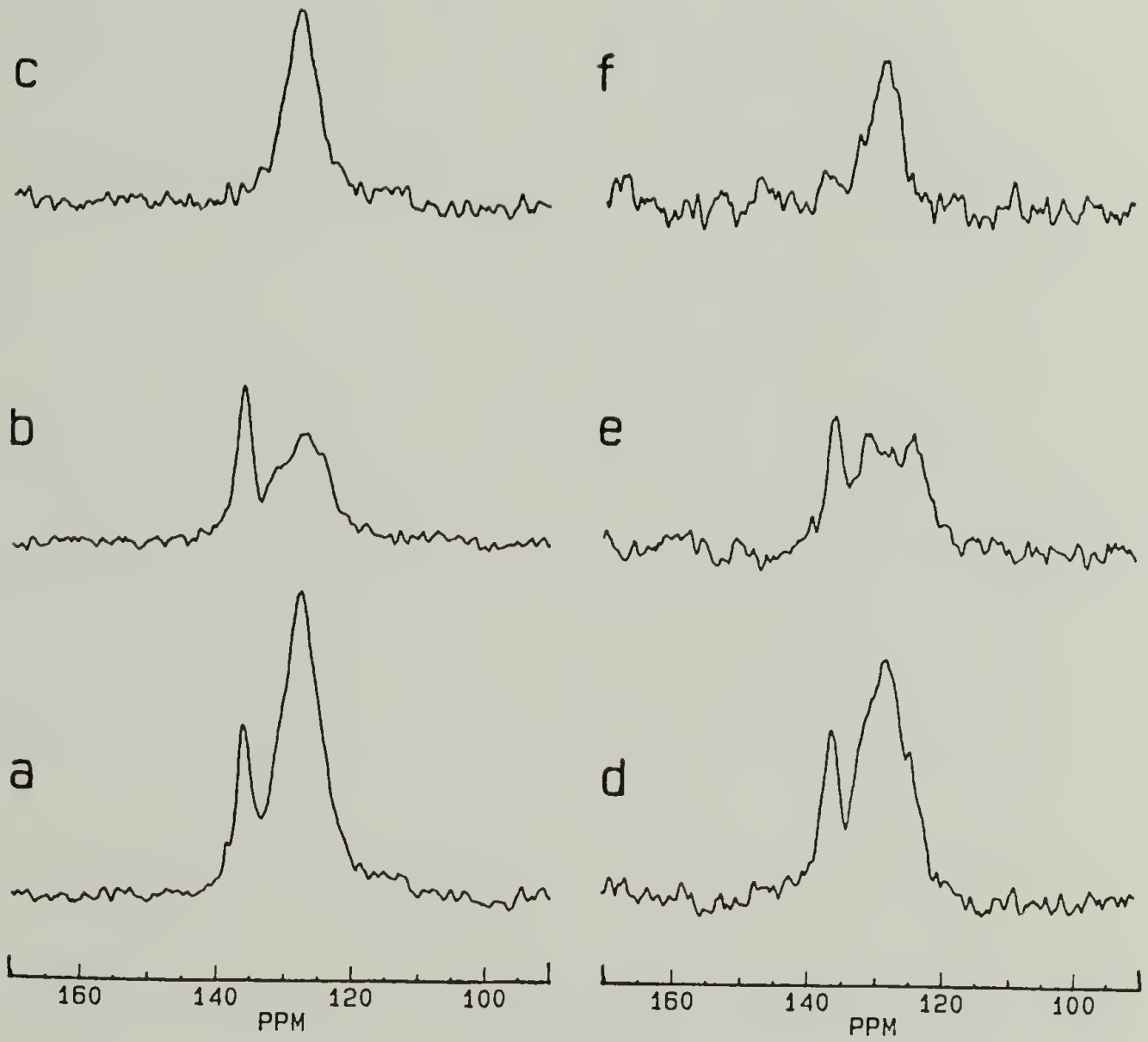

Figure 4.3 ^{13}C CPMAS NMR spectra of unstretched, annealed, ring-deuterated PPV film obtained at 75 MHz. Spectra were obtained at a) 25 °C; b) 25 °C with interrupted decoupling; and c) difference spectrum between a and b. Spectra were obtained at d) -25 °C, e) -25 °C with interrupted decoupling; and f) difference between d and e.

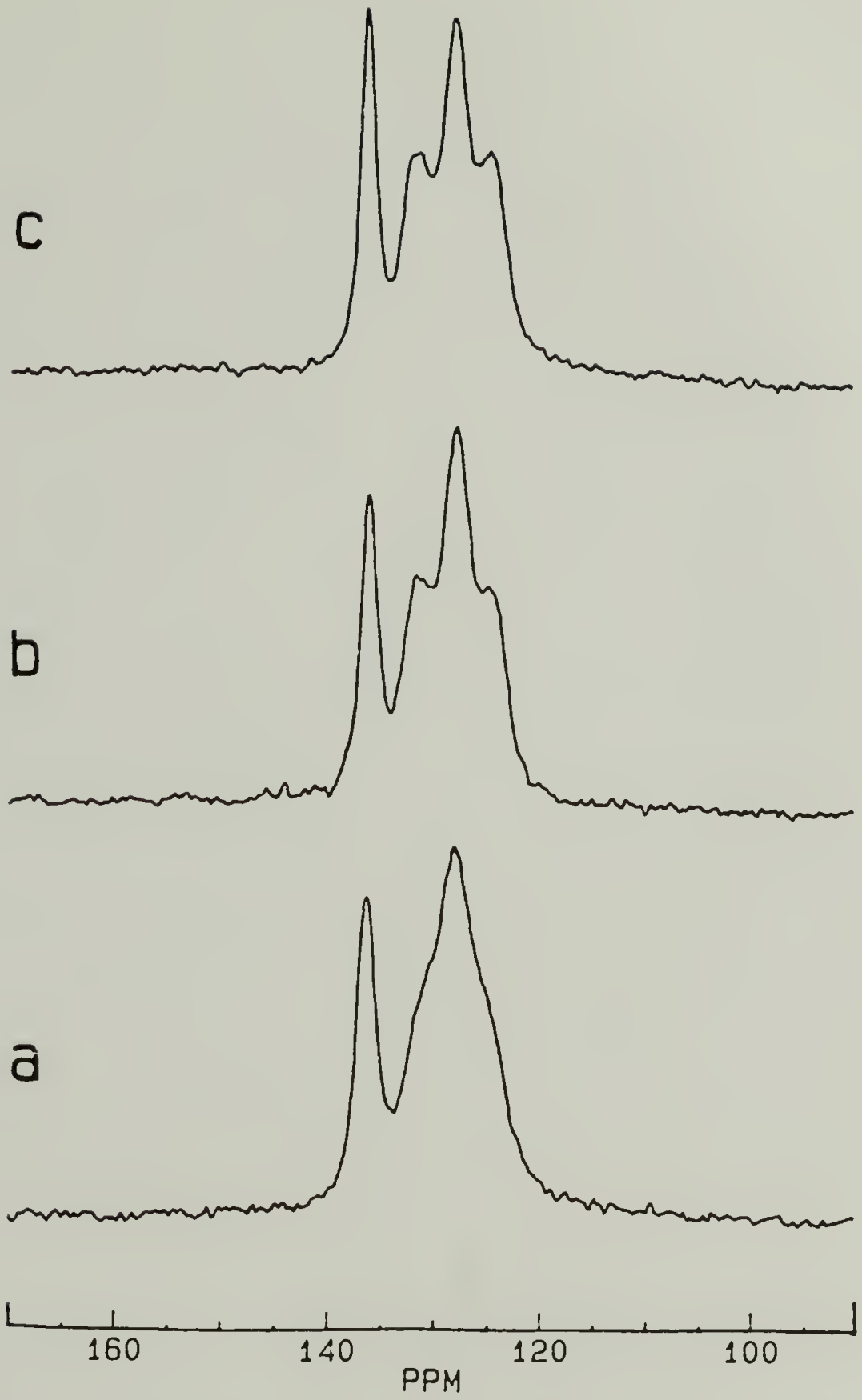

Figure 4.4 ^{13}C CPMAS NMR spectra of unstretched PPV films which had been annealed: a) 200 °C; b) 250 °C; c) 300 °C. Spectra were acquired at 25 °C.

CHAPTER 5

^{2}H NMR STUDIES OF PHENYLENE RING MOTION IN PPV

Both ^{2}H and ^{13}C NMR spectra of PPV films show that the phenylene rings of PPV undergo 180° rotational jumps about the 1,4 phenylene ring axis (ring flips) at routinely accessible temperatures. The ^{13}C data presented in chapter 4 have suggested that ring flips must occur within the crystalline domains of PPV. One might expect the crystalline structure and conjugation of PPV to preclude ring flip motion. Previously, ring flips have been observed only in the amorphous and crystallite bondary domains of semicrystalline polymers.[115] Also, PPV possesses a structure which is highly conjugated. Conjugation energy should contribute to the rotation energy barrier of ring flip motion.

This chapter presents a quantitative examination of the PPV phenylene ring flip motion through the analysis of ^{2}H quadrupole echo line shapes and spin lattice relaxation of a phenylene ring deuterated PPV (PPV-d_4). It will be shown that the distribution of phenylene ring flip rates is narrow, and that for PPV films the ring flip is a thermally activated process which can be described by a narrow distribution of activation energies. The data presented here do not distinguish between motion within crystallites and motion is disordered regions such as crystallite boundaries. Ring flips occur within PPV crystallites with a low activation energy. It is suggested that the ring flip motion in PPV is coupled to an efficient mechanism of chain motion within crystallites and that the experimental activation energy is dominated by the intramolecular barrier for rotation about phenylene-vinylene bonds. The implication of this result for the study of doped PPV is discussed.

5.1 ^{2}H Quadrupole Echo Powder Spectra of PPV Films

Figure 5.1a shows a structure of PPV-d_4 deuterated on the phenylene ring and describes the jump motion of the phenylene ring. Fast rotational jumps about the 1,4 axis of the ring interchange deuterons at C2 and C6 and at C3 and C5 and lead to a motionally average spectrum similar to the right hand spectrum of Figure 5.1b. Figure 5.2 shows ^{2}H quadrupole echo spectra of PPV-d_4 obtained at temperature between -23 and 225 °C. A low temperature spectrum (7 °C) is similar to the rigid lattice spectrum in Figure 5.1b and to that previously obtained for PPV-d_4. This spectrum results from phenylene rings for which molecular motion is slow (relative to the ^{2}H timescale of 10^6 s^{-1}) and have been described by a quadrupole splitting $\Delta\nu_Q$ = 133 kHz and η = 0.03. The high temperature spectrum (225 °C) is similar to the jump spectrum of Figure 5.1b and results from phenylene rings which undergo 180° rotational jumps about the 1,4 phenylene ring axis (ring flips). It can be seen that no trace of the static pattern remains at high temperature, and at elevated temperature all of the phenylene rings of PPV undergo fast ring flips on to the ^{2}H NMR timescale.

The intermediate temperature spectra in Figure 5.2a can be attributed to a thermally activated rotational jump, with a temperature-dependent jump rate of k = 10^2 to 10^8 s^{-1}. Simulations based upon this model are shown in Figure 5.2b, and the corresponding rates are listed in the figure caption. The change in jump rate with temperature is described by an Arrhenius expression:

$$\ln(k) = \ln(k_0) - E_a/RT \qquad (5.1)$$

where k_0 is the infinite temperature rate and E_a is the activation energy for jumps. A logarithmic plot of jump rate versus inverse temperature is linear and the sloped yields an activation energy of 15 kcal/mol, and k_0 = 10^{13} s^{-1}.

The spectra in Figure 5.2 shown the effect of anisotropic T_2 decay during the quadrupole echo, and this property uniquely supports the jump model.[104,140,158] The quadrupole echo intensity and spectra in Figure 5.2 have been scaled relative to the

intensity of a standard material (crystalline L-alanine-d_3, CIL, Inc., Boston, MA) to determine the change in the absolute echo intensity with temperature.[139,140] This procedure eliminates the effect of temperature-dependent probe response. The echo intensities for the spectra obtained at intermediate temperature (ca. 75 °C) decrease to 50% of those intensities at either high or low temperature. This decrease can be attributed to a substantial fraction of phenylene rings which undergo jumps for which k = 10^4 to 10^6 s^{-1}. At individual temperatures ^2H spectra also show a dependence upon quadrupole echo spacing consistent with intermediate exchange.

The magnitude of the absolute intensity chage can reveal the width of the distribution of jump rates. The spectra in Figure 5.2 have been simulated with a log-Gaussian distribution, as described in chapter 3. For a single intermediate jump rate the quadrupole echo intensity is known to decrease to 20% of its fast or slow exchange value.[140,171] The spectra for an infinitely broad distribution are virtually indistinguishable from the sum of a fast-jump line shape and a static line shape (Figure 5.1b) and show no intensity loss. The 50% decrease observed here corresponds to a Gaussian width of approximately $\Delta\log(k) = \pm 2.0$ or two orders of magnitude.[140] A distribution of rates can result from a distribution of activation energies:

$$\Delta\log(k) = 2.303\ \Delta E_a/RT \qquad (5.2)$$

or from a distribution of infinite temperature rates, $\Delta\log(k_0)$. With the assumption that $\Delta\log(k_0)$ is zero, the data shown that the maximum distribution of activation energies is ±2 kcal/mol or ±13% (T = 100 °C). Such a distribution of jump activation energies is in fact narrow for a polymer sample and only small molecular weight crystals have shown more homogeneous ring flip behavior.[140]

Careful examination of Figure 5.2a shows that high-temperature spectra have an overall spectra width which is narrower than that predicted by a simple ring flip model. This additional narrowing can be attributed to fast small-angle motion of the phenylene ring within each jump site. Over the observed temperature range the edges at ±61 kHz

narrow by about 10%. Also, the smaller edges which should occur at about ±15 kHz show a smaller change. Such a line shape change can be attributed to small angular torsional rotation about the 1,4 ring axis of about ±30°. A smaller wobble of the ring axis (< ±15°) may also be present. The above motions are fast relative to the ^2H time scale ($\geq 10^6$ s^{-1}) and may be attributed to the cumulative effects of fast libration about all the phenylene-vinylene bonds of the PPV chain, or could result from a particular mechanism for chain motion. It is noted that any mechanism for PPV chain motion must be consistent with the relatively small wobble of the 1,4 phenylene ring axis. Also, these measurements do not distinguish rotation about the phenylene ring axis from rotation about the chain axis. The angle of phenylene ring tilt relative to the chain axis is too small to have an observable effect on these spectra.

5.2 Measurement of ^2H Spin Lattice Relaxation Rates

Spin lattice relaxation time, T_1, have been obtained for PPV-d_4 as a function of temperature. The magnitude and anisotropy of T_1 support the ring flip mechanism described above. Figure 5.3 shows a logarithmic plot of T_1 versus inverse temperature. It can be seen that T_1 decreases from a value of 0.4 s at 25 °C to approximately 17 ms at 175 °C and it is noted that the value of T_1 decreasees with increasing temperature. Such behavior can be attributed to slow, large amplitude motion with a correlation time τ_c such that at $\omega_0\tau_c < 1.0$, (the nonextreme narrowing region) where $\omega_0 = 2\pi(46\ MHz)$, the resonance frequency. The curvature of the plot in Figure 5.3 may be attributed to the T_1 minimum and the data of Figure 5.2 show that jump rates at high temperature do approach the value of ω_0.

The spin lattice relaxation data indicate a distribution of correlation times. Figure 5.4 shows a logarithmic plot of scaled quadrupole echo intensity versus delay time from an inversion recovery measurement at (T = 75 °C). Figures 5.4a and b show the same plot with two different time axes. For a single T_1 value such a plot should be

linear with a slope proportional to T_1. However, Figure 5.4 shows curvature of over two orders of magnitude and is consistent with a distribution of T_1 values (and correlation times) which also span two orders of magnitude. The values of T_1 shown in Figure 5.3 are those of the fastest relaxing deuterons whereas the actual distribution of T_1 values is up to two orders magnitude longer.

Figure 5.5a shows a partially relaxed inversion recovery line shape obtained at 225 °C with a value of DE corresponding to the experimental null point. This spectrum shown the anisotropy of T_1, and the peaks with a long T_1 are inverted and peaks with a short T_1 are upright. The T_1 anisotropy of Figure 5.5a indicates that spin lattice relaxation for PPV-d_4 is determined by the jump mechanism and that the jump rate is in the nonextreme narrowing region. The slowest relaxation occurs for frequencies in the center of the spectrum and the most rapid relaxation occurs for two of the three tensor component frequencies, ν_{xx} and ν_{zz}. Figure 5.5b shows a simulation of Figure 5.5a based on the jump model. It is noted that here is disagreement between the spectrum and the simulation for the intensity at about 63 kHz (the ν_{yy} tensor frequency). The slower relaxation is due to the distribution of T_1 values. Phenylene rings which move slowly have a long T_1 and a static spectrum whose maximum intensity occurs at about ±63 kHz. At lower temperature spectra obtained at the null point show inverted peaks. In the linear region of Figure 5.3, the value of T_1 (determined from quadrupole echo height) can be calculated according to the expression:[140]

$$1/T_1 = (2k/5)(\omega_Q{}^2/\omega_0{}^2)\sin^2(2\pi/3) \qquad (5.3)$$

where $\omega_Q = 2\pi(133\text{ kHz})$ and $\pi/3$ is the angle between the phenylene C-D bond and the jump axis. Based on this expression, the data in Figure 5.3 indicate that the maximum jump rate varies between $7 \times 10^5\ s^{-1}$ at 25 °C and $1 \times 10^7\ s^{-1}$ at 125 °C. The T_1 distribution in Figure 5.4 suggest that jump rates extend about two orders of magnitude below these values. At 125 °C the jump rates determined from T_1 measurements are similar to those determined from line shapes. However, at low temperature T_1 data

indicate a greater jump rate than that obtained from line shape data, and show a shallower temperature dependence. An activation energy E_a = 7 kcal/mol is determined from the linear region in Figure 5.3. Also, the distribution of jump rates, detemined from T_1 ($\Delta\log(k) = \pm1$) is narrower than that determined from line shapes ($\Delta\log(k) = \pm2$).

The disagreement between the two sets of data may reflect the experimental uncertainty associated with both measurements. In this case one could conclude that the ring flip activation energy is between 7 and 15 kcal/mol and that the distribution width is ±1 to ±2 orders of magnitude. It is noted, however, that an additional motion such as a small angular torsional rotation could contribute to spin lattice relaxation at the lower temperatures. For example, a fast, small-angle torsional libration of the ring (with a correlation time, $\tau_c = 10^{-11}$ s and an amplitude of ±10°) would yield a T_1 of 1 s. Such a small angle of libration would be difficult to distinguish in line shapes. Alternatively, a diffusion of the position of minimum ring energy ($\tau_c = 10^{-7}$ s and an amplitude of ±10°) could contribute to T_1 with a similar magnitude. Deuteron spin diffusion may also average the long T_1 extremes of the jump rate distribution.[121] For these reason it is suggested that the true activation energy and the distribution width are probably closer to those determined from line shapes. It is noted that both the line shapes and the relaxation indicate a remarkably low and narrow activation energy distribution for the polymer.

5.3 The Rotational Potential of the Phenylene-Vinylene Bond

It is useful to contrast the ring motion of PPV with that of another semicrystalline polymer, polybutylene terephthalate (PBT)[172] and with that of purely amorphous polymers.[105,173,174] The ring motion observed here for PPV is intermediate between that typically observed for crystalline and amorphous domains. The activation energy for PPV is higher than that observed for amorphous polymers, and the

distribution of ring flip rates in PPV is narrower. For an amorphous morphology, a broad distribution of ring flip rates has been attributed to a broad distribution of local structure and of packing density.[115,172] The homogeneity of PPV ring flips can be attributed to a more regular structure, resulting from crystallinity. The ^2H spectra of ring-labeled PBT consist of a superposition of a static component and a jump component. The static component has been attributed to the crystalline domains of PBT. This static component persists at high temperature, has a long spin lattice relaxation time and is separable by T_1 selection methods. The jump component of PBT has been attributed to motion in the amorphous domains and interphase regions of PBT and shows a change in line shape with temperature which can be attributed to a thermally activated jump with an activation energy E_a = 5.9 kcal/mol. The ring flip rate distribution for PBT is broader than that of PPV and is similar to that of other purely amorphous polymers (the distribution of rates can be more than 7 orders of magnitude).[105,173,174]

The ring flip activation energy should be the sum of both an intramolecular component, E_a^{intra} (resulting from the phenylene-vinylene rotational barrier) and an intermolecular component, E_a^{inter} (resulting from the effective steric interaction of chain packing). The experimental activation energy place an upper limit upon the potential barrier to rotation about a phenylene-vinylene bond. The intramolecular barrier for rotation in an isolated stilbene molecule has been estimated to be 5-10 kcal/mol.[175] For PPV this barrier should depend upon the extent of electron delocalization in the conjugated structure, and the rotational barrier for PPV could be greater than that of stilbene.[99,176] A simple ring flip requires the concerted rotation about two phenylene-vinylene bonds and the intramolecular barrier could conceivably be 10-20 kcal/mol. These theoretical values are in rough agreement with the experimental value of 15 kcal/mol. The intramolecular barrier to rotation may determine the experimental value, and the effective steric contribution to the activation energy could in fact be small.

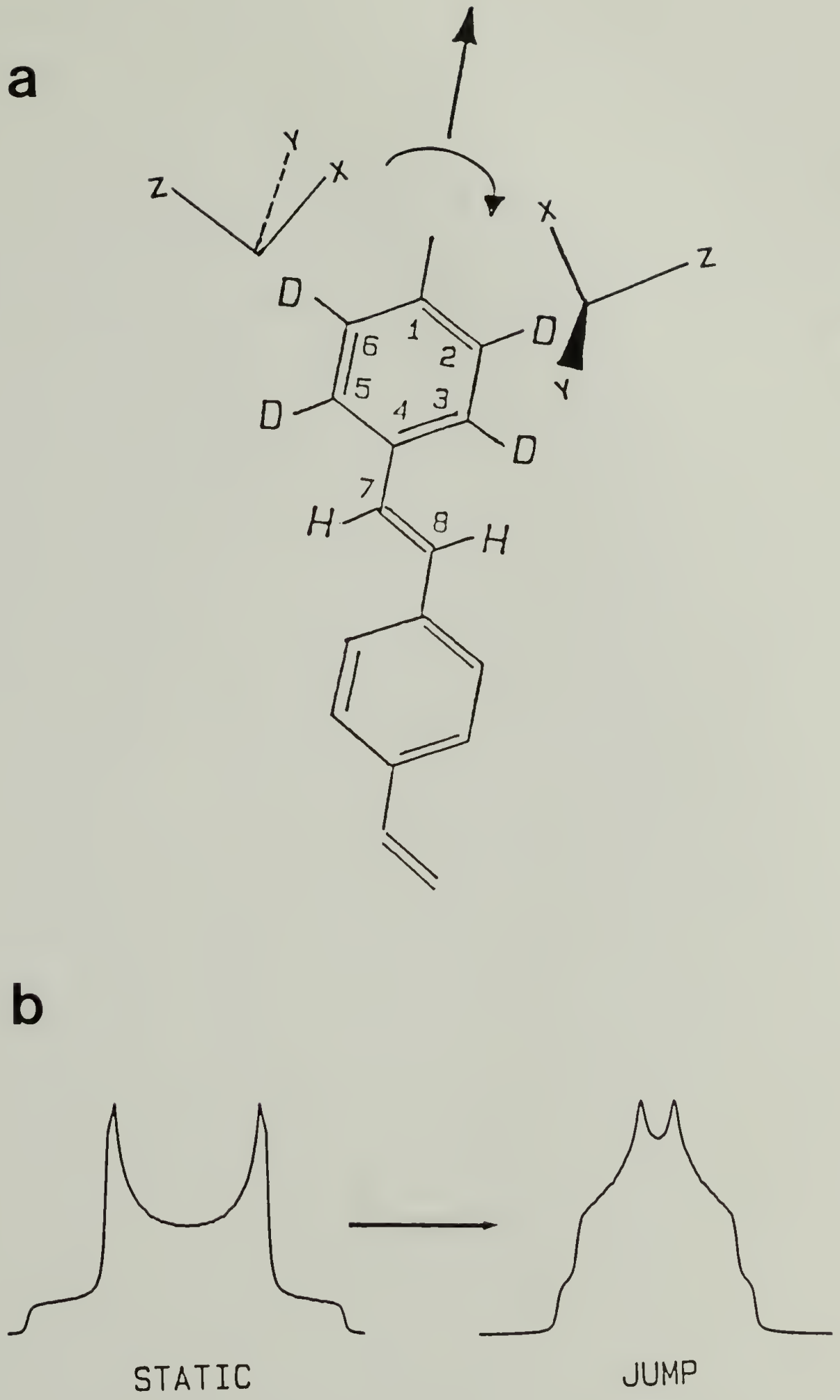

Figure 5.1 a) Structure of PPV-d_4; b) ^{2}H NMR line shapes that result from static and flipping phenylene rings.

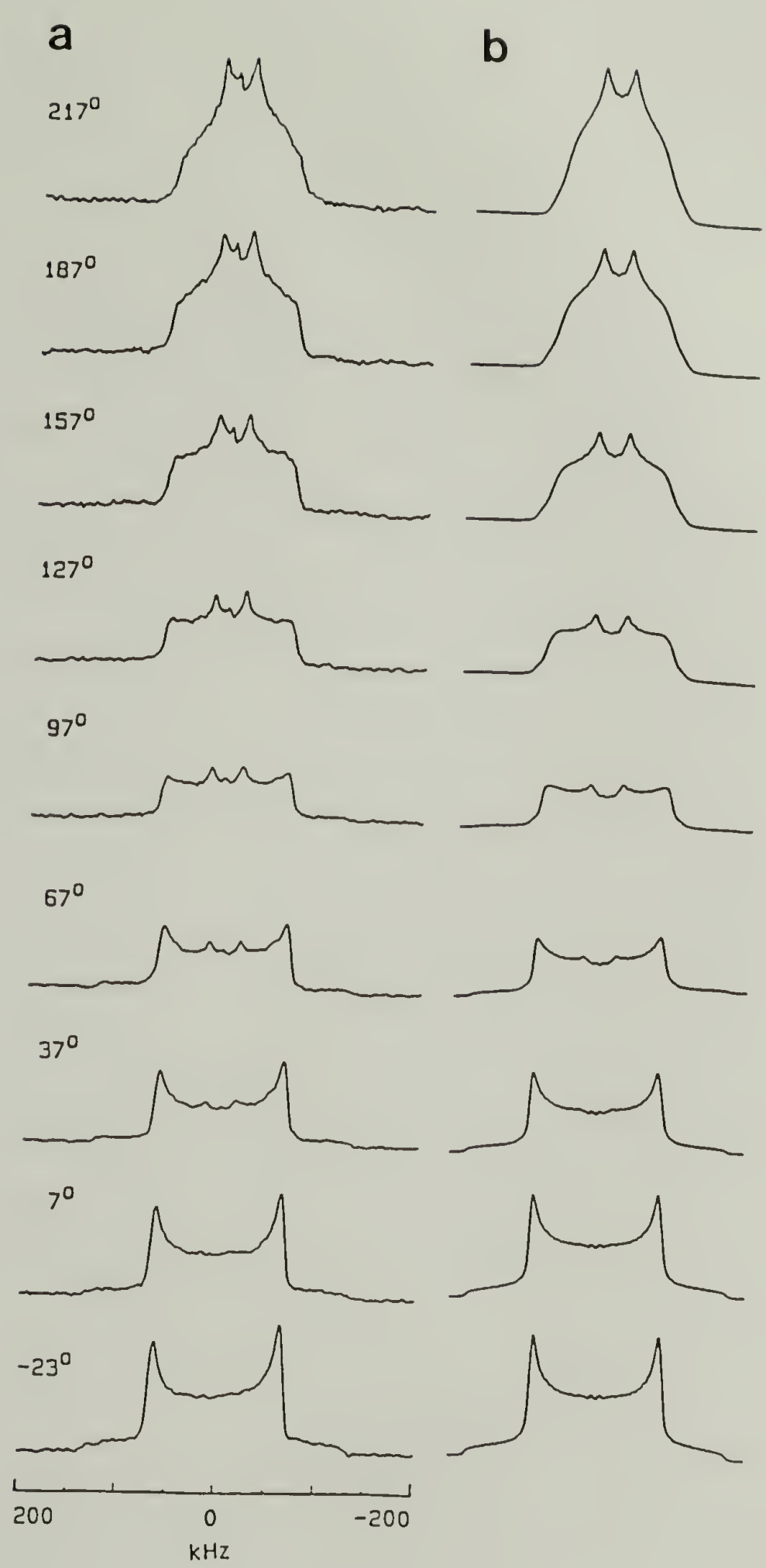

Figure 5.2 a) ^{2}H NMR line shapes of PPV-d_4 at various temperatures and b) the corresponding best-fit simulations based on a single adjustable parameter. The best-fit jump rates are k = $1x10^2$ s^{-1} (-23 °C), $6.3x10^2$ s^{-1} (7 °C), $4.0x10^3$ s^{-1} (37 °C), $2.5x10^4$ s^{-1} (67 °C), $1.6x10^5$ s^{-1} (97 °C), $1.0x10^6$ s^{-1} (127 °C), $6.3x10^6$ s^{-1} (157 °C), $4.0x10^7$ s^{-1} (187 °C) and $4.0x10^8$ s^{-1} (217 °C).

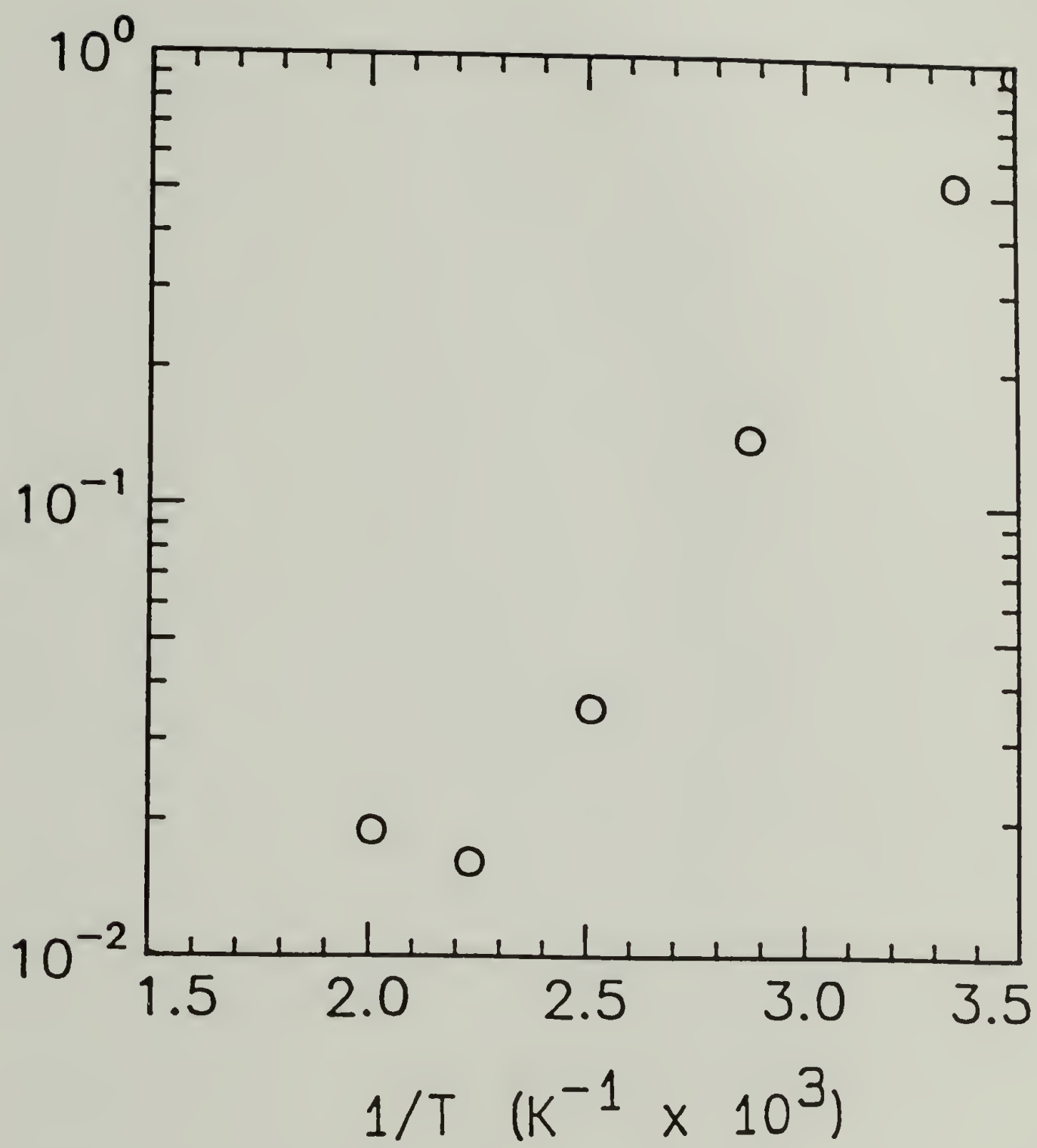

Figure 5.3 Logarithmic plot of the spin-lattice relaxation time, T_1, of PPV-d_4 versus inverse temperature.

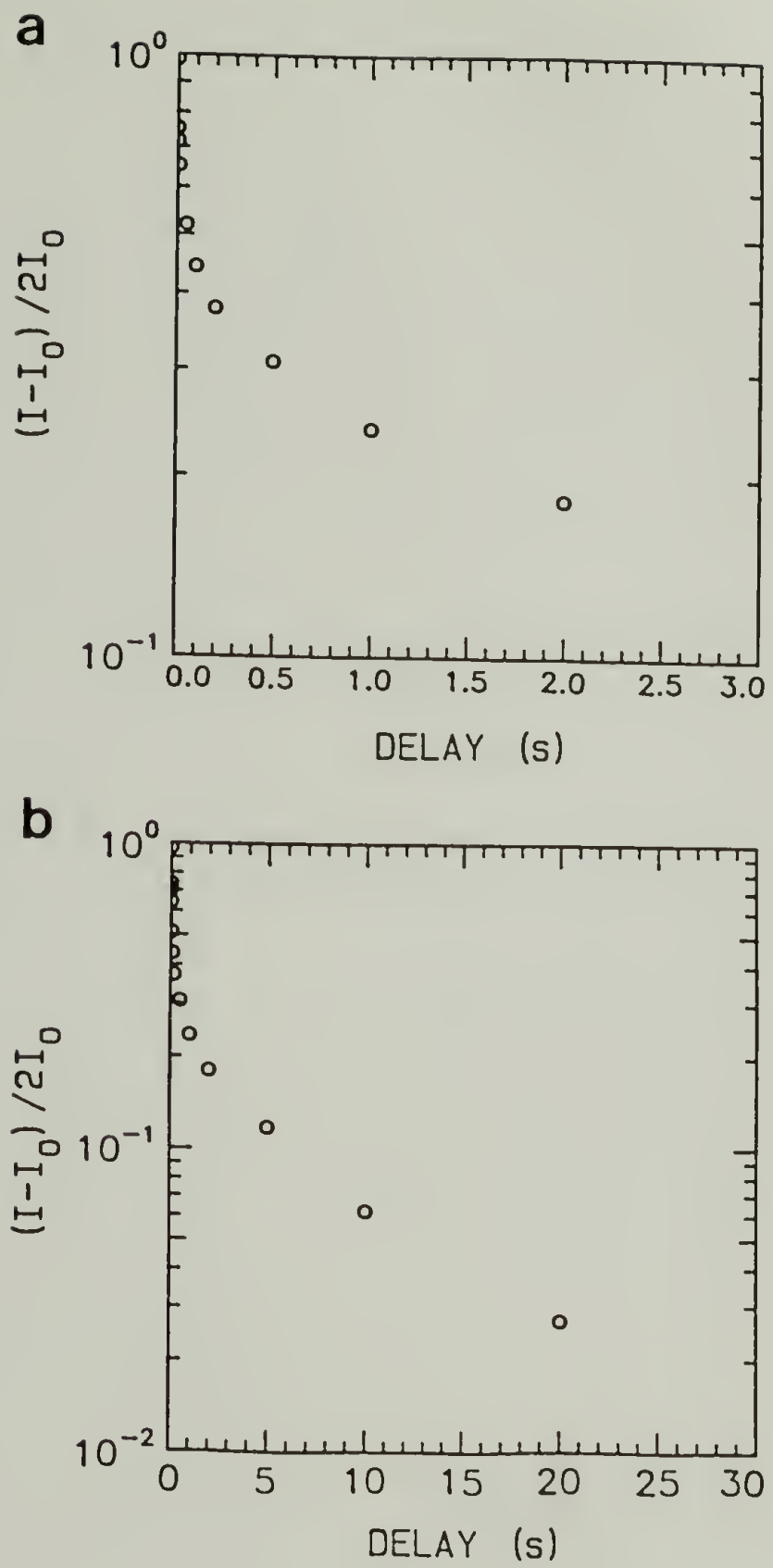

Figure 5.4 Logarithmic plot of quadrupole-echo intensity obtained from the inversion-recovery, quadrupole-echo pulse sequence of PPV-d_4 at 75 °C. a) For delays spanning 0.0 to 3.0 s; b) for delays between 0.0 and 30.0 s.

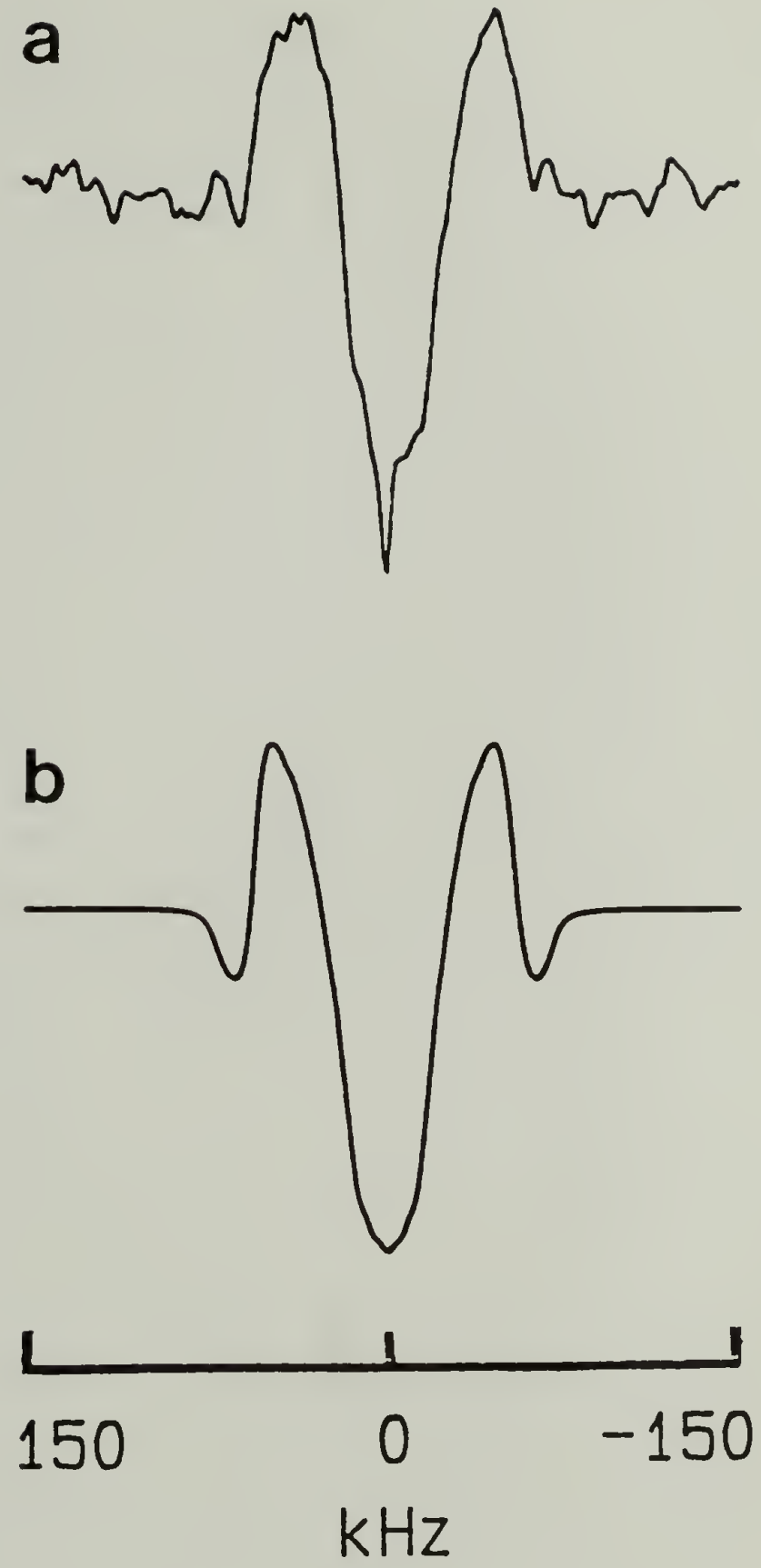

Figure 5.5 a) Partially relaxed inversion-recovery, quadrupole-echo NMR line shape of PPV-d_4 obtained at 225 °C with a delay, DE, of 7 ms (near the null point); b) simulation based upon the 180° jump model with a jump rate of 1.0×10^8 s^{-1}.

CHAPTER 6

EFFECTS OF H_2SO_4-DOPING ON PHENYLENE RING MOTION IN PPV

In this chapter, the effect of sample oxidation on the ring flip behavior of H_2SO_4-doped PPV-d_4 will be examined with solid state ^2H quadrupole echo NMR spectroscopy. Additional information about the chemistry of the doping process and the importance of thermal history will also be presented. Figure 6.1a shows how doping is expected to increase the double-bond character of the phenylene rings about which rotation occurs. Figure 6.1b shows the PPV repeat unit with the deuterons in place and the arrows indicated the bonds about which rotation occurs.

6.1 Comparison of ^2H Line Shapes from Pristine and Doped PPV-d_4

Figure 6.2a shows a solid state ^2H quadrupole echo NMR spectrum of a film of phenylene ring deuterated, H_2SO_4-doped PPV-d_4 obtained at ambient temperature and

Figure 6.2b shows a spectrum of a film of pristine PPV-d_4. It has been shown that the spectrum of pristine PPV results from two components in chapter 5. The outer Pake doublet[177] splitting results from static phenylene rings, compared to the ^2H quadrupole coupling constant ($\leq 10^6$ s^{-1}). The central splitting results from the peaks of a ring flip spectrum which results from phenylene rings which undergo fast 180° jumps ($\geq 10^6$ s^{-1}) about the 1,4 axis of the ring. For the doped PPV-d_4 sample, the ring flip component of the spectrum is attenuated. This attenuation has been attributed to a slowing of the flip rates resulting from an increase in the activation energy for the jump process. This increase might be caused by intermolecular effects such as steric hindrance from nearby dopant counterions or by an electronic effect such as the increase in the double bond character of the phenylene vinylene single bonds resulting from the delocalization of the positive charge of the oxidized PPV. The barrier to rotation about the single bonds of

trans-stilbene is estimated to be 5-10 kcal/mol.[175] The barrier for *cis-trans* isomerization of a vinylene group approaches 60 kcal/mol.[178] An increase in the double bond character of the phenylene vinylene single bonds is expected to increase the activation energy for the *p*-phenylene ring flip. For pristine PPV-d_4, the mean ring flip activation energy has been determined to be 15 kcal/mol in chapter 5 through measurment of the temperature dependence of the ring flip rate. This procedure can also be applied to H_2SO_4-doped PPV-d_4 to observe an increase associated with doping.

Figure 6.2c shows the spectrum obtained from a sample of H_2SO_4-doped PPV-d_4 which has been sealed in a glass tube and heated to a temperature of 125 °C. A narrow resonance is observed at the center of the spectrum. This center resonance is due to a mobile deuterium containing species in the sample tube. Subsequent cooling of the sample to ambient temperature does not remove the center resonance. This component is irreversibly removed from the sample by heating to 225 °C under vacuum and further heating *up to this temperature* yields no more of the mobile component. Only a small portion of the deuterium is removed from the sample, that which remains is still covalently bound to the *p*-phenylene ring. The absence of scrambling of deuterium between phenylene and vinylene groups was confirmed by solid state ^{13}C CPMAS NMR (using dipolar dephasing[148]) and also with ^2H quadrupole echo NMR (deuterium present on the vinylene group has a different quadrupolar splitting than on the phenylene ring, see chapter 7). Figure 6.3a shows the ^2H spectrum obtained from a sample of evacuated, heat treated, H_2SO_4-doped PPV-d_4 at 25 °C. The spectrum is similar to that obtained from H_2SO_4-doped PPV-d_4 before heating (Figure 6.2a).

6.2 Variable Temperature ^2H Line Shapes of Doped PPV-d_4

Figures 6.3a-e show five ^2H quadrupole echo NMR spectra acquired at temperatures ranging from 25 °C to 225 °C in 50 degree increments. Figures 6.3f-j show the corresponding best fit simulations of these spectra based upon a distribution of

ring flip rates as described in chapters 3 and 5. As in chapter 5, the quadrupolar coupling constant, $\Delta\nu_Q$, and the asymmetry parameter, η, are taken to be 133 kHz and 0.03, respectively. The two adjustable parameters of the present fitting procedure are the width of the rate distribution (which is the same for all of the simulations) and the median rate for each simulation. These spectra show that, as with pristine PPV-d_4, the population of rapidly flipping rings can be increased with increasing temperature. Unlike pristine PPV-d_4 at 225 °C, not all phenylene rings of doped PPV-d_4 undergo fast jumps. At any given temperature the number of fast moving rings is fewer than that observed for pristine PPV-d_4.

Doping also increases the width of the distribution of jump rates. When a ring flip occurs at an intermediate rate (approximately equal to the quadrupole coupling constant), its NMR signal will be attenuated due to relaxation during the quadrupole echo (echo distortions)[140,158,171]. If the distribution of jump rates for a given ensemble of spins is narrow, then the spectral intensity generated by these spins will show a marked drop over the temperature range where the observed line shape passes from the slow exchange line shape to the fast exchange line shape. The magnitude of this drop provides for measurement of the width of the jump rate distribution. For pristine PPV-d_4, the intensity drops by 40% at intermediate temperature, and this drop is consistent with a ring flip rate distribution of $\Delta\log(k) = \pm 2$. For doped PPV-d_4 there is no observable intensity drop and this behavior is consistent with a ring flip rate distribution of $\Delta\log(k) = \pm 4$ or greater. A log Gaussian distribution of rate has been chosen for simulations (see chapter 5). This broadening of the ring flip rate distribution indicates that doping introduces greater heterogeneity of the phenylene ring environment into doped PPV-d_4. A ring flip rate distribution width of seven orders of magnitude or greater is often observed for amorphous polymers, while a distribution width for pristine PPV-d_4 is similar to behavior observed in crystals of low molecular weight compounds in which there is homogeneity of ring environments.[105,173,174] Masse *et al.*[22,63] have

shown that H_2SO_4-doped PPV has a nearly completely crystalline structure. It seems most likely that the observed broadening is due to a greater range of crystalline environments in which the *p*-phenylene groups reside. To clarify the last point, it is noted that Masse[22] observed that the doping process begins at crystallite grain boundaries and other regions where the dopant molecules can more easily diffuse into the pristine PPV lattice and proceeds towards the center of the PPV crystallites. Because the new crystalline phase originates at a previously disordered site in the sample, it is expected that the degree of perfection of the new crystalline phase is lower than the old. This crystal transition is also evident when excess dopant is rapidly removed by washing with acetonitrile. An H_2SO_4-doped PPV film experiences local stresses that cause it to flex as excess dopant is removed. This view of how the doping process proceeds also has important implications regarding the reversibility of doping of PPV, particularly in light of the electrochemical applications that have been considered for these materials.

6.3 Median Jump Rates as a Function of Temperature

Figure 6.4 shows a plot of the logarithm of the calculated center rates for the ring flip process for pristine and H_2SO_4-doped PPV-d_4 versus inverse temperature according to the familiar Arrhenius expression: $\log(k) = \log(k_o) - 2.303\Delta E_a/RT$. The slope of the fitted line for the doped PPV-d_4 film is greater than that of the pristine film and the calculated activation energies are 21 and 15 kcal/mol, respectively. The distribution width can also be attributed to a distribution of activation energies and $\Delta\log(k) = -\Delta E_a/RT$. Through this equation the observed ring flip rate distribution ($\Delta\log(k) = \pm 4$) can result from $\Delta E_a = \pm 5$ kcal/mol. Doping increases the median activation energy by broadening the distribution of activation energies upward.

6.4 Levels of Dopant Uptake

When a sample of PPV is doped with H_2SO_4, its mass increases by approximately 60%±5%. This mass uptake corresponds to two H_2SO_4 molecules per three repeat (C_8H_6)

units. Earlier studies have shown there is a wide range of mass uptakes for this doping procedure[22,63] indicating that the chemical reactions here are not well defined. Some possible reasons for this are: 1) there may be complex equilibria involved with the chemical reactions occuring in the sample, for example in the crystalline regions as opposed to the crystallite grain boundaries or in the bulk compared to at the sample surface; 2) doping reaction products may experience difficulty in diffusing out of the sample so sample thickness may play a role in the mass uptake; 3) minor temperature variations may affect the kinetics of various competing doping reactions. Macroscopic heterogeneity of doping is not considered here because x-ray diffraction has shown that H_2SO_4 doping of PPV proceeds to completion in the samples used in the present studies,[22,63] yielding a completely new diffraction pattern with no residual of the pristine diffraction pattern. When a film of PPV is doped, its electrical conductivity increases dramatically.[179] For a sample of PPV drawn to ten times its original length, the conductance of the sample in the draw direction will increase from less than 10^{-10} S/cm to greater than 10^3 S/cm after doping.[22,63]

6.5 Heat Treatment of Doped PPV-d_4

The heat treatment associated with the elevated temperatures of ring flip rate measurements causes a loss of dopant. For the set of experiments performed, the weight loss was confined to a small range of values. After heat treatment a doped film typically loses two thirds of its dopant. Elemental analysis has shown that the volatile component contains sulfur and oxygen in addition to protons (and deuterons). The pH of this volatile component has also been tested and is found to be low (<1.0). It is concluded from these data that partially-deuterated H_2SO_4 is liberated from a doped sample upon heating.

A heat-treated, doped sample also loses its electrical conductivity. This could simply be a consquence of losing H_2SO_4 or it could be due to some other chemical

reaction such as sulfonation that renders the PPV chains unable to conduct electricity effectively. ^{13}C CPMAS NMR has shown no new resonances that would be attributable to this or similar chemical reactions. A sample of heat-treated, H_2SO_4-doped PPV will regain its conductivity if it is redoped with H_2SO_4 indicating that irreversible sample degradation has not taken place. Based on these data, we conclude that the measured ring flip activation energy for fully-doped PPV-d_4 is at least 21 kcal/mol and quite possibly greater because dopant is removed from the sample during measurement. The additional breadth of the ring flip rate distribution could also be due to a heterogeneous loss of dopant.

Before doping, a sample of PPV is yellow-orange in color. After doping, the sample takes on a much darker color (it will appear to be virtually black) with either a slight yellowish or a bluish hue. If a sample of H_2SO_4-doped PPV is exposed to the atmosphere at ambient temperatures for a period of several weeks or immersed in water for a shorter period, it will undope to the point were it is no longer conductive and it regains its former appearance. Initially, an H_2SO_4-doped film that is exposed to the atmosphere loses its shiny surface. This is due to the migration of H_2SO_4 to the sample surface where it picks up atmospheric moisture because of its hygroscopic nature. Over a period of time, the acid is eventually lost and the film completely undopes. The resulting film, though similar in color, is more brittle than before doping. The more brittle nature might be attributed to chain scission associated with local stresses brought on by the crystal-crystal phase transition that occurs upon doping[22,63] or by incomplete reversibility of the crystal transition. This has important implications regarding the mechanical stability of PPV films that might be used in electrochemical applications.[51] It is noted that a heat-treated, H_2SO_4-doped film will retain its optical characteristics longer than non-heat-treated PPV upon exposure to the atmosphere at ambient temperature. Heat treatment does fix some dopant in the film, but does not prevent restoration of conductivity.

a

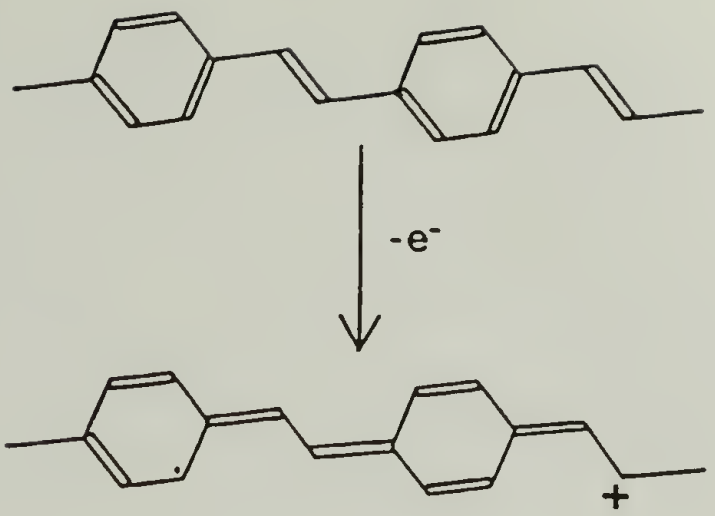

b

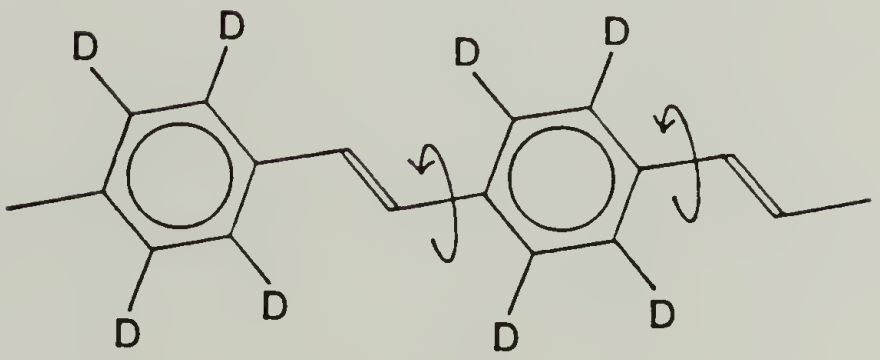

Figure 6.1 a) An illustration of how doping can increase the double bond character of the backbone single bonds; b) A section of PPV chain with its ring protons replaced with deuterons. Arrows indicated the bonds about which the ring rotates.

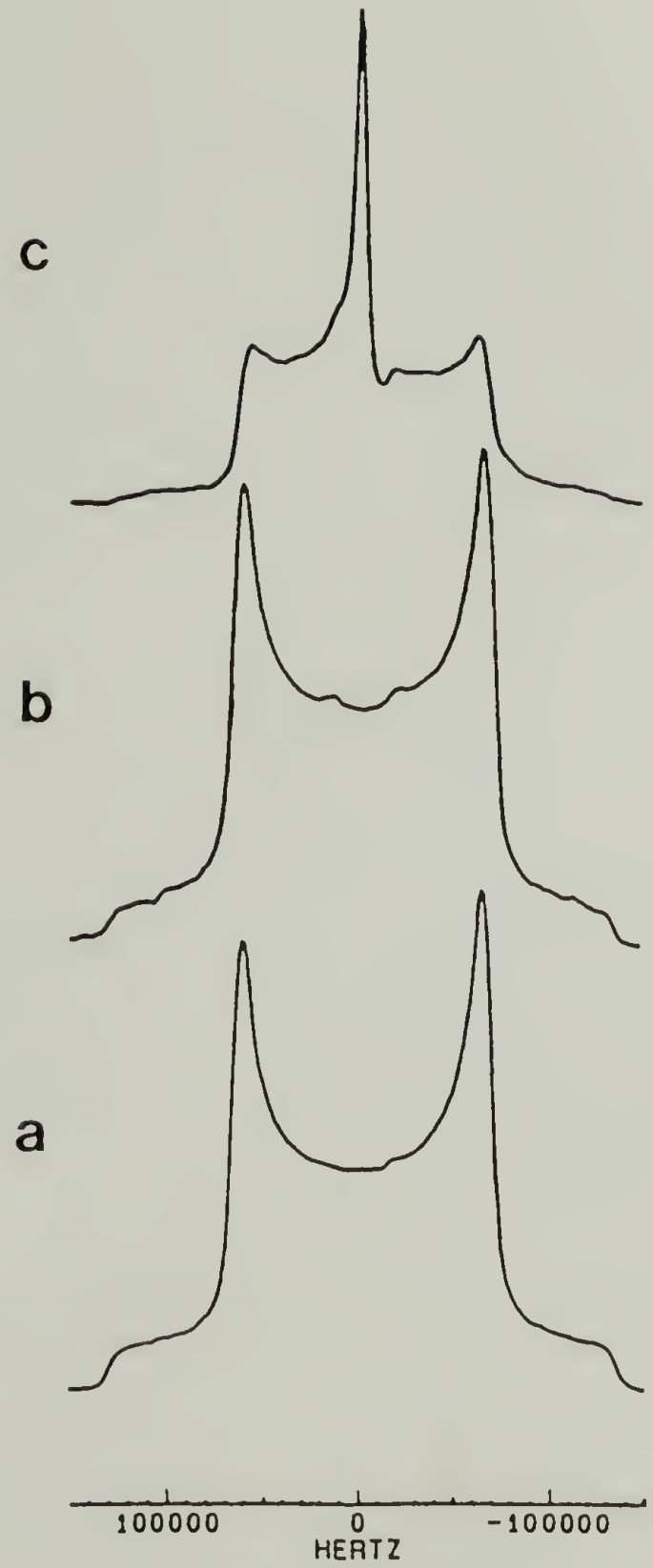

Figure 6.2 a) The ^{2}H quadrupole echo NMR spectrum obtained from a sample of H_2SO_4-doped PPV-d_4 at 25 °C; b) the spectrum obtained from a sample of pristine PPV-d_4 at 25 °C; c) the spectrum obtained from a sample of H_2SO_4-doped PPV-d_4 heated to a temperature of 125 °C.

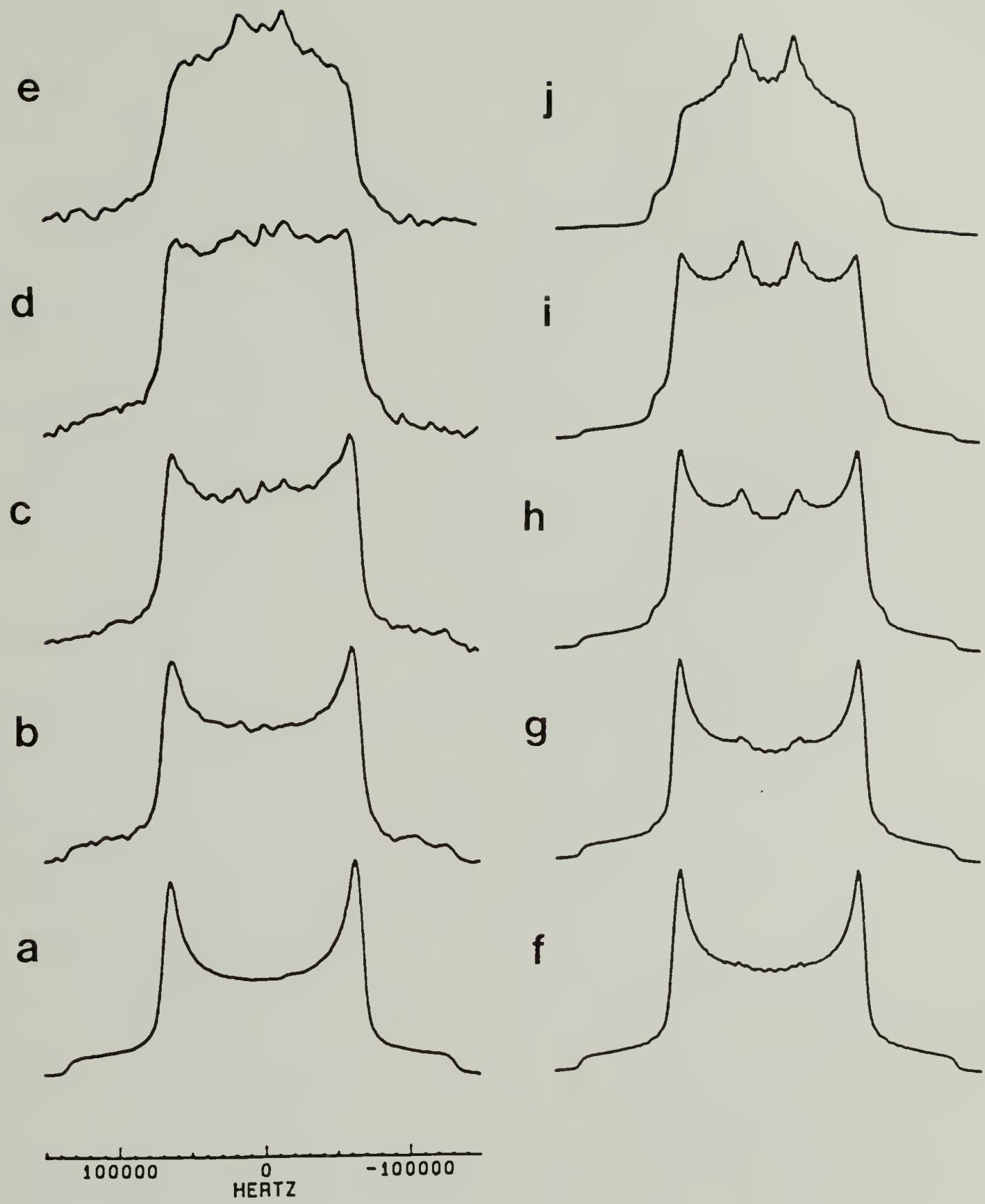

Figures 6.3 a-e The ^2H quadrupole echo NMR spectra obtained from a sample of H_2SO_4-doped PPV-d_4 at: a) 25 °C, b) 75 °C, c) 125 °C, d) 175 °C, e) 225 °C; f-j the corresponding best-fit simulations. The logarithm of the median jump rates are f) 1.2, g) 2.8, h) 4.2, i) 5.4, j) 7.6.

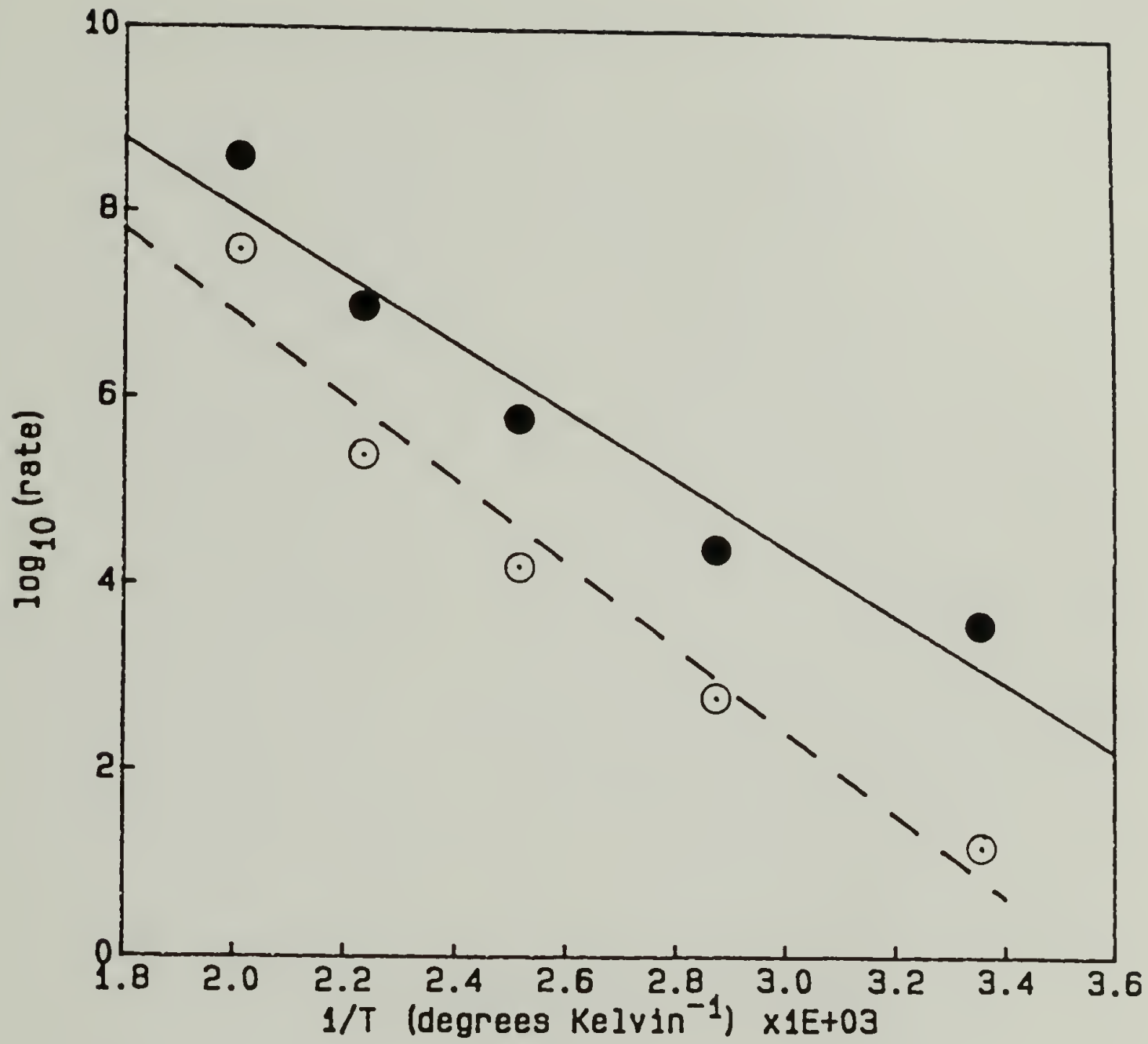

Figure 6.4 A plot of the logarithm of the mean rates of the best-fit simulations versus inverse temperature for undoped- (●) and doped- (⊙) PPV-d_4. The solid line is that calculated for the undoped median jump rates and the dashed line is that for the doped median jump rates.

CHAPTER 7

^{2}H NMR STUDY OF PPV CHAIN MOTION THROUGH VINYLENE-DEUTERATED PPV

For PPV-d_4, the rotation of the phenylene ring about its 1,4 axis obscures direct information about the motion of the chain. However, the ^{2}H line shape of a vinylene C-D bond must result directly from bond motion associated with the PPV chain itself. This chapter presents the ^{2}H quadrupole echo NMR spectra of stretched films of PPV deuterated on the vinylene carbons (PPV-d_2, Figure 7.1).

At ambient temperature, the ^{2}H quadrupole echo NMR spectra of field-aligned, drawn PPV-d_2 can be described with an orientation distribution similar to that of PPV-d_4 (see chapter 8) and that the orientation of the vinylene C-D bond relative to the chain axis is consistent with a *trans*-stilbene-like structure.

^{2}H quadrupole echo NMR spectra of PPV-d_2 show that PPV undergoes extensive chain motion at elevated temperatures. At 225 °C, the spectra of oriented PPV-d_2 films aligned in the magnetic field are the result of a motion which is best described as a two-fold jump of the PPV chain about its axis. Inversion recovery quadrupole echo spectra have been obtained for PPV-d_2 in order to characterize the magnitude and anisotropy of T_1.[104,140] Partially-relaxed inversion-recovery ^{2}H NMR spectra obtained near the null-point also support the 180° chain-jump mechanism. The relationship between the chain-jump mechanism and PPV paracrystallinity is discussed.

7.1 ^{2}H NMR Spectra of PPV-d_2 Obtained at 25 °C

Figure 7.2a shows a ^{2}H NMR powder spectrum obtained at 25 °C from an unoriented film (l/l_0 = 1) of PPV-d_2. This spectrum is characteristic of the spectrum of unoriented C-D bonds which undergo no molecular motion. Figure 7.2b shows a

calculated simulation of Figure 7.2a with a quadrupole splitting $\Delta\nu_Q$ = 129 kHz and an asymmetry parameter η = 0.03. These quadrupole coupling parameters are those which are expected for a vinylene C-D bond with sp^2 hybridization and are also similar to, though slightly smaller than, the quadrupole coupling parameters of the phenylene ring (see chapter 5 and references 137 and 140). Spectra similar to Figure 7.2a have also been obtained from stretched PPV-d_2 films (l/l_0 = 6) which have been mechanically disordered. Stretching does not affect the quadrupole coupling parameters of the vinylene C-D bond. A similar result was obtained for PPV-d_4 (see chapter 5).

Table 7.1 contains the quadrupole tensor components derived from Figure 7.2b and an assignment of these components to individual principal axes of the vinylene C-D bond (Figure 7.1). This assignment is based upon the assumption that the unique tensor axis ν_{zz} is aligned with the C-D bond and that the magnitude of ν_{yy} (the component perpendicular to the sp^2 plane) is greater than ν_{xx} (discussion in chapter 8).

The spectrum in Figure 7.2a shows no evidence of a motionally averaged component and at 25 °C all of the vinylene groups of PPV appear to be static on a timescale comparable to the quadrupole coupling frequency ($k < 10^6\ s^{-1}$). In contrast approximately 10% to 15% of the phenylene rings of similarly prepared PPV-d_4 are observed to undergo fast 180° rotational jumps (ring flips, see chapter 5)

Figure 7.2c shows a ^2H NMR spectrum obtained at 25 °C from a stretched film (l/l_0 = 6) of PPV-d_2 with its stretching axis aligned at Θ = 0° to the magnetic field. Figure 7.2e shows a spectrum obtained with Θ = 90°. These spectra indicate orientation of the vinylene groups of PPV. The best fit chain orientation distribution is similar to that observed for the phenylene rings of PPV-d_4 in chapter 8 (Figures 7.2d and 7.2f). Line shape differences between oriented PPV-d_2 and PPV-d_4 are attributable to the spatial orientation of the vinylene C-D bonds.[140] For a PPV chain modelled after the *trans*-stilbene molecule,[140] the vinylene C-D bond should be oriented at β_0 = 72.3° to the chain axis. Figure 7.2c shows the spectrum of a film aligned at Θ = 0°. The line

shape contains one doublet with a frequency splitting, $\Delta\nu$ = 44 kHz. Solving

$$\Delta\nu = \nu_{zz}\cos^2\beta_0 + \nu_{xx}\sin^2\beta_0 \qquad (7.1)$$

gives a value for β_0 of 71.9°, 1.4° below the value predicted based on *trans*-stilbene and in good agreement with the value of β_0 = 71.7±0.5° predicted from the study of oriented PPV-d_4 in chapter 8. It is noted that the frequency splitting between the peaks of Figure 7.2e (Θ = 90°) is slightly larger than that of Figure 7.2a. This additional splitting has been noted for PPV-d_4 and indicates that the ν_{yy} tensor component of the vinylene C-D bond is greater than the ν_{xx} component, verifying the assignments in Table 7.1.

7.2 ^{2}H NMR Spectra of PPV-d_2 Obtained at 225 °C

Figure 7.3a shows a ^{2}H NMR powder spectrum of an unoriented PPV-d_2 film obtained at 225 °C. This spectrum is narrower than the equivalent spectrum obtained at 25 °C (Figure 7.2a) and has a shape with substantial axial asymmetry (η = 0.14) which can be attributed to vinylene C-D bond motion with a rate greater than the quadrupole coupling (k > 10^6 s^{-1}). Thus the spectrum shows that the PPV chains undergo substantial molecular motion at elevated temperature. Figure 7.3a can be described by a set of motionally averaged quadrupole tensor components (Table 7.1) and each value can be assigned to one of three average tensor axes. The orientations of these axes can be determined from the spectra of oriented films and reveal the mechanism of motion.

Figure 7.4 depicts two mechanisms for chain motion: 180° jumps and small angle diffusion. Figure 7.4a shows the 180° rotational jump motion of the vinylene group about the chain axis which would result from a 180° jump of the PPV chain about the c axis of the unit cell and would leave the angle of inclination β_0 unchanged. Figure 7.3b shows a simulation resulting from such a jump motion with β_0 = 71.7°, the value determined from the study of PPV-d_4. Figure 7.4b shows a mechanism based upon small angle diffusion of the C-D bond about the chain axis. For this mechanism rotation about the chain axis occurs at all angles between two square-well boundaries at

$\pm\Phi$. This motion might result from small angle rotation of the PPV chain about the c axis of the unit cell (without a jump) or might approximate the cumulative result of small angle motion about all bonds of the PPV chain. A value of $\Phi = \pm 38°$ and $\beta_0 = 71.7°$ would reproduce the line shape shown in Figure 7.3a and the simulation is shown in Figure 7.3c. Both models adequately predict the observed spectrum (Figure 7.3a) and thus do not distinguish between the two mechanisms.

The spectra of oriented films favor the rotational jump mechanism of Figure 7.4a. Figures 7.3e (jump mechanism) and 7.3f (diffusion mechanism) are simulations of the spectra of the oriented PPV with $\Theta = 0°$ (Figure 7.3d). Figure 7.3e reproduces the experimental frequency splitting and the narrower line width of the spectrum while Figure 7.3f simulates the frequency splitting but does not simulate the narrower line width. The jump model predicts spectra which are relatively insensitive to crystallite misalignment and hence jump spectra have a narrower line width than spectra based on the diffusion model. The phenylene ring flip spectrum also has this property (see chapter 5).

Figures 7.3h (jump mechanism) and 7.3i (diffusion mechanism) are simulations of Figure 7.3g ($\Theta = 90°$). The two pairs of edges ($\Delta\nu$ = 102 kHz and $\Delta\nu$ = 58 kHz) in Figure 7.3g have the same splittings as the corresponding edges in the high temperature spectrum of an unoriented sample (Figure 7.3a) and correspond to the ν_{xx} and ν_{yy} tensor components. These splittings are narrower than the corresponding splittings at 25 °C (Figure 7.2e, $\Theta = 90°$) indicating that these tensor components are perpendicular to the chain axis, an attribute of the jump mechanism. The diffusion mechanism (Figure 7.3i) underestimates the central splitting of the high temperature, $\Theta = 90°$ spectrum while the jump mechanism (Figure 7.3h) overestimates the central splitting. The jump mechanism is nevertheless favored because the outer edges of Figure 7.3g are actually slightly smaller than those of of Figure 7.3h indicating that there is also some small angle diffusion ($\pm 20°$) within the two jump sites which serves to reduce the observed splittings.

A diffusion mechanism alone does not predict the magnitude of the central splitting while a jump mechanism with diffusion does. Evidence for this small angle diffusion at high temperature is also observed for the phenylene labeled material (PPV-d_4, see chapter 5).

^{2}H spectra obtained at temperatures between 25 °C and 225 °C have line shapes intermediate between those of Figures 7.2 and 7.3. The intermediate temperature line shapes can be attributed to the simplest jump model involving a jump between two sites with equal populations with a thermally activated rate. It is noted that intermediate temperature spectra do not show clear evidence for anisotropic T_2 relaxation (echo distortions),[171] due to rates for which $k \approx \Delta\nu$. This absence could be attributed to a broad jump rate distribution (which is expected for a polymer sample)[115] or to the relatively small difference between line shapes of the static and the jump spectra. However, these results do not exclude a model in which the populations of the two jump sites change with temperature. Unlike a phenylene ring, the PPV chain does not have strict C_2 symmetry and the possibility for unequal populations must be considered.[180,181] While the simulation of the high temperature spectra requires equal populations, the simulation of intermediate temperature spectra does not. Echo distortions are not expected for a model based upon changing populations.

7.3 Measurement of ^{2}H Spin Lattice Relaxation Time

Measurements of the magnitude and anisotropy of the spin lattice relaxation time, T_1, have been obtained. These data also favor a jump mechanism rather than rotational diffusion and suggest that the jump motion is the result of a thermally activated change in rate, rather than changing populations.

For most ^{2}H spectra the value of T_1 is anisotropic[104,140] - it depends upon the orientation of the C-D bond relative to the magnetic field. ^{2}H powder spectra

consequently often show a dependence of T_1 upon frequency. As with the line shape of an oriented sample, this dependence can be used to specify the mechanism of motion.

Figure 7.5 shows a logarithmic plot of T_1 versus inverse absolute temperature for PPV-d_2 determined by means of an inversion recovery quadrupole echo pulse sequence. These values are determined from the null point of the inversion recovery experiment and represent the fastest relaxing deuterons at each temperature. The T_1 values decrease with increasing temperature from 1.0 s at 25 °C to 30 ms at 225 °C. At each temperature PPV-d_2 films possess a broad distribution of T_1 values, spanning one to two orders of magnitude. Figure 7.6 shows a logarithmic plot of quadrupole echo intensity versus delay time from an inversion recovery experiment, obtained at a single temperature (75 °C). Figures 7.6a and 7.6b show the same curve with two different time axes. If a single T_1 were present, these plots would be linear and the slope would be proportional to T_1. However, Figure 7.6 shows curvature over two orders of magnitude indicating a distribution of T_1 values of *at least* two orders of magnitude.

The spin-lattice relaxation behavior of PPV-d_2 is consistent with a slow, large amplitude motion. The values of T_1 in Figure 7.5 decrease with increasing temperature and must result from a motion with a correlation time in the non-extreme narrowing region where $\omega_0\tau_c$ is greater than unity. For ^2H $\omega_0 = 2\pi(46MHz)$ and τ_c must be longer than $3.5x10^{-9}$ s. It has been shown that for a 180° jump in the non-extreme narrowing region that $1/T_1$ (measured from the quadrupole echo height) is proportional to the jump rate:[140]

$$1/T_1 = 2k\omega_Q{}^2\sin(2\beta_0)/(5\omega_0{}^2) \qquad (7.2)$$

For PPV-d_2 $\omega_Q = 2\pi(129\ kHz)$ and $\beta_0 = 71.7°$. If the T_1 of PPV-d_2 is the result of a jump mechanism, then (assuming a two order of magnitude distribution of jump rates based upon Figure 7.5) the jump rate must be $1x10^4\ s^{-1}$ to $1x10^6\ s^{-1}$ at 25 °C and $5x10^5\ s^{-1}$ to $5x10^7\ s^{-1}$ at 225 °C.

It is useful to compare the T_1 behavior of PPV-d_2 with that of PPV-d_4 as presented in chapter 5. T_1 values for the phenylene rings of PPV-d_4 show a similar temperature dependence and distribution, but the values of T_1 for PPV-d_4 are about two-fold shorter. This two-fold difference could be due solely to the different geometry of the phenylene and vinylene bonds. Equation 7.2 shows that T_1 depends upon the angle of inclination of the C-D bond to the jump axis and that:[140]

$$\frac{T_1^{\text{vinylene}}}{T_1^{\text{phenylene}}} = \frac{\sin^2(2\text{x}60.0°)}{\sin^2(2\text{x}71.7°)} = 2.11 \qquad (7.3)$$

If a thermally activated 180° jump of the PPV chain is responsible for the line shapes of PPV-d_2, then Equation 7.3 indicates a chain jump-rate distribution similar to the ring flip jump-rate distribution.

7.4 The Anisotropy of ^{2}H Spin Lattice Relaxation

Figure 7.7a shows an inversion recovery quadrupole echo NMR spectrum obtained at 225 °C for a value of the delay, DE = 12 ms, close to the null point. At this delay the spectral integral is close to zero and the frequency dependence of T_1 within the spectrum is evident. The intensities at frequencies with long T_1 are negative and intensities at frequencies with a short T_1 are positive. The resulting pattern has been shown to depend upon the mechanism of motion and to depend upon whether $\omega_0\tau_c$ is greater or less than unity. The anisotropy of T_1 can be calculated by methods similar to those used to simulate line shapes.[104,140,157,159] The T_1 anisotropy also supports the jump mechanism.

Figure 7.7b shows a simulation of the spectrum of Figure 7.7a based upon the 180° chain jump model and Figure 7.7c shows a calculated simulation of Figure 7.7a based upon the diffusion model. For the jump mechanism the fastest relaxation occurs for the 44 kHz splitting corresponding to the motionally averaged ν_{zz}. In contrast, the diffusion model predicts that the slowest relaxation should occur at 44 kHz. Both

mechanisms predict slow relaxation at low frequencies (near the center of the spectrum). In Figure 7.7a, the intensity at 44 kHz is positive and thus supports the jump model. For the jump model, a rate of $k = 6x10^7\ s^{-1}$ gives the best fit. It should also be noted that the spectral intensity at 64 kHz of Figure 7.7a is less than that in both Figures 7.7b and 7.7c. This difference is attributed to the T_1 distribution. Vinylene groups with the slowest jump rates and longest T_1 contribute an inverted Pake doublet line shape ($\Delta\nu$ = 64 kHz) and diminish the intensity most strongly at 64 kHz. As expected, negative peaks are observed in the null-point spectra obtained at lower temperatures where the jump rate is close to the quadrupole coupling frequency (spectra not shown).

7.5 A Jump Mechanism for PPV Chain Motion

A 180° chain jump within a PPV crystallite could result from the coupled rotation about two phenylene-vinylene bonds located on widely spaced segments. The PPV crystallite size is small (7 nm)[75] and such rotations might occur at crystallite boundaries where greater chain disorder may be present. A two-fold jump should be a natural motion for the PPV chain which itself has approximate two-fold symmetry. In comparison, the high temperature motion of polytetrafluoroethylene (PTFE) is axially symmetric and spectral data is consistent with the greater than three-fold symmetry of the PTFE chain.[181]

The chain jump mechanism is consistent with the data obtained for PPV-d_4 presented in chapter 5. The spectra of PPV-d_4 are dominated by the 180° jump motion of the phenylene rings about their 1,4 axis. Additional motion of the PPV chain should cause additional fluctuations of the ring axis tilt angle of $\pm\Psi = 7.7°$, as discussed in chapter 8. Motion of this magnitude has a negligible effect upon the ring flip spectrum if, as observed, both motions occur on the same timescale. The two motions may in fact be coupled by a common mechanism, but current NMR data does not specify this

mechanism unambiguously. Also, chain jumps of 180° alone cannot be responsible for the observed spectra of PPV-d_4.

7.6 NMR Data and PPV Paracrystallinity

PPV does not undergo a glass transition, nor does it undergo crystalline melting before the onset of thermal degradation upon heating.[182] Motions of the PPV chain must be thermally activated motions associated with the stable PPV crystal lattice. Dynamic disorder evident in the NMR spectrum at high temperature might be associated with static disorder of the PPV crystal structure at low temperature. It is useful to compare the structural implications of PPV chain motion with the disorder associated with the PPV unit cell.

Figure 7.8 shows a projection of the a,b plane of the PPV unit cell.[82] The PPV chain itself does not have C_2 symmetry and the arrows in Figure 7.8 can be associated with a positive direction of phenylene ring and vinylene tilt. Sites I and II of Figure 7.8 show two adjacent chains with opposite tilt. If the PPV chain occupies both rotational conformations with equal probability then one must conclude that the packing interactions associated with phenylene ring tilt do not significantly effect the energy of the two conformations. Granier *et al.*[81,82] have noted that diffraction data do not specify the direction of phenylene ring tilt. A 180° rotation about the chain axis is the simplest disorder which could be present within the PPV unit cell. These NMR data have shown that this disorder is present at elevated temperature and the T_1 data suggest that this disorder is also present at low temperature on a slower timescale.

Electron diffraction has further shown that there is a lack of axial registry between the chains of adjacent layers along the a direction of the unit cell.[81,82] Examination of Figure 7.8 shows that a 180° jump of the PPV chain would principally affect the inter-chain interaction in the a direction. A 180° jump at site II would tilt the phenylene and vinylene groups of chain II toward or away from site III, but would have little effect on

the chain of site I which is coplanar. Such a jump might be accompanied by an axial shift of chains in the adjacent layer to relieve steric crowding. Axial disorder should reduce the energy difference between the two chain jump conformations. Cooperative chain jumps might be coupled to slip between adjacent layers perpendicular to the a direction. These NMR data, however, provide no direct information about the slip motion.

NMR data have shown that rotational diffusion about the PPV chain axis is small. The rotation of ±38° implied by the diffusion mechanism would involve substantial disruption of the unit cell structure. Both electron diffraction data at room temperature and energy minimization calculations have shown that the setting angle (the angle between vectors 1 and 2 in Figure 7.8) is confined to a small range (56°-68°).[81,82] These NMR data suggest that the unit cell structure and setting angle remain well determined at high temperature. It should also be noted that the PPV-d_2 data are also inconsistent with a jump motion which interchanges the setting angle of adjacent layers (i.e. sites I-III of Figure 7.8). Such a motion would cause a greater than observed averaging of both the spectra of PPV-d_2 and PPV-d_4.

PPV films are unusual in that they show both high crystallinity and substantial ring flip motion. It has been suggested in chapter 5 that ring flip motion in PPV results from the particular paracrystalline disorder of the PPV unit cell. In the past, ring flip motion has been attributed to the amorphous and disordered boundary regions of semicrystalline polymers.[115] For example, the conjugated polymer, polyaniline, shows ^{2}H NMR spectra more consistent with the usual behavior of semicrystalline polymers (a population of static rings at all temperatures).[173] The NMR data presented here show that the phenylene ring flip of PPV is not an isolated motion but rather that the entire PPV chain is capable of undergoing substantial motion. The disorder of the axial registry between chains provides a plausible mechanism for PPV chain jumps, and may also provide a plausible mechanism for ring flips.

Table 7.1

Quadrupole Tensor Components in kHz for PPV-d_2

all values ±1 kHz

	ν_{xx}	ν_{yy}	ν_{zz}	η
Static (25 °C)	62.5	66.5	-129	.03
Motionally Averaged (225 °C)	-102	58	44	.14*

*calculated with ν_{xx} and ν_{zz} interchanged

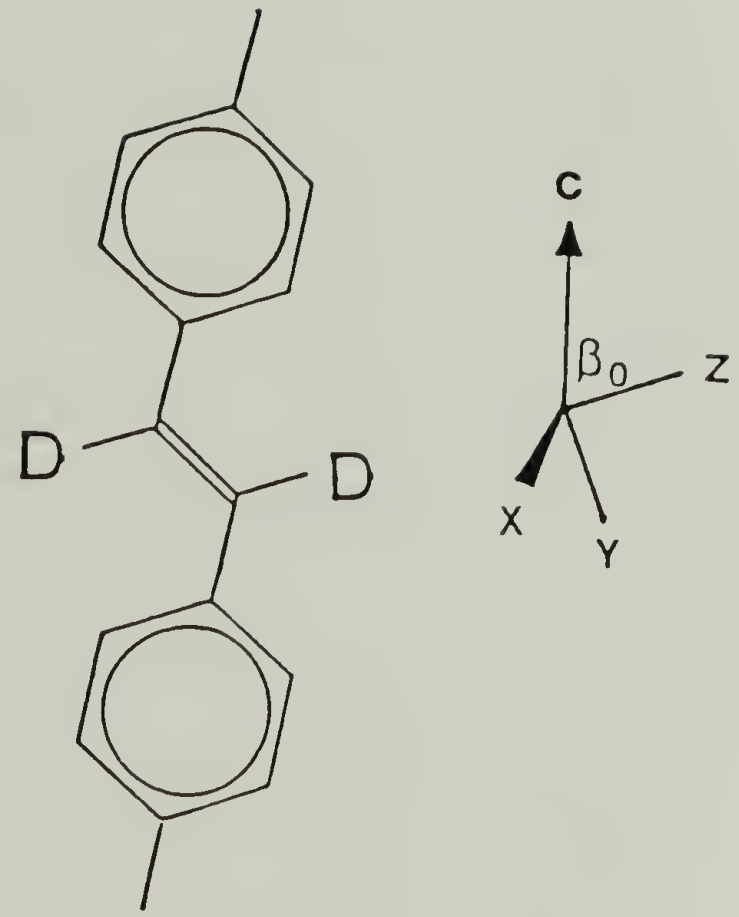

Figure 7.1 The structure of PPV-d_2. The principal axis system (PAS) of the vinylene C-D bond is shown. β_0 is the inclination of the vinylene C-D bond with respect to the chain axis **c**.

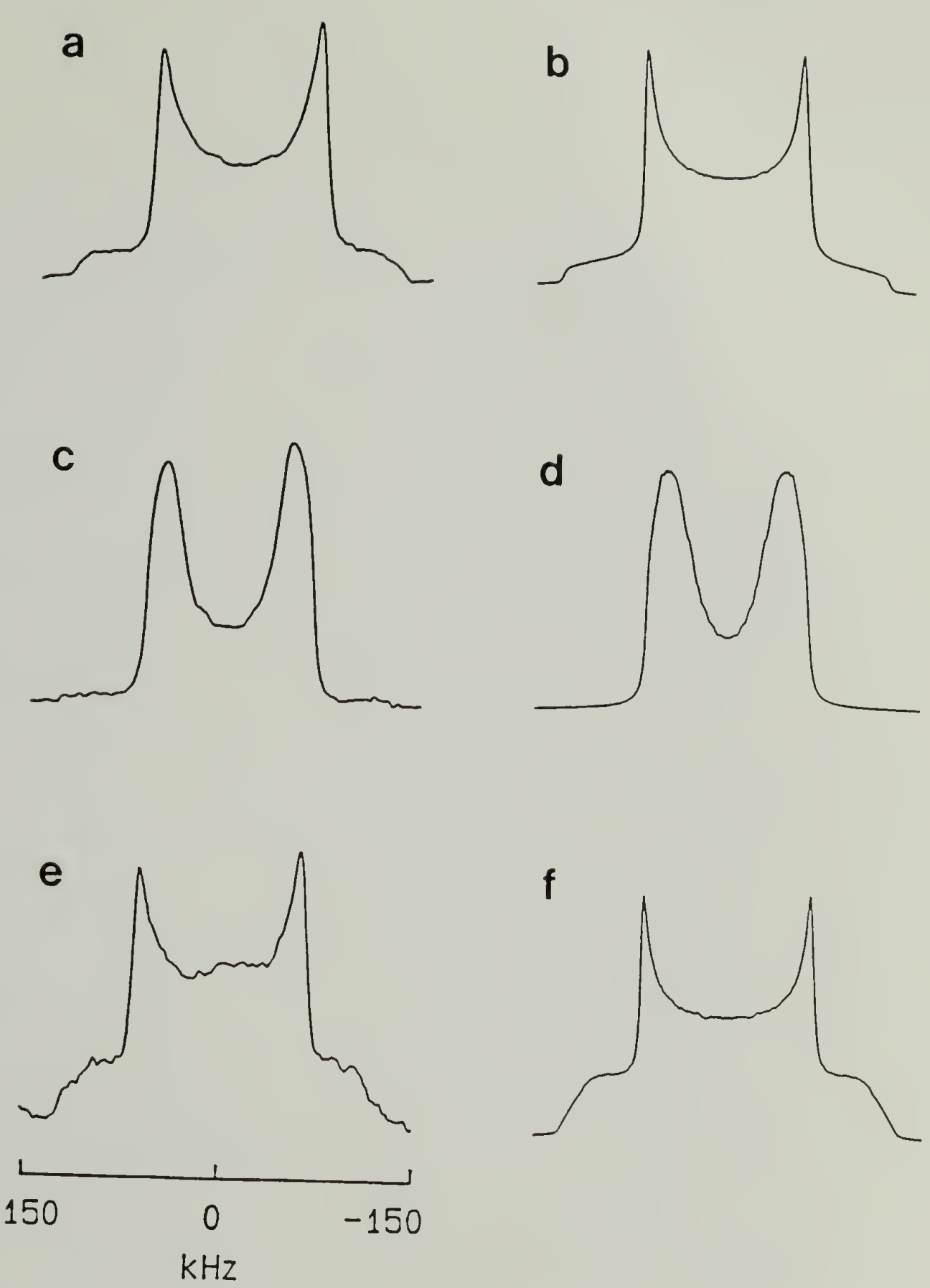

Figure 7.2 ^{2}H quadrupole echo NMR spectra of PPV-d_2 obtained at 25 °C and simulations: a) Powder spectrum obtained from an unoriented film and b) rigid lattice simulation with PAS tensor components of Table 7.1. c) Spectrum obtained from a stretched film, aligned in the magnetic field (Θ = 0°) and d) a simulation based upon the orientation distribution of chapter 8. e) a spectrum obtained from a stretched film, aligned in the magnetic field (Θ = 90°) and f) a simulation based upon the orientation distribution of chapter 8.

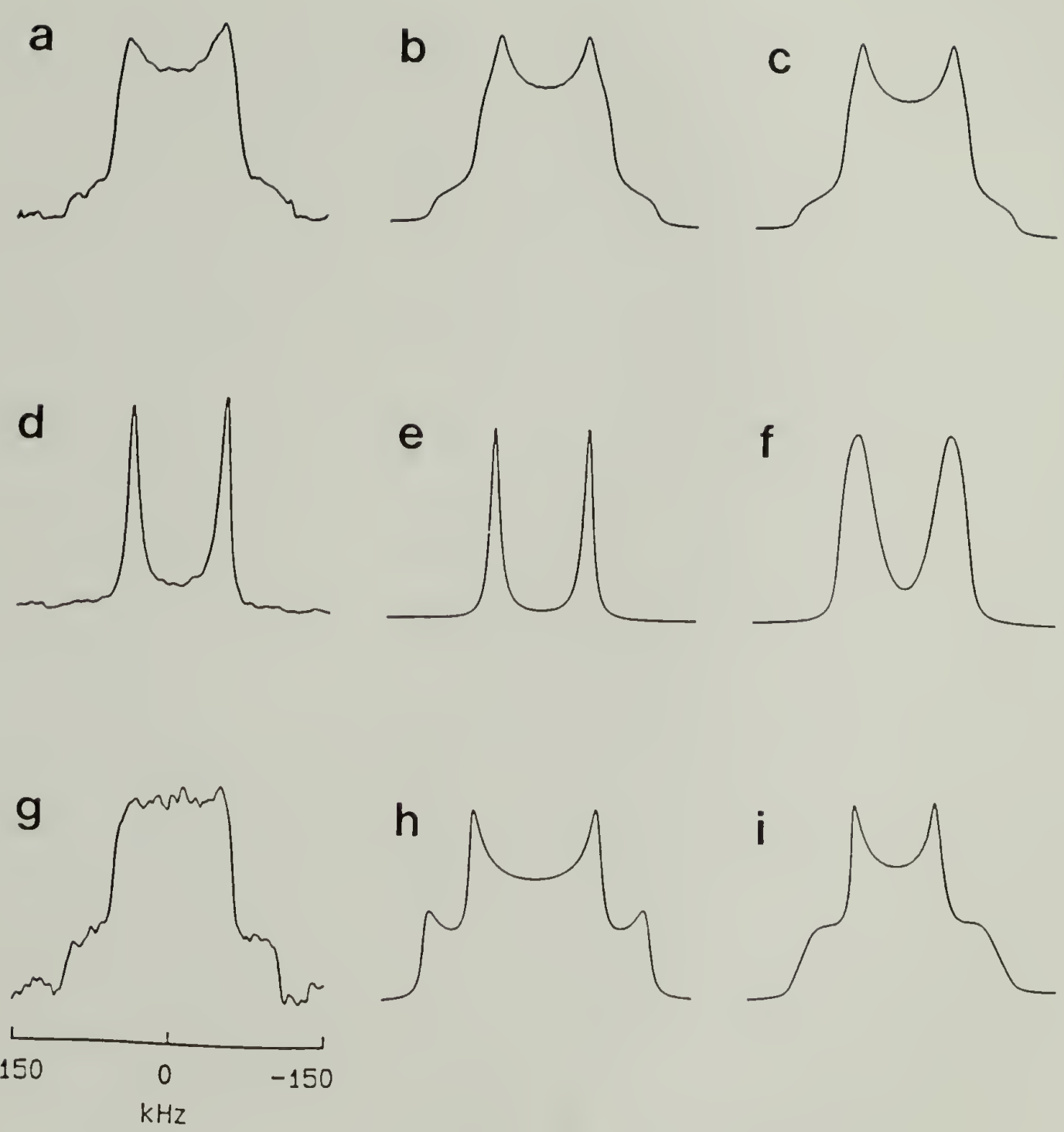

Figure 7.3 ^{2}H quadrupole echo NMR spectra and simulations of PPV-d_2 at 225 °C: a) Spectrum obtained from an unoriented film; b) a 180° jump model simulation; c) a diffusion model simulation; d) a spectrum obtained from a stretched film, aligned in the magnetic field (Θ = 0°); e) a 180° jump model simulation (Θ = 0°); f) a diffusion model simulation (Θ = 0°); g) a spectrum obtained from a stretched film, aligned in the magnetic field (Θ = 90°); h) a 180° jump model simulation (Θ = 90°) and i) a diffusion model simulation (Θ = 90°).

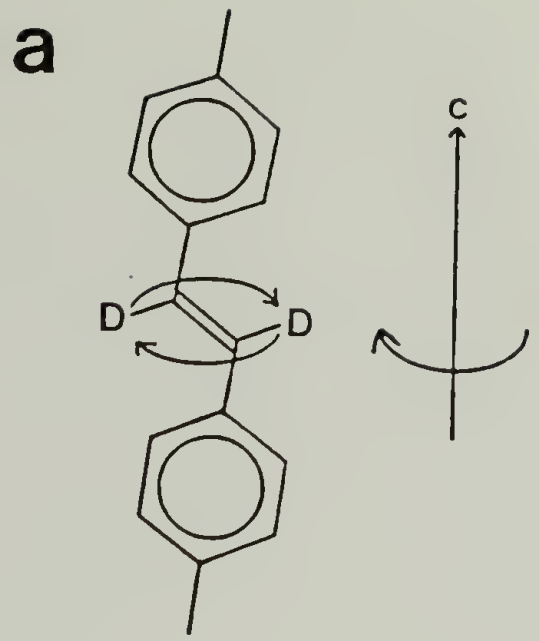

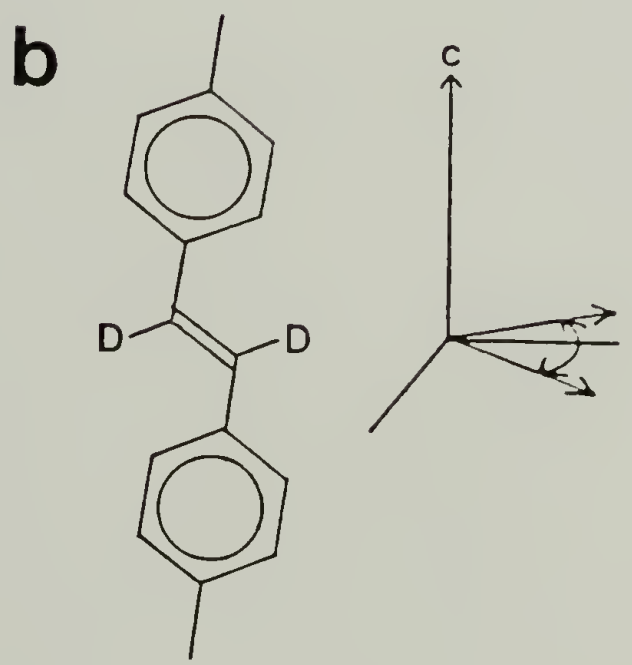

Figure 7.4 Two mechanisms for PPV chain motion at 225 °C. a) 180° jump about the **c** chain axis. The angle of inclination of the C-D bond is constant (β_0 = 71.7°). b) Small angle diffusion within the boundaries of a square well potential (Φ = ±38°).

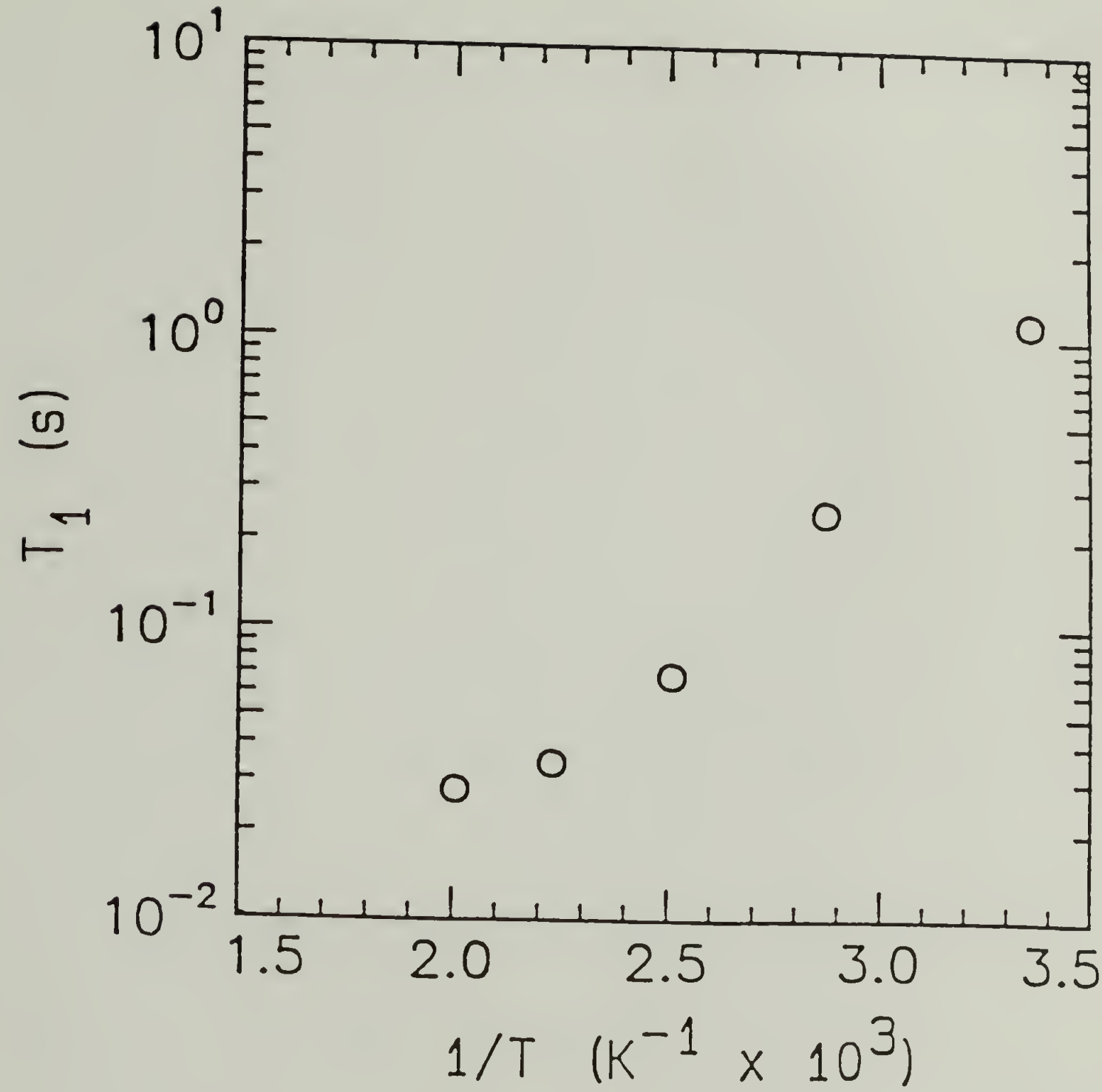

Figure 7.5 Logarithmic plot of spin lattice relaxation time, T_1, of PPV-d_2 versus inverse temperature. These T_1 values were obtained from the null point of an inversion recovery quadrupole echo (as described in chapter 3) and represent the fastest relaxing components of the T_1 distribution at each temperature.

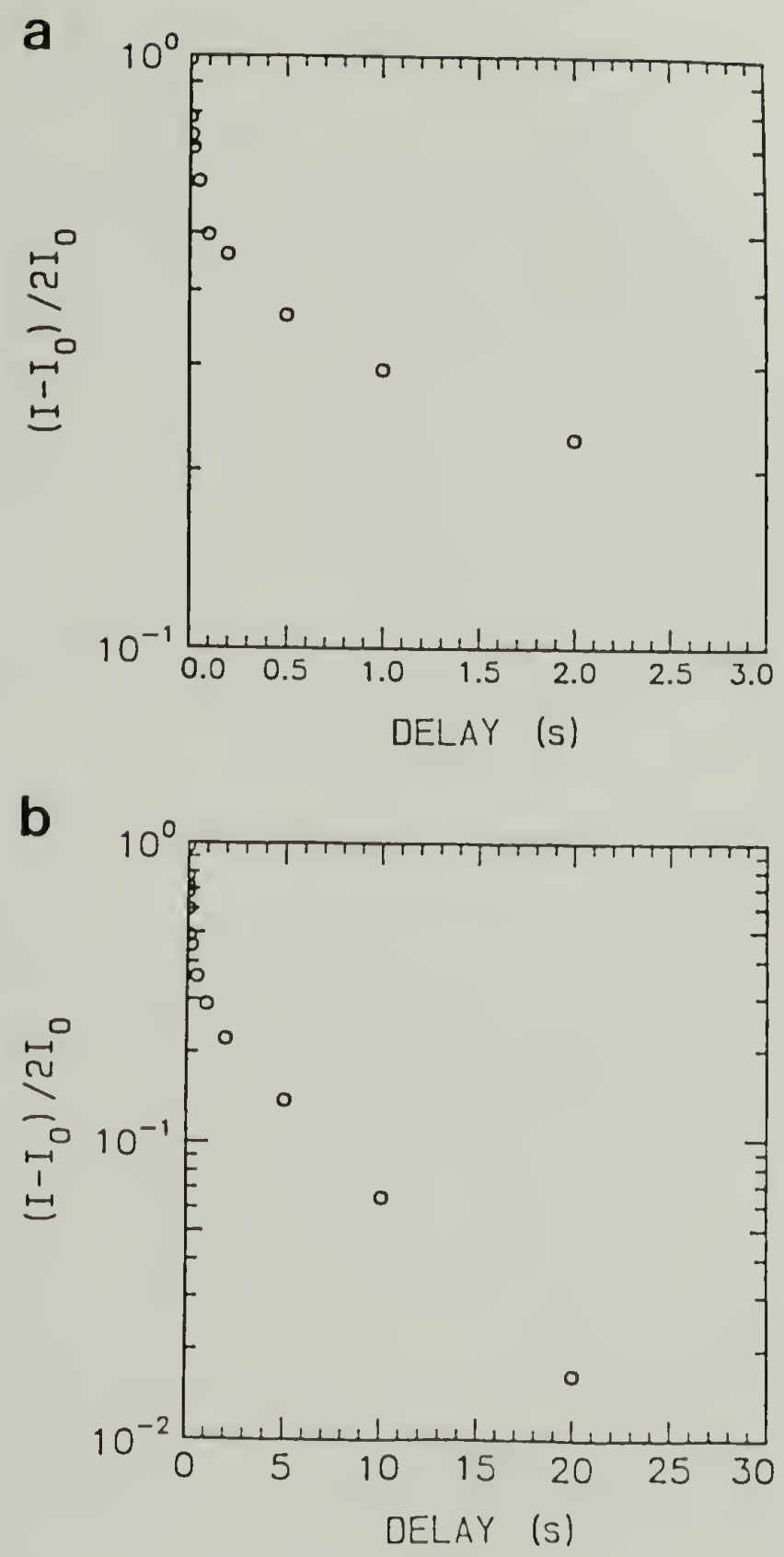

Figure 7.6 Logarithmic plot of scaled echo intensity from an inversion recovery quadrupole echo versus delay time (75 °C) a) for delays between 0.0 s and 3.0 s and b) for delays up to 30.0 s.

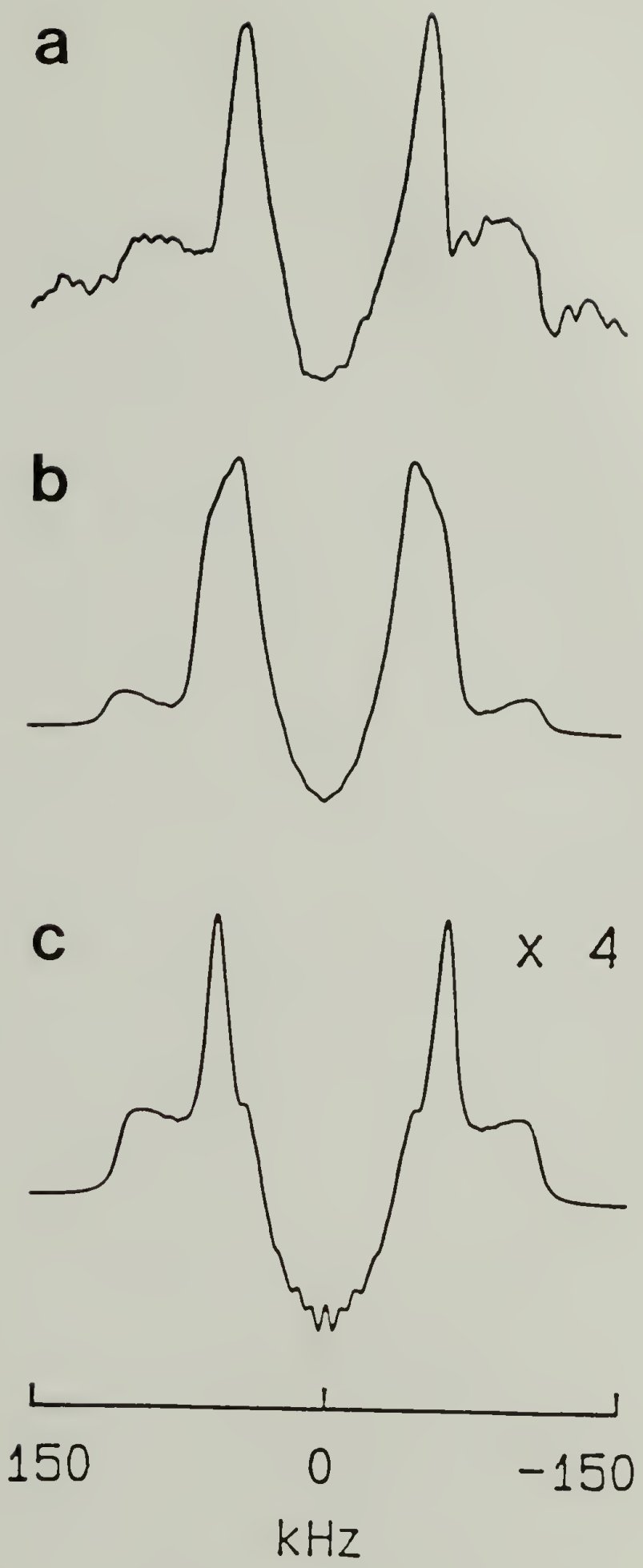

Figure 7.7 a) Partially relaxed inversion recovery quadrupole echo NMR spectrum of PPV-d_2 obtained at 225 °C with DE = 12 ms, near the null point; b) simulation based upon a 180° jump about the chain axis (Figure 7.4a) ($k = 6 \times 10^7\ s^{-1}$). c) a simulation based upon small angle diffusion about the chain axis (Figure 7.4b).

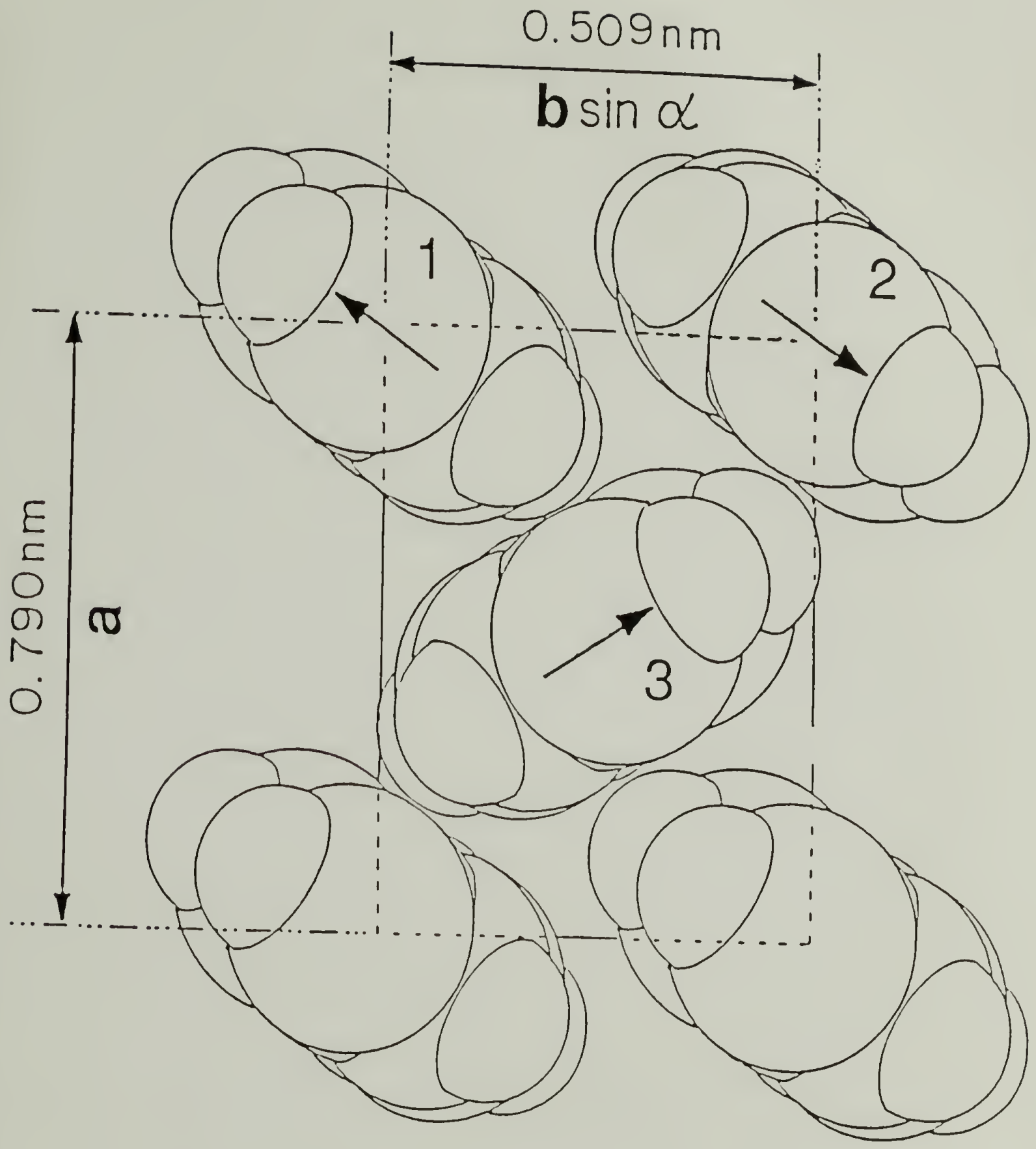

Figure 7.8 Projection of the PPV unit cell[81] perpendicular to the chain axis. The arrows point in the direction of positive phenylene ring tilt. A 180° jump motion (Figure 7.4a) at elevated temperature suggests disorder in the direction of tilt within a single plane (compare I and II).

CHAPTER 8

MEASUREMENT OF THE CHAIN ORIENTATION DISTRIBUTION IN PPV USING ^{2}H NMR

In this chapter the ^{2}H quadrupole echo NMR spectra of appropriately labeled PPV films are presented and analyzed to characterize the chain orientation distribution. As with any oriented, deuterated polymer, a drawn PPV-d_4 film, aligned in the NMR magnetic field will possess a ^{2}H spectral line shape which is dependent upon the orientation distribution of C-D bonds in the film.[137,138] The ^{2}H NMR line shape of ring-deuterated PPV (PPV-d_4) reveals the orientation distribution of the polymer chains relative to the stretching axis of the film, and thereby provides information about the chain conformational disorder. ^{2}H NMR spectra also provide measurement of the average tilt of the phenylene ring of PPV relative to the chain axis.

8.1 ^{2}H Quadrupole Echo Powder Spectra of PPV-d_4

Figure 8.1a shows the structure of PPV-d_4 in which the phenylene ring protons have been replaced with deuterium. Figure 8.2a shows the ^{2}H quadrupole echo powder spectrum of unstretched films of this material, obtained at -25 °C. The low temperature spectrum in Figure 8.2a is a Pake doublet spectrum which results from a random orientation of deuterated phenylene rings which undergo no observable molecular motion. For this spectrum the measured quadrupole splitting, $\Delta\nu_Q$ = 133±1 kHz and the asymmetry parameter, η = 0.03±0.01. A simulation is shown in Figure 8.2b and the quadrupole tensor components are shown in Table 8.1. These values are similar to those obtained for other deuterated phenyl and phenylene rings.[104,105,172]

It is noted that ^{2}H powder spectra of PPV-d_4 films which have been stretch-oriented and subsequently cut into pieces are similar to the spectra of unstretched PPV.

Stretching of PPV films has no effect upon the quadrupole coupling parameters nor upon the percentage of rings which undergo fast jumps at room temperature. If ring flips indicate regions of conformational disorder, stretching does not change the size of these regions.

8.2 ^{2}H Quadrupole Echo Spectra of Aligned Films of Oriented PPV-d_4

Figure 8.3 shows the ^{2}H quadrupole echo spectra of a partially oriented PPV-d_4 film which has been aligned in the NMR magnetic field. These spectra were obtained at -58 °C, a temperature at which the effects of ring motion are absent. The spectrum of Figure 8.3a was obtained from a sample with the stretching axis aligned at $\Theta = 0°$ to the magnetic field axis $\mathbf{B}_0$. For Figures 8.3b and 8.3c the stretching axis was tilted at $\Theta = 15°$ and $\Theta = 90°$ respectively. The spectrum of Figure 8.3a can be described as the sum of two components, a line shape similar to a Pake doublet which causes the outer splitting and a narrower line shape which appears to have a flat top. The narrow component can be attributed to PPV crystallites which are well oriented with their **c** axes close to the stretching axis. The broader component can be attributed to more poorly oriented crystallites.

For phenylene ring deuterated PPV, well oriented and poorly oriented chains can be expected to show distinguishable spectral shapes and one can expect to obtain precise details about structure unique to the spectra of oriented phenylene rings. The C-D bonds of a phenylene ring are oriented at 60° relative to the 1,4 ring axis, and for a PPV chain oriented near the magnetic field direction (Figure 8.1a), the C-D bonds are oriented at angles in the region of the magic angle, 54.7° to the field. At 54.7° the quadrupole splitting is zero, and a well oriented PPV chain should have a maximum intensity near zero frequency. In contrast, poorly oriented chains have a lineshape resembling a Pake doublet, regardless of the geometry of the C-D bond. Near 54.7° the quadrupole splitting is also most sensitive to changes in orientation, and the ^{2}H spectrum

of PPV shows this sensitivity. For comparison, the C-D bonds of an all-*trans* polymethylene chain are oriented 90° to the chain axis and the quadrupole splitting for a perfectly oriented polymethylene chain is similar to that of the Pake doublet.[x250] At an angle of 90° the quadrupole splitting of a C-D bond is much less sensitive to small changes in orientation.

8.3 Characterization of ^2H Line Shapes for Oriented PPV

The spectra of Figure 8.3 are compared with calculated simulations and can provide quantitative data about the crystallite orientation and chain structure in stretched PPV films. The calculated ^2H spectra presented here are based upon the current model for PPV structure as determined by x-ray and electron diffraction and by transmission electron microscopy.[47,75,81,82] In this model PPV films are thought to contain crystalline domains with an average crystallite size of 7 nm. The crystallinity is high and the above techniques provide no evidence for separate amorphous domains, though some disorder must be present at domain boundaries. Tensile stress during elimination causes orientation of the crystallite **c** axes and an orientation function of 0.90 or greater can be obtained for draw ratios less than $l/l_0 = 10$.[61]

Individual PPV chains are assumed to be present in the all-*trans* configuration (Figure 8.1a) with the chain axis oriented close to the crystallite **c** axis. The PPV chain is assumed to be planar and assumed to have a structure similar to *trans*-stilbene; all vinylene groups are assumed to be parallel to each other in a *transoid* structure.[75] For this structure (Figure 8.1a) the 1,4 axes of each phenylene ring should also be parallel to each other. The stilbene geometry predicts an angle of 9.2° between the phenylene ring axis and the crystallite **c** axis. This angle is referred to as the phenylene ring tilt and represented with the symbol Ψ.

Figure 8.4a shows the calculated ^2H line shape which is expected for a nearly perfectly oriented PPV film (crystallite misalignment of ±1°) with its stretch axis aligned

parallel to the magnetic field direction. The line shape consists of two quadrupole doublets which are associated with C-D bonds oriented at each of two angles to the chain axis (Figure 8.1a); the deuterons of the phenylene ring are oriented at 60° to the 1,4 ring axis. It can be seen from Figure 8.1a that deuterons at carbons C2 and C5 are oriented at an angle less than 60° to the chain axis due to the tilt of the phenylene ring. The inner splitting can be attributed to the deuterons at C3 and C6 which are oriented at an angle greater than 60° to the chain.

Figures 8.4b-e show the calculated line shapes expected for several other distributions of crystallite orientation of greater width. For the calculation of these line shapes the distribution of crystallite **c** axes was assumed to be a Gaussian function of the angle between the chain axis and the stretching axis as shown in Equation (8.1).

$$P(\alpha,\beta,\gamma) = \exp(-(\beta/\Delta\beta)^2) \qquad (8.1)$$

where the angular width $\Delta\beta$ is defined as the angle corresponding to $P(\alpha,\beta,\gamma) = 1/e$. The angles α, β and γ are the Euler angles that orient the C-D bond with respect to the magnetic field $\mathbf{B}_0$. Figure 8.2f is the Pake doublet line shape resulting from a completely isotropic distribution of crystallites.

The two components of Figure 8.3a can each be associated with a line shape similar to Figure 8.4 (calculated from a Gaussian crystallite distribution) and the spectrum can be simulated with a sum of these two line shapes. The crystallite orientation distribution can therefore be represented empirically by a sum of two Gaussian functions with different widths. The spectrum obtained at the $\Theta = 0°$ orientation can be deconvoluted into a narrow line shape similar to Figure 8.4, $\Delta\beta = 10°$ and a doublet similar to Figure 8.4, $\Delta\beta = 30°$. The two line shapes have intensities in a ratio of 1:0.67±0.01. A Hermans orientation function, f = 0.85 has been be calculated for the two component distribution. This value is consistent with that obtained from infrared dichroism data.[60]

The spectra of the films which have been rotated at angles of Θ = 15° (Figure 8.3b) and Θ = 90° (Figure 8.3c) are consistent with the two component Gaussian distribution. The overall change in spectral shape with alignment angle, Θ, is reproduced in simulations (Figures 8.3d-f). Observation of the expected change in spectral shape with film rotation verifies that the spectrum of Figure 8.3a is indeed the result of oriented chains.

Two features of the spectra and simulations of rotated films should be noted. First, the spectra at all orientations lack the step-function edges which are usually associated with the Pake doublet spectrum of an isotropic distribution. The lack of such edges distinguishes the spectrum of a 30° distribution (Figure 8.4, 30°) from that of an isotropic distribution (Figure 8.4, PAKE) and suggests that there are no unoriented segments within these films. Second, the apparent frequency difference between the peaks of Figure 8.3c (Θ = 90°) is about 3% greater than that between the peaks of Figure 8.3a (Θ = 0°). Also, this difference is 3% greater than that of the powder spectrum of Figure 8.2a. Simulations reproduce this change. The change in splitting can be attributed to the effect of the axial asymmetry of the C-D bond (η = 0.03) upon the line shape of the Θ = 90° orientation. The change cannot be attributed to a change in the quadrupole coupling tensor components with stretching because stretching does not affect the quadrupole splitting as measured from the powder spectrum. The 3% change in splitting also distinguishes the spectrum of the 30° distribution from that of the isoptropic distribution and establishes that all PPV segments in these samples are oriented. If a substantial population of unoriented PPV were present, a second narrower splitting would be present in Figure 8.3c.

The change also establishes that ν_{yy} (the quadrupole coupling tensor component perpendicular to the ring) is greater than ν_{xx}. If the opposite were true, the quadrupole splitting of Figure 8.3c would be 3% smaller than the powder splitting. It is important to note that this relationship between ν_{yy} and ν_{xx} is also necessary for the simulation of

the 30 kHz splitting of the ring flip component of Figure 8.2b and the asymmetry parameter of η = 0.63. The consistency of these two details supports the assumption that the ν_{zz} component of the quadrupole coupling tensor is oriented precisely along the C-D bond, and deviation of the ring flip asymmetry parameter from 0.60 can be attributed entirely to the rigid lattice asymmetry parameter of the C-D bond. The relative magnitudes of ν_{xx} and ν_{yy} are also consistent with the assignment of chemical shift tensor axes of aromatic rings.[109]

8.4 The Dependence of the Orientation Upon Draw Ratio

Figures 8.5a-c show three ^2H spectra of PPV films stretched to various draw ratios (l/l_0= 2.0, 3.0 and 6.0). Increasing the draw ratio decreases the intensity at outer frequencies of the spectrum and increases the intensity of the central component. These spectra have been simulated with the distribution used for Figure 8.3 (a sum of two Gaussian functions with $\Delta\beta$ = 10° and $\Delta\beta$ = 30°), and this distribution provides a good fit, as shown in Figures 8.5d to 8.5f. The two Gaussian functions have been weighted differently for each draw ratio, and the fractions P_{10} and P_{30} are shown for each draw ratio in Table 8.2. It should be noted that within the precision of these spectra, there is no need to alter the value of $\Delta\beta$ or add extra Gaussian components. The draw ratio dependence of ^2H spectra can be fit by changing one parameter, P_{10} (P_{30} = 1 - P_{10}).

An alternative fitting procedure can be employed in which the Gaussian width, $\Delta\beta$, is varied to fit the spectrum obtained from a PPV sample at each different draw ratio. For example, Figure 8.3a is adequately simulated by Figure 8.4, 20°. This method has not been used because it is inconsistent with the model of the well ordered crystallite surrounded by poorly ordered grain boundaries.

Table 8.2, column 3 also shows the value of the Hermans orientation function, f_{Gauss}, derived from each distribution. Column 6 contains the values of the orientation function, f_{IR}, obtained from the infrared dichroic ratios of similarly stretched,

protonated PPV films with the same draw ratio, l/l_0. For the lowest draw ratio, the orientation functions obtained from NMR and infrared spectroscopy are in good agreement. For the higher draw ratios, $f_{Gauss} < f_{IR}$. At higher draw ratios the difference can be attributed to uncertainty of film alignment. Infrared data can be obtained from a single film, while NMR data must be obtained from stacked films with a corresponding uncertainty of alignment. NMR measurements do not represent the narrowest components of the orientation distribution.

It is useful to compare the experimental spectra of Figure 8.5 with those which would result from the pseudo-affine or Kratky model.[161,183] The pseudo-affine model provides a theoretical relationship between orientation distribution and the experimental draw ratio, and has been used previously to characterize PPV orientation data obtained from the infrared dichroic ratio. It has been shown that PPV orientation is better than that predicted by the pseudo-affine model.[60,61] In particular the experimental orientation function, f_{IR}, obtained from the infrared dichroic ratio, is greater than that obtained by integration of the Kratky distribution when $l/l_0 = k$. The Kratky distribution is shown in equation 8.2 where α, β and γ have definitions the same as in Equation 8.1:

$$P(\alpha,\beta,\gamma) = \frac{k^{3/4}}{(k^{3/2}\sin^2\beta + k^{-3/2}\cos^2\beta)^{3/2}} \qquad (8.2)$$

The single parameter, k, is compared with the experimental draw ratio. Simulations of the experimental spectra with this distribution are shown in Figures 8.5g to 8.5i. The best fit values of k for each simulation with the Kratky distribution are shown in Table 8.2, column 4, along with the calculated orientation function, f_{Kratky} in column 5. For the draw ratios $l/l_0 = 2.0$ and 3.0 the Kratky distribution provides a reasonable fit of the experimental spectra, especially in the low frequency center of the spectrum. However, there are subtle differences between the high frequency edges of the experimental spectra and Kratky simulations. The best fit simulations with the Kratky

distribution include step-function edges which are not evident in experimental spectra. Also, the orientation functions derived from the Kratky distribution, f_{Kratky}, are smaller than those determined from the best fit Gaussian distribution, f_{Gauss}. The values of f_{Kratky} are also less than f_{IR}, the experimental orientation function determined from infrared dichroism.

For the draw ratio l/l_0 = 6.0, the Kratky simulation (Figure 8.5i) provides a reasonable fit to the edges of the spectrum and f_{Gauss} and f_{Kratky} are closer in magnitude. However, the center of the simulation of Figure 8.5i contains some structure which is only partially evident in the experimental spectrum. This structure can be attributed to a fraction of chains whose orientation angle is less than 10°. The spectrum of Figure 8.5c does not contain this structure, however, these very highly oriented chains should be unobservable due to the uncertainty of film alignment.

^{2}H NMR data suggest why the orientation functions determined from the infrared dichroic ratio are greater than those predicted by the pseudo-affine model. The step-function edges of the Kratky simulations result from very poorly oriented chains (at close to 90° to the stretching axis). The pseudo-affine model overestimates the number of these chains, resulting in the calculation of a substantially lower orientation function and dichroic ratio. The fraction of chains in the overestimation can be determined from the integrals of the spectra and simulations, and it should be noted that only a small fraction of chains are involved. These chains, however, substantially lower the orientation function because they are oriented at close to 90° to the stretching axis. For the low draw ratios the pseudo-affine model provides a good fit to the orientation distribution of the majority chains with low orientation angle and it can be seen in Table 8.2 that the values of k obtained by simulation (neglecting the difference at the edges) are similar to the experimental draw ratios. At high draw ratios, the pseudo-affine distribution properly describes the chains with large orientation angle, but overestimates the fraction of chains with alignment better than β = 10°.

Figures 8.3 and 8.5 show that, with the above qualifications, the orientation distribution for most of the segments of stretched PPV could readily result from the assumptions of the pseudo-affine model. It should be emphasized that the poorly oriented component of the empirical distribution does not necessarily represent a distinguishable domain, and that segments in both crystallites and boundary domains have orientations at least as good or better than that predicted by the pseudo-affine model.

The spectra of Figures 8.3 and 8.5 do not provide information about the relationship between domain structure and orientation. Dark field TEM pictures have suggested, however, that boundary domains may contribute preferentially to the broad component of the orientation distribution.[75] TEM data obtained from a partially oriented film similar to that of Figure 8.3 do not show a significant number of crystallites at angles greater than 10° from the stretching axis.[73] These data suggest that the more poorly oriented segments observed by NMR may exist within boundary domains where they are not observable by TEM.

8.5 ^{2}H Quadrupole Echo Spectra of Oriented PPV-d_4 at 25 °C

Figure 8.6 shows the ^{2}H spectra of an oriented PPV film obtained at 25 °C. The spectrum of Figure 8.6a, aligned at $\Theta = 0°$ to the field shows the presence of the two components of Figure 8.3a, but also contains an additional doublet with a quadrupole splitting about 25% of the Pake doublet splitting. This doublet can be attributed to the phenylene rings of well oriented crystallites which undergo rapid 180° rotational jumps. A similar spectrum has also been reported for the phenylene rings of an oriented side chain liquid crystalline polyacrylate, as shown by Pschorn *et al.*,[137] and our calculations show that it should also be expected for PPV. Figure 8.6d shows a simulation of Figure 8.6a which results from an orientation distribution with Gaussian components similar to those of Figure 8.3, except that 10% of the phenylene rings are represented by a fast

jump line shape. Rotation of the film axis away from the field axis (increasing Θ) causes the oriented ring flip doublet to disappear (Figures 8.6b and 8.6c). This disappearence is expected and has been reproduced in simulations (Figures 8.6e and 8.6f).

For semicrystalline polymers containing phenylene rings it has been noted that fast ring flips occur principally in amorphous or crystallite boundary domains[115] (including two related structures, poly(*p*-phenylene)[184] and polyaniline[173]). However, the observation of a well oriented ring flip component for PPV indicates that within the experimental precision of these spectra there is no correlation between the ring flip motion and orientation. Ring flips must be found in both well oriented and poorly oriented domains. If, as TEM data suggest, the well oriented domains are principally crystallites and the poorly oriented domains are principally boundary domains, then one must conclude that ring flips are present in crystallites as well as boundary domains. The temperature dependence of ^2H spectra also supports this conclusion.

These spectra do not rule out a more subtle relationship between ring flip motion and orientation. The powder spectrum of Figure 8.2b indicates a 15% fast jump component while Figure 8.6 indicates a 10% component. Also Figure 8.6 indicates a smaller percentage for the $\Delta\beta = 30°$ distribution than Figure 8.3. More precise simulation of the spectra of Figure 8.6 is possible, but this simulation would also require consideration of anisotropic T_2 decay and additional knowledge of the ring flip rate distribution. With the additional parameters, line shape simulation would not yield a clear answer, though two new two-dimensional NMR methods could provide additional data.[134,135] Stretched PPV films with their good orientation provide an excellent opportunity to study the mechanism of the ring flip motion and its relationship to orientational order.

8.6 Determination of the Phenylene Ring Tilt Angle

Simulation of the spectra of Figure 8.3 allows experimental determination of the angle of phenylene ring tilt, Ψ, relative to the chain axis. Figure 8.7 shows a set of simulations for Figure 8.3a for three tilt angles Ψ = 6.5°, 7.7° and 9.0°. A tilt angle of 7.7±0.5° has been found to best fit the experimental width of the central component of Figure 8.3a. Also, the use of a 7.7° tilt angle leads to values of the orientation function (Table 8.2) consistent with those obtained from infrared dichroism measurements. The experimental value is close to the value of 9.2° predicted for PPV with a *trans*, *transoid* configuration and a stilbene geometry, and the observation of phenylene ring tilt supports the assumption that PPV chains are well organized in this structure. The phenylene ring tilt has also been obtained from the measurement of infrared dichroism of protonated films (Ψ = 9°).[60,61]

NMR line shapes clearly distinguish a tilt angle of 7.7° from an angle of 9.2°. The width of the central component of Figure 8.7a is greater than that of Figure 8.7b and greater than the experimental width. Such a precise measurement of tilt is possible because the C-D bonds of well oriented chains are close to the magic angle (54.7°) where the quadrupole splitting is very sensistive to angle. Also, the orientation width ($\Delta\beta$ = 10°) is of the same magnitude as the tilt angle (Ψ = 7.7°), and so the effects of both parameters are equally evident in simulations. In particular, the tilt angle affects the frequency splitting of the deuterons at C3 and C6. For an orientation distribution with a finite width the two doublets are not distinguished and the result is apparent as a change in the overall width of the line shape. For a larger tilt angle the spectrum is broader with a more rectangular shape, and for a small tilt angle the spectrum is narrower and has a peak.

The 1.5° deviation can be attributed to disorder within the PPV structure, either within crystallites or at domain boundaries. To obtain a planar, *trans*, *transoid* PPV structure with a 7.7° tilt angle, the PPV segmental length would have to be stretched by

0.1 nm or the vinylene bond length would have to be decreased by 0.02 nm. Such structures would have chemically unlikely bond lengths and angles and would be in conflict with diffraction data. The deviation could, however, be explained with a non-planar PPV structure containing static rotational disorder about the phenylene-vinylene bonds. The planar PPV structure has a maximum value of phenylene ring tilt. Small angle rotation about phenylene-vinylene bonds would reduce the angle between the C-D bonds of C3 and C6 and the crystallite c axis and lead to a smaller apparent tilt angle.

Alternatively, the experimental tilt angle could result from a planar chain containing one or more segments in a *trans*, *cisoid* structure (Figure 8.1b). In this structure a single vinylene group is aligned in an opposite direction from its neighbors, and for a structure with an alternating *cisoid* configuration the phenylene ring tilt angle is zero. The 7.7° experimental tilt angle might be attributed to one cisoid configuration in about twelve segments. It should be noted that twelve PPV segments would easily span the crystallite length of 7 nm. A *cisoid* defect at the crystallite boundary would tilt the PPV chain about an axis perpendicular to its plane and and reduce the phenylene ring tilt angle relative to the crystallite c axis.

Table 8.1

Quadrupole Tensor Components in kHz for PPV-d_4

all values are ±1 kHz

	ν_{xx}	ν_{yy}	ν_{zz}
Rigid Lattice (-58 °C)	138	128	-266
Rigid Lattice (25 °C)	137	130	-266
Ring Flip (25 °C)	-168	137	32

Tensor axes are defined in the chapter 3

Table 8.2

Simulation Parameters and Orientation Functions
for the Spectra of Stretched PPV-d_4
at Three Draw Ratios

l/l_0	P_{10} ±0.02	P_{30} ±0.02	f_{Gauss}	k ±0.1	f_{Kratky}	f_{IR}
2.0	0.16	0.84	0.72	2.4	0.55	0.72
3.0	0.42	0.58	0.79	3.2	0.68	0.84
6.0	0.66	0.34	0.86	5.1	0.81	0.92

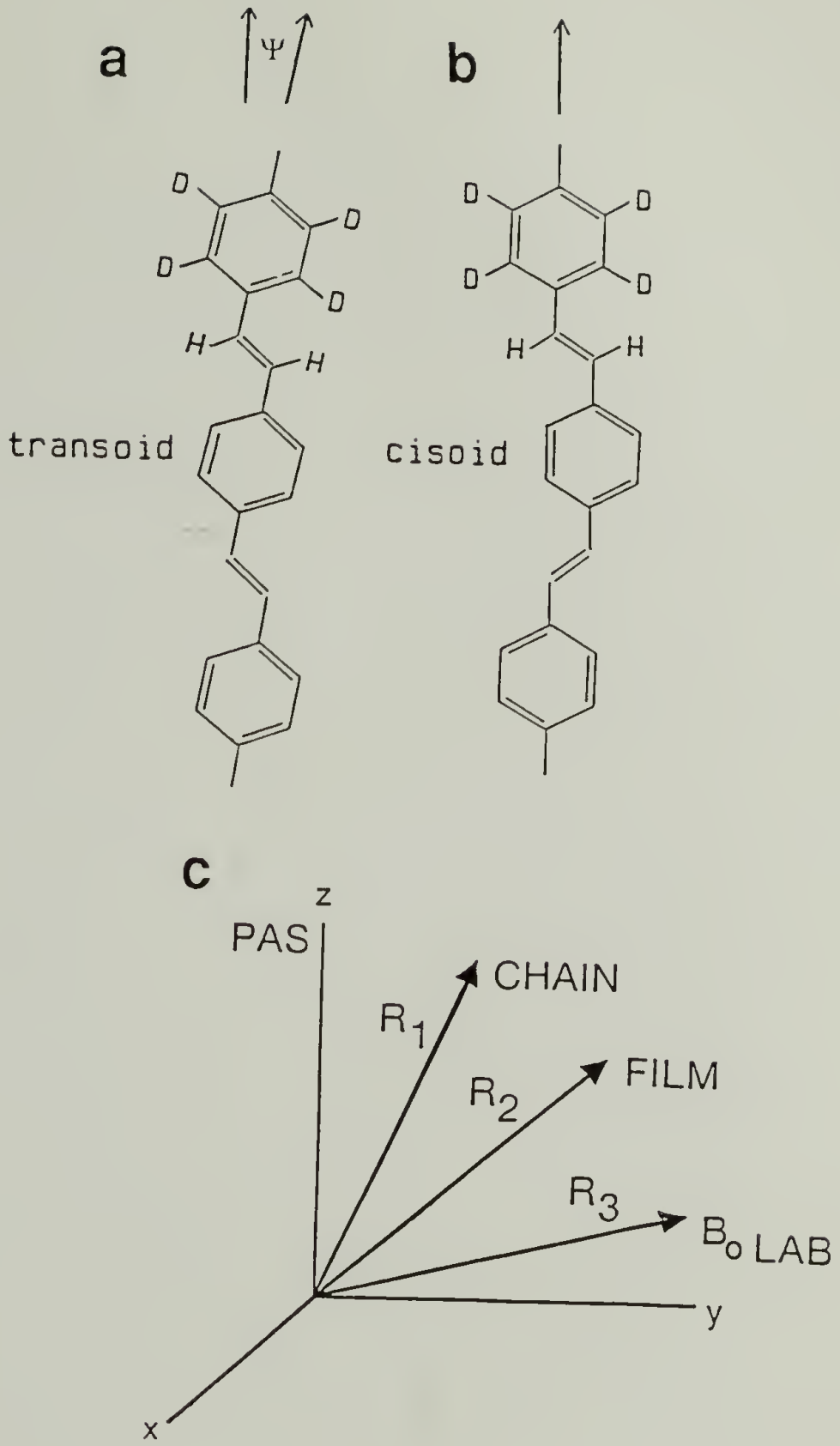

Figure 8.1 PPV structures showing coordinate axes and angles used to calculate the spectra of oriented films. a) All-*trans*, *transoid* structure with stilbene-like geometry; b) All-*trans*, *cisoid* structure; c) The magnetic field vector $\mathbf{B}_0$ is expressed in the C-D bond PAS through three rotation matrix transformations.

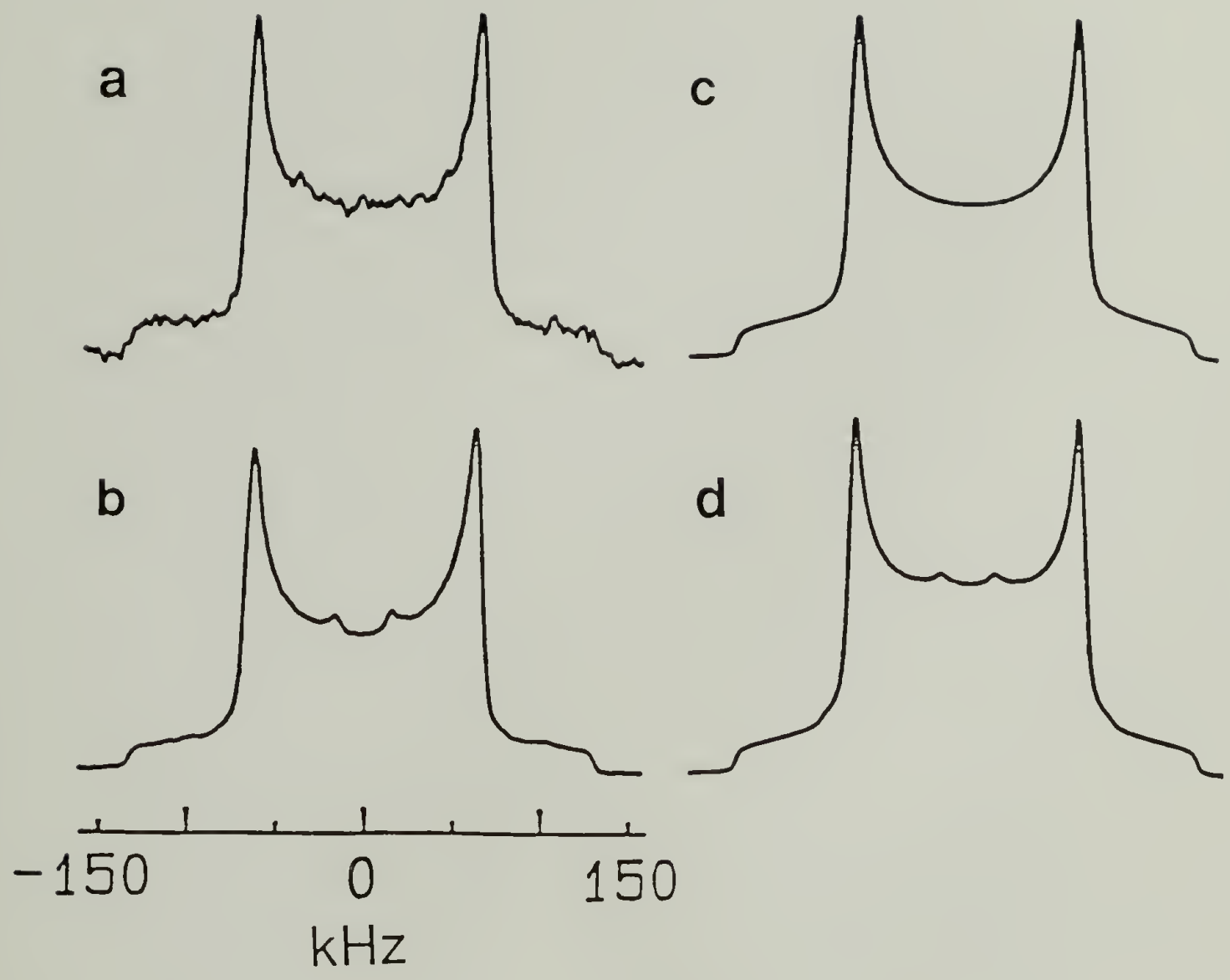

Figure 8.2 ^{2}H quadrupole echo NMR spectra of unoriented PPV film (25 mg) at a) -25 °C and b) 25 °C and their simulations c) $\Delta\nu_Q$ = 133 kHz and η = 0.03 and d) the sum of $\Delta\nu_Q$ = 84 kHz and η = 0.63) plus ($\Delta\nu_Q$ = 133 kHz and η = 0.03) in a 1:5.7 ratio.

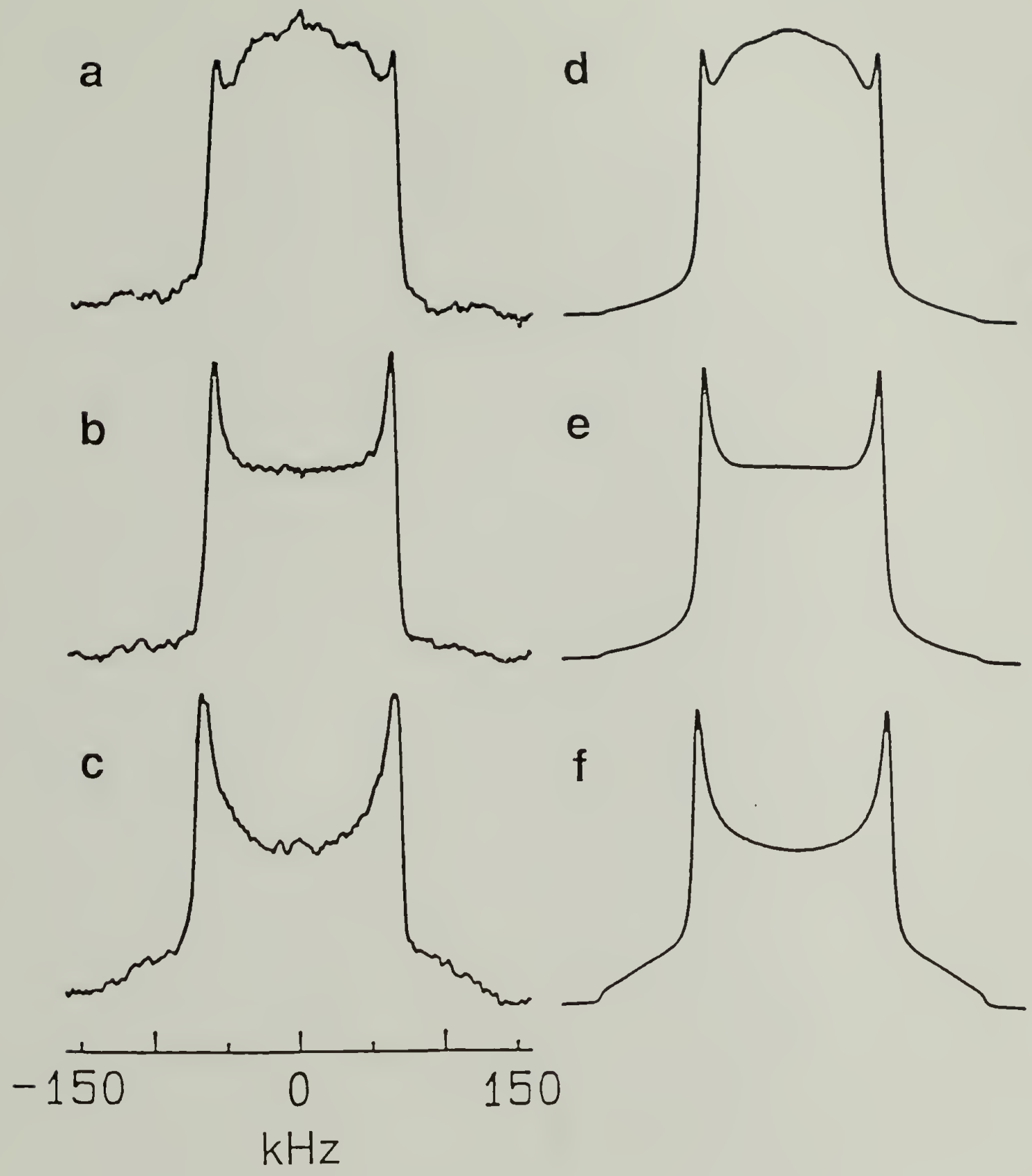

Figure 8.3 ^{2}H quadrupole echo NMR spectra of aligned, stretched films of PPV (10 mg) at -58 °C for: a) $\Theta = 0°$; b) $\Theta = 15°$ and c) $\Theta = 90°$. Simulations with ($\Psi = 7.7°$ and $\Delta\beta = 10°$) narrow component plus a ($\Psi = 7.7°$ and $\Delta\beta = 30°$) broad component in a 0.67:1 ratio for d) $\Theta = 0°$; e) $\Theta = 15°$ and f) $\Theta = 90°$. Quadrupole coupling parameters as Figure 8.2c.

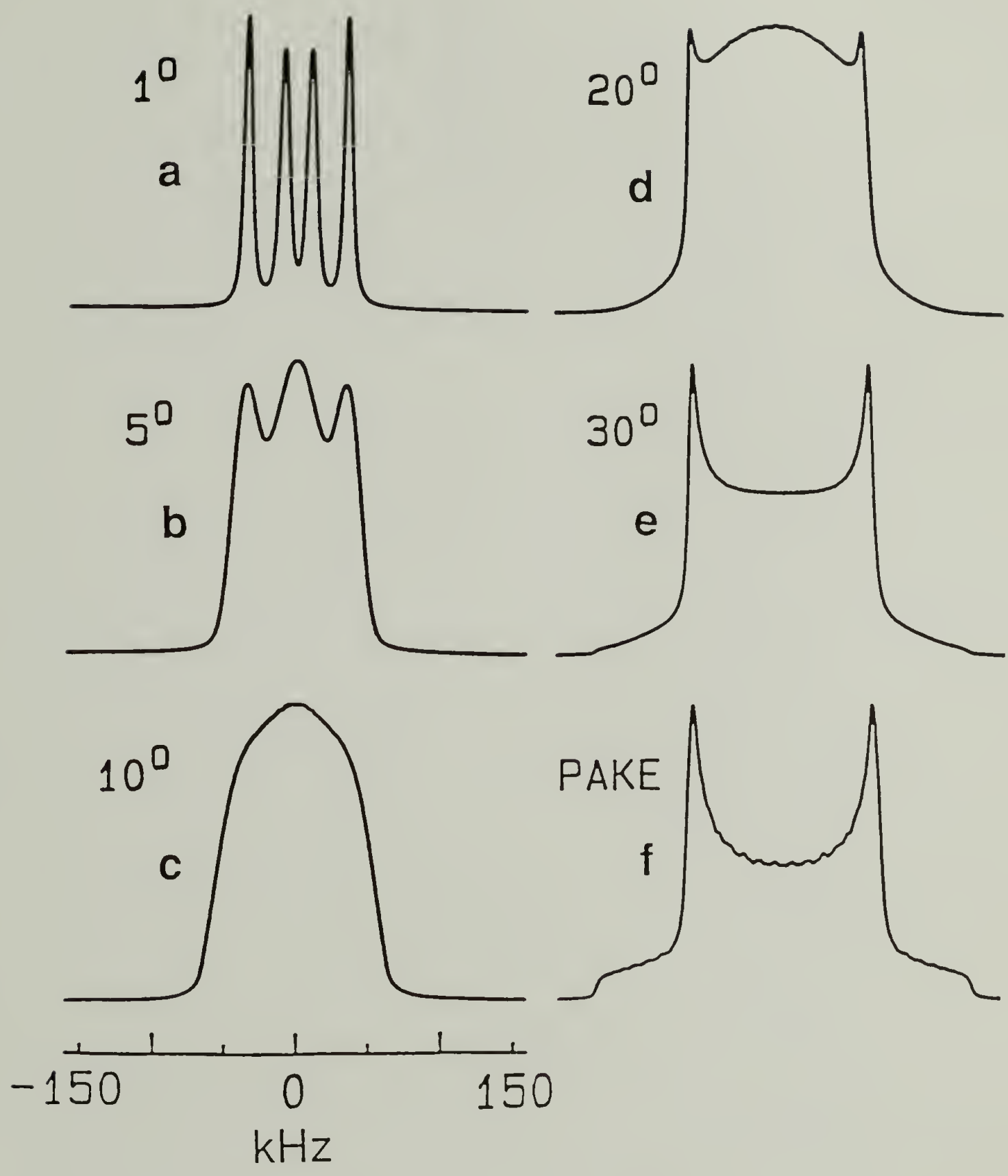

Figure 8.4 Calculated ^2H NMR spectra for several Gaussian orientation distributions with width, $\Delta\beta$, as indicated and $\Psi = 7.7°$.

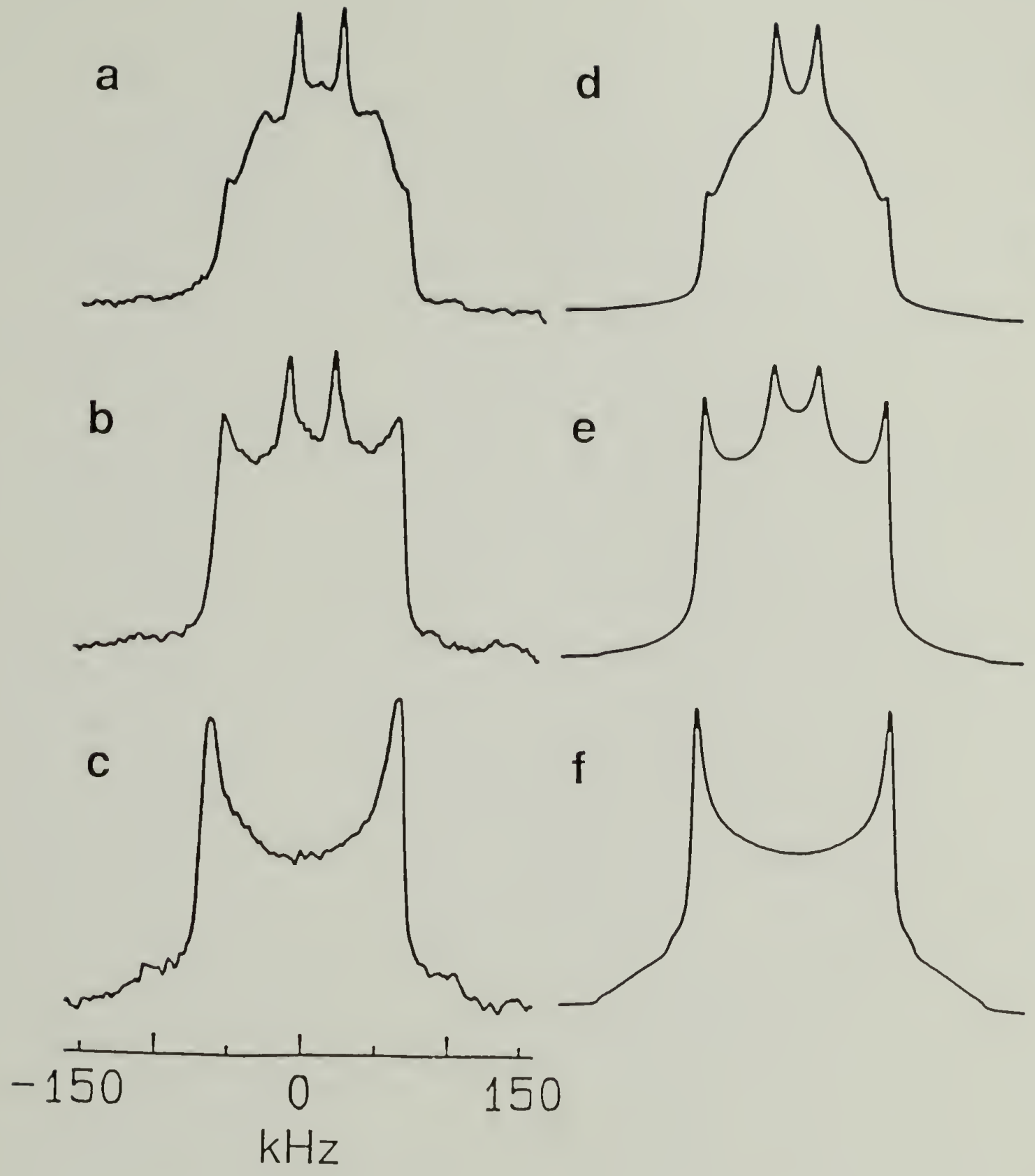

Figure 8.5 ^{2}H quadrupole echo NMR spectra of aligned, stretched films of PPV (10 mg) at 25 °C for: a) $\Theta = 0°$; b) $\Theta = 15°$ and c) $\Theta = 90°$. Simulations with ($\Psi = 7.7°$ and $\Delta\beta = 10°$) narrow component plus a ($\Psi = 7.7°$ and $\Delta\beta = 30°$) broad component in a 1.33:1 ratio, with static rings and flipping rings in a 9:1 ratio, for d) $\Theta = 0°$; e) $\Theta = 15°$ and f) $\Theta = 90°$. Quadrupole coupling parameters as Figure 8.2d.

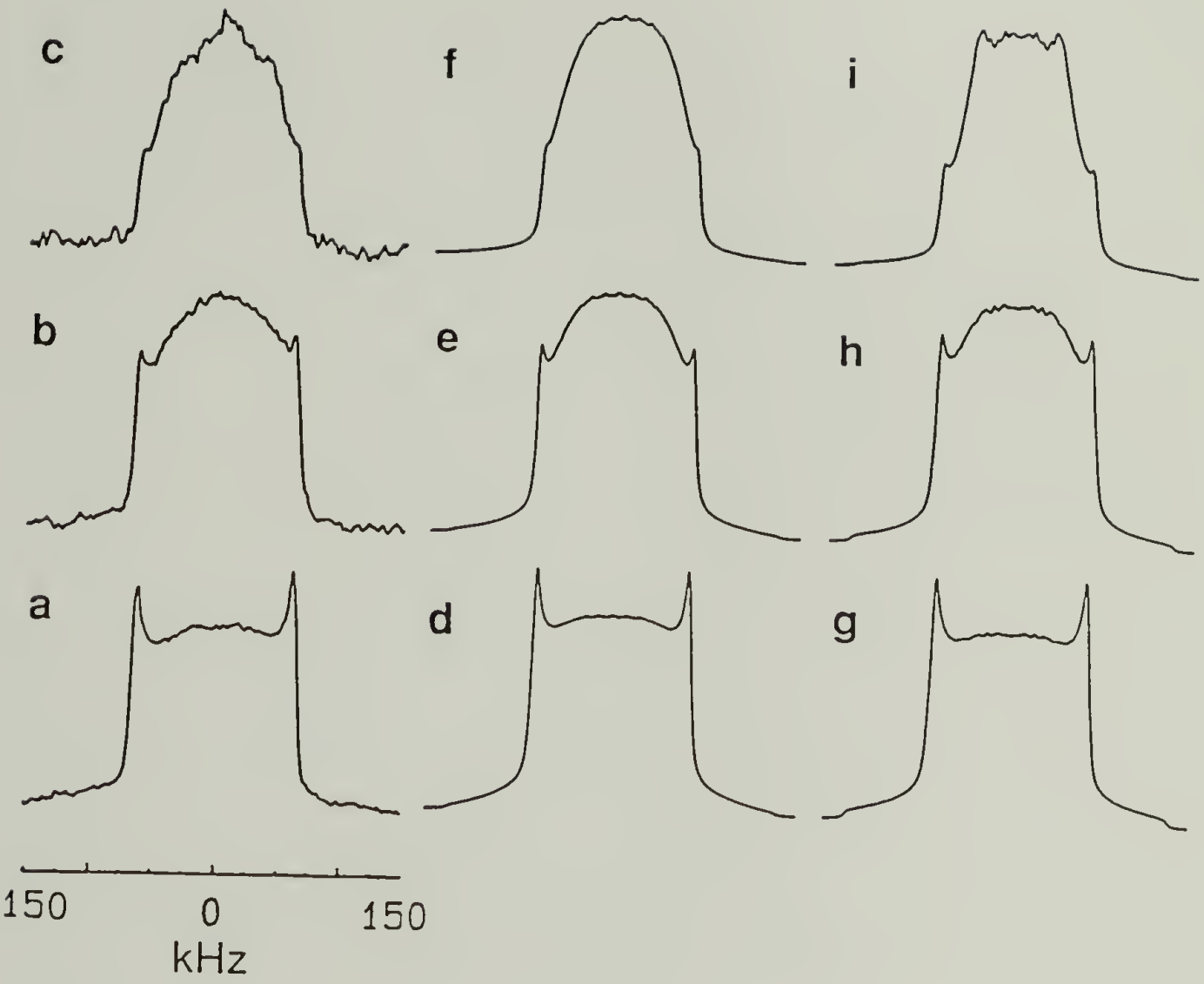

Figure 8.6 ^{2}H NMR spectra of mechanically stretched PPV aligned at $\Theta = 0°$ for several different draw ratios (left) and their simulations based upon a sum of Gaussian distributions (center) or upon the pseudo-affine distribution (right): a) $l/l_0 = 2.0$; b) $l/l_0 = 3.0$ and c) $l/l_0 = 6.0$.

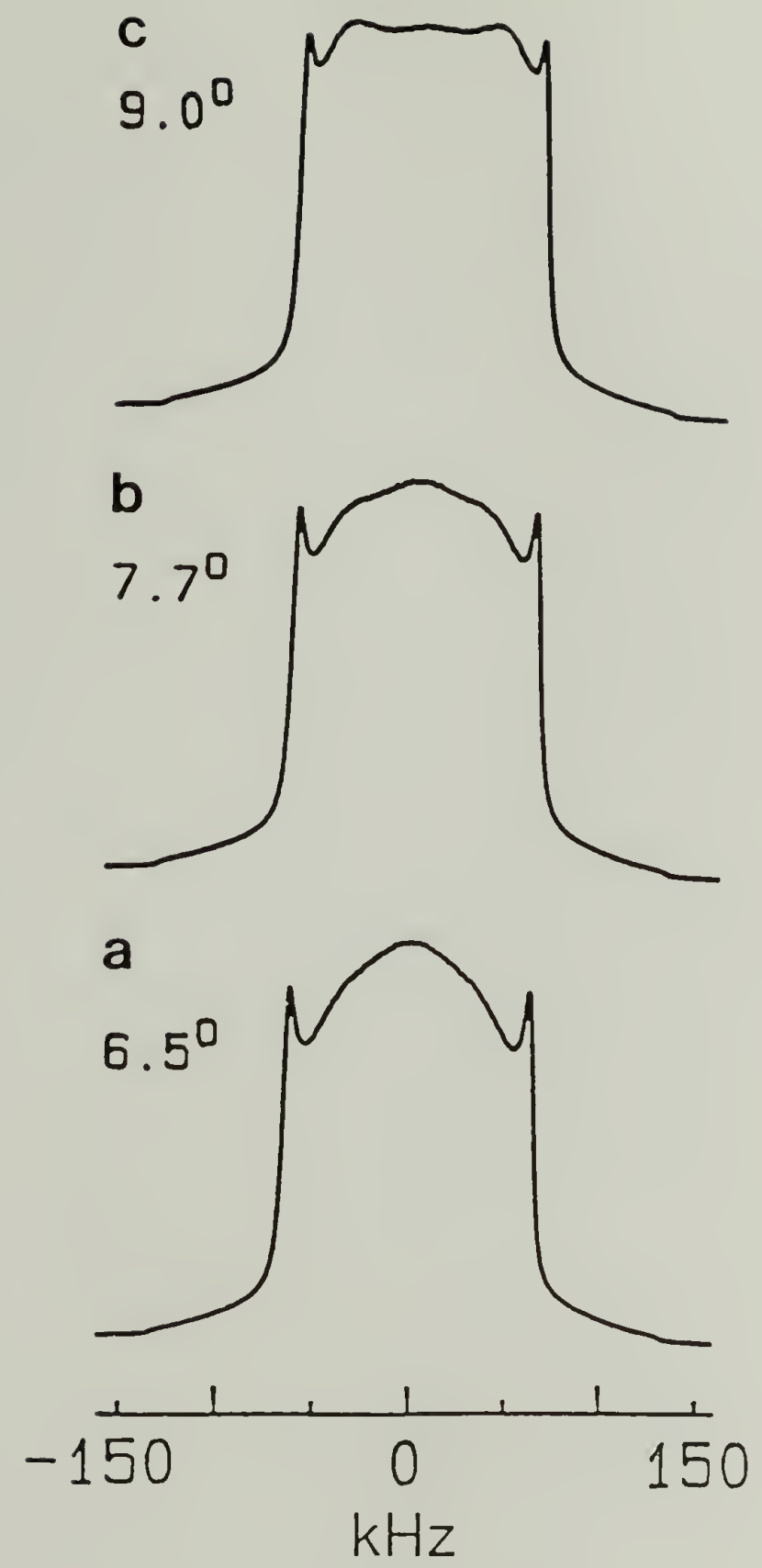

Figure 8.7 Calculated ^2H spectra for three phenylene ring tilt angles, Ψ = 6.5°, 7.7° and 9.0°. Other parameters as in Figure 8.3d.

CHAPTER 9

A STUDY OF THE SODIUM DOPING OF PPV

This chapter focuses on the chemical and physical changes brought about in the PPV lattice upon doping with sodium vapor. By combining the data obtained with various complementary methods, a more complete picture of the n-doping process of PPV emerges. In particular, elemental analysis reveals the stochiometry of the sodium doping reaction of PPV. ESR spectroscopy has been used to follow the concentration of unpaired spins in the sample at various levels of sodium uptake. The high dopant uptake suggests that there must be substantial coulombic repulsion between adjacent sodium ions in the columnar structure of PPV observed with x-ray diffraction. Deuterium NMR of ring-deuterated PPV (PPV-d_4) reveals a component of the ^{2}H line shape which suggests the presence of sodium hydride (sodium deuteride). The abstraction of ring protons (deuterons) as hydride (deuteride) ions that pack between adjacent sodium ions in the columns of sodium ions explains the dense packing of the sodium ions in the unit cell of sodium-doped PPV. The ^{2}H NMR line shapes of sodium-doped PPV-d_4 also show that the electronic structure of the PPV chain is altered by doping. The results of these experiments are compared and contrasted to the results of Chen *et al.*[69] who have also studied the sodium doping of PPV using x-ray diffraction.

9.1 Preliminary Considerations of Sodium Doping

Figure 9.1a shows several repeat units of the PPV chain. Note that PPV adopts an all *trans* configuration with the *trans*-vinylene groups aligned in a predominantly parallel configuration.[20,60,62,81] This latter condition is referred to as the *transoid* structure of PPV. In the crystalline unit cell,[81,82] the PPV chains are aligned parallel to

each other. Viewed end-on (along the crystallographic **c** axis), the chains pack in a herringbone fashion.

Sodium doping of PPV induces a structural change in the unit cell.[69] In particular, sodium doping rearranges the unit cell of PPV such that three PPV chains surround a column of sodium ions. These structures are in turn packed in a hexagonal arrangement. The unit cell of pristine PPV is shown in Figure 9.1b and the hexagonal phase of sodium-doped PPV is shown in Figure 9.1c. Another crystal phase is also observed for sodium doped PPV at higher levels of dopant uptake (> 55% of sodium ions per repeat unit).[69] The unit cell for this structure is similar to the hexagonal phase of sodium doped PPV except that the lateral spacings are larger and the length of the repeat unit (along the crystallographic **c** axis) are reduced, suggesting that the PPV repeat unit is folded or distorted in some manner and is no longer planar. Chen *et al.*[69] have suggested that this is due to sodium ions occupying sites outside of the sodium channels.

When PPV is sodium doped, the reaction is observed to proceed in a heterogeneous manner. Figure 9.2 show this schematically. The regions of the film that are nearest to the chunk of molten sodium metal are observed to dope most quickly and those regions of the film that are farthest dope the slowest. Chen *et al.*[69] have noted that the kinetics of doping exhibit a strong dependence on doping vessel geometry. As the reaction proceeds, the PPV film will change in color from yellow-orange to dark blue and then to a metallic gold. In the limit of very long doping times, portions of the sample will take on a mottled, gray-black color with what appears to be an ashy surface texture. These three states of sodium-doped PPV have been empirically designated the blue phase, the gold phase and the gray phase.

The blue phase has also been observed by Chen *et al.*[69] at very short doping times. The ^{2}H NMR quadrupole echo NMR line shape (not shown) obtained from a sample of blue-phase, sodium-doped PPV-d_4 was virtually identical to the line shape

obtained from pristine (undoped) PPV-d_4. Chen *et al.*[69] have suggested that this phase is due to the incorporation of a limited amount of sodium ions into the PPV structure such that the amount of dopant incorporated is not sufficient to convert the bulk PPV from the pristine PPV unit cell to the hexagonal phase unit cell.

Furthermore, Chen *et al.*[69] have determined with x-ray diffraction that the transformation of the unit cell of PPV from the pristine PPV unit cell to the hexagonal phase unit cell does not proceed continuously. That is, at a certain level of sodium uptake a threshhold is reached wherein the PPV lattice undergoes a phase transition. Masse *et al.*[63] have also observed analogous behavior for various p-doped PPVs. The blue phase is hence assigned to PPV that has only incorporated a limited amount of dopant insufficient to bring about the transformation of the unit cell.

Using the experimental procedure described above, it is difficult to obtain a sample that is uniformly doped to the blue phase. Holding a typical sample of the blue phase up to an incandescent light source shows that there are still regions of undoped PPV which are translucent in the middle of what at first glance appears to be pure blue phase material. This suggests that the blue phase may be thermodynamically unstable with respect to the gold phase that corresponds to higher levels of sodium uptake. The blue phase is likely produced by the diffusion of sodium into regions of the PPV lattice which are more disordered and hence more accessable to dopant molecules

Supporting this idea is a result of Chen *et al.*[69] that the residual pristine PPV left undoped as the sodium doping reaction proceeds has slightly smaller lattice constants. That is, some of the x-ray diffraction peaks shift to slightly larger angles as the doping reaction proceeds indicating that those crystalline regions left undoped are more dense than those that first undergo doping.

Another indication that the blue phase is lightly doped PPV is that a film of blue phase material still possesses qualitatively similar mechanical properties to pristine PPV.

In sharp contrast, the gold phase material is extremely brittle. A pristine PPV film converted into the gold phase has an extremely reflective surface. Also, a 30 μm thick film of the gold phase is completely opaque. The gray phase of sodium-doped PPV also has very poor mechanical properties. Once a region of the PPV film has reached this state, its surface will no longer be shiny and its texture will appear to be rough. It is possible that this phase is due to the aggregation of small regions of sodium metal on the film surface or that the rough appearance of the film surface is caused by a complete breakdown of the PPV sample morphology. Chen *et al.*[69] have suggested that at high levels of sodium uptake, sodium ions no longer confine themselves to the channels shown in Figure 9.1c but additionally occupy interstitial sites thus distorting the PPV chains from their planar configurations. This conclusion is based on the observation that the distance of the PPV repeat unit is reduced from 0.662 nm to 0.654 nm as the dopant uptake increases from the range of 52-62% (as measured by x-ray diffraction) to some greater, unspecified value.

At the greater levels of sodium uptake corresponding to the production of saturation phase PPV, x-ray diffraction does not specifically locate the sodium ions in the lattice.[69] This indicates that x-ray diffraction alone is not ideally suited to following the incorporation of sodium into the structure of PPV.

9.2 Elemental Analysis of Sodium-Doped PPV

The ratio of carbon to sodium has been determined with elemental analysis. Table 9.1 shows the results for the blue phase, the gold phase and the gray phase. The uncertainties in the composition of the blue phase and the gray phase of sodium-doped PPV are much larger than the uncertainty determined for the gold phase material. This is due to the fact that the blue phase and the gray phase are extremely difficult to obtain in their pure forms. The sample of blue phase material that was analyzed had small regions of pristine and gold phase material present whose effects should roughly

offset but certainly add a greater uncertainty to this result. The gray phase material also had regions of the gold phase present, indicating that the sodium content should in fact be larger than the value listed for the gray phase. Columns 1 and 2 of Table 9.1 show the relative percentage by weight of carbon and sodium in the samples. Column 3 lists the number of sodium atoms per C_8H_6 repeat unit.

The elemental analysis data obtained for the gold phase of sodium-doped PPV clearly show that the doping reaction occurs with a well-defined stochiometry. This is the first report of sodium doping of PPV occuring with a well-defined stochiometry. However, potassium doping of polyacetylene has been report to occur stochiometrically.[185] For the gold phase of sodium-doped PPV, one sodium atom is incorporated into the PPV structure for every repeat unit. This level of dopant uptake is significantly higher than any other levels previously reported for PPV polymers and stretches the formal definition of this redox process as doping.

One important question that arises from this result is how do the sodium ions pack into the PPV lattice? Since the driving force for the incorporation of sodium into the PPV structure is the redox reaction in which the sodiums donates an electron to PPV, the dense packing of the sodium ions into the lattice must give rise to substantial coulombic repulsion. This is especially acute in this case because the unit cell of sodium-doped PPV confines the sodium ions in channels between three PPV chains. The **c**-axis of the unit cell measures 0.662 nm, leaving barely enough room for three sodium ions to fit. The diameter of the sodium ion is 0.195 nm,[186] implying that if the sodium ions pack three per repeat unit into these channels then the distance between adjacent positive charges is only 0.220 nm!

Chen *et al.*[69] have suggested that the increase in the lateral lattice constants (normal to the **c** axis of the unit cell) that occurs in progressing from the hexagonal phase to the saturation phase could give the sodium ions room to stagger in the channels.

This would reduce the coulombic repulsions expected for this high level of sodium uptake but not to the degree required.

9.3 ESR Results of Sodium-Doped PPV at 25 °C and -196 °C

Another important aspect of the sodium doping process of PPV is the evolution of unpaired spins as a function of the dopant uptake. Table 9.2 shows ESR results obtained from samples of the blue phase and the gold phase of sodium doped PPV-d_4. The table lists the g-values, the peak-to-peak widths, and spin concentrations at 25 °C and -196 °C. Column 1 of the table shows the g-value obtained for the two phases at the two temperatures. Note that these values (g = 2.0032 and 2.0037 for the blue phase and the gold phase, respectively) are indicative of carbon based radicals. These values are similar to those observed for polyacetylene.[3,4] Column 2 of the table gives the peak-to-peak widths of the resonances. Interestingly, the widths of the resonances decrease from around 6 G to around 4 G upon cooling of the samples - a result not expected for an organic free radical. This behavior is more characteristic of metallic than organic systems. That is, the thermal vibrations of the lattice appear to be the dominant contributor to the observed radical line widths. For most solid-state organic radicals, decreasing the sample temperature will increase the line width due to a slowing of the mobility of the radicals. For metallic systems, the radicals are confined in a finite region. Thermal vibrations serve to impede the free movement of these radicals and hence confine them to smaller regions. This reduction in mobility gives rise to an increase in the radical line width.

Column 3 of Table 9.2 shows the concentration of spins in the samples at two temperatures. Here there is another result which is not in keeping with the conventional view of organic radicals. At the lower temperatures, the concentration of spins is observed to increase, indicating that the unpaired spins are not thermally generated. Further, the concentration of spins does not scale with the amount of sodium

incorporated into the samples. That is, the concentration of spins is higher per dopant ion at low dopant ion concentrations.

This discrepancy cannot be attributed to a concentration of unpaired spins in any pristine PPV present in the blue phase because PPV is known to possess very low unpaired spin concentrations in its undoped form[97] (this was confirmed experimentally). Instead, the ESR results indicate that at higher dopant uptake, the redox reaction driving the reaction donates electrons to the PPV chains and these electrons pair to form bipolarons[21,91] or some other spinless entity. This general phenomenon has been observed to hold true for p-doped PPV and other conducting polymers. At low doping levels, the free spins (polarons[91]) are present in a low enough concentration so that they do not combine to form spinless bipolarons. At higher concentrations, however, the polarons combine and hence the concentration of spins reaches a limiting value at relatively low dopant uptakes.

The increase in the concentration of the spins for both the blue and the gold phase at reduced temperatures suggests that as the lattice cools, bipolarons are broken up to form polarons. The most obvious phenomenon associated with cooling of a solid material is that the lattice motions decrease. Chen *et al.*[69] have observed that cooling of the sample slightly shrinks the lateral unit cell parameters by approximately 1%. This small shrinkage may well be the reason for the increase in spin concentration at low temperatures. The geometrical distortions of the PPV chains caused by cooling may disrupt the extended conjugation between widely separated repeat units. Where there are already significant distortions of the PPV chains, the slight shrinkage of the lattice may kink the chains sufficiently so that some of the bipolarons are broken up into polarons. That is, the slight shrinkage of the PPV lattice may shift the equilibrium of paired versus unpaired electrons for a small fraction of the PPV chains in the samples.

9.4 ^{2}H NMR Line Shape of Sodium-Doped PPV-d_4 at 25 °C

Futher insight into the doping process is gained by examining the changes brought about in the ^{2}H NMR line shape of ring-deuterated PPV upon sodium doping. PPV-d_4 is known to undergo thermally-activated *p*-phenylene ring flips at ambient and super-ambient temperatures (see chapter 5). Cooling a sample of PPV-d_4 will cease the flip motion of the rings on the NMR time scale and yield a ^{2}H NMR line shape known as the Pake line shape.[177] Figure 9.3a shows the line shape obtained from a sample of pristine PPV-d_4 at a low temperature. The quadrupolar splitting, $\Delta\nu_Q$ is 133 kHz and the asymmetry parameter, η, is 0.03.

The activation energy of the PPV-d_4 ring flip has been measured in chapter 5. H_2SO_4 doping of PPV-d_4 is observed to increase the ring flip activation energy from 15 kcal/mol to 21 kcal/mol (see chapter 6). There are two potential reasons for this increase. One is that the electronic structure of the PPV backbone may be altered. Specifically, doping of the PPV chain may introduce more double bond character into the single bonds about which the rotation occurs. The other possibility for the increase in the ring flip activation energy could be due to steric considerations. H_2SO_4-doped PPV is known to possess a different crystal structure than does pristine PPV.[22,63] Along with a new unit cell, the steric constraints imposed on the phenylene rings may well be significantly different. Because sodium doping of PPV is known to change the crystal structure of PPV and also changes the electronic structure of the polymer backbone, it was expected that sodium doping might similarly effect the rates of phenylene ring flips as measured by ^{2}H NMR.

Figure 9.3b shows the line shape obtained from a sample of sodium-doped PPV-d_4. This line shape is composed of two distinct components (and perhaps three). One can clearly be attributed to static deuterons still on the *p*-phenylene rings, the other(s) is(are) less clear. The second component is narrower, with a splitting, $\Delta\nu$, of 64 kHz. There may, in addition, be a third component at ±0 kHz. Figure 9.3c shows the line

shape that results after subtraction of the standard Pake pattern line shape (Figure 9.3a) from the line shape shown in Figure 9.3b.

The edges of the difference line shape shown in Figure 9.3c (Figure 9.3b minus 9.3a) have a peculiar modulation due to the decrease in the coupling constant of the static C-D bonds in the sodium doped sample. Sodium doping induces a change in the electronic environment of the polymer chains such that the electrical field gradient is reduced in magnitude. The overall quadrupolar splitting observed for PPV-d_4 drops from 133 kHz to 131 kHz upon doping with sodium.

The difference line shape shown in Figure 9.3c is qualitatively similar to the line shape that is obtained from deuterated phenylene rings undergoing 180° flips. Figure 9.3d shows the high temperature line shape obtained from PPV-d_4. Note the third (centermost) component in Figure 3b (at ±0 kHz) which suggests there exists an additional phase of deuterated material undergoing rapid, isotropic motion on the NMR time scale. For H_2SO_4-doped PPV-d_4, deuterons have been abstracted from the phenylene rings at elevated temperatures in the form of D_2SO_4 or $HDSO_4$ (see chapter 6). The deuterated sulfuric acid is mobile at ambient temperatures and contributes a spike to the center of the ^2H NMR line shape. The possibility that the centermost component (at ±0 kHz) is due to some mobile species must be considered.

Besides being due to molecular motion, the center components of Figure 9.3b could also be caused by deuterium present in some other chemical form, i.e. as sodium deuteride. In order to determine whether the second component (at ±32 kHz) of the observed line shape (Figure 9.3b) is due to motion, the temperature of the sample was varied. If the component were due to a thermally-activated molecular motion, one would expect that temperature variation would bring about a change in the percentage of rings undergoing this motion on the NMR time scale with a corresponding change in the observed ^2H NMR line shape.

9.5 Variable-Temperature ^2H NMR Line Shapes of Sodium-Doped PPV-d_4

Figure 9.4 shows a number of ^2H NMR line shapes obtained from a sample of sodium-doped PPV-d_4 at temperatures varying from -175 °C to 175 °C. Note that the ^2H NMR line shape is very insensitive to changes in temperature. This is in sharp contrast to undoped PPV-d_4 or even H_2SO_4-doped PPV-d_4 (see chapters 5 and 6). For undoped PPV-d_4 the line shape varies greatly over the same temperature range. This fact indicates that the narrow component of the sodium-doped PPV-d_4 ^2H NMR line shape is due to either a separate mobile phase of deuterated phenylene rings that undergo discreet flips even at very low temperatures or to deuterons in a different chemical environment - i.e. deuterons not bound to carbon atoms. If the energy barrier for ring rotations were near zero, then the resulting line shape would be a further collapsed with a quadrupolar splitting one eighth that of the static Pake pattern (the line shape that results from phenylene rings undergoing free rotational diffusion).[104-106,108]

The possibility that there are two phases that are formed upon sodium doping of PPV-d_4 to the gold phase seems unlikely. Since the coulombic repulsion associated with the products of the doping reaction is expected to be large, a heterogeneous distribution of material phases with one phase being particularly mobile seems remote. Nevertheless, the authors constructed a special solid-state ^2H NMR probe insert to obtain the ^2H NMR line shape of sodium-doped PPV-d_4 at -196 °C. Figure 9.5 shows that line shape. While the signal to noise is poorer than those line shapes shown in Figures 9.3 and 9.4, the line shape nevertheless shows that the narrow component of the sodium-doped PPV-d_4 persists at -196 °C. The presence of this component at this temperature strongly suggests that it is not due to phenylene rings undergoing discreet flips.

The alternative to the motional collapse of the quadrupolar splitting is that the deuterons are present in some chemical species in the sample other than the carbon-deuterium bond. Theoretical calculations on the quadrupolar coupling of the gas-phase sodium deuteride molecule[187] are in excellent agreement with the observed quadrupolar

splitting of this second component. Abstraction of hydride ions from the phenylene rings of PPV also helps explain how the positively charged sodium ions are able to pack so tightly into the sodium-doped PPV unit lattice. By incorporating hydride ions near the sodium ions, the sodium ions are able to pack closely into the unit cell without paying the energy penalty associated with putting like charges in close proximity. Even if the sodium deuteride ion pairs are not exclusively confined to the former sodium ion columns, the pairing of these ions helps explain the high density of sodium in the samples.

Other investigations of alkali-doped, fully conjugated polymers have also shown the presence of hydrides.[188,189] Polyacetylene doped with potassium has been observed to form hydrides, thus lending support to the idea that sodium hydride is formed at high levels of sodium uptake in PPV.

Abstraction of hydride ions from the PPV chains is also expected to induce large geometrical distortions in the PPV chain. Recall that Chen *et al.*[69] observed both a lateral swelling of the hexagonal phase of the sodium-doped PPV to form the saturation phase and also a reduction in the length of the repeat unit suggesting the chains were no longer planar. It should also be noted that the abstraction of hydride ions from the PPV chains is consistent with the ESR results shown in Table 9.2. The hydride ion will, like the bipolaron, go undetected using this technique.

It is important to note that the levels of sodium uptake determined in this study are much larger than those observed with x-ray diffraction.[69] This indicates that the distribution of sodium ions in the PPV samples is not regular (or commensurate) with respect to the PPV chains in the unit cell. Using the sodium doping procedure described in reference 69, weight uptake measurements[190] indicate that the levels of sodium uptake are larger than those indicated by x-ray diffraction (they are in the range of 0.7 to 1.0 sodium ions per repeat unit). Whether sodium ions and sodium hydride pair occupy sites outside of the sodium channels remains to be determined. It is possible that the sodium

hydride pairs are the cause of the lateral (normal to the c axis) swelling of the unit cell or that sodium ions are located in poorly defined regions in the sample. It is clear, however, that at very high dopant uptakes that the unit cell of the material is greatly disrupted and the PPV chains undergo scission resulting in greatly reduced mechanical stability.

Table 9.1

Elemental Analysis Results for Sodium-Doped PPV

Phase	%Carbon	%Sodium	Na's per C_8H_6 repeat
Blue	88-92	2-6	0.08-0.22
Gold	76±3	18±1	0.98±0.04
Gray	<73	>22	>1.24

Table 9.2

ESR Results for Sodium-Doped PPV

Phase	g-Value	Peak-to-Peak Width		Repeat Units per Spin	
		25 °C	-196 °C	25 °C	-196 °C
Blue	2.0032	5.6	3.6	730	850
Gold	2.0035	7.0	3.9	400	270

a

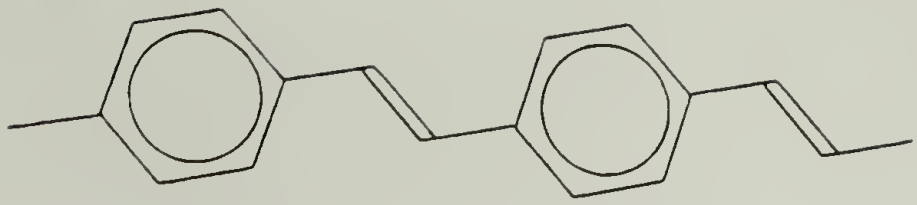

b

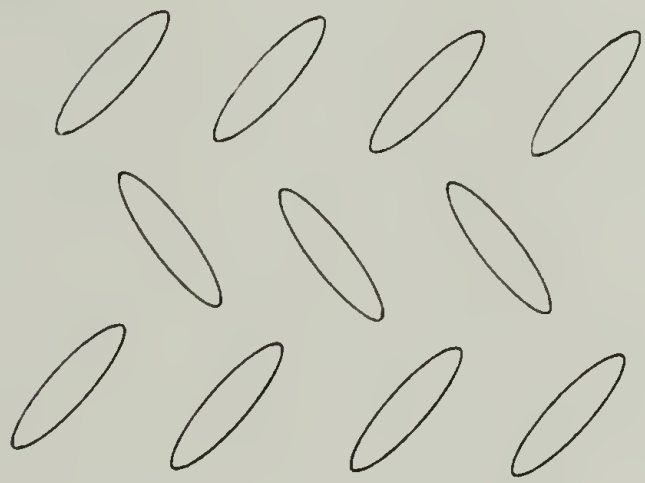

c

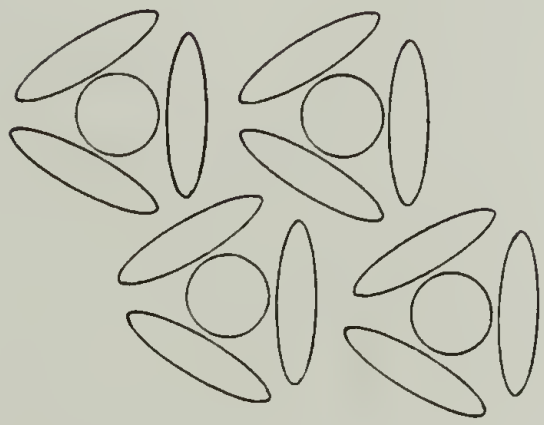

Figure 9.1 a) Structure of the PPV repeat unit; b) herringbone packing arrangement of the chains when viewed end-on; c) hexagonal packing arrangement of chains viewed from same perspective. The circles denote the sodium channels.

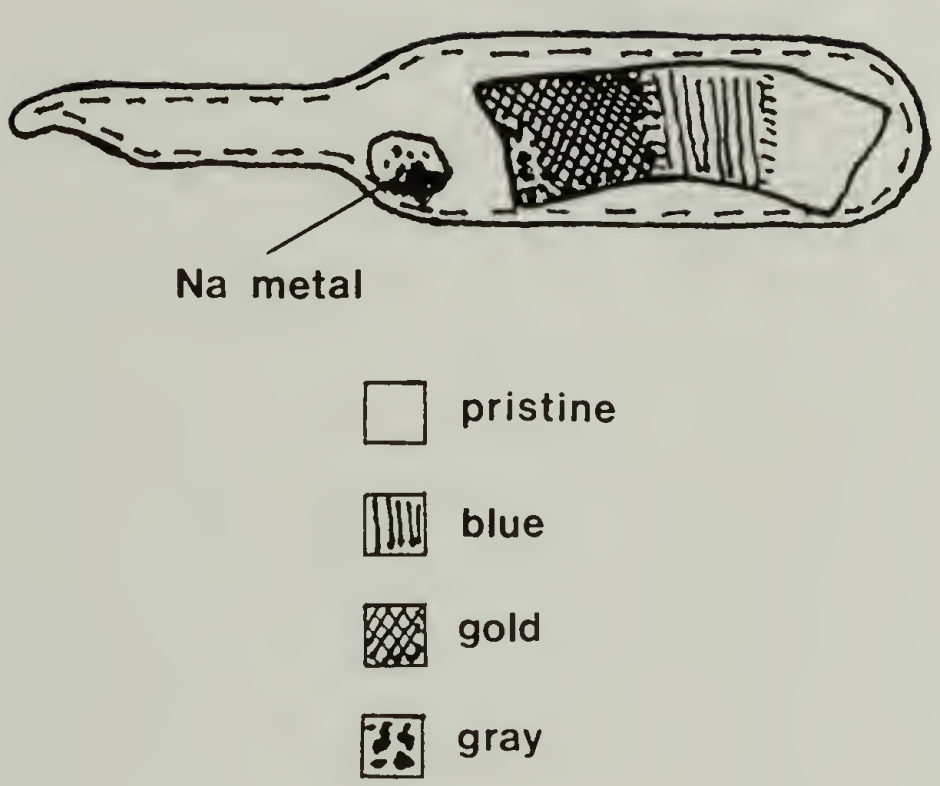

Figure 9.2 An illustration of the heterogeneity of the doping reaction which results under the conditions employed (see chapter 3 for more detail).

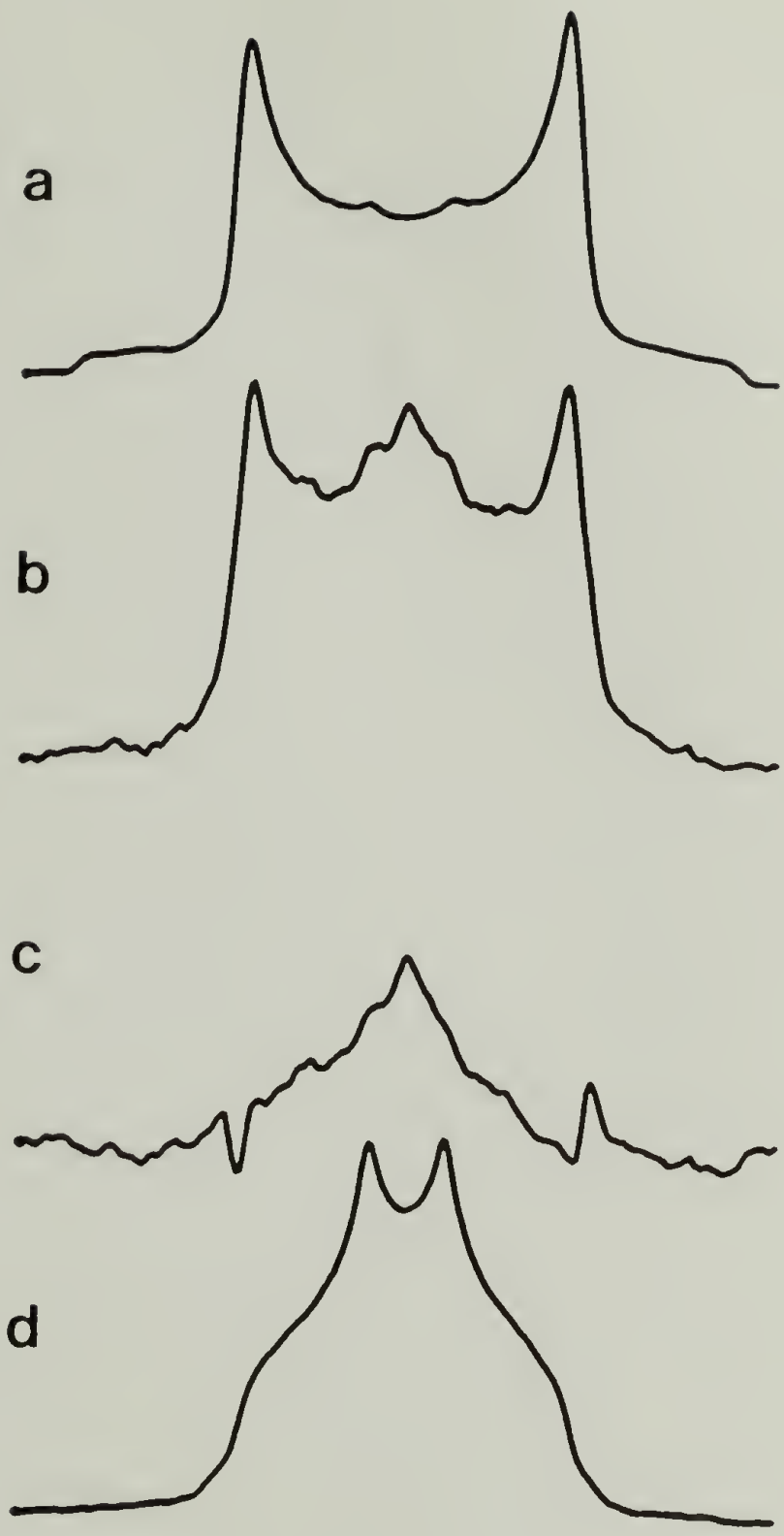

Figure 9.3 ^{2}H NMR line shapes of a) pristine PPV-d_4 at 25 °C; b) sodium-doped (gold phase) PPV-d_4; c) the line shape b minus a; d) PPV-d_4 at 225 °C. Note the similarity between c and d.

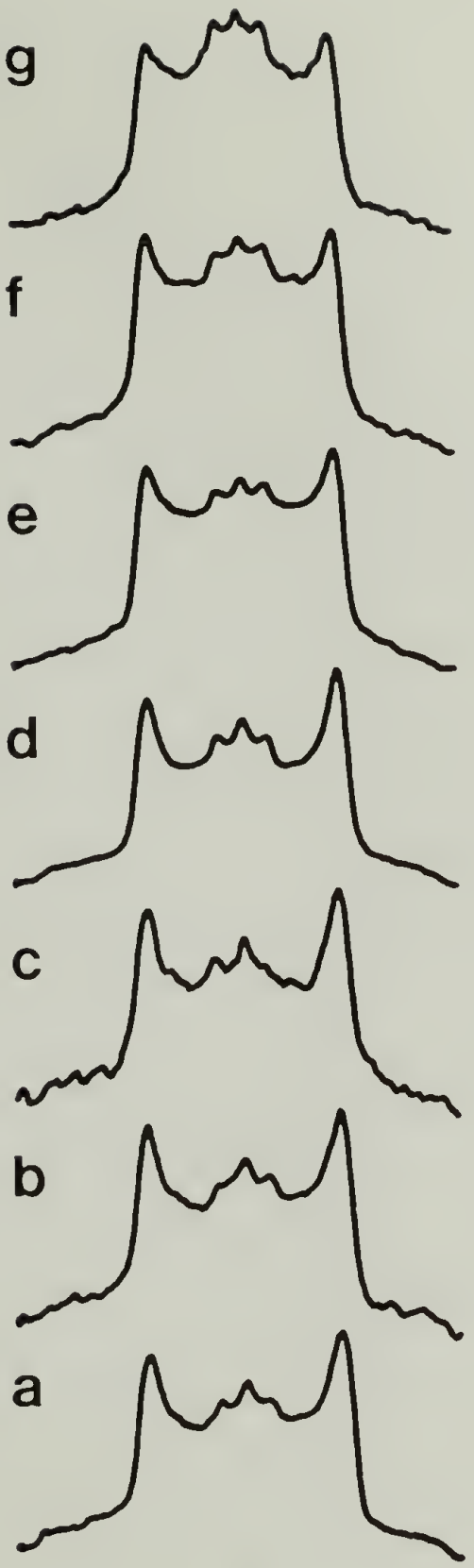

Figure 9.4 Stack plot of ^2H NMR line shapes obtained from sodium-doped (gold phase) PPV-d_4 at a) -125 °C; b) -75 °C; c) -25 °C; d) 25 °C; e) 75 °C; f) 125 °C; g) 175 °C. Note that the line shape is extremely insensitive to temperature changes.

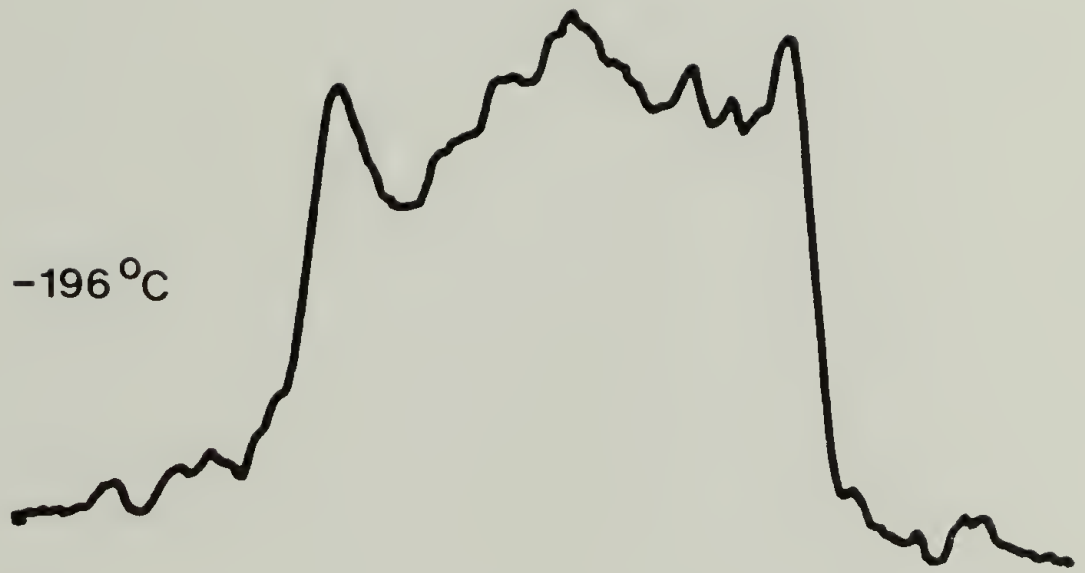

Figure 9.5 ^{2}H NMR line shape of sodium-doped (gold phase) PPV-d_4 obtained at -196 °C.

CHAPTER 10

USE OF TWO-DIMENSIONAL ^{1}H-^{13}C HETERONUCLEAR CORRELATION NMR TO DETERMINE THE CONFORMATION OF THE PDMPV REPEAT UNIT

This chapter presents two-dimensional NMR data on a functionalized PPV: poly(2,5-dimethoxy-*p*-phenylene vinylene) (PDMPV). The NMR technique makes use of the dipolar interaction between protons by allowing them to transmit phase information (encoded during part of the pulse sequence) between themselves and then cross-polarizing this information (via the magnetization) to attached carbon nuclei for detection. By following the evolution of the phase information transferred to the carbon nuclei, one can determine the rates of phase information transfer and these rates can be related to the interproton distances. The interproton distances are then used to calculate the conformation of the repeat unit of PDMPV.

In order to have the rates to yield distance information, a standard with precisely know interproton distances must be used for calibration. Figure 10.1a shows the structure of the standard used in this experiment: 1,4-dimethoxybenzene (DMB). Note how similar the structure of DMB is to that of PDMPV (Figure 10.1b).

10.1 Spectral Assignments

Figure 10.2 shows 2D HETCOR NMR spectra for DMB[191] and PDMPV acquired with a minimal dipolar mixing period. The vertical axes show the ^{1}H chemical shift range and the horizontal axes show the ^{13}C chemical shift range. One-dimensional projections are to the left and above the 2D spectra for the ^{1}H and ^{13}C nuclei, respectively. For the ^{1}H projection of DMB, all three ^{1}H shifts can clearly be seen. The ^{1}H projection of PDMPV shows only two distinct chemical shifts because the protons bound to the aromatic and vinylene carbons have similar chemical shifts. The

difference between the ^{13}C line widths of the low molecular weight material and the polymer is the result of greater chemical shift heterogeneity in the polymer sample due to greater local conformational heterogeneity.

Tables 10.1 and 10.2 show the NMR resonance assignments for DMB and PDMPV, respectively. For DMB, the methoxy ^{13}C resonance at 56 ppm (MeO, Figure 10.2a) is correlated with an upfield ^{1}H shift from the methoxy protons at 3.8 ppm, as is expected. The upfield protonated aromatic carbon resonance at 112 ppm (Up.Ar., Figure 10.2a) derives its intensity from the more upfield of the remaining two ^{1}H resonances at 5.2 ppm. The downfield protonated aromatic carbon resonance at 118 ppm (Dn.Ar., Figure 10.2a) has a cross-peak with the most downfield ^{1}H resonance at 7.0 ppm. The non-protonated carbon of DMB appears at 154 ppm (N.P.Ar., Figure 10.2a) but lacks cross-peaks above the contour intensity threshold in the figure. HETCOR spectra with dipolar mixing provide data that will be shown to confirm the ^{13}C assignments of DMB obtained previously from a single-crystal, chemical shift tensor analysis.[192] Dipolar mixing of the methoxy and aromatic ^{1}H magnetization as a function of time will be analyzed below to yield rate constants for the dipolar magnetization transfer, which will in turn yield intermolecular distances used for assignment and the determination of the local conformation.

The assignments of the three protonated ^{13}C resonances in the projection of PDMPV are shown in Table 10.2. The methoxy ^{13}C resonance at 56 ppm (MeO, Figure 10.2b) has a cross peak with the ^{1}H resonance at 3.8 ppm. The resonance spanning 108 to 111 ppm (Ar., Figure 10.2b) is assigned to the protonated aromatic carbon. This assignment is based upon a comparison with DMB. The protonated aromatic ^{13}C resonance derives its polarization from part of the broad downfield ^{1}H resonance at 8.0 ppm due to protons on both the vinylene and the aromatic rings. The resonance spanning 120 to 126 ppm (Vn., Figure 10.2b) is assigned to the vinylene carbon and also derives its magnetization from the ^{1}H resonance at 8.0 ppm. This assignment is in

agreement with that obtained from the solid state ^{13}C NMR spectrum of poly(*p*-phenylene vinylene) (PPV) for which the resonance of the vinylene carbon is assigned at 128 ppm (see chapter 4) The broadness of the latter two carbon resonances is attributed to local conformational heterogeneity in PDMPV and is discussed below.

10.2 Analysis of Spectra as a Function of Mixing Time

Protons with distinct chemical shifts exchange magnetization during the dipolar mixing period. The ^{1}H slices obtained at specific carbon chemical shifts change from their parent line shape, corresponding to the chemical shift of the attached proton, to a line shape similar to the ^{1}H projection for the entire 2D spectrum, which is invariant with time. Columns of the 2D spectra of DMB are extracted and are shown in Figure 10.3. The slice at the bottom of each stack-plot consists only of its parent ^{1}H shift (methoxy, Figure 10.3a; upfield aromatic, Figure 10.3b; and downfield aromatic, Figure 10.3c). The top spectra in each stack-plot are similar to each other, indicating the approach to equilibrium.

The ^{1}H slices of Figure 10.3 are deconvoluted into their three parent ^{1}H components to obtain the rates of dipolar magnetization transfer. The buildup and decay of each of the three ^{1}H components, associated with each of the three protonated carbons, yields a set of nine curves for DMB. Three of the curves, corresponding to the methoxy ^{13}C resonance of DMB, are shown in Figure 10.4a. For PDMPV, the chemical shifts on the aromatic and vinylene protons are coincident, yielding only six curves. Figure 10.4b shows three of these curves for PDMPV, corresponding to the development of methoxy ^{1}H character for each of the ^{13}C resonances.

Examination of Figure 10.1 shows that the three ^{1}H types in DMB (3 Meo, 1 H_u, 1 H_d) and PDMPV (3 MeO, 1 H_a, 1 H_v) each form a pair of coupled spin systems in which ^{1}H-^{1}H distances are 0.3 nm or less. These spin systems are effectively isolated from other protons during the initial ^{1}H mixing period. Figure 10.5 shows the model

which is applied to characterize the dipolar mixing of DMB and PDMPV. The dipolar mixing is modeled with irreversible first order kinetics and six exchange rates (three forward and three reverse), and spin lattice relaxation is neglected). Note that the assumption of irreversible mixing is an approximation and neglects the coherence associated with the dipolar interaction. This coherence under conditions of MAS would be evident in Figure 10.5 as a rotational spin echo at one rotor period (250 μs for DMB and 273 μs for PDMPV). It can be seen experimentally that this echo is absent and the mixing curves have approximate exponential character. Therefore, the exponential approximation is sufficient to model the initial rate of mixing. Also, it should be noted that for an exchange model the assumption of microscopic reversibility relates the forward and reverse rates, reducing the number of independent rates to three. However, in this experiment detection requires the presence of a fourth spin (a ^{13}C nucleus), and the ^{13}C-^{1}H dipolar interaction could potentially affect the rate of dipolar mixing between the protons.[193] Under these conditions the assumption of microscopic reversibility is not formally correct. Nevertheless, analysis of the data with three and six rates yields the same result, indicating microscopic reversibility is applicable. The ^{1}H-^{13}C dipolar interaction probably contributes only to the exponential damping.

An application of the model shown in Figure 10.6 to the data for DMB and PDMPV yields the rates of dipolar magnetization transfer between the three ^{1}H spins in DMB and PDMPV. For DMB, the methoxy protons are designated $H_{[1]}$ in Figure 10.6. The downfield aromatic protons (H_d, Figure 10.1b) are designated $H_{[2]}$, and the upfield aromatic protons (H_u, Figure 10.1b) are designated $H_{[3]}$. Note that the upfield aromatic protons are separated by a large distance (approximately 0.5 nm) from the methoxy protons. For this structure the rate of magnetization transfer between these two protons should be small. Figure 10.4a contains the best-fit buildup and decay curves for the DMB data shown in Figure 10.3. Note that the methoxy carbon loses its parent methoxy ^{1}H character and gains downfield aromatic ^{1}H character more rapidly than it gains

upfield aromatic ^{1}H character. The difference in rates must result from the structure of DMB - the upfield aromatic ^{1}H magnetization must first mix with the downfield aromatic proton before magnetization can in turn be passed to the methoxy protons. The ^{13}C assignment of DMB is immediately evident from this data and a comparison with the crystal structure. In order to have the greater rate of transfer the downfield proton must be that which is close to the methoxy group. This assignment confirms that of Carter *et al.*,[192] which was previously obtained from a novel ^{13}C chemical shift tensor analysis which required a single crystal of DMB. In contrast, this assignment based upon dipolar mixing is obtained from a powder.

The model shown in Figure 10.5 is also applied to the data for PDMPV (Figure 10.4b). In this case the structure is unknown, and the NMR data is used to place limits upon the local conformation. The methoxy protons are designated $H_{[1]}$, the aromatic protons (H_a, Figure 10.1a) are designated $H_{[2]}$ and the vinylene protons (H_v, Figure 10.1a) are designated $H_{[3]}$. One possible PDMPV conformation is shown in Figure 10.1a. For this conformation, note that the methoxy and vinylene protons are also separated by a large distance. As with DMB, the direct rate of mixing between these two protons is small. It can be seen in Figure 10.4b that the protonated aromatic carbon gains methoxy ^{1}H character more rapidly than does the vinylene carbon, a result consistent with the possibility that the vinylene protons obtain their methoxy proton character indirectly via the aromatic protons. A structure similar to Figure 10.1a must be the predominant conformation.

A distribution of methoxy conformations is probably present in largely amorphous PDMPV and that the curves of Figure 10.4b may result from an average over this distribution. In this model, however, the predominant conformation of the methoxy group must be towards the aromatic proton as shown in Figure 10.1a. Otherwise, the rate of methoxy proton magnetization transfer to the aromatic protons would be similar to that of the vinylene protons. A distribution of methoxy configurations could

potentially explain the broadness of the protonated aromatic ^{13}C resonance (Ar., Figure 10.2b) analogous to the two shifts for the protonated aromatic sites of DMB. However, all ^{1}H slices for this carbon site have a similar rate of dipolar mixing with the methoxy protons (as do all vinylene ^{1}H slices). Therefore, it is suggested that the distribution of methoxy conformations must be small. Two distinct vinylene conformations may be the cause of the chemical shift heterogeneity in Figure 10.2b. Proton chemical shifts show a strong dependence upon methoxy conformation, as seen in Figure 10.2a for DMB, but are less affected by the conformation of the vinylene group (as determined from the HETCOR spectrum of PPV[194]). The ^{1}H chemical shift heterogeneity associated with the PDMPV aromatic resonance is small, consistent with a distribution of vinylene conformations.

Table 10.3 shows the individual rate constants for the dipolar magnetization transfer in DMB and PDMPV. For the DMB data-set the rate constant between the methoxy protons ($H_{[1]}$) and the upfield aromatic protons ($H_{[3]}$) is assumed to be zero. The rate constant between the downfield aromatic protons ($H_{[2]}$) and the methoxy protons is 0.0165±0.0012 μs^{-1}, confirming that the methoxy group points toward the downfield aromatic carbon and proton. The rate constant for magnetization transfer between the downfield ($H_{[2]}$) and upfield ($H_{[3]}$) aromatic protons is 0.0153±0.0019 μs^{-1}. For the PDMPV data-set, the rate constant between the aromatic protons ($H_{[2]}$) and the methoxy protons ($H_{[1]}$) is 0.0118 μs^{-1} and the rate constant between the aromatic protons ($H_{[2]}$) and the vinylene protons ($H_{[3]}$) is 0.0208 μs^{-1}.

10.3 Computation of Interproton Distances

10.3.1 The Relationship Between Mixing Rate and Distance

The relationship between the rate of magnetization transfer and the distance between protons can be expressed more quantitatively and, with the known interproton distances for DMB, the magnetization transfer rates in PDMPV can be empirically

converted to average interproton distances. Limits for the dihedral angles ϕ_1 and ϕ_2 (Figure 10.1a) of PDMPV can be estimated, based upon the expected bond lengths and valence bond angles in PDMPV.

To calculate an exact expression relating the full dipolar interaction to interspin distances would require solution for the four-spin case (three ^1H and one ^{13}C) under conditions of MAS. The methodology for this type of calculation has recently been presented by Levitt *et al.*[193] However, the solution of a four spin system has not been obtained, and one might argue that a precise solution is not necessary, since these buildup curves are approximately exponential and coherences are absent. Useful data appears to be limited to the initial period of the curves. For the approximate calculation of buildup curves, the dipolar Hamiltonian is summed pairwise and the heteronuclear interaction and correlation terms are neglected. The Hamiltonian describing the homonuclear dipolar interaction of the two ^1H spins $\mathbf{I}_1$ and $\mathbf{I}_2$ is:

$$\mathbf{H}_D = \frac{-2\,\gamma^2\,\hbar}{r_{12}^{\,3}}\,\mathbf{I}_1\cdot\underline{\underline{\mathbf{D}}}\cdot\mathbf{I}_2 \qquad (10.1)$$

where γ is the magnetogyric ratio of the proton, r_{12} is the distance between the two spins and $\underline{\underline{\mathbf{D}}}$ is the dipolar coupling tensor. For a static sample, the frequencies of dipolar coupling are dependent on the angle, θ, between r_{12} and the applied field $\mathbf{B}_0$, and the time evolution is similar to the free induction decay associated with a Pake doublet spectrum. Frequencies of a Pake doublet $\omega_D(\theta)$ are given by:[193,195]

$$\omega_D(\theta) = \pm(\gamma^2\,\hbar\,/\,r_{12}^{\,3})\,(3/2\,\cos^2\theta - 1/2) \qquad (10.2)$$

The initial rate is approximately determined by the width of the Pake doublet as $\theta = 90°$, and this width is scaled by the factor[193] of $r_{12}^{\,-3}$:

$$\omega_D(90°) = \gamma^2\,\hbar\,/\,r_{12}^{\,3} \qquad (10.3)$$

Under conditions of MAS, the free induction decay should be transformed to a pattern of rotational spin echoes, but as noted experimentally the magnetization transfer is

strongly damped. The damping leads to an approximately exponential decay which can be characterized with a rate constant k_{12}, where:

$$k_{12} = (G / r_{12})^3 \tag{10.4}$$

Equation 10.4 is solved for the proportionality constant G using DMB data. For DMB, the distance between the downfield aromatic protons and the methoxy protons is 0.253 nm and yields G = 0.0644±0.0016. The distance between the upfield and downfield aromatic protons is 0.248 nm. Solving equation 10.4 for the latter case yields G = 0.0615±0.0026. The two values agree within experimental error - the average is G = 0.0629±0.0021.

10.3.2 Dihedral Angle Calculations From Distances

The value of G obtained from the DMB data set is then used together with the rate constants for magnetization transfer to calculate distances in PDMPV. An approximate planar model for the PDMPV repeat unit can be constructed based on diffraction studies of DMB,[192,196] *trans*-stilbene,[162] and PPV.[82] This model predicts a distance of 0.253 nm between the methoxy protons and the aromatic protons and a distance of 0.198 nm between the aromatic protons and the vinylene protons. It is expected from the small value of this latter distance that there will be a significant amount of steric crowding that will result in distortion of bond lengths and angles or require a non-zero dihedral angle (ϕ_2, Figure 10.1a). Both of the experimentally determined distances are larger than the planar model predicts: 0.276±0.009 nm between the methoxy protons and the aromatic protons, and 0.229±0.008 nm between the aromatic protons and the vinylene protons. These results suggest that the PDMPV repeat unit is not planar. If a single conformation of the PDMPV repeat unit were present, the dihedral angle, ϕ_1, between the O-CH_3 bond of the methoxy group and the plane of the aromatic ring would be ϕ_1 = 35±8° and the dihedral angle, ϕ_2, between the C=C bond of the vinylene group and the plane of the aromatic ring would be ϕ_2 = 33±4°. It is expected that the bond lengths and

bond angles in PDMPV may also vary from typical values to relieve crowding. A relaxation of the bond angle and length constraints used to determine the theoretical interproton distances can reduce the calculated dihedral angles (Bond angles and lengths are either increased or decreased by a percentage of their magnitude so that the change will always increase the calculated interproton distances). A 3% distortion of all of the bond distances and valence bond angles that affect the interproton distances reduces the calculated dihedrals to $\phi_1 = 25\pm13°$ and $\phi_2 = 19\pm8°$, respectively. A 5% distortion reduces the dihedrals to $\phi_1 = 14\pm14°$ and $\phi_2 = 0\pm9°$, respectively. Variation of only the backbone valence angle of the vinylene carbon while maintaining a planar repeat unit requires that the valence angle change from 128°[82,162] to 140°. This latter value is unreasonable, indicating that other distortions must be present to account for the measured interproton distances.

That a conjugated organic system such as PDMPV may lack planarity is not unexpected. For example, Bradley[47] has noted in an infrared transition moment analysis of oriented PPV that a non-planar repeat unit may account for some of his experimental observations. The solid state ^{13}C CP-MAS data presented in chapter 4 has suggested that the vinylene group in PPV may not be in the plane of the aromatic ring. Winokur and coworkers[69] have also suggested based on x-ray diffraction studies that the vinylene group of PPV may contain a dihedral angle on the order of 10-20°, and the value of ϕ_2 determined here for PDMPV is in excellent agreement with this value. The assumption of planarity in conjugated polymers has gained some acceptance due to the ease with which diffraction data may thereby be analyzed and because of its intuitive appeal in terms of molecular orbital theory. On the contrary, the present NMR results corroborate a growing body of evidence suggesting that certain conjugated systems previously assumed to be planar are in need of reevaluation.

Table 10.1

NMR Chemical Shifts of DMB

Nucleus	Shift	Assignment
^{13}C	56 ppm	Methoxy
"	112 ppm	Protonated aromatic attached to H_u, Figure 10.1b
"	118 ppm	Protonated aromatic attached to H_d, Figure 10.1b
"	154 ppm	Non-protonated aromatic
^{1}H	3.8 ppm	Methoxy
"	5.2 ppm	H_u, Figure 10.1b
"	7.0 ppm	H_d, Figure 10.1b

Table 10.2

NMR Chemical Shifts of PDMPV

Nucleus	Shift	Assignment
^{13}C	56 ppm	Methoxy
"	108-111 ppm	Protonated aromatic (attached to H_a, Figure 10.1a)
"	120-126 ppm	Vinylene (attached to H_v, Figure 10.1a)
^{1}H	3.8 ppm	Methoxy
"	8.0 ppm	H_a and H_v, Figure 10.1a

Table 10.3

Rate Constants for Dipolar Proton Magnetization Transfer

System	Rate	Assignment	Distance
DMB	0.0165 μs^{-1}	From downfield aromatic to methoxy	0.253 nm*
DMB	0.0153 μs^{-1}	From downfield aromatic to upfield aromatic	0.248 nm*
PDMPV	0.0118 μs^{-1}	From aromatic to methoxy	0.276 nm
PDMPV	0.0208 μs^{-1}	From aromatic to vinylene	0.229 nm

*values obtained from references 192 and 196

a

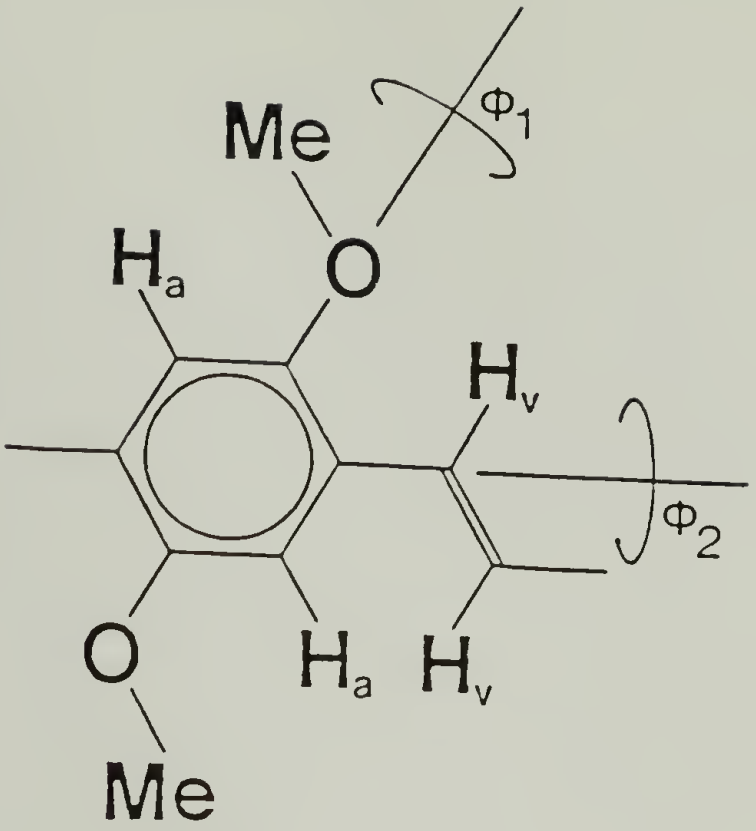

b

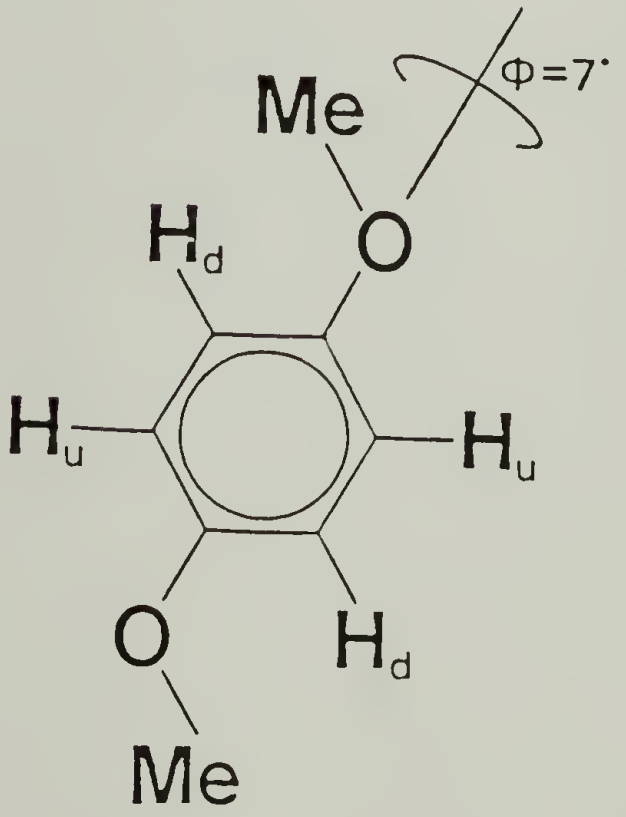

Figure 10.1 a) The structure of PDMPV. The two dihedral angle ϕ_1 and ϕ_2 which determine the conformation of the repeat unit. b) The structure of DMB. The dihedral angle between the the O-CH_3 bond of the methoxy group and the plane of the ring is 7°.[192]

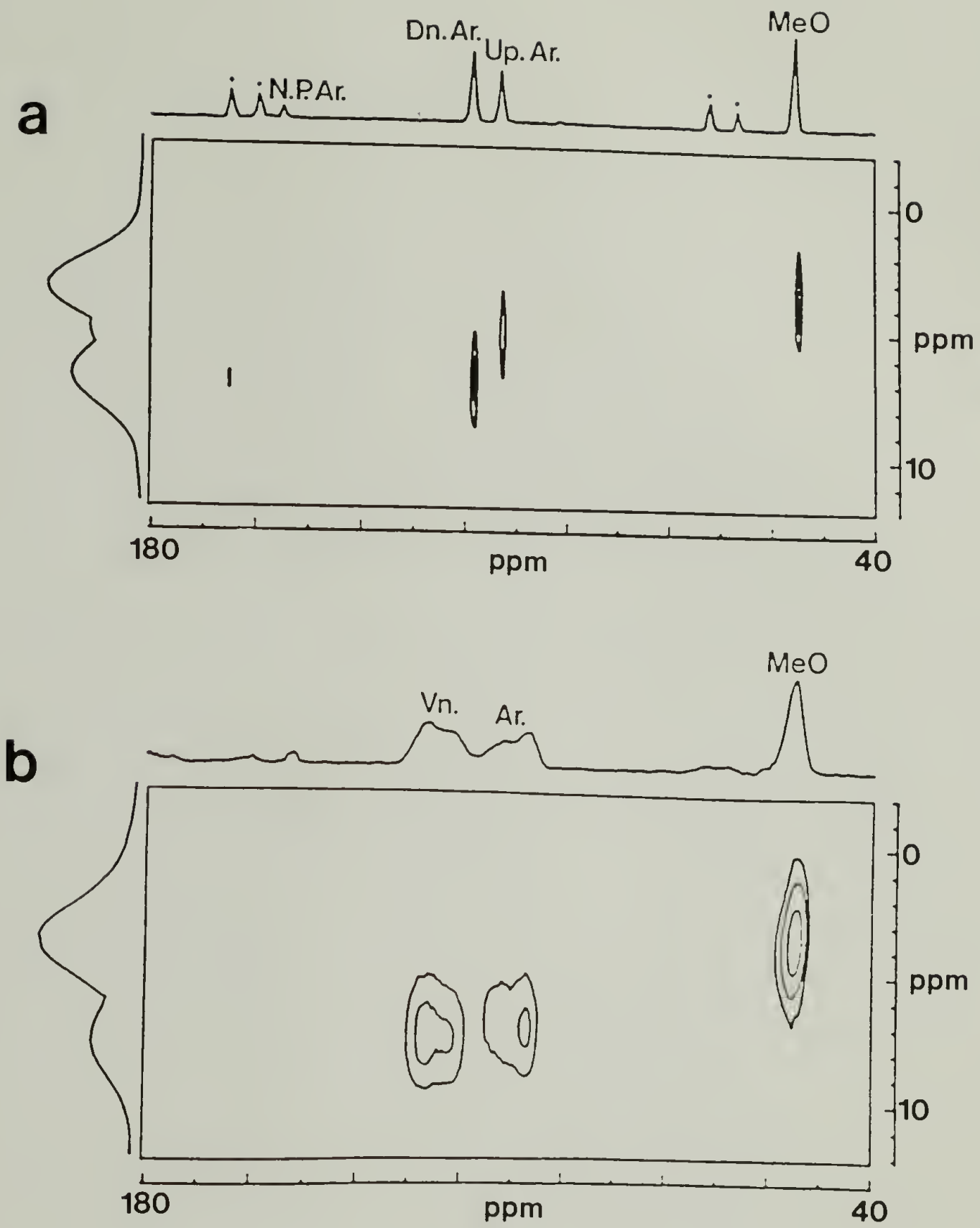

Figure 10.2 a) The 2D NMR spectrum of DMB with 10 μs of dipolar mixing. The vertical projection shows the solid state ^{13}C NMR spectrum of DMB and the horizontal projection shows the solid state ^{1}H NMR spectrum. Spinning sidebands are labeled with asterices. b) The 2D NMR spectrum of PDMPV with no dipolar mixing. The vertical projection shows the solid state ^{13}C NMR spectrum of PDMPV and the horizontal projection shows the solid state ^{1}H NMR spectrum.

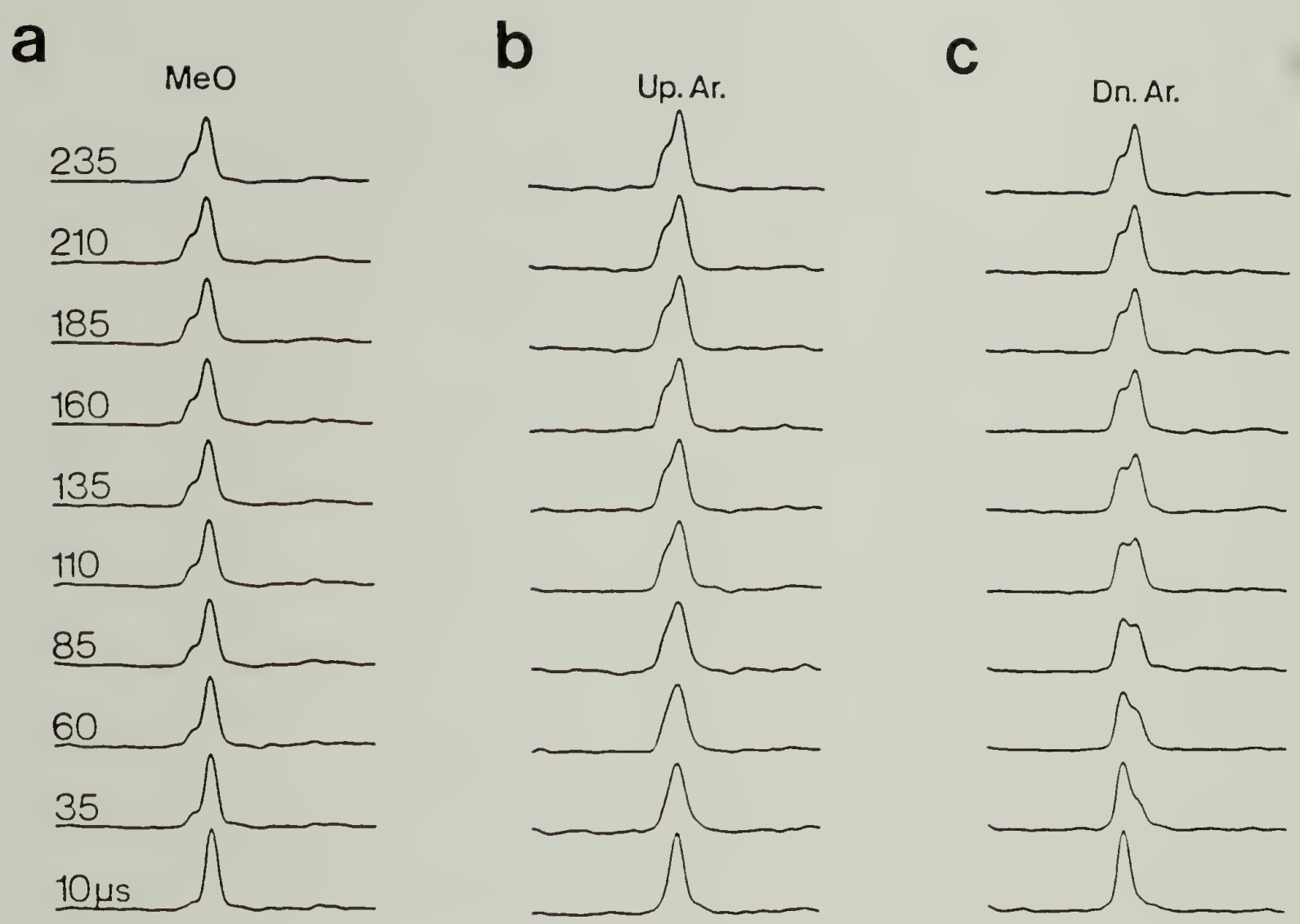

Figure 10.3 Three plots showing the evolution of the ^{1}H magnetization corresponding to the protonated ^{13}C of DMB. The parent proton chemical shifts are labeled. The bottom spectrum in each column is acquired with 10 μs of dipolar mixing, for the top spectrum, 235 μs. a) ^{1}H spectra obtained from the methoxy ^{13}C resonance at 56 ppm, b) ^{1}H spectra obtained from the aromatic ^{13}C resonance at 112 ppm, and c) ^{1}H spectra obtained from the aromatic ^{13}C resonance at 118 ppm.

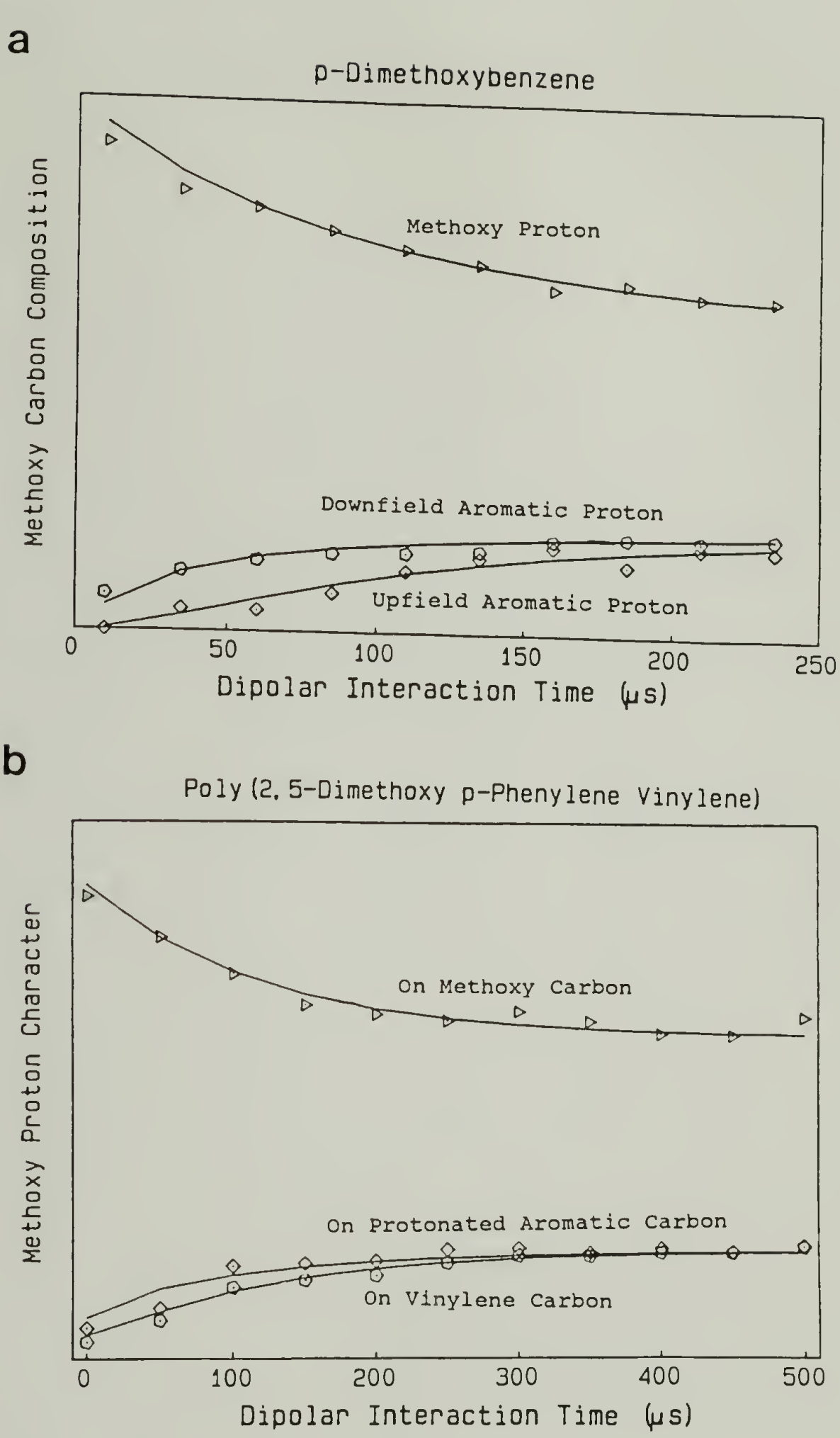

Figure 10.4 Buildup and decay curves for the dipolar magnetization transfer. a) Evolution of the ^{1}H components for the methoxy ^{13}C. b) The methoxy ^{1}H character for each of the three protonated ^{13}C resonances as a function of dipolar mixing time.

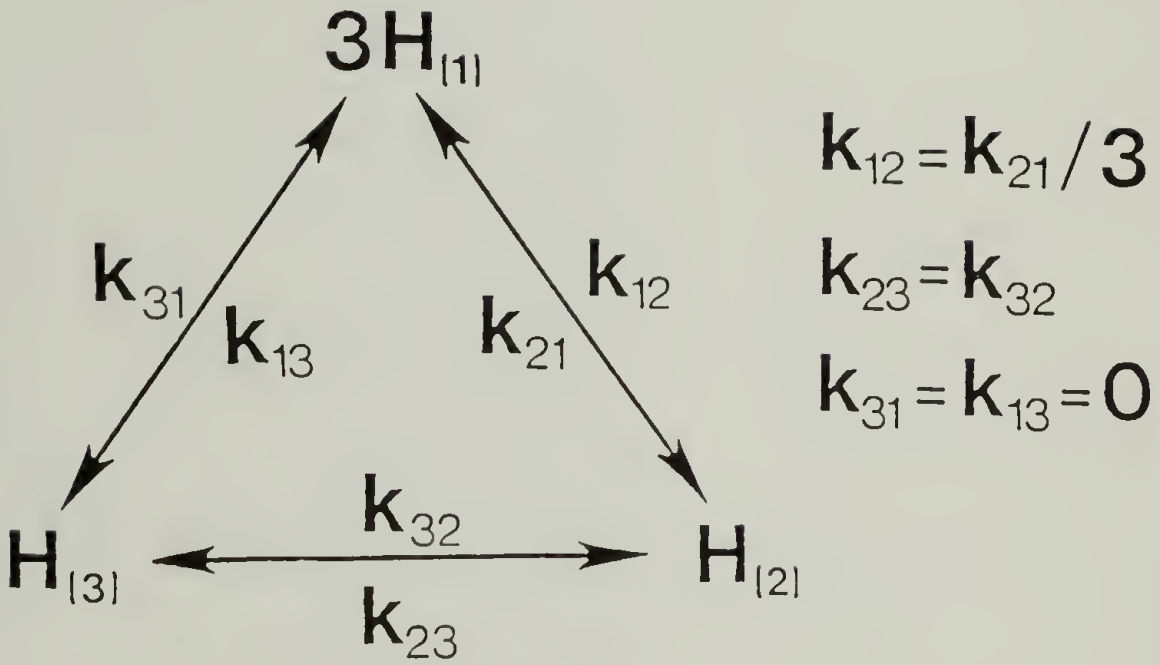

Figure 10.5 A schematic diagram of the kinetic model used to fit the data for both DMB and PDMPV. $H_{[1]}$ denotes the methoxy ^{1}Hs in both cases, $H_{[2]}$ denotes the downfield aromatic ^{1}H in DMB and the aromatic ^{1}H in PDMPV, $H_{[3]}$ denotes the upfield aromatic ^{1}H in DMB and the vinylene ^{1}H in PDMPV.

CHAPTER 11

SUMMARY AND SUGGESTED FUTURE DIRECTIONS

11.1 Summary of Results

Carbon and deuterium NMR have been used to study PPV in both its undoped and doped forms. The bonding, crystallinity, defect structure, chain orientation and molecular dynamics have all been investigated to varying degrees.

All four resonances of the ^{13}C CPMAS spectrum of PPV have been assigned, and these assignments have been proved through the observation of interrupted decoupling spectra of a deuterated PPV-d_4. NMR spectra of PPV are largely consistent with diffraction and TEM data and largely confirm that both stretched and unstretched PPV films have similarly high crystallinity. NMR resolution can be improved by increasing the annealing temperature, and TEM data show that the improvement is accompanied by an increase in crystallite size.

^{13}C NMR spectra of PPV-d_4 show evidence that a portion of PPV segments contain phenylene rings which undergo 180° rotational jumps. The short rotating-frame spin-lattice relaxation time of PPV has been atttributed to these flips, and the similar effect on the four PPV resonances through spin diffusion suggests that flipping rings are distributed homogeneously throughout the film. The ring-flip population increases with increasing temperature.

All phenylene rings of an PPV-d_4 have been shown to be capable of undergoing 180° rotational jumps about the 1,4 phenylene ring axis. The dependence of the median jump rate on temperature can be described by Arrhenius equation and with a median activation energy of 15 kcal/mol. The phenylene rings of PPV show relatively homogeneous behavior and the observed distribution of ring flip rates could be caused by a maximum distribution of activation energies of ±2 kcal/mol. Phenylene ring

motion with a low activation energy is unusual for a polymer with a high crystallinity such as PPV. However, paracrystalline disorder of the PPV unit cell may allow cooperative chain motion and effectively reduce the intermolucular packing contribution to the experimental activation energy.

H_2SO_4-doped PPV-d_4 has been characterized with ^2H quadrupole echo NMR spectroscopy. It has been shown that ^2H NMR can provide new information about the chemistry of PPV doping, and through ring flip rates indirectly provide data about the electronic structure of the phenylene vinylene bond. Doping increases the *p*-phenylene ring flip activation energy from 15 kcal/mol in the pristine state to at least 21 kcal/mol. This increase can be attributed to an increase in the double bond character of the phenylene vinylene bonds. The width of the distribution of ring flip rates also increases from $\Delta\log(k) = \pm 2$ in the pristine state to $\Delta\log(k) = \pm 4$ in the doped state, indicating that a greater degree of sample heterogeneity exists. This heterogeneity is attributed to a lower degree of crystalline perfection in the new crystalline (doped) phase and also to the indeterminate placement of the dopant counterions in the unit cell of the doped material.

H_2SO_4-doped samples are found to lose some of their dopant upon heating and also undergo a chemical reaction that fixes dopant into their structure. Nevertheless, heating does not permanently destroy sample conductivity. Subsequent redoping will restore electrical conductivity. Upon exposure to ambient conditions, an unheated, doped sample will eventually lose all its dopant and regain its former (undoped) appearance but with a significant loss of its mechanical properties.

^2H quadrupole echo NMR spectra and spin lattice relaxation data confirm that structure of PPV is similar to that of *trans*-stilbene. ^2H spectra obtained at elevated temperature show that the C-D bond motion has effective C_2 symmetry about the chain axis. A 180° vinylene rotational jump is the simplest motion with these attributes. Rotational small angle diffusion without a jump is inconsistent with the observed

spectra. ^2H spin lattice relaxation data also support a jump model and indicate that the the vinylene and phenylene jump rate distributions are similar.

A two fold jump motion is a natural motion for the PPV chain and a two-fold disorder about the PPV chain axis is the simplest type disorder associated with PPV paracrystallinity. This disorder may be related to the lack of axial registry which occurs for adjacent planes along the **a** axis of the unit cell. The actual mechanism of PPV chain motion may be more complex than a two-fold jump and perhaps involve a particular coupled motion of phenylene and vinylene groups. Any motion, however, should preserve the effective two-fold symmetry about the chain axis, evident in high temperature ^2H spectra.

^2H NMR spectra have provided new details about crystalline structure and chain disorder within stretched PPV films. NMR data confirm the results of diffraction experiments which show that the PPV chain has a high crystallinity. ^2H spectra show independently that the phenylene ring is tilted relative to the crystallite **c** axis, as expected for segments with a *trans*, *transoid* structure and a stilbene geometry. A 1.5° discrepancy between the predicted and experimental tilt has been attributed to the presence of chain disorder at crystallite boundaries or to small angle rotational disorder about the phenylene-vinylene bonds at each segment.

NMR data show that PPV films are highly oriented by stretching, and the orientation function determined by NMR is similar to that obtained from the infrared dichroic ratio. NMR spectra provide information about the shape of the orientation distribution and show that the orientation distribution for most segments can be adequately described by the pseudo-affine model. However, stretched PPV films possess fewer chains at 90° to the stretching axis than predicted by the pseudo-affine model. Though the fraction of chains involved is small, this difference can explain the higher orientation functions obtained for PPV from the infrared dichroic ratio.

NMR spectra show that at room temperature a fraction of PPV segments contain phenylene rings which undergo 180° rotational jumps. This jump motion is also present in stretched samples, and the existence of a well oriented jump spectrum suggests that this motion can occur within PPV crystallites as well as boundary domains. PPV is the first polymer for which this motion has been detected in both crystalline and boundary domains.

PPV doped with sodium metal has been observed to form at least three distinct phases (blue, gold, and gray) which have been characterized with elemental analysis, ESR and ^2H NMR spectroscopy. Elemental analysis indicates that the most easily prepared of the three phases corresponds to PPV with one sodium ion per C_8H_6 repeat unit. The evolution of unpaired spins has been examined for the blue and the gold phases at -196 °C and 25 °C. The ESR behavior of these systems is more characteristic of metallic than conventional organic radical systems.

^2H NMR spectra of sodium-doped, phenylene-ring deuterated PPV (PPV-d_4) show a line shape that is insensitive to temperature, suggesting that the doping process raises the activation of phenylene ring flips sufficiently such that the rings no longer flip on the NMR time scale even at 175 °C. A central component of the line shape has been assigned to the abstraction of deuterons from the phenylene rings to form sodium hydride. Sodium hydride screens out the extreme coulombic repulsions otherwise associated with the high sodium ion concentration in the samples. The hydride formation also accounts for the severe geometrical distortions observed at high doping levels.

Solid state 2D HETCOR NMR spectra with dipolar mixing have been presented for DMB and PDMPV. The ^{13}C assignment of DMB has been confirmed and the ^{13}C assignment of PDMPV has been presented. Proton dipolar magnetization transfer in DMB and PDMPV has been followed with 2D NMR and has been modeled with first order kinetics using a two parameter fit. Precise distance information for DMB has been

combined with rate constants for magnetization transfer in DMB to give distance information for the polymer PDMPV. Dihedral angles for the methoxy and vinylene groups have been determined and show that the repeat unit of PDMPV is not planar.

This modified version of the solid state HETCOR experiment has been shown to be a useful method for characterizing local polymer conformation in an unoriented material such as PDMPV. This method may also be used to provide CPMAS assignments in low molecular weight, crystalline materials where conformation brings about chemical shift inequivalence. Without this technique, such assignments would require a more laborious, single-crystal, chemical shift tensor analysis. Previously it has been assumed that the ^1H spin systems of most solids are too complex to provide data in all but the spin diffusion limit. We have shown here that useful data can also be obtained in the short-distance limit and a simple empirical model suffices to explain it. It is expected that this approach will also prove valuable for the characterization of NLO materials where precise conformational data is important.

11.2 Future Studies

As PPV continues to be found suitable for new applications, it is expected that fundamental research similar to that contained in this work will be viewed as vital in furthering our understanding of these systems. Perhaps the most important data presented in this work is the molecular motion data and the effects of doping on these rates.

Some of the NMR work that still needs to be done involves the characterization of how doping affects the dynamics of PPV-d_2. Specifically, various dopants should be employed in a systematic study of the vinylene group dynamics.

In addition, the high-level of sodium uptake poses the question of why diffraction methods do not observe this. Furthermore, the blue phase of sodium-doped PPV shows promise as a conductive polymeric material that possesses decent mechanical

properties. It is expected that this material might show especially good properties for high-frequency conduction because of the surface conduction that is well known for this frequency range.

The HETCOR pulse sequence should also be employed to investigate other systems where it will be possible to determine the conformation of repeat units. Perhaps a number of well-characterized, low molecular weight compounds should be examined to determine if there is a universal G value that governs the rate of dipolar mixing of encoded proton phase information for all systems. One caveat associated with this technique is the extreme dependence of the kinetics on the initial points. It appears that some initial mixing of the proton spins occurs prior to the start of the dipolar mixing period. It is unclear if this is due to some interaction that is not properly accounted for in the pulse sequence or if this is due to improperly tuned pulses.

REFERENCES

1. Shirakawa, H. and Ikeda, S. "Infrared Spectra of Poly(Acetylene)" *Polym. J.* **2** 231-244 (1971).

2. Chiang, C.K., Fincher, C.R., Park, Y.W., Heeger, A.H., Shirakawa, H., Louis, S.C., Gau, E.J. and MacDiarmid, A.G. "Electrical Conductivity in Doped Polyacetylene" *Phys. Rev. Lett.* **39** 1098-1101 (1977).

3. Chien, J.C.W. *Polyacetylene: Chemistry, Physics and Material Science* Academic, New York, 1984.

4. Skotheim, T.A., ed. *Handbook of Conducting Polymers* Vol. I & II, Marcel-Dekker, New York, 1986.

5. Burroughs, J.H., Bradley, D.D.C., Brown, A.R., Marks, R.N., Mackay, K., Friend, R.H., Burns, P.L. and Holmes, A.B. "Light-Emitting Diodes Based on Conjugated Polymers" *Nature* **347** 539-541 (1990).

6. Chien, J.C.W. and Schlenoff, J.B. "Limiting Battery Performance Parameters for Polyacetylene" *Nature* **311** 362-363 (1984).

7. Prasad, P.N. "Polymeric Materials for Non-Linear Optics and Photonics" *Polymer* **32** 1746-1751 (1991).

8. Burzynski, R., Prasad, P.N. and Karasz, F.E. "Large Optical Birefringence in Poly(*p*-Phenylene Vinylene) Films Measured by Optical Waveguide Techniques" *Polymer* **31** 627-630 (1990).

9. Reynolds, J.R., Karasz, F.E., Chien, J.C.W., Gourley, K.D. and Lillya, C.P. "Electrically Conducting Aromatic Polymers: Poly(*p*-Phenylene Vinylene) and its Analogs" *J. De Physique* **44** C3 693-696 (1983).

10. Wnek, G.E., Chien, J.C.W., Karasz, F.E. and Lillya, C.P. "Electrically Conducting Derivative of Poly(*p*-Phenylene Vinylene)" *Polymer* **20** 1441-1443 (1979).

11. Gourley, K.D., Lillya, C.P., Reynolds, J.R. and Chien, J.C.W. "Electrically Conducting Polymers: AsF_5-Doped Poly(Phenylene Vinylene) and its Analogues" *Macromolecules* **17** 1025-1033 (1984).

12. Dai, L. and White, J.W. "Soluble Conducting Polymers from Polyisoprene" *Polymer* **32** 2120-2127 (1991).

13. Tawansi, A., Migahed, M.D. and El-Hamid, M.I.A. "Electrical Conduction of Poly(Vinyl Alcohol) Films" *J. Polym. Sci., Polym. Phys. Ed.* **24** 2631-2642 (1986).

14. Patil, A.O., Ikenoue, Y., Wudl, F. and Heeger, A.J. "Water-Soluble Conducting Polymers" *J. Am. Chem. Soc.* **109** 1858-1859 (1987).

15. Furakawa, Y., Ueda, F., Hyodo, Y., Harada, I., Nakajima T. and Kawagoe, T. "Vibrational Spectra and Structure of Polyaniline" *Macromolecules* **21** 1297-1305 (1988).

16. Mitchell, G.R. and Geri, A. "Molecular Organisation of Electrochemically Prepared Conducting Polypyrrole Films" *J. Phys. D. Appl. Phys.* **20** 1346-1353 (1987).

17. Wessling, R.A. and Zimmermann, R.G "Polyelectrolytes From Bis-Sulfonium Salts" U.S. Pat. # 3,401,152 (1968).

18. White, D. and Bott, D.C. "The Production of Oriented, Crystalline Poly(Acetylene) by the Durham Route" Polymer Comm. **25** 98-99 (1984).

19. Gagnon, D.R., Capistran, J.D., Karasz, F.E. and Lenz, R.W. "Conductivity Anisotropy in Oriented Poly(*p*-Phenylene Vinylene)" *Polym. Bull.* **12** 293-298 (1984).

20. Gagnon, D.R., Karasz, F.E., Thomas, E.L. and Lenz, R.W. "Molecular Orientation and Conductivity in Highly Drawn Poly(*p*-Phenylene Vinylene)" *Synth. Met.* **20** 85-95 (1987).

21. Chance, R.R., Bredas, J.L. and Silbey, R. "Bipolar Transport in Doped Conjugated Polymers" *Phys. Rev. B* **29** 4491-4495 (1984).

22. Masse, M.A. "Stucture and Morphology of Electrically Conducting Poly(*p*-Phenylene Vinyelene)" Ph.D. Dissertation, University of Massachusetts, Amherst, Massachusetts (1989).

23. MacDiarmid, A.G. and Heeger, A.J. "Organic Metals and Semiconductors: The Chemistry of Polyacetylene, $(CH)_x$, and its Derivatives" *Synth. Met.* **1** 101-118 (1979).

24. Park, Y.W., Druy, M.A., Chiang, C.K., MacDiarmid, A.G. and Heeger, A.J. "Anisotropic Electrical Conductivity of Partially Oriented Polyacetylene" *J. Polym. Sci., Poly. Lett. Ed.* **17** 195-201 (1979).

25. Wessling, B. and Volk, H. "Post-Polymerization Processing of Conductive Polymers: A Way of Converting Conductive Polymers to Conductive Materials?" *Synth. Met.* **15** 183-193 (1986).

26. Shi, S. and Wudl, F. "Recent Progress Towards Water Soluble PPV" *Polym. Mater. Sci. Eng.* **59** 1164-1166 (1988).

27. Basescu, N., Liu, Z.-X., Moses, D., Heeger, A.J., Naarmann, H. and Theophilou, N. "High Electrical Conductivity in Doped Polyacetylene" Nature **327** 403-405 (1987).

28. Krichene, S., Lefrant, S., Froyer, G., Maurice, F. and Pelous, Y. "Raman Scattering Induced by Undoped and Doped Polyparaphenylene" *J. De Physique* **44** C3 733-736 (1983).

29. Enkelmann, V., Wieners, G. and Eiffler, J. "Model Structures for the Conducting Phase of Poly(1,4-Phenylene)" *Makromol. Chem. Rapid Comm.* **4** 337-340 (1983).

30. Creculius, G., Stamm, M., Fink, J. and Ritsko, J.J. "AsF_5-Doped Polyparaphenylene: Evidence for Polaron and Bipolaron Formation" *Phys. Rev. Lett.* **50** 1498-1500 (1983).

31. Cao, Y., Andreatta, A., Heeger, A.J. and Smith, P. "Influence of Chemical Polymerization Conditions on the Properties of Polyaniline" *Polymer* **30** 2305-2311 (1989).

32. Annis, B.K., Specht, E.D., Theophilou, N. and MacDiarmid, A.G. "Structural Aspects of Stretched Emeraldine as Determined by X-ray Scattering" *Polymer* **32** 1160-1166 (1991).

33. Jenekhe, S.A. "A Class of Narrow-Band-Gap Semiconducting Polymers" *Nature* **322** 345-347 (1986).

34. Tourillon, G. and Garnier, F. "Morphology of Conducting Organic Polymers: Polythiophene and Poly(3-Methyl Thiophene)" *J. Polym. Sci., Polym. Phys. Ed.* **22** 33-39 (1984).

35. Skotheim, T.A., Florit, M.I., Melo, A. and O'Grady, W.E. "Ultrahigh-Vacuum *in situ* Electrochemistry with Solid Polymer Electrolyte and X-ray Photoelectron Spectroscopy Studies of Polypyrrole" *Phys. Rev. B* **30** 4846-4849 (1984).

36. De Paoli, M.-A., Waltman, R.J., Diaz, A.F. and Bargon, J. "Conductive Composites from Poly(Vinyl Chloride) and Polypyrrole" *J. Chem. Soc., Chem. Comm.* 1015-1016 (1984).

37. Antoun, S., Karasz, F.E. and Lenz, R.W. "Synthesis and Electrical Conductivity of Poly(Arylene Vinylene). I. Poly(2,5-Dimethoxyphenylene Vinylene) and Poly(2,5-Dimethylphenylene Vinylene)" *J. Polym. Sci., Polym. Chem. Ed.* **26** 1809-1817 (1988).

38. Capistran, J.D., Gagnon, D.R., Antoun, S., Lenz, R.W. and Karasz, F.E. "Synthesis and Electrical Conductivity of High Molecular Weight Poly(Arylene Vinlenes)" *ACS Polym. Preprints* **25** 282-283 (1984).

39. Helbig, M., Horhold, H.-H. and Gyra, A.-K. "Investigation of Poly(Arylenevinylenes), 2) Electrochemical Redox Reactions of Poly(1,4-Phenylene-1,2-Diphenylvinylene)" *Makromol. Chem. Rapid Comm.* **6** 643-648 (1985).

40. Liang, W. and Karasz, F.E. "Molecular Orientation of Highly Drawn Poly(*p*-2-Methoxyphenylene Vinylene)" *Polymer* **32** 2363-2366 (1991).

41. Nouwen, J., Vanderzande, D., Martens, H., Gelan, J., Yang, Z. and Geise, H. "Solid State Cross Polarization/Magic Angle Spinning ^{13}C NMR Investigation of Alkoxy-Substituted Poly(*p*-Phenylene Vinylene) Homo- and Copolymers" *Synth. Met.* **46** 23-44 (1992).

42. Schlenoff, J.B., Obrzut, J. and Karasz, F.E. "Transport, Magnetic, and Optical Properties of Electrochemically Doped Poly(1,4-Dimethoxy Phenylene Vinylene)" *Phys. Rev. B.* **40** 822-833 (1989).

43. Laakso, J., Hortling, B., Levon, K. and Lindberg, J.J. "The Electrical Conductivity Properties and Structures of Substituted Poly(Phenylene Sulphides), Synthesized from Phenols and Sulphur" *Polym. Bull.* **14** 225-231 (1985).

44. Han, C.-C., Lenz, R.W. and Karasz, F.E. "Highly Conducting, Iodine-Doped Copoly(Phenylene Vinylene)s" *Polymer Comm.* **28** 261-262 (1987).

45. Lenz, R.W., Han, C.-C. and Lux, M. "Highly Conducting, Iodine-Doped Arylene Vinylene Copolymers with Dialkoxyphenylene Units" *Polymer* **30** 1041-1047 (1989).

46. Polis, D.W., Young, C.L., McLean, M.R. and Dalton, L.R. "Synthesis and Characterization of Copolymers of Aniline and Thiophene" *Macromolecules* **23** 3231-3236 (1990).

47. Bradley, D.D.C. "Precursor-Route Poly(*p*-Phenylene Vinylene): Polymer Characterisation and Control of Electronic Properties" *J. Phys. D., Appl. Phys.* **20** 1389-1410 (1987).

48. Horhold, H.-H. and Helbig, H. "Poly(Phenylenevinylene)s - Synthesis and Redoxchemistry of Electroactive Polymers" *Makromol. Chem. Macromol. Symp.* **12** 229-258 (1987).

49. Fink, J., Creculius, G., Ritsko, J.J., Stamm, M., Freund, H.J. and Gonska, H. "Pi Electron Delocalization in Poly-(*p*-Phenylene) (PPP), Polyphenylene Sulfide (PPS) and Polyphenylene Oxide (PPO) and AsF_5 Doping of PPP" *J. De Physique* **44** C3 741-744 (1983).

50. Crecelius, G., Fink, J., Ritsko, J.J., Stamm, M., Freund, H.-J. and Gonska, H. "π-Electron Delocalization in Poly(*p*-Phenylene), Poly(*p*-Phenylene Sulfide), and Poly(*p*-Phenylene Oxide)" *Phys. Rev. B* **28** 1802-1808 (1983).

51. Schlenoff, J.B., Machado, J.M., Glatkowski, P.J. and Karasz, F.E. "Chemical and Electrochemical Doping in Poly(Paraphenylene Vinylene) Blends" *J. Polym. Sci., Polym. Phys. Ed.* **26** 2247-2256 (1988).

52. Tieke, B. and Gabriel, W. "Conducting Polypyrrole-Polyimide Composite Films" *Polymer* **31** 20-23 (1990).

53. Machado, J.M., Karasz, F.E. and Lenz, R.W. "Electrically Conducting Polymer Blends" *Polymer* **29** 1412-1417 (1988).

54. Pradere, P. and Boudet, A. "Influence of the Mode of Synthesis on the Morphology and Structure of Polyparaphenylene" *J. Mater. Sci.* **22** 4240-4246 (1987).

55. Karasz, F.E., Capistran, J.D., Gagnon, D.R. and Lenz, R.W. "High Molecular Weight Polyphenylene Vinylene" *Mol. Cryst. Liq. Cryst.* **118** 327-332 (1985).

56. Machado, J.M., Denton III, F.R., Schlenoff, J.B., Karasz, F.E. and Lahti, P.M. "Analytical Methods for Molecular Weight Determination of Poly(*p*-Xylylidene Dialkyl Sulfonium Halide): Degree of Polymerization of Poly(*p*-Phenylene Vinylene) Precursors" *J. Polym. Sci., Polym. Phys. Ed.* **27** 199-203 (1989).

57. Antoun, S., Gagnon, D.R., Karasz, F.E. and Lenz, R.W. "Synthesis and Electrical Conductivity of AsF_5-Doped Poly(Arylene Vinylenes)" *Polym. Bull.* **15** 181-184 (1986).

58. Murase, I., Ohnishi, T., Noguchi, T., Hirooka, M. and Murakami, S. "Highly Conducting Poly(*p*-Phenylene Vinylene) Prepared from Sulfonium Salt" *Mol. Cryst. Liq. Cryst.* **118** 333-336 (1985).

59. Machado, J.M., Karasz, F.E., Kovar, R.F., Burnett, J.M., and Druy, M.A. "A Continuous Process for Preparing Highly Conducting, Uniaxially Oriented Poly(Phenylene Vinylene) Film" *New. Polym. Mater.* **1** 189-208 (1989).

60. Bradley, D.D.C., Friend, R.H., Lindenberger, H. and Roth, S. "Infra-Red Characterization of Oriented Poly(Phenylene Vinylene)" *Polymer* **27** 1709-1713 (1986).

61. Machado, J.M. "New Processes and Materials in Conducting Polymers" Ph.D. Dissertation, University of Massachusetts, Amherst, Massachusetts (1988).

62. Bradley, D.D.C., Evans, G.P. and Friend, R.H. "Characterization of Poly(phenylenevinylene) by Infrared and Optical Absorption" *Synth. Met.* **17** 651-656 (1987).

63. Masse, M.A., Schlenoff, J.B., Karasz, F.E. and Thomas, E.L. "Crystalline Phases of Electrically Conductive Poly(*p*-Phenylene Vinylene)" *J. Polym. Sci., Polym. Phys. Ed.* **27** 2045-2059 (1989).

64. Machado, J.M., Masse, M.A. and Karasz, F.E. "Anisotropic Mechanical Properties of Uniaxially Oriented Electrically Conducting Poly(*p*-Phenylene Vinylene)" *Polymer* **30** 1992-1996 (1989).

65. Gagnon, D.R. "Chemical. Structural, and Electrical Characterization of Poly(p-Phenylene Vinylene)" Ph.D. Dissertation, University of Massachusetts, Amherst, Massachusetts (1986).

66. Ohnishi, T., Murase, I., Noguchi, T. and Hirooka, M. "Highly Conductive Graphite Film Prepared from Pyrolysis of Poly(*p*-Phenylene Vinylene)" *Synth. Met.* **14** 207-213 (1986).

67. Ueno, H., Nogami, K. and Yoshino, K. "Electrical Conductivity and Optical Reflectance of Potassium-Intercalated Graphitized Poly(*p*-Phenylene Vinylene) Films" *Phys. Rev. B* **36** 8142-8146 (1988).

68. Ueno, H. and Yoshino, K. "Properties of $FeCl_3$-Intercalated Graphite Film Prepared by Heat Treatment of Poly(*p*-Phenylene Vinylene) Film" *Phys. Rev. B* **36** 8138-8141 (1988).

69. Chen, D., Winokur, M.J., Masse, M.A. and Karasz, F.E. "Structural Phases of Sodium-Doped Polyparaphenylene Vinylene" *Phys. Rev. B* **41** 6759-6767 (1990).

70. Heiney, P.A., Fischer, J.E., Djurado, D., Ma, J., Chen, D., Winokur, M.J., Coustel, N., Bernier, P. and Karasz, F.E. "Channel Structures in Alkali-Metal-Doped Conjugated Polymers: Broken-Symmetry Two-Dimensional Intercalation Superlattices" *Phys. Rev. B* **44** 2507-2515 (1991).

71. Winokur, M.J., Chen, D. and Karasz, F.E. "Structural Studies of Alkali-Doped Polyparaphenylene Vinylene" submitted to *Phys. Rev. B.*

72. Yoshino, K., Takiguchi, T., Hayashi, S., Park, D.H. and Sugimoto, R.-I. "Electrical and Optical Properties of Poly(*p*-Phenylene Vinylene) and Effects of Electrochemical Doping" *Jap. J. Appl. Phys. I* **25** 881-884 (1986).

73. Masse, M.A. and Karasz, F.E., unpublished results.

74. Masse, M.A., Composto, R.J., Jones, R.A.L. and Karasz, F.E. "Dopant Concentration Profiles in Conducting Poly(*p*-Phenylenevinylene) by Rutherford Backscattering Spectrometry" *Macromolecules* **23** 3675-3682 (1990).

75. Masse, M.A., Martin, D.C., Thomas, E.L., Karasz, F.E. and Petermann, J.H. "Crystal Morphology in Pristine and Doped Films of Poly(*p*-Phenylene Vinylene)" *J. Mater. Sci.* **25** 311-320 (1990).

76. Masse, M.A., Machado, J.M. and Karasz, F.E., unpublished results.

77. Glatkowski, P.J. and Karasz, F.E., unpublished results.

78. Lefrant, S., Perrin, E. and Buisson, J.P. "Vibrational Studies of Polyparaphenylene-Vinylene (PPV)" *Synth. Met.* **29** E91-E96 (1989).

79. Machado, J.M., Masse, M.A., Karasz, F.E., Burnett, J.M., Kovar, R.F. and Druy, M.A. "Processing and Characterization of a Biaxially Oriented Conducting Polymer" *Brit. Polym. J.* **22** 59-64 (1990).

80. Bradley, D.D.C., Friend, R.H., Hartmann, T., Marseglia, E.A., Sokolowski, M.M. and Townshend, P.D. "Structural Studies of Oriented Precursor Route Conjugated Polymers" *Synth. Met.* **17** 473-478 (1987).

81. Granier, T., Thomas, E.L. and Karasz, F.E. "Paracrystalline Structure of Poly(Paraphenylene Vinylene)" *J. Polym. Sci., Polym. Phys. Ed.* **27** 469-487 (1989).

82. Granier, T., Thomas, E.L., Gagnon, D.R., Karasz, F.E. and Lenz, R.W. "Structural Investigation of Poly(*p*-Phenylene Vinylene)" *J. Polym. Sci., Polym. Phys. Ed.* **24** 2793-2804 (1986).

83. Ezquerra, T.A., Lopez-Cabarcos, E., Balta-Calleja, F.J., Stenger-Smith, J.D. and Lenz, R.W. "Real-Time X-ray Scattering Study During the Thermal Conversion of a Precursor Polymer to Poly(*p*-Phenylene Vinylene)" *Polymer* **32** 781-785 (1991).

84. Moon, Y.B., Rughooputh, S.D.D.V., Heeger, A.J., Patil, A.O. and Wudl, F. "X-ray Scattering Study of the Conversion of Poly(*p*-Phenylene Vinylene) Precursor to the Conjugated Polymer" *Synth. Met.* **29** E79-E84 (1989).

85. Wilke, W. "General Lattice Factor of the Ideal Paracrystal" *Acta Cryst.* A39 864-867 (1983).

86. Hosemann, R. "Crystalline and Paracrystalline Order in High Polymers" *J. Appl. Phys.* **34** 25-41 (1963).

87. Clark, E.S. and Muus, L.T. "The Relationship between Bragg Reflections and Disorder in Crystalline Polymers" *Z. Krist.* **117** 108-118 (1962).

88. Hosemann, R. and Bagchi, S. *Direct Analysis of Diffraction by Matter* North-Holland, Amsterdam, 1962.

89. Thakur, M. "A Class of Conducting Polymers Having Nonconjugated Backbones" *Macromolecules* **21** 661-664 (1988).

90. Shuai, Z. and Bredas, J.L. "Electronic Structure of Conducting Polymers with Nonconjugated Backbones: 1,4-Polybutadiene and 1,4-Polyisoprene" *Macromolecules* **24** 3723-3724 (1991).

91. Bredas, J.L. and Street, G.B. "Polarons, Bipolarons, and Solitons in Conducting Polymers" *Acc. Chem. Res.* **18** 309-315 (1985).

92. Rebbi, C. "Solitons" *Sci. Amer.* **240** 92-116 (1979).

93. Heeger, A.J., Kivelson, S., Schrieffer, J.R. and Su, W.-P. "Solitons in Conducting Polymers" *Rev. Mod. Phys.* **60** 781-850 (1988).

94. Spangler, C.W., Hall, T.J., Sapochak, L.S. and Liu, P.-K. "Polaron and Bipolar Formation in Model Oligomeric Extended π-Electron Systems: Studies Towards the Rational Design of ElectroactivePolymers for Non-Linear Optics Applications" *Polymer* **30** 1166-1169 (1989).

95. Grant, P.M. and. Batra, I.P "Electronic Structure of Conducting π-Electron Systems" *Synth. Met.* **1** 193-212 (1979).

96. Yamabe, T., Tanaka, K., Koike, T. and Ueda, M. "Electronic Structures of Conjugated Polymers and Conducting Mechanism" *Mol. Cryst. Liq. Cryst.* **117** 185-192 (1985).

97. Kuroda, S., Murase, I., Ohnishi, T. and Noguchi, T. "ESR and ENDOR Study of Poly (Phenylene Vinylene)" *Synth. Met.* **17** 663-666 (1987).

98. Lahti, P.M., Obrzut, J. and Karasz, F.E. "Use of the Pariser-Parr-Pople Approximation to Obtain Practically Useful Predictions for Electronic Spectral Properties of Conducting Polymers" *Macromolecules* **20** 2023-2026 (1987).

99. Obrzut, M.J. and Karasz, F.E. "X-ray Photoelectron Spectroscopy of Neutral and Electrochemically Doped Poly(*p*-Phenylene Vinylene)" *Macromolecules* **22** 458-464 (1989).

100. Takiguchi, T., Park, D.H., Ueno, H. and Yoshino, K. "Photoconductivity and Carrier Transport Process in Poly(*p*-Phenylene Vinylene) Film" *Synth. Met.* **17** 657-662 (1987).

101. Braun, D. and Heeger, A.J. "Visible Light Emission from Semiconducting Polymer Diodes" *Appl. Phys. Lett.* **58** 1982-1984 (1991).

102. Maricq, M.M. and Waugh, J.S. "NMR in Rotating Solids" *J. Chem. Phys.* 70 3300-3316 (1979).

103. Yannoni, C.S. "High-Resolution NMR in Solids: the CPMAS Experiment" *Acc. Chem. Res.* 15 201-208 (1982).

104. Griffin, R.G., Beshah, K., Ebelhaeuser, R., Huang, T.H.,. Olejniczak, E.T, Rice, D.M., Siminovitch, D.J. and Wittebort, R.J. "Ch 7: Deuterium NMR Studies of Dynamics in Solids" in *The Time Domain in Surface and Structural Dynamics* G.J. Long and F. Grandejeon, eds, Kluwer, 1988 pp. 81-105.

105. Spiess, H.W. "Deuteron NMR - a New Tool for Studying Chain Mobility and Orientation in Polymers" *Adv. Pol. Sci.* **66** 23-58 (1985).

106. Spiess, H.W. "Molecular Dynamics of Solid Polymers as Revealed by Deuteron NMR" *Colloid & Polymer Sci.* **261** 193-209 (1983).

107. Spiess, H.W. "Pulsed Deuteron NMR Investigations of Structure and Dynamics of Solid Polymers" *J. Mol. Struct.* 111 119-133 (1983).

108. Spiess, H.W. "Deuteron NMR Methods for Studying Molecular Order and Motion in Solid Polymers and Liquid Crystalline Polymers" *Pure & Appl. Chem.* 57 1617-1626 (1985).

109. Mehring, M. *High Resolution NMR of Solids*, 2nd ed., Springer-Verlag, Berlin, 1983.

110. Slichter, C.P. *Principles of Magnetic Resonance*, 2nd ed., Springer-Verlag, Berlin, 1978.

111. Abragam, A. *Principles of Nuclear Magnetism*, Clarendon Press, New York, 1961.

112. Harris, R.K. *Nuclear Magnetic Resonance Spectroscopy*, Longman, Avon, 1986.

113. Schaefer, J., Stejskal, E.O. and Buchdahl, R. "High-Resolution Carbon-13 Nuclear Magnetic Resonance Study of Some Solid, Glassy Polymers" *Macromolecules* **8** 291-296 (1975).

114. Lyerla, J.R. "Chapter 3: High-Resolution NMR of Glassy Amorphous Polymers" in *High-Resolution NMR Spectroscopy of Synthetic Polymers in Bulk* Komoroski, R.A., ed. VCH, Weinheim, Germany, 1986, pp. 63-119.

115. Jelinski, L.W. "Deuterium NMR of Solid Polymers" in *High Resolution NMR Spectroscopy of Synthetic Polymers in Bulk* Komoroski, R.A., ed., VCH, Weinheim, Germany, 1986.

116. Euler, W.B. and Roberts, J.E. "Solid-State ^{13}C NMR Study of Oligomeric and Polymeric Azines" *Macromolecules* **22** 4221-4225 (1989).

117. Gomez, M.A. and Tonelli, A.E. "Carbon-13 Nuclear Magnetic Resonance Study of Chain Conformation in the Solid Polymorphs of Syndiotactic Polystyrene" *Macromolecules* **23** 3385-3386 (1990).

118. Sullivan, M.J. and Maciel, G.E. "Structural Resolution in the Carbon-13 Nuclear Magnetic Resonance Spectrometric Analysis of Coal by Cross Polarization and Magic-Angle Spinning" *Anal. Chem.* **54** 1606-1615 (1982).

119. Henrichs, P.M., Nicely, V.A. and Fagerburg, D.R. "Sub-T_g Dynamic Processes in Amorphous Solids: A Deuterium and ^{13}C NMR Study of Poly(Phenylene Sulfide)" *Macromolecules* **24** 4033-4037 (1991).

120. Erb, H.-P. and Bluhm, T. "^{13}C NMR Spectra of Diazastilbenes" *Org. Magn. Res.* **14** 285-289 (1980).

121. Van der Hart, D.L. and Garroway, A.N. "Resolution in ^{13}C NMR of Organic Solids Using High-Power Proton Decoupling and Magic-Angle Sample Spinning" *J. Magn. Reson.* **44** 361-401 (1981).

122. Schaefer, J., Stejskal, E.O. and Buchdahl, R. "Magic-Angle ^{13}C NMR Analysis of Motion in Solid Glassy Polymers" *Macromolecules* **10** 384-405 (1977).

123. Koegler, G., Hasenhindl, A. and Moeller, M. "Solid-State NMR Studies on the Molecular Structure and Dynamics of Poly(Diethylsiloxane) Polymorphs" *Macromolecules* **22** 4190-4197 (1989).

124. Lebek, B., Menge, H., Schlothauer, K., Schneider, H., Kivayeva, L.S. and Fedotov, V.D. "^{13}C NMR Investigation of the Microdynamics of Poly(Vinyl Butyral)" *Polymer* **32** 2335-2339 (1991).

125. Morin, F.C. and Marchessault, R.H. "Solid-State ^{13}C NMR Study of the Molecular Dynamics in Amorphous and Crystalline Poly(β-Hydroxyalkanoates)" *Macromolecules* **25** 576-581 (1992).

126. Henrichs, P.M. and Nicely, V.A. "^{13}C NMR Study of the Conformation and Dynamics of Bisphenol A Polycarbonate" *Macromolecules* **24** 2506-2513 (1991).

127. Poliks, M.D. and Schaefer, J. "Characterization of the Chain Dynamics of PEEK by CPMAS ^{13}C NMR" *Macromolecules* **23** 3426-3431 (1990).

128. Jelinski, L.W., Dumais, J.J. and Engel, A.K. "Multitechnique Solid-State NMR Approach to Assessing Molecular Motion: Poly(Butylene Terephthalate) and Poly(Butylene Terephthalate)-Containing Segmented Copolymers" *Macromolecules* **16** 403-409 (1983).

129. Liu, Y., Roy, A.K., Jones, A.A., Inglefield, P.T. and Ogden, P. "An NMR Study of Plasticization and Antiplasticization of a Polymeric Glass" *Macromolecules* **23** 968-977 (1990).

130. Jeener, J., Meier, B.H., Bachmann, P. and Ernst, R.R. "Investigation of Exchange Processes by Two-Dimensional NMR Spectroscopy" *J. Chem. Phys.* **71** 4546-4553 (1979).

131. Schleicher, A., Mueller, K. and Kothe, G. "Two Dimensional Nuclear Magnetic Resonance Relaxation Spectroscopy of Molecular Solids" *J. Chem. Phys.* **92** 6432-6440 (1990).

132. Blumich, B. and Spiess, H.W. "Two-Dimensional Solid-State NMR Spectroscopy: New Possibilities for the Investigation of the Structure and Dynamics of Solid Polymers" *Angew. Chem. Int. Ed. Engl.* 27 1655-1672 (1988).

133. Bax, A. and Lerner, L. "Two-Dimensional Nuclear Magnetic Resonance Spectroscopy" *Science* 232 960-967 (1986).

134. Schmidt, C., Bluemich, B. and. Spiess, H.W "Deuteron Two-Dimensional Exchange NMR in Solids" *J. Magn. Reson.* 79 269-290 (1988).

135. Yang, Y., Hagemeyer, A. and Spiess, H.W. "Order-Exchange Correlated Two-Dimensional NMR Study of Slow Molecular Motion in Highly Oriented Crystalline Poly (Oxymethylene)" *Macromolecules* 22 1004-1006 (1989).

136. Thomas, A.F. *Deuterium Labelling in Organic Chemistry* Appleton, New York, 1976.

137. Pschorn, U., Spiess, H.W., Hisgen, B. and Ringsdorf, H. "Deuteron NMR Study of Molecular Order and Motion of the Mesogenic Side Groups in Liquid-Crystalline Polymers" *Makromol. Chem.* **187** 2711-2723 (1986).

138. Spiess, H.W. "NMR in Oriented Polymers" in *Developments in Oriented Polymers-1* Ward, I.M., ed., Applied Science, London, 1982.

139. Beshah, K., Olejniczak, E.T. and Griffin, R.G. "Deuterium NMR Study of Methyl Group Dynamics in L-Alanine" *J. Chem. Phys.* **86** 4730-4736 (1987).

140. Rice, D.M., Meinwald, Y.C., Scheraga, H.A. and Griffin, R.G. "Tyrosyl Motion in Peptides: ^{2}H NMR Line Shapes and Spin-Lattice Relaxation" *J. Am. Chem. Soc.* **109** 1636-1640 (1987).

141. Wittebort, R.J. and Szabo, A. "Theory of NMR Relaxation in Macromolecules: Restricted Diffusion and Jump Models for Multiple Internal Rotations in Amino Acid Side-Chains" *J. Chem. Phys.* **69** 1722-1736 (1978).

142. Jelinski, L.W., Dumais, J.J., Cholli, A.L., Ellis, T.S. and Karasz, F.E. "Nature of the Water-Epoxy Interaction" *Macromolecules* **18** 1091-1095 (1985).

143. Jelinski, L.W., Dumais, J.J., Stark, R.E., Ellis, T.S. and Karasz, F.E. "Interaction of Epoxy Resins with Water. A Quadrupole Echo Deuterium NMR Study" *Macromolecules* **16** 1019-1021 (1983).

144. Hirschinger, J., Schaefer, D., Spiess, H.W. and Lovinger, A.J. "Chain Dynamics in the Crystalline α-Phase of Poly(Vinylidene Fluoride) by Two-Dimensional Exchange ^{2}H NMR" *Macromolecules* **24** 2428-2433 (1991).

145. Schaefer, D., Spiess, H.W., Suter, U.W. and Fleming, W.W. "Two-Dimensional Solid-State NMR Studies of Ultraslow Chain Motion: Glass Transition in Atactic Poly(Propylene) Versus Helical Jumps in Isotactic Poly(Propylene)" *Macromolecules* **23** 3431-3439 (1990).

146. Pschorn, U., Roessler, E., Sillescu, H., Kaufmann, S., Schaefer, D. and Spiess, H.W. "Local and Cooperative Motions at the Glass Transition of Polystyrene: Information from One- and Two-Dimensional NMR as Compared with Other Techniques" *Macromolecules* **24** 398-402 (1991).

147. Liang, W., Rice, D.M. and Karasz, F.E. "Preparation of Poly(*p*-Phenylene Vinylene) Deuterium Labeled in the Vinylene Positions" submitted to *Polym. Comm.*

148. Opella, S.J. and Frey, M.H. "Selection of Non-Protonated Carbon Resonances in Solid-State Nuclear Magnetic Resonance" *J. Am. Chem. Soc.* **101** 5854-5856 (1979).

149. Tokito, S., Momii, T., Murata, H., Tsutsui, T. and Saito, S. "Polyarylene Films Prepared from Precursor Polymers Soluble in Organic Solvents" *Polymer* **31** 1137-1141 (1990).

150. Program SIMFIT, Barron, P., Bruker Instruments Inc., Billerica, Ma.

151. Burum, D.P., Linder, M. and Ernst, R.R. "Low-Power Multipulse Line Narrowing in Solid-State NMR" *J. Magn. Res.* **44** 173-188 (1981).

152. Bielecki, A., Burum, D.P., Rice, D.M. and Karasz, F.E. "A Solid State Two-Dimensional ^{13}C-^{1}H Correlation (HETCOR) NMR Spectrum of Amorphous Poly(2,6-dimethyl-*p*-phenylene oxide) (PPO)" *Macromolecules* **24** 4820-4822 (1992).

153. Caravatti, P., Braunschweiler, L. and Ernst, R.R. "Heteronuclear Correlation Spectroscopy in Rotating Solids" *Chem. Phys. Lett.* **100** 305-310 (1983).

154. LINESIM program supplied by Bruker Instruments, Billerica, Massachusetts.

155. Press, W.H., Flannery, B.P., Teukolsky, S.A. and Vetterling, W.T. *Numerical Recipes in FORTRAN* Cambridge Univ. Press, New York, 1986, pp. 289-293.

156. Bevington, P.R. *Data Reduction and Error Analysis for the Physical Sciences* McGraw Hill, New York, 1969, pp. 242-245.

157. Wittebort, R.J., Olejniczak, E.T. and Griffin, R.G. "Analysis of Deuterium Nuclear Magnetic Resonance Line Shapes in Anisotropic Media" *J. Chem. Phys.* **86** 5411-5420 (1987).

158. Spiess, H.W. and Sillescu, H. "Solid Echoes in the Slow-Motion Regime" *J. Magn. Reson.* **42** 381-389 (1981).

159. Torchia, D.A. and Szabo, A. "Spin-Lattice Relaxation in Solids" *J. Magn. Reson.* **49** 107-121 (1982).

160. Bloom, M., Davis, J.H. and Valic, M.I. "Spectral Distortion Effects Due to Finite Pulse Widths in Deuterium Nuclear Magnetic Resonance Spectroscopy" *Can. J. Phys.* **58** 1510-1517 (1981).

161. Ward, I.M., ed. *Structure and Properties of Oriented Polymers* Wiley, New York, 1975.

162. Finder, C.J., Newton, M.G. and Allinger, N.L. "An Improved Structure of *trans*-Stilbene" *Acta Cryst.* **B30** 411-415 (1974).

163. Schroter, B., Horhold, H.H. and Raabe, D. "Investigation of Poly(Arylenevinylenes): 24 High-Resolution Solid-State ^{13}C NMR Spectroscopy" *Makromol. Chem.* **182** 3185-3193 (1981).

164. Gibson, H.W., Pochan, J.M. and Kaplan, S. "^{13}C Magic Angle NMR Study of the Isomerization of *cis*- to *trans*-Polyacetylene" *J. Am. Chem. Soc.* **103** 4619-4620 (1981).

165. Herzfeld, J. and Berger, A.E. "Sideband Intensities in NMR Spectra of Samples Spinning at the Magic Angle" *J. Chem. Phys.* 73 6021-6030 (1980).

166. Suwelack, D., Rothwell, W.P. and Waugh, J.S. "Slow Molecular Motion Detected in the NMR Spectra of Rotating Solids" *J. Chem. Phys.* 73 2559-2569 (1980).

167. Grobelny, J., Obrzut, J. and Karasz, F.E. "Solid-State ^{13}C NMR Study of Neutral Insulating and Electrochemically Doped Conducting Poly(*p*-Phenylene Vinylene)" *Synth. Met.* **29** E97-E102 (1989).

168. Aujla, R.S., Harris, R.K., Packer, K.J., Parameswaran, M., Bunn, A. and Cudby, M.E.A. "Discriminatory Experiments in High-Resolution ^{13}C NMR of Solid Polymers" *Polym. Bull.* **8** 253-260 (1982).

169. Grobelny, J., Rice, D.M., Karasz, F.E. and MacKnight, W.J. "High Resolution Solid-State ^{13}C Nuclear Magnetic Resonance Study of Poly(Ether Sulphone)/Polyimide Blends" *Polym. Comm.* 31 86-89 (1990).

170. Stejskal, E.O., Schaefer, J., Sefcik, M.D. and McKay, R.A. "Magic-Angle Carbon-13 Nuclear Magnetic Resonance Study of the Compatibility of Solid Polymeric Blends" *Macromolecules* **14** 275-279 (1981).

171. Rice, D.M., Wittebort, R.J., Griffin, R.G., Meirovitch, E., Stimson, E.R., Meinwald, Y.C., Freed, J.H. and Scheraga, H.A. "Rotational Jumps of the Tyrosine Side Chain in Crystalline Enkephalin. ^{2}H NMR Line Shapes for Aromatic Ring Motion in Solids" *J. Am. Chem. Soc.* **103** 7707-7710 (1981).

172. Cholli, A.L., Dumais, J.J., Engle, A.K. and Jelinski, L.W. "Aromatic Ring Flips in a semicrystalline polymer" *Macromolecules* **17** 2399-2404 (1984).

173. Kaplan, S., Conwell, E.M., Richter, A.F. and MacDiarmid, A.G. "Ring Flips as a Probe of the Structure of Polyanilines" *Macromolecules* **22** 1669-1675 (1989).

174. Dumais, J.J., Cholli, A.L., Jelinski, L.W., Hedrick, J.L. and McGrath, J.E. "Molecular Basis of the β-Transition in Poly(Arylene Ether Sulfones)" *Macromolecules* **19** 1884-1889 (1986).

175. Fischer, E. "Selective Photoexcitation of Rotamers of 1,2-Diarylethylenes" *J. Mol. Struct.* **84** 219-226 (1982).

177. Pake, G.E. "Nuclear Resonance Absorption in Hydrated Crystals: Fine Structure of the Proton Line" *J. Chem. Phys.* **16** 327-336 (1948).

178. Morrison, R.T. and Boyd, R.W. *Organic Chemistry* 2nd ed., Allyn and Bacon, Boston, 1970, p. 149.

179. Murase, I., Ohnishi, T., Noguchi, T. and Hirooka, M. "Highly Conducting Poly(Phenylene Vinylene) Derivatives via Soluble Precursor Process" *Synth. Met.* **17** 639-644 (1987).

180. Fleming, W.W., Fyfe, C.A., Lyerla, J.R., Vanni, H. and Yannoni, C.A. "Variable Temperature High-Resolution Carbon-13 NMR Spectra of Solid Fluoropolymers" *Macromolecules* **13** 460-462 (1980).

181. Boyd, R.H. "Relaxation Processes in Crystalline Polymers: Experimental Behavior - a Review" *Polymer* **26** 323-347 (1985).

182. Gagnon, D.R., Capistran, J.D., Karasz, F.E., Lenz, R.W. and Antoun, S. "Synthesis, Doping and Electrical Conductivity of High Molecular Weight Poly(*p*-Phenylene Vinylene)" *Polymer* **28** 567-573 (1987).

183. Kratky, O. "Zum Deformationsmechanismus der Faserstoffe, I." *Kolloid. Z.* **64** 213-222 (1933).

184. Dumais, J.J., Jelinski, L.W., Galvin, M.E., Dybowski, C., Brown, C.E. and Kovacic, P. "Solid-State Deuterium NMR Studies of Poly(*p*-Phenylene) and *trans*-Polyacetylene as a Blend in Polystyrene" *Macromolecules* **22** 612-617 (1989).

185. Murthy, N.S., Shacklette, L.W. and Baughman, R.H. "Effect of Charge Transfer on Chain Dimension in *trans*-Polyacetylene" *J. Chem. Phys.* **87** 2346-2348 (1987).

186. Weast, R.C., ed., *CRC Handbook of Chemistry and Physics* 63rd edn., CRC Press, Boca Raton, FL, 1982-3, p. F-179.

187. Mokarram, M. and Ragle, J.L. "On the Relationship Between Deuteron Quadruple Coupling Constants and Force Constants in Diatomic Hydrides" *J. Chem. Phys.* **59** 2770-2771 (1973).

188. Billaud, D., Saldi, F., Ghanbaja, J., Begin, D. and Lelaurain, M. "Structural Variations of Oriented Polyacetylene upon Intercalation with Selected Electron Donating and Accepting Species" *Synth. Met.* **35** 113-121 (1990).

189. Saldi, F., Ganbaja, J., Begin, D., Lelaurin, M. and Billaud, D. "Insertion de Metaux Alcalins Dans le Polyacetylene: Etude Structurale des Phases les Plus Riches en Metal" *C. R. Acad. Sci* **309** 671-675 (1989).

190. Winokur, M.J., private communication.

191. Bielecki, A., Burum, D.P., Rice, D.M. and Karasz, F.E., unpublished results.

192. Carter, C.M., Facelli, J.C., Aldermann, D.W., Grant, D.M., Dalley, N.K. and Wilson, B.E. "Carbon-13 Chemical-Shift Tensors in Single-Crystal Methoxybenzenes" *J. Chem. Soc., Faraday Trans. 1* **84** 3673-3690 (1988).

193. Levitt, M.H., Raleigh, D.P., Creuzet, F. and Griffin, R.G., "Theory and Simulations of Homonuclear Spin Pair Systems in Rotating Solids" *J. Chem. Phys.* **92** 6347-6364 (1990).

194. Rice, D.M. and Karasz, F.E., unpublished data.

195. Munowitz, M.G. "High-Resolution Dipolar Nuclear Magnetic Resonance Spectroscopy in Solids" Ph.D. Dissertation, Harvard University, Cambridge, Massachusetts (1982).

196. Goodwin, T.H., Przybylska, M. and Robertson, J.M. "The Crystal and Molecular Structure of 1:4-Dimethoxybenzene" *Acta Cryst.* **3** 279-284 (1950).